The Dissertation Committee for Lauren Fay Greenlee Certifies that this is the approved version of the following dissertation:

Enhancing Recovery of Reverse Osmosis Desalination: Side-Stream Oxidation of Antiscalants to Precipitate Salts

Committee:

Benny D. Freeman, Supervisor

Desmond F. Lawler, Co-Supervisor

Philippe Moulin

Douglas R. Lloyd

Donald R. Paul

Lynn E. Katz

Enhancing Recovery of Reverse Osmosis Desalination: Side-Stream Oxidation of Antiscalants to Precipitate Salts

by

Lauren Fay Greenlee, B.S.E.; M.S.

Dissertation

Presented to the Faculty of the Graduate School of

The University of Texas at Austin

in Partial Fulfillment

of the Requirements

for the Degree of

Doctor of Philosophy

The University of Texas at Austin

August 2009

Dedication

To my parents and my sister, for believing in me and supporting me through all of my endeavors. I would not have made it here without you.

Acknowledgements

I would like to thank my two advisors at UT, Desmond Lawler and Benny Freeman. I chose to come to UT because of the opportunity to work with both of you, not knowing exactly what that meant but somehow knowing that it was the best fit for me. You both have given me incredible opportunities to learn, develop my own research project, travel, meet fellow researchers and colleagues, and begin my own career as a researcher, mentor, and educator. You are the reason I stayed at UT and finished my Ph.D., and it has been a truly rewarding experience to be able to work with both of you.

I would also like to thank my host and advisor at the Laboratoire Mécanique, Modélisation et Procédés Propres in Aix en Provence, France, Philippe Moulin. My year abroad in France conducting research during my Ph.D. was quite a challenge, and I learned to become part of a new laboratory, a new group of researchers, and a foreign culture and language with your help and support. Thank you for your patience and encouragement, particularly with my early attempts at talking about research and engineering in French, and thank you for traveling to Austin for my Ph.D. defense.

I would like to thank my three other committee members, Lynn Katz, Don Paul, and Doug Lloyd. Dr. Katz, thank you for help in all matters water chemistry and for your advice on becoming a faculty member and finding the right fit in a department. Dr. Paul, thank you for your advice on pursuing postdoctoral and faculty positions, as well as teaching me about polymers and helping me understand the solution-diffusion model of RO transport. Dr. Lloyd, thank you for your early advice on my research project; the most important question that I was asked during my Ph.D. proposal oral exam, one that has kept me thinking and helped to direct my research, was your question – even if your

process does not work, how will your research further scientific understanding and contribute outside of your specific research project?

I would also like thank both the Freeman and Lawler research groups for support, advice, laboratory lessons, and fun times outside of the lab. In particular, thanks to Liz, Alyson, Brandon, Bryan, Hao, Richard, Scott M., Scott, and Roy from the Freeman group and thanks to Jeff, Ana, Jenny, Marion, Hector, Scott, Mike, Lee, Yamuna, Katie, Francois, and Younggy from the Lawler group. Special thanks go to Pat, Shane, and Corin, for all of our great conversations on research and on life. I look forward to continuing as colleagues with all of you throughout our careers. Thank you as well to all of the other students in EWRE that have helped me and given me advice – Lauren S., Nate, Susan, Mara, Andrew W., Lily, and Julian, to name a few. Also thank you to all members of Philippe Moulin's research group who made me feel welcome and helped me while I was in France. In particular, thank you to Ludiwine, Elise, Georgette, and Jeremy.

My family, my parents and my sister, Emily, have been supportive, encouraging, positive, and understanding throughout my time in graduate school, and I thank them for every visit they have made down to Austin, Texas and every minute they have spent on the phone and on email talking with me and staying in touch. With my family in Pennsylvania, I feel I have made some other "family" here, and I would like to thank these special people for their support and friendship throughout my years in Austin. Carrie, thank you for being the best roommate, friend, and running partner during my first two years at UT. Ana, it has been wonderful getting to know you since your days in EWRE, and you are a great friend who is always there to listen and talk. Ellison, I never thought I would find another running partner, and I am so happy we tried it out. You are an amazing, inspiring, hardworking, intelligent, motivating, and beautiful person, and you

have helped me through conversations and runs too numerous to count. Thank you for being such a wonderful friend and colleague. I look forward to many more conversations.

I would also like to acknowledge several colleagues for help in obtaining experimental data. Thank you to Dr. Elise Barbot for helping with the particle size measurements and for helping with the pilot RO study. Thank you to Fabrice Testa for helping with ozonation, precipitation, and filtration experiments; Fabrice contributed to the experimental work described in Chapters 4, 5, 8, and 9. Also, a special thanks to Daniel Dreyer and Professor Christopher Bielawski in the Department of Chemistry and Biochemistry at The University of Texas for performing the NMR analysis of the polymer antiscalant. Thank you to Dr. Hugo Celio for help and training on the SEM equipment.

Finally, I would like to acknowledge the University of Texas Thrust 2000 program for a four-year fellowship and the National Science Foundation for a three-year Graduate Research Fellowship and an International Research and Education in Engineering fellowship. I would also like to acknowledge the local Austin chapter of the P.E.O. International women's society for their help in obtaining a P.E.O. Scholar Award and P.E.O. itself for giving me the award. Thank you to Dr. J.P. Nicot and the Bureau of Economic Geology for financial support during my first year of graduate school and the opportunity to learn about desalination facilities in Texas. Thank you to both of my advisors for financial support to attend numerous meetings and conferences and for funding during my first year of graduate school.

Enhancing Recovery of Reverse Osmosis Desalination: Side-Stream Oxidation of Antiscalants to Precipitate Salts

Publication No._____

Lauren Fay Greenlee, Ph.D.

The University of Texas at Austin, 2009

Supervisors: Benny D. Freeman, Desmond F. Lawler

Brackish waters are now considered valuable alternative water resources. Reverse osmosis (RO) membranes are the most promising candidate for drinking water production through desalination. Low recovery (the fraction of influent water that becomes product water) prevents widespread application of RO inland because of the high cost of waste disposal. The recovery of a brackish RO system is limited by sparingly soluble salts that become supersaturated and precipitate on the membrane surface. Precipitation is controlled through pH adjustment and antiscalant addition; however, at high salt supersaturation, antiscalant control is overcome and precipitation occurs. To further increase RO recovery and avoid precipitation, a three-stage process treated the waste stream (concentrate) of a brackish water RO system through antiscalant degradation, salt precipitation, and solid/liquid separation.

Ozone (O_3) and hydrogen peroxide (H_2O_2) were used to degrade antiscalants, pH elevation and base ($NaOH/NaHCO_3$) addition were used to precipitate sparingly soluble salts, and microfiltration (0.1 μm) was used to separate precipitated solids from the water.

Optimal parameters (pH, ozone dose, H_2O_2/O_3 ratio, antiscalant type and concentration, water composition) for antiscalant oxidation were determined. The influence of antiscalant type and concentration and pH was investigated for the precipitation and filtration stages. Results were obtained for particle size distribution, extent of precipitation, particle morphology, and particle composition. The effect of ozonation on precipitation and filtration was evaluated, with a comparison to two-stage treatment consisting of precipitation and filtration.

Antiscalant oxidation is controlled by bivalent cation coordination, while pH and ozone dose significantly affect the extent of oxidation. The addition of antiscalant prior to precipitation caused changes to particle size and morphology, and results varied with water composition and antiscalant type and concentration. Ozonation, even for small times such as one minute, prior to precipitation and filtration increased calcium precipitation and decomposed the antiscalant enough to remove the effect of the antiscalant on particle characteristics. During ozonation, antiscalants were not completely oxidized, but the partial oxidation products did not seem to affect precipitation. Ozonation also reduced the fouling of microfiltration membranes used for solid/liquid separation. Results indicated concentrate treatment can significantly increase the overall recovery of an RO system.

Table of Contents

List of Figures

List of Tables

Chapter 1: Introduction

BACKGROUND

Sources of fresh water in the U.S. are becoming increasingly scarce, particularly in the arid Southwest (Texas to California) and states, such as Florida, where a large percentage of resources are brackish or sea waters. The production of drinking water in the U.S. currently relies primarily on freshwater sources, but as the demand increases and sources are depleted, other sources, with new treatment technologies and treatment options, must be explored. The most promising method of drinking water production from non-traditional sources is desalination, the process of turning sea water or brackish water into fresh water. Desalination processes fall into two main categories, thermal processes or membrane processes. Thermal desalination (distillation) has been used for hundreds of years to produce fresh water, but large scale municipal drinking water distillation plants began to operate during the 1950's (Gleick, 2006). While thermal desalination has remained the primary technology of choice in the Middle East, membrane processes have rapidly developed since the 1960's (Loeb and Sourirajan, 1963) and now surpass thermal processes in new plant installations.

The two most common desalination membrane processes are reverse osmosis (RO) and electrodialysis (ED). With the invention of structured membranes that allow RO membranes to consist of a thin layer for the separation and a support layer for structural integrity, RO can operate at far lower pressures than earlier membranes and has become much cheaper than in previous years; as a result, reverse osmosis has essentially replaced ED as the method of choice for drinking water desalination.

The U.S. is just beginning to take advantage of the desalination process to aid in its drinking water production. Several desalination plants in California, Florida, and Texas are already in operation or will be in operation within the next 5 years. Most of these plants are located on the coast, where the salty waste water (concentrate) can be pumped back into the ocean.

PROBLEM STATEMENT

A central problem in the use of RO for desalination is that the recovery is limited; recovery is the fraction of influent water that becomes product (drinking) water. For reasons delineated below, recovery is virtually always less than 80%, meaning that the concentrate is always greater than 20% of the influent volume. The disposal of this high volume of waste can pose a problem even for coastal plants, but it will be considered unacceptable as desalination plants are built farther inland.

The research described in this dissertation was designed to develop a treatment system for the waste concentrate of the current type of RO facilities that would allow some of the concentrate to become product water, thereby improving the overall recovery. While often considered unnecessary for coastal systems, the auxiliary treatment could be economically viable for inland systems treating brackish water supplies.

With an RO system enhanced by concentrate treatment, inland facilities would use brackish waters that were once thought to be impossible to develop as water supplies but are now being considered as valuable resources. Reverse osmosis is the most likely treatment for such waters, but low recovery of RO systems prevents its widespread adoption; the huge volume of waste produced is generally unacceptable. Current inland disposal options include deep well injection, release to local water bodies, evaporation ponds, and enhanced evaporation. These methods can negatively affect local ecosystems

and resources, particularly freshwater sources such as surface waters and aquifers. In addition, these methods of concentrate disposal do not help to improve the product recovery; they are merely temporary solutions that will eventually ruin freshwater sources and create an even greater need for brackish water treatment and new disposal options.

Reverse osmosis systems for brackish water desalination are operated in a series-parallel arrangement, usually in three stages in which the concentrate from one stage becomes the influent to the next. The rejected ions build to higher concentrations in each stage, and the possibility of inorganic solid precipitation increases. For an RO system with a recovery of 80% and salt rejection between 95% and 99%, salt concentrations in the concentrate are nearly fives times that of the feed. When salt concentrations are pushed above saturation in a solution, seed crystals begin to form, and additional precipitation continues until the salt concentration is at or below its saturation point. When precipitates form during RO filtration, the solids can build up on the surface of the membrane, reducing water flux and often permanently fouling the membrane. This process of precipitate buildup is termed scaling. Scaling is further promoted by concentration polarization, the accumulation of excess ions in a thin layer next to the surface of the membrane. The most common precipitates involved in scaling are referred to as sparingly soluble salts, and include calcium carbonate (mostly in the form of calcite) and calcium sulfate (gypsum $CaSO_4*2H_2O$ and anhydrite $CaSO_4$) (Nicot and Chowdhury, 2005). Other problematic scales include barium sulfate, strontium sulfate, magnesium hydroxide, and ferric hydroxide.

Scaling, the irreversible accumulation of salt precipitates on a membrane, must be avoided because it causes product water flux decline and forces membrane replacement. In most cases, scaling is prevented by adding antiscalant compounds—complexing agents

that allow operation of the system under conditions in which precipitates would otherwise be formed. Without antiscalants, RO system recovery in brackish water applications is rarely more than 70%, and even with them, recovery is rarely more than 85 - 90%. In conventional water treatment systems, recovery approaches 99%. Unless recovery is improved, RO use will be limited to coastal areas, where waste stream disposal into the ocean is considered acceptable. Water shortages, of course, are far more severe in inland areas, so improving recovery in RO systems is essential.

OBJECTIVES

The broad objective of the research was to develop a novel side-stream system to increase recovery in RO preparation of drinking water. The treatment system takes concentrate from a conventional RO system, removes salts, and allows much of the liquid to be recovered; a schematic is shown in Figure 1. A conventional RO system is the first two membrane stages in the upper left of the figure. In the proposed system, the concentrate is treated to (I) deactivate the antiscalants, (II) encourage precipitation, and (III) perform a solid/liquid separation (*e.g.*, microfiltration). The resulting liquid stream is then sent to an additional RO unit to improve overall system recovery dramatically and reduce concentrate volume.

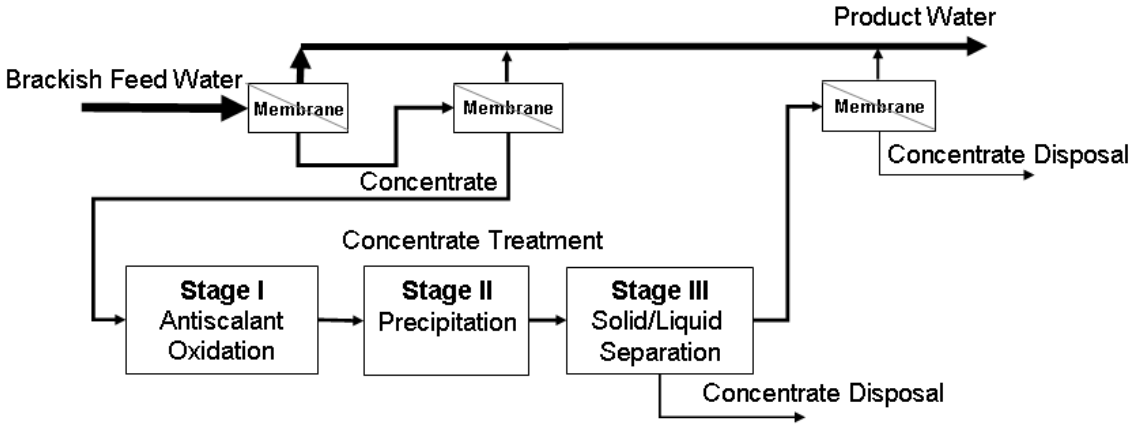

Figure 1. Proposed enhanced RO treatment system: Antiscalant degradation, salt precipitation, and solid/liquid separation.

The primary objectives of the experimental research were to:

1) determine the experimental parameters that control antiscalant oxidation by ozone (with or without hydrogen peroxide) and the optimal ranges of operation for these parameters in model RO concentrate solutions;
2) determine how antiscalants impact salt precipitation and solid/liquid separation by filtration;
3) determine how antiscalant oxidation impacts salt precipitation and filtration; and
4) evaluate the three-stage concentrate treatment process by quantifying the possible improvement in RO recovery.

APPROACH

The research objectives were primarily achieved through experimental investigation, with the aid of thermodynamic equilibrium software, which was used to predict salt precipitation, calculate activity coefficients, and calculate speciation distributions of antiscalant-cation complexes. Most of the experiments were performed

on a synthetic model brackish water, and a series of simplified synthetic water compositions were used to delineate the effect of specific water components on the three-stage treatment. Each stage of the concentrate treatment process was studied through batch experiments; ozone (O_3) (with and without hydrogen peroxide (H_2O_2)) was chosen as the oxidation system for Stage I, addition of sodium hydroxide (NaOH) and sodium bicarbonate ($NaHCO_3$) was used to precipitate salts (Stage II), and dead-end microfiltration (0.1 μm pore size) was used as the solid/liquid separation step (Stage III). The first stage was examined in detail to determine the oxidation pathway for ozonation of phosphonate antiscalants and the key parameters that affect oxidation. In addition, the effect of antiscalant oxidation on the precipitation and separation stages was examined by comparison to concentrate treatment consisting of only the precipitation and separation stages.

The three treatment stages were studied together using gaseous addition of ozone to the aqueous system. Ozonation parameters important to the precipitation and separation stages were varied, including the ozone dose (controlled by ozonation time), pH (of both the ozonation and precipitation stages), antiscalant type, and antiscalant concentration. The influence of antiscalants on salt precipitation was evaluated through a study of dissolved ions remaining in solution after precipitation, particle composition, particle size distributions, and particle morphology. Permeate flux data were compared to determine the influence of the parameters mentioned above on the microfiltration step.

Stage I was studied individually using an ozone stock solution (60 – 70 mg/L O_3), and an aqueous ozone aliquot was added to each batch experiment. While gaseous ozone addition was a more relevant experimental setup based on current practice in water treatment plants and ozone disinfection, using the ozone stock solution allowed small ozone doses and revealed relationships between antiscalant oxidation and parameters

such as pH, ratio of hydrogen peroxide to ozone (H_2O_2/O_3 mole/mole), cation type and cation concentration. Four antiscalants were used in experiments, including three phosphonate antiscalants and one polyacrylate blend polymer.

The subsequent chapters are organized as follows: Chapter 2 contains a literature review of desalination and reverse osmosis membranes, advanced oxidation processes, activity coefficient calculations, antiscalants, and precipitation; Chapter 3 details the materials and methods used for experimental work, while Chapters 4 through 8 are the five papers written on experimental results obtained. Chapters 4 and 5 present results on the effect of antiscalants on salt precipitation and microfiltration. Chapter 6 contains results on the ozonation of phosphonate antiscalants. Chapter 7 presents results on the effect of antiscalant oxidation on precipitation and separation, and Chapter 8 contains a pilot RO system study performed on a natural brackish water. Chapter 9 contains conclusions and recommendations for future work, and supplemental results are located in Appendices A through C.

SIGNIFICANCE

The overall result of the research is an intermediary process capable of dramatically decreasing the scaling potential of brackish RO concentrate; this type of concentrate treatment could increase overall RO recovery well beyond that currently possible in brackish water desalination. This treatment of antiscalant degradation, salt precipitation, and solid/liquid separation has the potential to shift inland desalination from a rarely used system to a widely applied solution where freshwater supplies are limited; this potential derives from the joint benefits of decreased costs and decreased environmental impact with the reduced volume of concentrate requiring disposal. The concentrate treatment process could also reduce costs and labor associated with membrane fouling and failing problems.

While other researchers are investigating new processes and improvements in RO systems, including possible intermediary options for RO membranes in series, this project fills an important niche that has not been studied. Most RO research has focused on areas such as novel membrane development and scaling issues, including the design and use of antiscalants, but the *deactivation* and *manipulation* of antiscalants off-line from the RO process has not been the emphasis of current or past relevant research to the best of our knowledge. In addition, the development of a complete side-stream process, such as that proposed in Figure 1, provides the process framework for incorporating the RO research of others and ultimately makes a significant and usable contribution to the field of desalination.

Furthermore, this research has resulted in a greater understanding of how phosphonate compounds are oxidized in an ozone system and what parameters affect phosphonate ozonation. In addition, the influence of antiscalants on salt precipitation and filtration has been studied in detail. Phosphonate compounds are used in many industries as scale inhibitors, and will continue to be a component of waste streams; successful waste stream treatment depends on a fundamental understanding of phosphonate chemistry. The research reported in this dissertation contributes to that understanding.

Chapter 2: Literature Review

DESALINATION AND REVERSE OSMOSIS MEMBRANES

The U.S. Geological Survey (Gleick, 1996) found that 96.5% of Earth's water is located in seas and oceans, and 1.7% of Earth's water is located in the ice caps. Of the remaining 1.8%, approximately 0.8% is considered to be fresh water, or water with a total dissolved solids (TDS) content of 1000 mg/L or less. The remaining percentage is made up of brackish water, slightly salty water found as surface water in estuaries and as groundwater in salty aquifers. Water shortages have plagued many communities, and humans have long searched for a solution to Earth's meager fresh water supplies. Thus, desalination is not a new concept; the idea of turning salt water into fresh water has been developed and used for centuries.

In the modern world, desalination first began to be developed for commercial use aboard ships. Distillation, the process of using a heat source to separate water from salt, was used to provide drinking water to ocean-bound ships to avoid the possibility of depleting onboard fresh water supplies (Seigal and Zelonis, 1995). Eventually distillation units were developed to provide make-up water for steam ship boilers; the U.S. began to develop distillation technology in the late 18^{th} century. The first countries to use desalination on a large scale for municipal drinking water production were in the Middle East. Seawater distillation plants were first developed in the 1950's, and in the 1960's, the first industrial desalination plant opened in Kuwait. In the following decade, membranes began to enter the desalination market, and over the past 30 years, RO membrane technology has improved dramatically to elevate RO as the primary choice for desalination facilities.

Today, there are approximately 15,000 desalination plants worldwide, and approximately 50% of those are RO plants (Frenkel, 2000). The Middle East holds approximately 50% of the world's production capacity (and 2.9% of the world's population), and in 2005, Israel opened the world's largest RO desalination plant, with a production capacity of 100 million m^3/yr (Sauvet-Goichon, 2007). In contrast, for many years, most regions in the U.S. did not have large water shortages. The first desalination pilot plant opened in 1961 in Freeport, TX, but desalination has not been widely implemented as a drinking water production strategy. Today, the U.S., with 4.6% of the world's population, has 17% of the world's desalination production capacity (Huntington, 2006; Wolff, 2006), and severe water shortages exist throughout the southern and southwestern states. RO has emerged as the leader in desalination, and it will be the key to increasing water supplies for drinking water production throughout the country. Outside of the Middle East, new RO desalination installations have been steadily increasing; in 2001, 51% of new installed desalination capacity used RO desalination, and in 2003, RO desalination accounted for 75% of new production capacity (Wolfe, 2005).

RO membranes are considered to be nonporous and lie at one extreme of commercially-available membranes. RO can reject the smallest contaminants, monovalent ions, while other membranes, including nanofiltration (NF), ultrafiltration (UF), and microfiltration (MF), remove larger compounds, bacteria, and particles. The range of each membrane type is displayed in Figure 2.

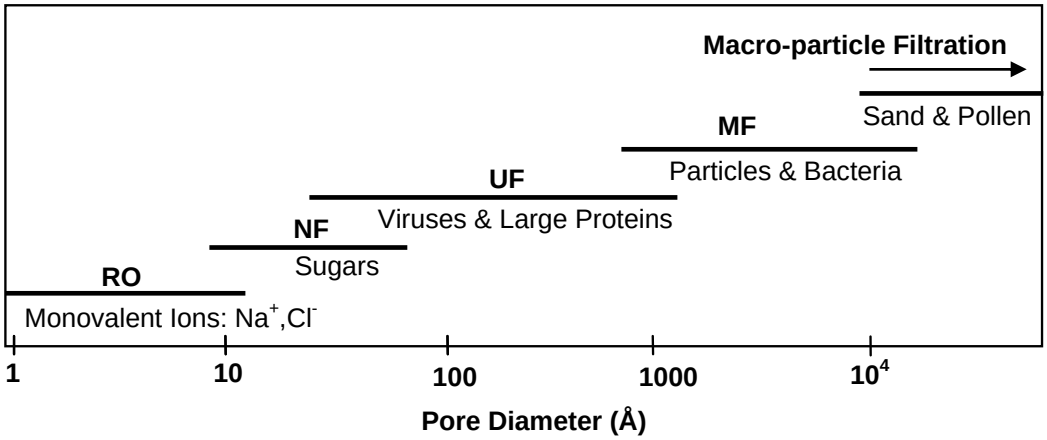

Figure 2. Range of nominal pore sizes for commercially available membranes (Perry and Green, 1997).

Membranes can be used in either dead-end (water flow perpendicular to the membrane surface) or crossflow (water flow parallel to the membrane surface) applications. RO membranes are typically operated in crossflow mode and are most commonly available as spiral wound modules, where the membrane sheets are wound around an inner tube that collects the concentrate (Baker, 2004). Most membranes allow filtration through pore flow, where the fluid is forced through the membrane by a positive hydrostatic pressure. The fluid flow depends upon the membrane porosity, the fraction of membrane volume that is void space and can contain liquid, and tortuosity, the distance a molecule must travel through the membrane divided by the thickness of the membrane. Fluid flux also occurs due to diffusion, and the relationship that describes transport due to pore flow and diffusion can be expressed as follows (Bird, et al., 2002):

$$N_{Ax} = \frac{\rho_A \kappa}{\mu} \frac{dp}{dx} - D_{AB} \frac{d\rho_A}{dx} \qquad (1)$$

where N_{Ax} is the mass flux in the x-direction (perpendicular to the membrane surface), ρ_A is the mass density, κ is the permeability, μ is the viscosity, dp/dx is the pressure gradient

in the x-direction, and D_{AB} is the binary diffusion coefficient. For MF and UF membranes, the diffusion term is negligible compared to the pressure term.

Transport through RO membranes, however, is controlled by diffusion, and no open channels exist for pore flow; the RO transport mechanism has been termed solution-diffusion (Lonsdale, et al., 1965; Merten, 1963; Paul, 1972; Paul, 2004; Wijmans and Baker, 1995). In the solution-diffusion model, water transport across an RO membrane occurs in three separate steps: absorption onto the membrane surface, diffusion through the thickness of the membrane, and desorption from the permeate surface of the membrane. Once a water molecule has absorbed onto the membrane surface, the water concentration gradient (of the water-membrane system) across the membrane causes the water molecules to diffuse down the concentration gradient to the permeate side of the membrane. The water molecule then desorbs from the membrane and becomes part of the bulk permeate. A complete development and explanation of the solution-diffusion model for transport through RO membranes can be found elsewhere (Lonsdale, et al., 1965; Paul, 2004). An RO membrane is operated by achieving a hydrostatic pressure greater than the osmotic pressure of the solution. The positive difference in pressure creates a chemical potential difference (concentration gradient) across the membrane that drives the liquid through the membrane against the natural direction of osmosis (the movement of water molecules from an area of high concentration to an area of low concentration), while the salts are retained and concentrated on the influent surface of the membrane. Some salt passage through the membrane does occur; salt passage for the same membrane increases with salt concentration and temperature. Mass transport through RO membranes can be described as follows:

$$N_A = L(\Delta p - \Delta \pi) \qquad (2)$$

where N_A is liquid (water) flux through the membrane, L is the permeability coefficient, Δp is the transmembrane pressure difference, and $\Delta\pi$ is the osmotic pressure difference between the influent and the product water (permeate). The osmotic pressure, π, depends on the solution concentration and the solution temperature. The relationship is described as follows:

$$\pi = CRT \tag{3}$$

where C is the ion concentration (molar units), R is the ideal gas constant, and T is the operating temperature.

The permeability coefficient, L, depends on characteristics of the membrane and is described by (Wijmans and Baker, 1995):

$$L = \frac{DSV}{RTl} \tag{4}$$

where D is the water diffusivity, S is the water solubility, V is the water molar volume, R is the ideal gas constant, T is the operating temperature, and l is the membrane thickness. This definition of L is based on the solution-diffusion model of water transport across a RO membrane (Bird, et al., 2002).

RO membrane performance can be measured by salt flux through the membrane, but it is more often measured by salt rejection. Salt flux is a function of salt concentration, and occurs from a region of high salt concentration to a region of low salt concentration. Salt flux is given by (Baker, 2004):

$$N_s = B\left(C_{feed} - C_{permeate}\right) \tag{5}$$

where N_s is the salt flux across the membrane, B is a constant (similar to L in the water flux equation) that depends on membrane characteristics, C_{feed} is the ion concentration in the feed solution, and $C_{permeate}$ is the ion concentrate in the permeate. B is described by:

$$B = \frac{D_s K_s}{l} \tag{6}$$

where D_s is the salt diffusivity through the membrane, K_s is the salt partition coefficient, and l is the membrane thickness.

Membrane salt rejection is a measure of overall membrane system performance, and membrane manufacturers typically state a specific salt rejection for each commercial membrane available. Salt rejection through a RO membrane (crossflow operation) is nominally given by:

$$R = \left(1 - \frac{C_{permeate}}{C_{feed}}\right) \times 100\% \tag{7}$$

where R is salt rejection, $C_{permeate}$ and C_{feed} are defined as in equation (5).

OXIDATION AND ADVANCED OXIDATION PROCESSES (AOPS)

Oxidation processes are used throughout environmental and chemical engineering applications and are powerful tools to control water composition and desired products. Specifically, in water and wastewater treatment, oxidation enables disinfection, control of unwanted tastes and odors, color removal, controlled precipitation and coagulation of inorganic contaminants, and destruction of toxic organic compounds. A variety of specific processes have been developed that cause oxidation by chemical, catalyzed, and electrolytic reactions. Traditional oxidation reactions include a relatively stable oxidant and one or more reactants. More recently, oxidants have been combined to form

advanced oxidation processes (AOPs). The commonality among AOPs is the production of the hydroxyl radical, *OH, which is a highly unstable molecule that reacts spontaneously with a large number of organic and inorganic compounds. Radicals are compounds with a single (unbalanced) electron in the orbital structure, a situation that makes them highly reactive and electrophilic. Hydroxyl radicals (or, in some cases, other radicals) accomplish much or all of the oxidation in AOPs. In particular, organic compounds previously thought to be highly recalcitrant to biological or chemical degradation have been successfully degraded with AOPs, either in an isolated process or in conjunction with additional biological/chemical treatment. AOPs have become a primary focus in water treatment, and results have shown a great potential for integration in conventional treatment systems.

A conventional oxidation-reduction (redox) reaction consists of two separate half reactions. When these two reactions are combined, the oxidant accepts electrons and is reduced, thereby oxidizing the other reactant involved. A generic half reaction appears as follows:

$$Ox + n_e e^- + n_H H^+ \leftrightarrow Red \qquad (8)$$

where n_e is the number of electrons, n_H is the number of hydrogen ions, *Ox* is the species form that accepts electrons to become reduced, and *Red* is the reduced form of the oxidant. Perhaps the simplest half reaction is that of hydrogen (H_2) and the hydrogen ion, H^+:

$$H^+ + e^- \leftrightarrow \frac{1}{2} H_2(g) \qquad (9)$$

For this, or any, half reaction, an equilibrium relationship can be written:

$$K = \frac{a_{H_2(g)}^{1/2}}{a_{H^+} a_{e^-}} \qquad (10)$$

where each *a* is the activity of that species, and *K* is the equilibrium constant. In this equilibrium expression, the presence of the electron activity presents a problem for calculations. In contrast to other ions in solution, electrons are unstable in aqueous solutions and the activity, a_{e^-}, cannot be measured. To circumvent this issue, the established convention dictates a_{e^-} be assigned a value of 1.0 in equation (10), when a_{H^+} and $a_{H2(g)}$ both equal 1.0 and the system is at equilibrium. Thus, the value of the equilibrium constant for the half reaction shown in equation (9) is 1.0, and equilibrium constants for all other half reactions can be calculated from this convention.

The a_{e^-} for a solution is calculated using the pH and hydrogen gas partial pressure, and the resulting value (like pH) is often displayed as the negative logarithm of the activity, or *pe*. Another convention in water chemistry is to define a standard equilibrium constant for a half reaction, written as a reduction (*e.g.,* equation (9)), for the transfer of one electron; the equilibrium constant for a half reaction written as such is pe^o. Pe^o replaces the notation "log K" in the equilibrium relationship, and the equation can be transformed:

$$K = \frac{a_{H_2(g)}^{1/2}}{a_{H^+} a_{e^-}} \Rightarrow -\log\left(a_{e^-}\right) = \log K - \log\left(\frac{a_{H_2}^{1/2}}{a_{H^+}}\right) \Rightarrow pe = pe^o - \log\left(\frac{a_{H_2}^{1/2}}{a_{H^+}}\right) \qquad (11)$$

Or, more generally:

$$K = \frac{a_{\mathrm{Re}\,d}}{a_{Ox} a_{e^-}^{n_e}} \Rightarrow pe = pe^o - \frac{1}{n_e}\log\left(\frac{a_{Red}}{a_{Ox}}\right) \qquad (12)$$

Many half reactions also transfer hydrogen ions as well as electrons, and a term is added to equation (12) to account for this additional component:

$$pe = pe^o - \frac{n_H}{n_e} pH - \frac{1}{n_e} \log\left(\frac{a_{Red}}{a_{Ox}}\right) \quad (13)$$

Values for K and pe^o have been tabulated and are readily available in most aquatic chemistry resources (Morel and Hering, 1993; Snoeyink and Jenkins, 1980; Stumm and Morgan, 1996).

Typical oxidation treatment processes include oxygen, chlorine, chloramines, chlorine dioxide, ozone, and potassium permanganate; ozone is the focus of this discussion as it is a component of AOPs of interest. Ozone, O_3, is an unstable molecule that readily decomposes and acts as a strong oxidant for many compounds (Acero and von Gunten, 2001). Ozone decomposition occurs through several reactions (Elliot and Mccracken, 1989; Sehested, et al., 1984; Staehelin and Hoigné, 1982):

$$O_3 + OH^- \rightarrow HO_2^- + O_2 \quad (14)$$

$$O_3 + HO_2^- \rightarrow {}^*OH + O_2^{*-} + O_2 \quad (15)$$

$$O_3 + O_2^{*-} \rightarrow O_3^{*-} + O_2 \quad (16)$$

with equations (15) and (16) having the higher rate constants of 2.8×10^6 $M^{-1}s^{-1}$ and 1.6×10^9 $M^{-1}s^{-1}$ as compared to the rate constant, 70 $M^{-1}s^{-1}$, for equation (14). Oxidation by ozone occurs both through reactions with the ozone molecule itself and with the hydroxyl radicals produced through decomposition (von Gunten, 2003). As ozone decomposes, the radical compounds produced react immediately with other reactants in solution; often the reactions are self-propagating and produce additional hydroxyl radicals. The decomposition of ozone is highly dependent on pH and increases as pH increases (Elovitz, et al., 2000), as well as being affected by the presence of other compounds in solution. Compounds such as natural organic matter (NOM), carbonate

(CO_3^{-2}), and bicarbonate (HCO_3^-) can scavenge ozone and can have a positive or negative effect on the treatment process.

Since ozone is unstable, it is typically produced (in gaseous form) as needed at the point of treatment within a facility, and either air or oxygen can be used as the feed gas. Ozone generators use an electrolytic cell to convert a percentage of the oxygen in the inflow to ozone; use of air typically produces a gas stream with 1-3 wt% ozone, while an oxygen feed produces a stream with 5-7 wt% ozone (Hoigné, 1998).

AOPs encompass a variety of methods and chemicals used to create hydroxyl radicals, but not all methods have the potential to be incorporated into existing or new treatment plants even though they may be successful on a small scale in the laboratory. The overall cost of using an AOP in a treatment process is generally similar to well established technologies (Munter, et al., 2001). The AOPs reviewed include: ozonation at elevated pH (>8.5), ozone and hydrogen peroxide (H_2O_2), ozone and a catalyst, the Fenton system (H_2O_2/Fe^{2+}), ozone and ultraviolet radiation (UV), H_2O_2 and UV, ozone, H_2O_2, and UV, and photo-Fenton systems.

Ozone at elevated pH is considered an AOP because as the pH increases above 8.0, its decomposition in water increases, and the rate of oxidative attack by *OH molecules is much greater than that of ozone molecules. The major cost would be electricity needed for ozone generation, however, the process is not a good choice for drinking water because of the elevated pH. The O_3/H_2O_2 system, however, is operated at a lower pH range (7-8), and has been shown to achieve improved contaminant degradation in comparison to treatment with ozone alone (Fahmi, et al., 2003; Ito, et al., 1998; Munter, et al., 2001). Fahmi showed that O_3/H_2O_2, along with biological treatment, can reduce dissolved organic carbon in secondary waste water effluent by more than 70%, and Munter reported that pesticides in river water were better degraded

by O_3/H_2O_2 than by ozone alone. The O_3/H_2O_2 system is an accepted treatment in water and wastewater facilities and has been used for approximately 10 years in the U.S. to treat trichloroethylene and tetrachloroethylene in ground water. Such a system could potentially be incorporated into existing ozone treatment units or added onto a conventional treatment system. Disadvantages include scavenger compounds, such as carbonate, that reduce *OH efficiency, poor knowledge of oxidation product toxicity, and the production of dissolved organic carbon (which supports biological growth) (Suty, et al., 2004).

Metal oxides and metal ions, such as Fe_2O_3, MnO_2, Al_2O_3, TiO_2, Fe^{2+} and Mn^{2+}, have been used as catalysts with ozone to accelerate *OH production (Munter, et al., 2001). Addition of catalyst is more effective than ozone alone, and the system has been shown to degrade such compounds as chlorobenzenes, succinic acid, salicylic acid, and oxalic acid. The primary disadvantage is the unlikely feasibility of full scale implementation.

The Fenton system of H_2O_2 and Fe^{2+} and Fenton-like systems, such as Fe^{3+} added to an H_2O_2/UV system, have been the focus of much research, but industry has shown little interest. Ferrous iron is not typically a component of drinking water sources because it is easily oxidized in the presence of oxygen to ferric iron (Fe^{3+}). However, ferric iron acts as a catalyst for H_2O_2 decomposition, producing ferrous iron. Ferrous iron is then available to react with H_2O_2 to form hydroxyl radicals. The reaction scheme is as follows (Munter, et al., 2001):

$$Fe^{3+} + H_2O_2 \leftrightarrow H^+FeOOH^{2+} \quad (17)$$

$$FeOOH^{2+} \rightarrow HO_2^* + Fe^{2+} \quad (18)$$

$$Fe^{2+} + H_2O_2 \rightarrow Fe^{3+} + OH^- + {}^*OH \quad (19)$$

Successful contaminant degradation using the Fenton process typically requires molar ratios of H_2O_2 to contaminant of 2:1 to 10:1, and the available iron must be in excess of the H_2O_2 (Bowers, et al., 1989; Sedlak and Andren, 1991; Watts, et al., 1993). From drinking water data collected thus far, ferric iron concentrations range from 0.01 mg/L to 1.9 mg/L, which corresponds approximately to a range of 0.05 mg/L – 9.5 mg/L ferric iron in an RO feed (assuming 80% recovery). Comparatively, a relatively low antiscalant (ATMP, Figure 3) dose of 4 mg/L in the RO feed would require 14 mg/L ferrous iron, assuming a H_2O_2 to contaminant molar ratio of 2:1 and a ferrous iron to H_2O_2 molar ratio of 2.5:1. Therefore, the iron naturally present in RO feed water is at too low a concentration to serve as the sole iron source in the Fenton process. A salt, such as ferrous sulfate ($FeSO_4$), is often used to dose iron (Watts, et al., 1993).

Fenton systems require a low pH and the addition of iron, and produce a waste sludge of ferric hydroxide (FeOH) precipitate. Photo- or electro-assisted Fenton systems, as well as the Fe(III)-H_2O_2 system, do not produce the waste sludge, but require equipment setups unlikely to be used at full scale. Only one research group has attempted to degrade antiscalants with AOPs, and they used the electro-Fenton system, where the ferric iron was electrogenerated from a small sheet of iron metal (Yang, et al., 2004). However, the strict pH control required and additional waste product make these systems an improbable candidate for drinking water treatment.

The AOPs involving UV (with O_3, H_2O_2, or both) can degrade chemicals as effectively as the O_3/H_2O_2 system, but the UV processes require additional energy input and equipment (UV lamps and process modifications to include UV treatment). The key disadvantage to the UV processes is: more energy is required, than when the H_2O_2/O_3 system is used, to produce the same quantity of *OH molecules. The UV/O_3 system produces H_2O_2, which then degrades to *OH; since H_2O_2 is a relatively inexpensive

chemical compared to the cost of operating a UV lamp, this system achieves the same result as the H_2O_2/O_3 system at a much higher energy expense. The H_2O_2/UV system requires more energy and produces less *OH than O_3/UV; in addition, H_2O_2 absorbs UV light and reduces the system effectiveness.

Among the AOPs described above, the O_3/H_2O_2 system appears to be the most efficient and inexpensive process for treating micro-pollutants, chemicals that are present in low concentrations, in drinking water. Each system has advantages and disadvantages, and the water to be treated and system requirements dictate the choice of AOP. For this project, the O_3/H_2O_2 system was chosen as the best oxidation treatment option. A summary of possible AOPs is shown in Table 1.

Table 1. Advanced oxidation processes available for antiscalant degradation.

AOP	Advantages	Disadvantages
O_3 at elevated pH	O_3 decomposition increases No chemical additions	High pH Electricity for O_3 generation
O_3/H_2O_2	More *OH for reaction H_2O_2 inexpensive O_3 already accepted as a treatment option	Scavengers reduce efficiency Electricity for O_3 generation By-product toxicity
O_3 + catalyst	More effective than O_3 Variety of catalyst choices	Additional metals in system Scale-up issues
Fenton systems	Fe is abundant and nontoxic Shown to degrade antiscalants	Low pH required High Fe^{2+} concentration FeOH sludge produced
UV/O_3, UV/H_2O_2, $UV/O_3/H_2O_2$	UV already used in treatment processes As effective as O_3/H_2O_2	Additional power requirements UV difficult to use in water systems H_2O_2 absorbs UV light

DETERMINATION OF ACTIVITY COEFFICIENTS

As ionic strength increases, activity coefficients first decrease, and the concentrations of ions appear thermodynamically to be less than they actually are. Two phenomena occur that cause this effect: electrostatic interactions and ion complexing. When ions dissolve in water, water molecules surround each ion, and prevent ions from interacting and precipitating. When ionic strength increases, additional oppositely-charged ions surround each ion, increasing the electrostatic shielding and further preventing precipitation. In addition to electrostatic interactions, ions can form new

complexes, or ion pairs, through interactions where the ions are separated by only one layer of water molecules. These complexes are less likely to precipitate, and they also effectively reduce the apparent concentration of the salt.

The activity of a species, a_i, is often written as $\{I\}$, and is the product of the activity coefficient, γ_i, and the species molar concentration, *[I]*:

$$a_i = \{I\} = \gamma_i [I] \tag{20}$$

To obtain the activity of an ion in solution, the activity coefficient must be calculated, and there are both physical and chemical models that have been empirically derived to describe the change in activity coefficient with change in solution composition. All models use ionic strength, I, as a parameter:

$$I = \frac{1}{2} \sum_i \left(C_i Z_i^2 \right) \tag{21}$$

Where C_i is the concentration of I (moles/kg) and Z_i is the charge of i. Calculations are often done with C_i in moles/L (M) because the density of water is 1000 kg/m^3, and changes in density account for less than 1% change in activity coefficient values.

For dilute solutions (ionic strength less than 1x10^{-4} M), the ions can be assumed to behave ideally, and all activity coefficients have a value of approximately 1. As the ionic strength increases, ion activity coefficients decrease, and this decrease is more dramatic for ions with greater valences. For rigorous calculations, the activity coefficients may be calculated, and the Debye-Huckel equation is valid for I less than 0.1 M (Pytkowicz, 1979; Snoeyink and Jenkins, 1980):

$$\log(\gamma_i) = -A_{DH} Z_i^2 \left(\frac{I^{1/2}}{1 + a_{DH} B_{DH} I^{1/2}} \right)$$
$$A_{DH} = 1.82x10^6 (\varepsilon T)^{-3/2} \quad (22)$$
$$B_{DH} = 50.3(\varepsilon T)^{-1/2}$$

where A_{DH} and B_{DH} are temperature-dependent constants, ε is the dielectric constant of water, a_{DH} is the ionic size parameter, and all other variables are defined as above.

Most RO concentrate solutions have ion strengths of greater than 0.1 M, and it is necessary to account for non-ideality. The Davies equation may be used for an ionic strength of less than 0.5 M, and the Pitzer equations are useful for even higher ionic strength solutions (Pitzer, 1991). The Davies equation is as follows:

$$\log(\gamma_i) = -A_{DH} Z_i^2 \left(\frac{I^{1/2}}{1 + I^{1/2}} - 0.2I \right) \quad (23)$$

The Pitzer equation was developed using the Debye-Huckel equation (22) and adding on terms for ion-ion interactions. The Pitzer terms relevant to this project are (Pitzer, 1991):

$$\ln(\gamma_M) = z_M^2 F + \sum_a m_a (2B_{Ma} + ZC_{Ma}) + |z_M| \sum_c \sum_a m_c m_a C_{ca} +$$
$$\sum_c m_c \left(2\Phi_{Mc} + \sum_a m_a \Psi_{Mca} \right) + \sum_{a<} \sum_{a'} m_a m_{a'} \Psi_{Maa'} \quad (24)$$

with:

$$F = -A_\phi \left[\frac{I^{1/2}}{1 + bI^{1/2}} + \frac{2}{b} \ln(1 + bI^{1/2}) \right] + \sum_c \sum_a m_c m_a B'_{ca} +$$
$$\sum_{c<} \sum_{c'} m_c m_{c'} \Phi'_{cc'} + \sum_{a<} \sum_{a'} m_a m_{a'} \Phi'_{aa'} \quad (25)$$

where A_Φ, b, B_{Ma}, Z, C_{Ma}, B'_{ca}, and C_{ca} are constants dependent on temperature, ionic strength, and ion charge, γ_M denotes the activity coefficient of cation M, $m_c/m_{c'}$ and $m_a/m_{a'}$ denote molar concentrations of cations and anions, respectively, and subscripts c and a denote all other cations and anions, respectively, in solution. The variable Φ denotes a constant that describes pairwise interactions, and the variable Ψ denotes a constant that describes triplet interactions. A similar set of equations, (24) and (25), can be written for anion X (Pitzer, 1991). Additional terms can be added to equation (24) when significant neutral species are present, and the full equation can be found in Pitzer.

The general behavior of an ion, with increasing ionic strength, is first a parabolic decrease in activity coefficient and then a parabolic increase, so that γ_i reaches a minimum value. The Pitzer model is the most complex physical model of ion activity, and takes into account pairwise and triplet interactions between ions of like charge and ions of opposite charge. The empirical equation stems from Young's Rules, which describe the effects of non-ideal mixing on the excess free energy, and thus on the relative chemical potential of each solution component.

Models, such as the Pitzer model, express activity coefficients as either mean-ion or total single-ion values (Pytkowicz, 1979). Mean-ion activity coefficients can be used in single salt solutions, but the total single-ion coefficients were more appropriate to the proposed project because all solutions were mixtures of several different ion pairs.

ANTISCALANT DEGRADATION: SELECTION OF ANTISCALANTS AND AOP

Two common classes of antiscalants are used in drinking water RO applications. Both are synthetic organic polymers, with one based on phosphonates alone and the other based on acrylic acid with or without blending with phosphonates. The defining characteristic of phosphonates is a phosphorus-carbon (P-C) bond, but the antiscalants

also have at least one fully-substituted amino group (nitrogen bonded to three carbons). Several commercial products are available, with their differences designed to target specific potential scaling compounds (*e.g.,* calcium carbonate, calcium sulfate, several metal silicates, and strontium and barium salts). The P-C bonds of phosphonates are considerably more difficult to degrade (either chemically or biologically) than the phosphorus-oxygen bonds (P-O) of traditional phosphate antiscalants. Some research (Hayes, et al., 2000; Krzysko-Lupicka, et al., 1997) has indicated that phosphonates are biodegradable by some microorganisms, including some halophilic (salt-loving) bacteria, but little research has investigated chemical oxidation of these compounds.

In a review of the appropriate literature, only one research group was found to have published an article specifically on using an oxidation process to degrade antiscalant compounds (Yang, et al., 2004). Yang *et al*. used the Fenton process (Munter, et al., 2001), an electrochemical oxidation process with iron (Fe^{2+}) and H_2O_2, to degrade antiscalants. This process was successful in degrading antiscalants but would not be easily applied in municipal drinking water treatment systems.

While the Fenton process is difficult to operate at full-scale, ozone and the combination of ozone and hydrogen peroxide (O_3/H_2O_2, often referred to as peroxone) have both been shown to successfully degrade recalcitrant compounds in both drinking water and waste water and could more easily be integrated into treatment systems (Fahmi, et al., 2003; Ikehata and El-Din, 2004; Ledakowicz and Solecka, 2001). It has also been shown that both P-C and C-N bonds of compounds similar in structure to phosphonate antiscalants are susceptible to oxidative attack by hydroxyl radical (*OH), the principal product when ozone and H_2O_2 react (Frost, et al., 1987; Shadyro, et al., 2003). Because this previous research suggests that the peroxone process can be

expected to degrade phosphonate antiscalant molecules, it has been chosen for the proposed research on antiscalant degradation.

Other researchers have begun to explore a variety of topics aimed at the overall improvement and understanding of aspects of the desalination process, such as water flow, scale formation, membrane use, and water chemistry (Bonné, et al., 2000; Kim and Hoek, 2005; Lee, et al., 2003). In particular, the focus on increased product recovery has motivated new approaches to modifying the RO process. Pretreatment and interstage treatment options including non-thermal precipitation have been investigated (Almulla, et al., 2002; Gabelich, et al., 2004; Gilron, et al., 2005; Mickley, 2004; Rahardianto, et al., 2007; Williams and Cohen, 2004; Williams, et al., 2002). In addition, characterization of mineral scale formation has become critical to progress in RO recovery. Researchers are studying inorganic scales of different types that are problematic during RO operation; these compounds include calcium carbonate, calcium sulfate, barium sulfate, silicates, and strontium sulfate. The choice of compounds to study depends on the research focus; for example, water sources used for drinking water in Texas and New Mexico have high silica content, and many silicate precipitates can form (Pacheco, 2005), while drainage waters in southern California have the potential to precipitate calcium and barium salts (Rahardianto, et al., 2008). In many cases, antiscalants are used in bench scale or pilot plant operations as a component required in full-scale facilities, but the compounds are not often considered directly in the research. Different types of antiscalant compounds are used in experiments that consider issues such as membrane fouling, inception of salt precipitation and scale formation, but they are rarely studied beyond the point of varying the type of compound to obtain differences in membrane performance.

Several examples of typical antiscalants used in RO applications are shown in Figure 3. These compounds were chosen specifically for their different scale inhibition

abilities; for example, DQ2054 is particularly successful in preventing calcium sulfate ($CaSO_4$) precipitation, while DQ2006 is used when calcium carbonate ($CaCO_3$) is the major potential precipitate (Dequest, 2006; Luu, 1994). Both of these salts are considered to be sparingly soluble and they are often found, even in fresh waters, at natural concentrations above their solubility limits. As a result, these calcium salts often become the limiting factor for increased recovery.

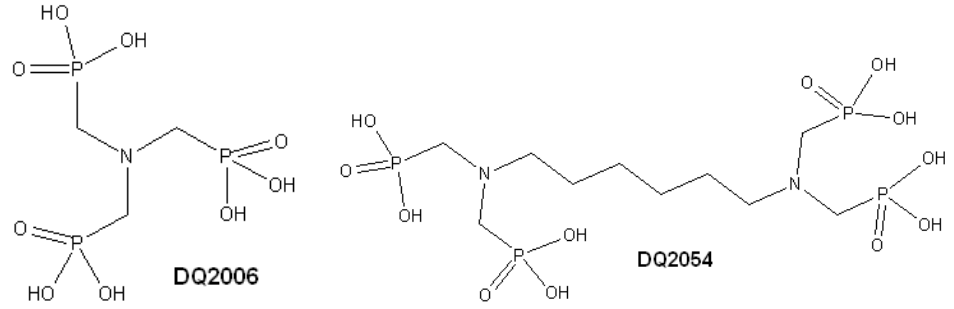

Figure 3. Examples of phosphonate antiscalant compounds.

The initial focus on calcium salts resulted from a review of literature and typical water compositions in water-short regions of the U.S.; calcium salts are some of the most troublesome compounds for desalination (Lee, et al., 2003; Mickley, 2001; Nicot and Chowdhury, 2005). For example, in some areas of Texas, water sources are already at the solubility limit for calcium carbonate, and water sources in California have high sulfate concentrations, resulting in calcium sulfate precipitation. These two compounds seem to be of importance in most regions attempting desalination and are typically the most common scales to form. Two other compounds of interest are barium sulfate and strontium sulfate; barium sulfate is highly insoluble and strontium sulfate is only slightly more soluble. It is also possible for barium and strontium to coprecipitate with calcium.

If a phosphonate antiscalant is completely oxidized by ozone or peroxone, the carbon atoms would be released as carbon dioxide (CO_2), the phosphorus atoms as orthophosphate (H_3PO_4), and the nitrogen atoms as nitrate, (NO_3^-). All three of these noted products are, of course, acid/base species with conjugates, so referring to the products in each case as a single species is simply shorthand. Ozonation or peroxone treatment typically causes a portion of the organic compounds to be completely oxidized, but partial oxidation products are also formed (Klinger, et al., 1998; Nowack and Stone, 2000; von Gunten, 2003).

During radical oxidation of aliphatic amines, ammonia is initially formed; an *OH causes the addition of an oxygen atom to the carbon atom adjacent to the nitrogen, and the bond between the nitrogen and carbon atom is broken (Shadyro, et al., 2003). A hydrogen atom replaces the previous C-N bond, and eventually the fully substituted nitrogen atoms shown in Figure 3 are reduced to ammonia. Ammonia is not easily oxidized by ozone or *OH molecules (at low pH) but may be oxidized to nitrate under conditions of excessive ozone or by radicals at pH values greater than 8 (von Gunten, 2003). Previous research has shown that ammonia has a half-life of 96 hours at pH 7 with an ozone concentration of 1 mg/L (Hoigné, et al., 1985).

Two pathways have been proposed for C-N and C-P bond cleavage (Frost, et al., 1987; Shadyro, et al., 2003). In the first case, the *OH removes a hydrogen atom from the amino group and eventually removes the amino group, forming an aldehyde:

$$CH_3CH_2NH_2 \xrightarrow{*OH} CH_3CH_2\overset{*}{N}H \rightarrow CH_3CHNH \xrightarrow{H_2O} CH_3CHO + NH_3 \quad (26)$$

The aldehyde group can continue to be oxidized to a carboxylic acid. If the aldehyde is methanal (HCHO), the compound will be oxidized further to water and $CO_{2(g)}$. During

C-P bond cleavage, the *OH separates the phosphate group from the organic carbon atom, forming inorganic orthophosphate and a methyl group:

$$R - CH_2PO_3H_2 \xrightarrow{*OH} R - CH_3 + H_3PO_4 \quad (27)$$

Many other molecules can be oxidized by either ozone or hydroxyl radicals, and these reactions have the potential to significantly reduce the oxidative capacity of the peroxone system. A system of reactions has been proposed for ozone decomposition in the presence of H_2O_2 (Staehelin and Hoigné, 1985; Tomiyasu, et al., 1985). In this system, ozone combines with H_2O_2 to produce hydroxyl radicals (*OH), the molecules that oxidatively attack many different compounds. Without H_2O_2, ozone spontaneously reacts with water molecules and self-decompose into *OH, but the addition of H_2O_2 greatly increases the decomposition process. As ozone decomposes, these *OH molecules begin a self perpetuating cycle of radical-based oxidative attack.

The decomposition of ozone and production of hydroxyl radicals can be greatly affected by variation of experimental parameters and water composition. Both temperature and pH can affect the rate of ozone decomposition; as temperature increases, ozone decomposition increases, and as pH increases (within the range of 6 – 9), ozone decomposition also increases (Elovitz, et al., 2000). Different components in the water, such as the carbonate system (bicarbonate, HCO_3^- and carbonate, CO_3^{2-}) and natural organic matter (NOM), also affect ozone decomposition.

Bicarbonate, carbonate, and NOM are examples of *OH scavengers, defined as any molecule that reacts with *OH, preventing the radical from oxidatively attacking other compounds (Acero and von Gunten, 2000). An *OH scavenger can either combine with *OH, effectively removing it from the oxidative cycle, or an *OH scavenger can

combine with *OH to produce superoxide, O_2^{*-}, which continues the ozone decomposition process. These scavengers are called inhibitors and promoters, respectively. Bicarbonate, carbonate, and NOM all act as inhibitors to ozone decomposition. However, when H_2O_2 is added into the system, both carbonate compounds become promoters instead of inhibitors. When bicarbonate or carbonate combines with an *OH molecule, $CO_3{}^{*-}$ is formed. This molecule then reacts with H_2O_2 to produce CO_3^{2-} and O_2^{*-}, thus perpetuating the ozone decomposition cycle. These reactions and the spontaneous decomposition reactions of ozone are shown in Figure 4.

The total carbonate and NOM concentrations and the pH can increase or decrease the oxidation capacity of the *OH in solution. Acero and von Gunten (2000) define oxidation capacity as the relative disappearance of a probe compound that only reacts with *OH. The reaction of the probe compound with *OH is used to determine the amount of *OH obtained through O_3 decomposition and the lifetime of *OH molecules in water (Acero and von Gunten, 2000). Two competing processes affect *OH effectiveness. First, carbonate and bicarbonate molecules scavenge H_2O_2 molecules and reduce the possibility of *OH reacting with target reactants; second, the scavenging process mentioned actually increases the decomposition of O_3 into *OH (Acero and von Gunten, 2000). Carbonate and bicarbonate concentrations affect the consumption of H_2O_2, but the *OH oxidation capacity depends only on the total scavenging rate, not on the proportion of H_2O_2 that reacts with carbonate and bicarbonate. Therefore, an increase in the overall scavenging rate decreases the *OH oxidation capacity, but an increase in the fractional contribution of carbonate and bicarbonate to the overall scavenging rate (with the overall rate remaining constant) increases the *OH oxidation capacity.

In waters where the contribution of the carbonate system on *OH scavenging is large, compared to the contribution of NOM (NOM concentrations less than 1 mg/L), the

rate of target pollutant oxidation by *OH can increase significantly. The rate of ozone decomposition also increases, and the ozone oxidation capacity decreases. Acero and von Gunten (2000) showed that the *OH oxidation capacity was reduced from 73% to 26% when the bicarbonate concentration was increased from 0.002 M to 0.1 M at pH 7, thus increasing the overall scavenging rate. The researchers also showed that, for a constant overall scavenging rate, the consumption of the *OH probe compound was faster when bicarbonate was the dominant scavenger (as compared to tert-butanol, an inhibitor); this result indicates a higher *OH concentration during O_3 decomposition and increased degradation of target pollutants. Furthermore, for waters with a high concentration of NOM, ozonation alone is considered to be an advanced oxidation process (Acero and von Gunten, 2001; Buffle, et al., 2006a); ozone molecules react directly with specific moieties of NOM, including double bonds, aromatic systems, amines, and sulfides, producing radicals (von Gunten, 2003), and the addition of hydrogen peroxide does not significantly increase radical production or oxidation (Buffle, et al., 2006a).

The competing effects of scavenging and decomposition can be managed by adjusting the operating pH and the ratio of H_2O_2 concentration to O_3 concentration in the system. In waters with high total carbonate concentrations, the optimal operating pH may decrease because the reaction of CO_3^{2-} with *OH (3.9×10^8 M^{-1} s^{-1}) is faster than that of HCO_3^- with *OH (8.5×10^6 M^{-1} s^{-1}). Yet in waters with increased NOM concentrations, the optimal pH may increase to take advantage of the faster reaction rate of CO_3^{2-} and shift the relative contributions of NOM and carbonate to scavenging. Since O_3 decomposition depends on the H_2O_2 concentration in solution (because of the reaction between O_3 and HO_2^-), the optimal $[H_2O_2]$ also varies with total carbonate concentration. Acero and von Gunten (2000) found the optimal ratio, $[H_2O_2]/[O_3]$, to be 0.72 for a

bicarbonate concentration of 0.1 M, and the optimal ratio value decreased to 0.1 or less for low bicarbonate concentrations.

Thus, the peroxone process is a powerful oxidative tool for molecular degradation, and creates a cyclic production of *OH molecules. The process is promoted by the most important system of molecules found in natural waters, the carbonate system, and carbonate and pH must be taken into account during process optimization.

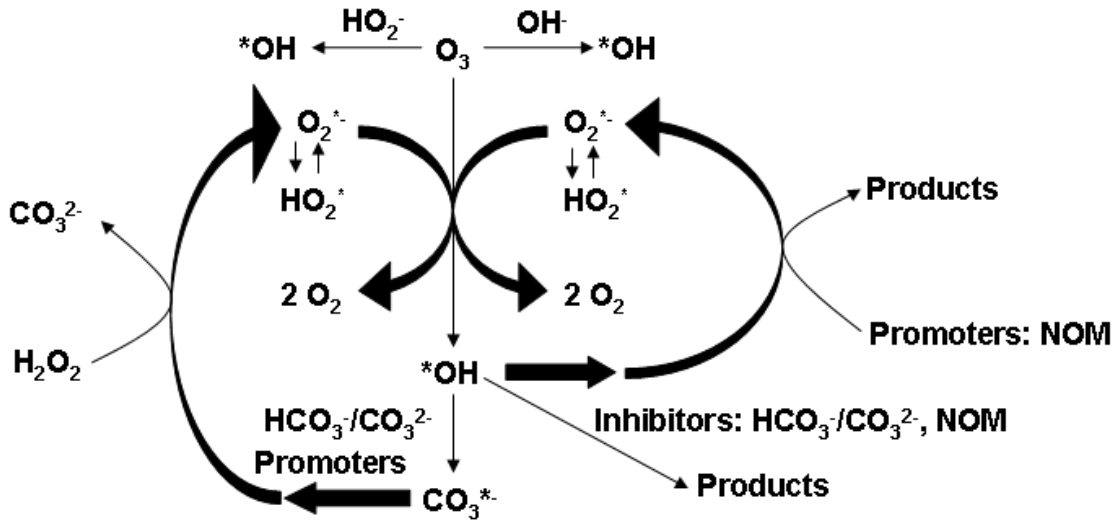

Figure 4. Depiction of ozone decomposition in water and effects of inhibitors and promotors. Adapted from Figure 1 of Acero and von Gunten (2000).

PRECIPITATION

After degradation of the antiscalant compounds in the concentrate of RO systems, the ionic strength of the solution is be high and the potential for a wide variety of compounds to precipitate is present. The equilibrium relationship between a dissolved salt and its corresponding precipitate is commonly called the solubility product, or K_{so}. K_{so} describes the general equation:

$$A_z B_{y(S)} \leftrightarrow zA^{y+} + yB^{z-} \tag{28}$$

where A_zB_y is the solid precipitate of cation A^{y+} and anion B^{z-}. The corresponding equilibrium equation is (Snoeyink and Jenkins, 1980):

$$K_{so} = \frac{\{A^{y+}\}^z \{B^{z-}\}^y}{\{A_z B_{y(S)}\}} \tag{29}$$

where the ions and precipitate are given as activities. For an ideal solution, calculations with ion concentrations are sufficient, but non-ideal solutions require calculations using activity. The concentration or activity of the solid phase is taken to be 1.0. The activity coefficients can be calculated with the Pitzer equation, as explained above, and K_{so} can be modified (Snoeyink and Jenkins, 1980) to give the apparent (concentration-based) equilibrium constant ${}^cK_{so}$:

$${}^cK_{so} = \left[A^{y+}\right]^z \left[B^{z-}\right]^y = \frac{K_{so}}{\left(\gamma_{A^{y+}}\right)^z \left(\gamma_{B^{z-}}\right)^y} \tag{30}$$

where γ_{Ay+} and γ_{Bz-} are activity coefficients of cation *A* and anion *B*.

An equilibrium equation like (28) can be written for the speciation of each acid-base pair in solution. The waters tested had the carbonate system as the natural buffering system, and the speciation can particularly affect calcium precipitates. Carbonate speciation also affects sulfate and magnesium because these two metals often co-precipitate with calcium, forming solid solutions where solid activities are not equal to one (Falini, et al., 2009; Kralj, et al., 2004; Loste, et al., 2003; Meldrum and Hyde, 2001; Nicot and Chowdhury, 2005). The carbonate speciation is dependent on the partial pressure of $CO_{2(g)}$ in the local atmosphere and the pH of the solution. The chemical equations are as follows:

$$CO_{2(g)} \leftrightarrow H_2CO_3^* \tag{31}$$

$$H_2CO_3^* \leftrightarrow H^+ + HCO_3^- \tag{32}$$

$$HCO_3^- \leftrightarrow H^+ + CO_3^{2-} \tag{33}$$

where $H_2CO_3^*$ denotes dissolved $CO_{2(g)}$ in solution in its acidic form. In a brackish water RO concentrate, the total carbonate concentration is expected to be greater than that dictated by the partial pressure of $CO_{2(g)}$ in air, and equilibrium would not be achieved during a typical RO desalination process; therefore, the carbonate system can be considered to be a closed system, and the pH primarily controls carbonate speciation. The corresponding equilibrium equations are:

$${}^cK_H = \frac{[H_2CO_3^*]}{pCO_2} = \frac{K_H}{\gamma_{H2CO3*}} \tag{34}$$

$${}^cK_{a1} = \frac{[H^+][HCO_3^-]}{[H_2CO_3^*]} = \frac{K_{a1}\gamma_{H2CO3*}}{\gamma_{H+}\gamma_{HCO3-}} \tag{35}$$

$${}^cK_{a2} = \frac{[H^+][CO_3^{2-}]}{[HCO_3^-]} = \frac{K_{a2}\gamma_{HCO3-}}{\gamma_{H+}\gamma_{CO3^{2-}}} \tag{36}$$

Where *[A]* denotes a component concentration (mol/L), γ_i denotes an activity coefficient, and ${}^cK_i$ denotes an equilibrium constant adjusted for non-ideal solution behavior. These equations, along with a carbonate mass balance and the pH, can be used to calculate the concentration of each carbonate system species:

$$C_{T,CO3} = [H_2CO_3^*] + [HCO_3^-] + [CO_3^{2-}] \tag{37}$$

$$[H_2CO_3^*] = C_{T,CO3}\left[1 + \frac{{}^cK_{a1}}{[H^+]} + \frac{{}^cK_{a1}\,{}^cK_{a2}}{[H^+]^2}\right]^{-1} \tag{38}$$

$$[HCO_3^-] = C_{T,CO3}\left[\frac{[H^+]}{{}^cK_{a1}} + 1 + \frac{{}^cK_{a2}}{[H^+]}\right]^{-1} \tag{39}$$

$$\left[CO_3^{2-}\right] = C_{T,CO3}\left[1 + \frac{\left[H^+\right]}{{}^cK_{a1}} + \frac{\left[H^+\right]^2}{{}^cK_{a1}\,{}^cK_{a2}}\right]^{-1} \qquad (40)$$

where C_{TCO3} is total carbonate and $[H^+]$ is hydrogen ion concentration (mol/L). Equations (37) – (40) can be used to create a speciation graph, shown in Figure 5, for the carbonate acid-base system. The system shown is specific to the water composition used for synthetic RO concentrates in this research.

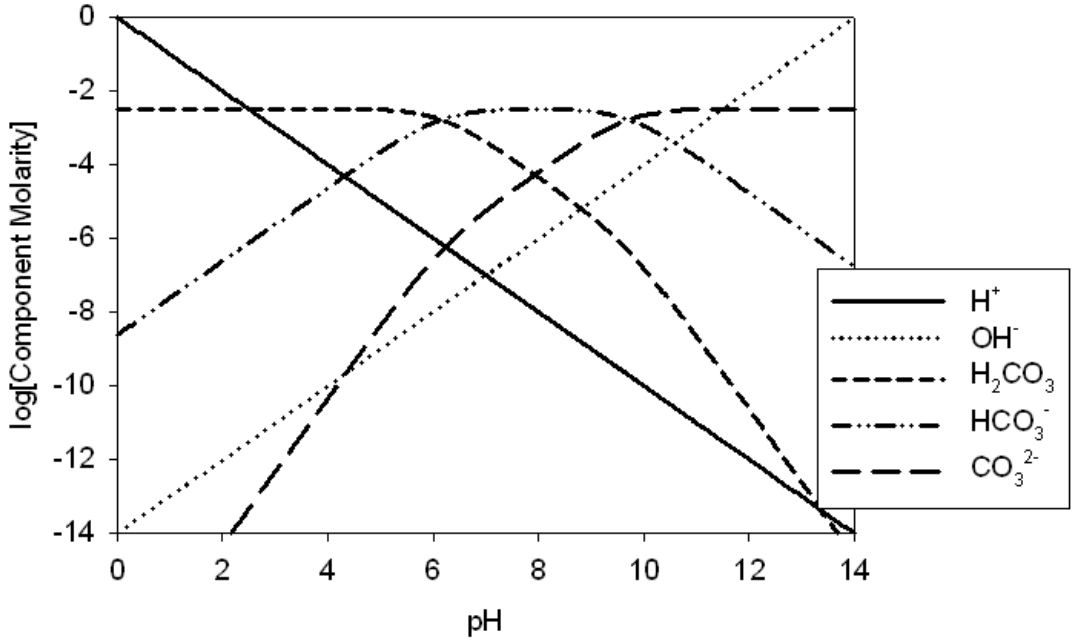

Figure 5. Speciation of the carbonate system, $C_{TCO3} = 3.23\text{x}10^{-3}$M, ${}^cK_i$ calculated at pH = 7.5.

For most natural waters (pH 6.5 – 9.5), bicarbonate is the dominant species. When a system is assumed to behave ideally, the K_i values remain constant and the speciation figure can be used given C_{TCO3}. However, when activity coefficients deviate from unity, K_i are replaced by ${}^cK_i$, and the calculations for ionic strength, activity, and carbonate speciation become interdependent. Therefore, an iterative process is used to adjust these three calculations at the desired pH.

Another measure of the likelihood of precipitation is given by the saturation index, SI, or the logarithm of SI (known specifically as the Langlier Saturation Index, LSI, for calcium carbonate). The SI is given by (Stumm and Morgan, 1996):

$$SI = \log_{10}\left(\frac{IAP}{{}^{c}K_{so}}\right) \tag{41}$$

where *IAP* is the ion activity product, or the product of the actual activities of the specific ions in solution. If the *SI* is negative, the salt does not precipitate, and a positive *SI* indicates supersaturation and the probability of precipitation. A positive *SI* does not guarantee precipitation because the kinetics involved may be too slow, or it may be affected by the presence of other ions or particles or by temperature and pressure.

Chapter 3: Materials and Methods

THREE-STAGE TREATMENT EXPERIMENTAL DESIGN: SELECTION OF EXPERIMENTAL PARAMETERS

Several experimental parameters were considered for the three-stage treatment. These parameters and the specific parameter ranges included:

- Precipitation pH (8.0, 9.0, 10.5, 11.0);
- Ozonation time (0, 1, 10, or 30 minutes) for a gaseous ozone flow of 3 mg/min;
- Precipitation time (30 or 60 minutes);
- Water composition (several synthetic water compositions and one natural water sample);
- Commercial antiscalant type (phosphonate and acrylic polymer); and
- Antiscalant concentration (2 – 100 mg/L).

Several ozonation parameters, such as ozonation pH, molar ratio of H_2O_2/O_3, buffer system, and ozone dose (in mg/L, added as an aqueous stock solution) were tested in detail when the ozonation step (Stage I) was studied individually. These experiments are explained in detail below. For the three-stage treatment experiments, these ozonation parameters were set at pH = 6.0, H_2O_2/O_3 = 0.8, carbonate as the buffering system, and gaseous ozone addition.

The synthetic concentrates used for precipitation experiments were based on the chemical composition of a brackish groundwater in Maricopa County, Arizona, USA (Jurenka and Chapman-Wilbert, 1996). Four different water compositions, shown in Table 7, were tested to determine the effect of major ions such as magnesium and sulfate on calcium precipitation and antiscalant performance. The data shown in Table 7 were

determined based on a theoretical 80% recovery and 100% rejection of all ions. The simplification of assuming 100% rejection resulted in synthetic RO concentrate that was five times as concentrated as the feed. In an operating reverse osmosis system, the membranes can have rejections of greater than 99% for most ions. The initial pH of the synthetic concentrates was 7.8.

Table 2. Composition of waters used for precipitation experiments.

	Water Type and Composition (mg/L)			
Component	**Simplified Maricopa (SM)**	**Simplified Maricopa + Na_2SO_4**	**Simplified Maricopa + $MgCl_2$**	**Complete Maricopa**
Na^+	1,552	2,027	548	849
Ca^{2+}	1,330	1,330	1,330	1,330
Mg^{2+}	---	---	514	514
Ba^{2+}	---	---	---	2.0
Fe^{3+}	---	---	---	2.3
Cl^-	4,163	4,163	4,114	3,933
SO_4^{2-}	---	991	---	991
NO_3^-	---	---	---	89
Alkalinity (as $CaCO_3$)	780	780	780	780
Total Dissolved Solids (TDS)	8,037	9,503	7,499	8,790

OZONE GENERATOR EXPERIMENTAL SETUP

The experimental setup for ozonation, shown schematically in Figure 6, included an ozone generator, gas washing bottles, digital flow meter, tubing, fittings, and catalytic ozone destructors. The gas washing bottles contained the test solution or a solution of 20 g/L potassium iodide (KI). The gas outflow from the generator was first split using a three-way fitting; one direction lead to an ozone destructor, and the other direction lead to the gas washing bottles. The three-way valve was used to completely shut off gas flow during different stages of experiments. All materials that came into contact with ozone were made of glass, Teflon, or stainless steel, since these three materials withstand degradation by ozone. The gas washing bottles were glass with fitted glass tops that contain glass tubes reaching down to the bottom of the bottles and ending in diffusers. The ozone generator used oxygen as the gas inflow and an electrolytic cell to produce ozone.

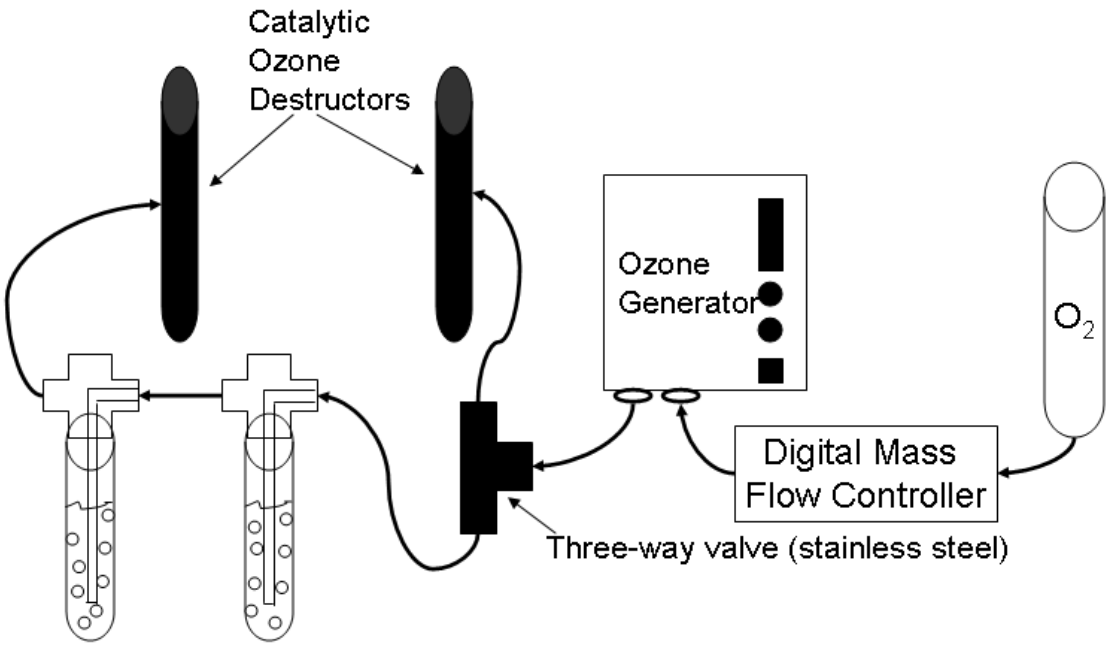

Figure 6. Schematic of ozone generator experimental setup.

The ozone generator (OzoneLab™ Model OL80W/FM100VT) used for experiments was obtained from Ozone Services, a division of Yanco Industries, Ltd. (Burton, British Columbia, Canada). The oxygen flow to the ozone generator was controlled by a digital mass flow meter and controller (Mass Flo© Model 1179A-01522CS1BV), obtained from MKS Instruments (Wilmington, MA, USA). The flow meter was calibrated by MKS for oxygen flow at room temperature (20 ^{o}C) and was powered by a single channel power supply (15 pin Model 246C). The ozone generator was operated a maximum oxygen gas pressure of 10 psi. The ozone offgased was captured by two catalytic ozone destructors. All experiments that tested the three stages of the concentrate treatment process together (Chapters 7 and 8) used gaseous ozone addition. For experiments containing hydrogen peroxide (H_2O_2), the H_2O_2 was added from the working solution of 10,000 mg/L to the experiment before ozone was dosed.

OZONE MASS FLOW

The 20 g/L KI solution was used to measure the mass flow of the ozone and to create a set of calibration curves correlating ozone mass flow to the gas flow and to the specific frequency regulator settings on the ozone generator. The 10-turn regulator (0 - 10 in integer increments) controlled the frequency of the high voltage discharge in the ozone-producing cell and therefore controlled the mass concentration of ozone in the gas stream; the digital mass flow controller was used to vary the oxygen flow to the ozone generator. When ozone reacted with KI, the solution turned a yellow/brown color. It was assumed that all ozone entering the KI solution completely reacted, so that no ozone was lost in the off-gas flow. The gas washing bottle(s) were attached in series using Teflon tubing and stainless steel fittings with Teflon ferrules. Two gas washing bottles were used in series to react with all of the ozone flowing from the generator. If all of the KI was quenched in the first bottle, the second bottle would begin to react and catch the ozone coming from the first. For each flow meter reading, the KI solution was ozonated for a specific amount of time (usually 3 - 5 minutes), and a 20 mL sample was removed from the washing bottle for titration with 0.01 N sodium thiosulfate. Before titration, 1 mL of 2 N H_2SO_4 was added to acidify the sample. Acidification allows complete reaction of iodide with sodium thiosulfate. This method was adapted from the Ozone Demand/Requirement-Semi-Batch Method (2350 E) (Eaton, et al., 2005).

Based on ozone flow measurements, ozone generator settings were set at 30 mL/min gas flow, with the frequency regulator set at four. The fraction of ozone in the gas outflow was approximately 5% (wt). The ranges of gas flows and frequency regulator settings are shown in Figure 7. The choice of 30 mL/min gas flow and a regulator setting of four allowed operation within the linear range of the curves; at larger

oxygen gas flow rates, increasing the gas flow did not significantly increase the ozone flow for each regulator setting.

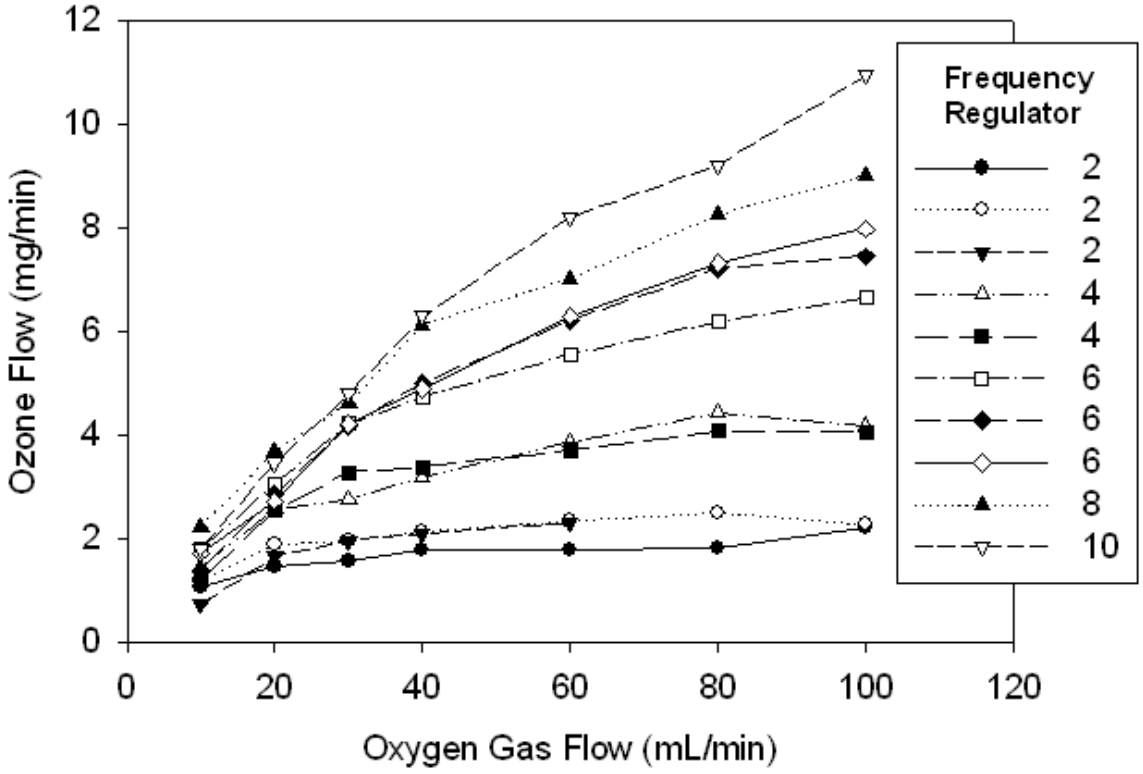

Figure 7. Calibration curves for the ozone generator and gaseous ozone flow. The legend depicts the frequency regulator settings tested within an integer range of 0 – 10.

PRECIPITATION EXPERIMENTAL SETUP

Precipitation experiments were performed in a jar test apparatus (Fisherbrand model 10008 or Phipps & Bird Stirrer model 7790-400), with agitation by stainless steel paddles (2.5 cm wide and 7.5 cm in length). Each solution was rapid-mixed at the start while sodium bicarbonate and sodium hydroxide were added. Then the solution was mixed at 60 rpm for one hour. One liter beakers or square jars were used.

Most of the precipitation experiments were performed at pH 10.5, except for a pH study that evaluated pH values of 8.0, 9.0, 10.5, and 11.0. When appropriate, antiscalant was added from a stock solution prior to carbonate addition and pH elevation. For most experiments, the antiscalant concentrations tested were 0, 0.1, 0.5, and 2.1 mg/L as dissolved organic carbon (DOC) in the hypothetical RO feed stream; therefore, actual antiscalant concentrations in the synthetic RO concentrate were 0, 0.5, 2.5, and 10.5 mg/L DOC. Additional antiscalant concentrations were tested for some experiments where additional data points were necessary. The order of addition of antiscalant and dissolved salts did not affect the precipitation results. To initiate precipitation, additional carbonate was added as $NaHCO_3$ (26 mM) in excess of the molar calcium concentration (to enable complete precipitation of calcium and stabilize the precipitation pH). A solution of 6 M NaOH was used to increase the pH.

MICROFILTRATION EXPERIMENTAL SETUP

The solid/liquid separation step was performed using 0.1 μm pore size Millipore nitrocellulose membranes in either a dead-end pressurized (0.5 bar) cell with a stir bar or using a Millipore glass filter holder assembly (47 mm diameter, 300 mL filter holder) under vacuum. A pore size of 0.1 μm was chosen based on the typical particle diameter of precipitated calcium carbonate (8 – 15 μm); using a membrane with significantly smaller pores (as compared to the particle size) allows complete particle removal from the water. The dead-end filtration cell was used with a digital mass balance to measure filtrate (permeate) flux as the precipitated solution was filtered. A stopwatch was used to record mass measurements every five to 10 seconds during filtration. The effect of antiscalant addition on flux was evaluated. Samples filtered with the vacuum assembly were analyzed for dissolved calcium.

ANTISCALANT SELECTION

Phosphonate antiscalant samples were obtained from Dequest Water Management Additives, a subsidiary of Thermophos. The antiscalants included the penta-sodium salt of aminotri(methylene phosphonic acid), or ATMP, the hexa-potassium salt of hexamethylenediamine tetra(methylenephosphonic acid), or HDTMP, and the hepta-sodium salt diethylenetriamine penta(methylene phosphonic acid) or DTPMP. Dequest refers to ATMP as DQ2006, to HDTMP as DQ2054, and to DTPMP as DQ2066. Dequest recommends DQ2006 and DQ2066 for general purpose metal ion control, while DQ2054 is specifically recommended for calcium sulfate precipitation control. The longer carbon chain in DQ2054 is designed to allow the antiscalant to adsorb to the needle-like calcium sulfate particles, while the more compact structures of DQ2006 and DQ2066 are better able to adsorb onto spherical or rhombohedral particles, such as calcium carbonate. The polymer antiscalant was obtained from Coatex S.A. (France) and is a proprietary polymer containing 19% acrylic acid, 20% methacrylic acid, and 61% itaconic acid. Proton nuclear magnetic resonance (NMR) spectroscopy was used to determine the composition of this polymer. Results from the NMR analysis are located in Appendix D. Total organic carbon (TOC) and total solids analysis were used to determine the mass and organic carbon concentrations of all the antiscalants. The four antiscalants used in this research are shown in Figure 8.

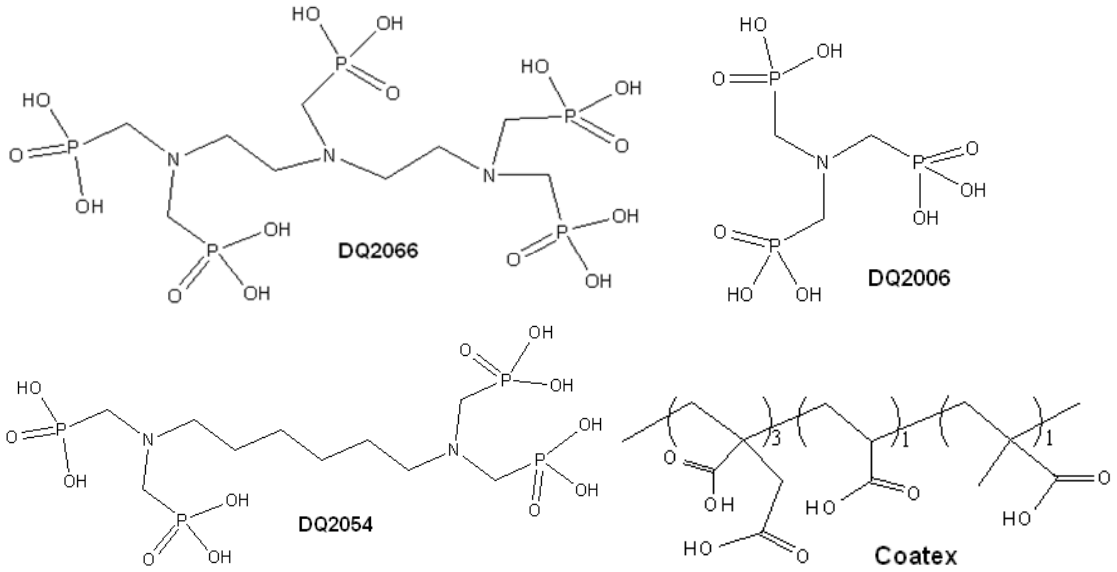

Figure 8. Chemical structures of phosphonate antiscalants DQ2006, DQ2066, (recommended for general metal ion control), DQ2054 (recommended for calcium sulfate control), and polymer antiscalant Coatex. All four antiscalants were used to evaluate three-stage process, while only phosphonate antiscalants were used in the ozone parameter study (Chapter 6).

TOC was measured on a Teckmar-Dohrman Apollo 9000 Combustion Analyser, where, first, CO_2 (inorganic carbon) was removed from each sample through addition of 21% phosphoric acid and subsequent oxygen sparging. The sample then passed through a catalyst and was oxidized in a furnace at 680 ^{o}C. Raw data counts from the detector, a Nondispersive Infrared (NDIR) sensor, were correlated to organic carbon concentration through a calibration curve. The calibration curve was obtained from a series of five standards, analyzed at the beginning and end of the sample set. Total solids was determined by placing an aqueous antiscalant sample of known mass in an oven (100 ^{o}C) overnight and then measuring the remaining mass after water evaporation. The ratio of the remaining mass to the starting mass is the total solids content.

Each antiscalant was tested for a range of concentrations. The concentrations were chosen based on a range of dissolved organic carbon (DOC) concentrations and a theoretical RO recovery of 80%, with a salt rejection of 100%. These assumptions resulted in a concentration factor of five for antiscalants in the RO concentrate. The range of feed antiscalant concentrations was 0.4 – 20 mg/L, resulting in RO concentrate concentrations of 2 – 100 mg/L antiscalant. For most experiments, the range of antiscalant mass concentrations used resulted in a dissolved organic carbon concentration range of 0.5 to 10.5 mg/L DOC. Two antiscalant concentrations tested, 100 mg/L DQ2066 and 50 mg/l Coatex, had higher DOC concentrations (19 and 30 mg/L, respectively). The specific concentrations tested for each antiscalant in synthetic RO concentrate are shown in Table 3.

Table 3. Concentrations tested for each antiscalant in the synthetic RO concentrate. Feed concentrations were assumed to be 0.2 of the value present in the synthetic RO concentrate.

Antiscalant	**Concentrations Tested (mg/L)**
DQ2006	4, 21, 40, 60, 85
DQ2054	2, 10, 43
DQ2066	3, 13, 56, 100
Coatex	2, 10, 50

pH METER CALIBRATION AND pH MEASUREMENT

A particular issue of importance throughout this research was the effect of high ionic strength on sample analysis and process chemistry. One expected effect was the

reduction of real pH values due to high salt concentrations in sample solutions. This effect, often referred to as the "sodium error," occurs because the activity of water decreases from unity as ionic strength increases, causing underestimates in pH readings. pH meters that have been calibrated with standard buffer solutions yield erroneous results because the liquid junction potential of the buffer solution (low ionic strength) is different than that of the high ionic strength samples. Also, the glass electrode of a pH probe can be affected by high ionic strength. A pH probe typically works by measuring the H^+ ions aligned on the sample side of the glass, but a high concentration of another ion can interfere with the H^+ measurement. Interfering ions can lower the pH of experimental solutions by as much as 0.75 pH units (Baumann, 1973). To avoid this problem, buffers at high ionic strength were used.

All pH measurements were taken with a Thermo Electron Corp. pH meter (Orion 720 A+), calibrated with three buffers (pH 4, 7, and 10 standard buffers). Based on the ionic strength of the synthetic RO concentrates, 8 g/L NaCl (0.14 M) was added to each of the three standard buffer solutions, and the salted buffers were used to calibrate the pH meter at 4.0, 7.0, and 10.0. The addition of salt to a standard buffer also causes the pH of the buffer solution to change, and the actual pH of each buffer solution must be recalculated based on the pH probe cell potential (mV) readings and a series of acid and base titrations (Wiesner, et al., 2006). However, based on work by Wiesner, et al. (2006), the addition of 8 g/L sodium chloride caused the pH of the buffers to decrease by no more than 0.1 pH units (Baumann, 1973; Wiesner, et al., 2006). Therefore, no recalculation of the buffer pH values was performed, and all pH values in this work are reported as measured, based on the salted-buffer calibration curve.

ANTISCALANT OXIDATION: SELECTION OF EXPERIMENTAL PARAMETERS

Antiscalant oxidation was studied in detail, and the following parameters were evaluated:

- pH (5.0, 6.0, 7.0, and 8.0);
- Molar ratio of H_2O_2/O_3 (0, 0.2, 0.5, and 0.8);
- Cation concentration (calcium, magnesium, ferric iron, and barium; 0 – 50 mM);
- Total carbonate concentration (0 – 30 mM);
- Ozone concentration (1, 5, 10 mg/L);
- Number of ozone doses added to an experiment (1, 2, or 3 additions);
- Phosphonate antiscalant type and concentration (as described above);
- Water composition (water compositions similar to those shown in Table 2); and
- Addition of an *OH scavenger, tert-butanol (t-BuOH) (0 or 10 mM for all experiments).

OZONE STOCK SOLUTION

For the detailed study on antiscalant ozonation (Chapter 6), all experiments were performed using an aliquot of ozone stock solution to add ozone and start the experiment (Acero and von Gunten, 2000). The stock solution was made by bubbling gaseous ozone through deionized water in a gas washing bottle. The gas washing bottle was placed in a bucket of ice to increase the solubility of ozone in water; the oxygen gas flow was set to 40 mL/min and the generator knob was set to 10. Higher oxygen gas flows did not significantly increase the stock solution ozone concentration. The stock solution typically had an ozone concentration between 1.25 mM (60 mg/L) and 1.66 mM (80 mg/L). Ozone concentrations used in experiments included 1, 5, and 10 mg/L O_3. All experiments were dosed with a specific volume of aqueous ozone based on the measured ozone concentration, and the same glass pipet was pretreated with ozone and used for

aqueous ozone addition. For experiments containing hydrogen peroxide (H_2O_2), the H_2O_2 was added from the working solution of 1,000 mg/L to the experiment before ozone was dosed. The aqueous ozone concentration was measured on a UV/visible spectrophotometer (Agilent model 8453) at 258 nm in a one centimeter quartz cuvet. To prepare a sample for measurement, an aliquot was removed from the stock solution and added to 5 mM phosphate buffer (pH 3) to stabilize the ozone. The sample was measured within approximately 30 seconds on the spectrophotometer.

ORTHOPHOSPHATE MEASUREMENT

The extent of phosphonate antiscalant oxidation was measured by the amount of orthophosphate produced during ozonation. The initial solution, before ozonation, was also tested for orthophosphate. The amount of available phosphorus was calculated for a specific antiscalant concentration, based on the known molecular structure of the antiscalant. Therefore, a fractional orthophosphate production could be calculated as the ratio of the orthophosphate measured after ozonation (minus the initial orthophosphate concentration) to the phosphate available in the original antiscalant molecules. Standard method 4500-P E (Ascorbic Acid Method) was used to measure orthophosphate in aqueous solutions (Eaton, et al., 2005). A UV/visible spectrophotometer (Agilent model 8453) was used to measure reacted orthophosphate in test samples. A new calibration curve from known phosphate concentrations was made for each set of samples tested. Phosphate samples were taken from the initial solution and after ozonation. A one centimeter quartz cuvet was used for all measurements.

HYDROGEN PEROXIDE MEASUREMENT

The stability of hydrogen peroxide stock was a concern, since the compound is light-sensitive and can be highly reactive in the presence of oxygen and transition metals

such as iron and manganese. Most available hydrogen peroxide contains stabilizer compounds to help prevent decomposition. These stabilizers work by chelating the metals and preventing reaction with hydrogen peroxide; unfortunately, the stabilizers are often organophosphates, exactly the type of compound that was studied. Thus, unstabilized hydrogen peroxide was required for experiments to prevent other oxidation reactions that were not part of the system in question.

Since unstabilized hydrogen peroxide degrades more rapidly than the other commercial products, two different methods were used to evaluate H_2O_2 concentration during experiments. Both methods utilized spectrophotometric detection. The first method, described by Klassen et al., used potassium permanganate ($KMnO_4$) to titrate H_2O_2 (Klassen, et al., 1994). The limit of detection was reported as approximately 3 μM. The H_2O_2 stock was tested with this method. For more dilute solutions, *i.e.*, experimental samples, a second method, which employs titanium oxalate in the presence of sulfuric acid to produce a titanium-peroxysulfate complex, was used (Pobiner, 1961; Schick, et al., 1997). This method had a determination limit of approximately 0.7 μM.

PRECIPITATION AND SOLID/LIQUID SEPARATION: PREDICTING PRECIPITATION

Along with individual calculations for each potential precipitate based on the equations developed by Pitzer, chemical equilibrium modeling programs such as Visual Minteq (version 2.50, 2006) or PHREEQC (version 2.15.0.2697, 2008) were used. For this project, these programs helped to guide the experiments in creating conditions for precipitation and to interpret the results. Visual Minteq was a more straightforward program to use and provided a first prediction of precipitation, but ultimately PHREEQC was used because the program contains a database of thermodynamic equilibrium relationships based on the equations developed by Pitzer for high ionic strength solutions (Pitzer, 1991).

DISSOLVED IONIC SPECIES

Inductively coupled plasma atomic emission spectroscopy (ICP-AES) was used to analyze metal concentrations before and after precipitation experiments. A Spectro Ciros CCD Model (Spectro AI GmbH) was used with Smart Analyzer data acquisition software (version 3.2, 1995-2000). Samples were analyzed for calcium, magnesium, barium, and iron. Standards were made with appropriate sodium chloride additions to avoid ion effects on ICP concentration results. Samples were prepared in 15 mL screw-cap polypropylene centrifuge tubes with concentrated nitric acid added for a final concentration of 1.5% (v/v). If necessary, samples were stored at 4 ^{o}C for no longer than 2 weeks before analysis. Scandium (1 ppm in 2% HNO_3) was used as the reference line, and argon is the monitor line. Standards were made to measure Na^{+}, Ca^{2+}, Cl^{-}, Ba^{2+}, Mg^{2+}, and Fe^{3+} simultaneously in the range 0 – 10 mg/L. Sample solutions were run in several dilutions to capture all ions within the linear range established by the standards. All samples and standards contained 1.5% HNO_3. Some calcium and magnesium measurements were made using standard titrations for calcium and hardness with ethylenediaminetetraacetic acid (EDTA) (Eaton, et al., 2005).

An ion chromatography system (Metrohm 700 series, column Metrosep A Supp 5, 150/4.0 mm) was used to measure sulfate concentrations after precipitation and filtration. Some sulfate measurements were taken with a Hach Ratio/XR turbidimeter; the turbidimeter was used to measure barium sulfate turbidity and to ultimately obtain sulfate concentrations in filtered precipitated samples (Eaton, et al., 2005).

Carbonate was measured through alkalinity titrations with 0.36 M standardized hydrochloric acid (HCl). The pH was recorded initially and after each volume addition of HCl, and the equivalence of acid added was correlated to the alkalinity and total carbonate concentrations of the sample.

PRECIPITATE PARTICLE CHARACTERISTICS

A light microscope (Lamp 12v/20W, B2 series, MOTIC, 50x magnification) and a LEO 1530 scanning electron microscope (SEM) were used to obtain images of the precipitates. Two different scanning electron microscopes (SEM), a LEO 1530 and a Hitachi S-5500, were used to obtain images of the precipitates. Both SEMs were equipped with energy dispersive x-ray (EDX) elemental analysis. Samples were mounted on adhesive carbon tabs; precipitates were placed directly onto the carbon tab or were on a nitrocellulose microfilter that was placed on the carbon tab. All samples were sputter coated with silver (30 seconds). Samples used for SEM analysis were taken from a set of repeat precipitation experiments performed under identical conditions as those performed to obtain particle size distribution measurements; SEM data and particle size distribution data were used together to explain changes caused by antiscalant addition.

Particle size distributions were obtained using a laser granulometer Mastersizer S (Malvern Instruments). The Mastersizer S is a static laser light scattering instrument. A polydisperse deconvolution algorithm and the Fraunhofer theory were used to translate the detected light scattering data (diffraction intensity with as a function of diffraction angle) into a best-fit particle size distribution. Except for several experiments performed several days after precipitation, precipitated samples were measured on the Mastersizer S directly following precipitation. The samples were placed in a 500 mL or 1 L glass beaker and stirred using the same jar test apparatus used during precipitation. The sample was passed through the light scattering glass cell with Masterflex Tygon tubing and a peristaltic pump. The tubing was removed and cleaned with a brush and deionized water after each sample measurement.

PILOT RO MEMBRANE OPERATION

Two spiral wound membrane models were used for the pilot RO study. The first RO treatment stage was performed using a Koch Ultra Low Pressure (ULP) RO membrane (Model# 2540ULP). The secondary RO treatment stage was performed using a Koch high pressure SWRO membrane (Fluid Systems TFC, part number 8254004, Model 2540 SW). The average permeability for the ULP model was 1.20 L/m^2-h-bar, and the average permeability for the SWRO module was 1.38 L/m^2-h-bar. The pilot RO membrane was operated in either permeate recycle mode or permeate withdrawal mode; in both cases, the concentrate from the membrane unit was recycled back to the feed tank. For the permeate recycle mode, the permeate line was also recycled back into the feed tank, and the salt concentration in the feed tank was assumed constant. For the permeate withdrawal mode, permeate was collected in a separate tank that was placed on a digital balance to record accumulated mass, and the concentration of the feed tank increased during the experiment. The pilot RO feed tank was temperature controlled; however, the temperature still increased over time when the pilot RO system was operated in permeate withdrawal mode. The temperature varied between 18 and 22 ^{o}C during operation of the ULP module. The variation of the viscosity with water temperature was taken into account for this temperature range. Each module was rinsed before and after each test run with distilled water in recycle mode until the initial permeability (measured before each test) was recovered. If the initial permeability was not achieved, a chemical wash was performed to clean the membrane module. The first RO stage was performed at a pressure of 20 bar and the second RO stage was performed at 50 bar. During pilot system operation, measurements were taken in the permeate and concentrate for instantaneous dissolved calcium concentration, conductivity, temperature, and pH. After the end of

each experiment, final measurements were taken in the permeate and concentrate for calcium, magnesium, sulfate, conductivity, turbidity, temperature, and pH.

A water sample was obtained from a natural karstic spring in Marseille, France. The water was analyzed for dissolved calcium, magnesium, sulfate, carbonate, turbidity, and conductivity. Sodium and chloride concentrations were estimated from previous measurements taken on a similar karstic spring in southern France (Blavoux, et al., 2004). A summary of the composition for the water sample obtained is shown in Table 15. While the water composition has a salinity typical of a brackish water (1 – 10 g/L total dissolved solids (TDS)), the water sample is atypical of many brackish water sources, primarily due to the high sulfate and magnesium concentrations. In addition, a typical brackish groundwater has a higher alkalinity (Jurenka and Chapman-Wilbert, 1996). The natural pH of the water sample was 7.6. The pH was adjusted to 6.5 prior to primary RO treatment with the ULP RO module. A synthetic version of the water sample was made in the laboratory; the synthetic water was made as RO concentrate, based on the recovery (67%) and concentration factor (~3) calculated from primary RO treatment of the real water sample. The RO concentrate treatment process was evaluated with the synthetic concentrate, and results were compared to data obtained from concentrate treatment of the real water RO concentrate.

Table 4. Composition of water sample obtained from a karstic spring in Marseille, France.

Component	**Concentration**	**Units**
Sodium (Na^{+})	2,500 – 2,800	mg/L
Chloride (Cl^{-})	5,200 – 5,900	mg/L
Calcium (Ca^{2+})	173	mg/L
Magnesium (Mg^{2+})	387	mg/L
Bicarbonate (HCO_3^{-})	65	mg/L
Sulfate (SO_4^{2-})	787	mg/L
Alkalinity	1	meq/L
Turbidity	0.19	NTU*
Conductivity	15	mS/cm at 20^{o}C

*NTU = Nephelometric Turbidity Units

Chapter 4: The effect of antiscalant addition on calcium carbonate precipitation for a simplified synthetic brackish water reverse osmosis concentrate[1]

ABSTRACT

The primary limitation to inland brackish water reverse osmosis (RO) desalination is the cost and technical feasibility of concentrate (i.e., salty waste stream) disposal. To decrease concentrate volume, a side-stream process can be used to precipitate problematic scaling salts and then remove the precipitate from the aqueous solution with a solid/liquid separation step. The treated concentrate can then be purified through a secondary reverse osmosis stage to increase overall recovery and decrease the volume of waste requiring disposal. A key component of most RO concentrates is antiscalant; antiscalants are used in an RO system to prevent salt precipitation but might affect side-stream treatment of the concentrate. Precipitation experiments were performed on a synthetic RO concentrate with and without antiscalant; of particular interest was the precipitation of calcium salts, especially calcium carbonate. Particle size distributions, calcium precipitation, microfiltration flux, and scanning electron microscopy were used to evaluate the effect of antiscalant type, antiscalant concentration, and precipitation pH on calcium carbonate precipitation and filtration. Results show that antiscalants can decrease precipitate particle size and change the shape of the particles; smaller particles can cause an increase in microfiltration flux decline and result in poorer performance during the solid/liquid separation step. The presence of antiscalant during precipitation can also decrease the mass of precipitated calcium carbonate.

[1] Manuscript to be submitted to the journal Water Research.

Key Words

Brackish water, reverse osmosis, antiscalant, calcium carbonate, precipitation, concentrate treatment

Nomenclature

ATMP	Aminotri(methylene phosphonic acid)
DOC	Dissolved organic carbon concentration (mg/L)
DTPMP	Diethylenetriamine penta(methylene phosphonic acid)
EDTA	Ethylenediaminetetraacetic acid
HDTMP	Hexamethylenediamine tetra(methylenephosphonic acid)
$K_{sp,x}$	Solubility product of x
IAP	Ion activity product
MF	Microfiltration
NMR	Nuclear magnetic resonance
Q	Volumetric flow rate (L/m^3)
RO	Reverse osmosis
SEM	Scanning electron microscopy
SI	Saturation index
t	Time
TDS	Total dissolved solids concentration (mg/L)
TOC	Total organic carbon concentration (mg/L)
V	Volume (L)

INTRODUCTION

Reverse osmosis (RO) membrane desalination has emerged as the primary choice for new and expanding desalination plants (Wolfe, 2005), and most plants today are located in coastal regions. Coastal RO desalination plants can use brackish water (1 – 10 g/L total dissolved solids (TDS)) or seawater (30 – 45 g/L TDS) and typically dispose of the salty RO waste stream (concentrate) back into the ocean or sea. Many countries, including the United States, also have large brackish aquifers inland and could use this salty water as an additional water resource (Sandia, 2003). The application of RO desalination inland has been limited due to the technical and financial challenges of concentrate disposal.

Brackish water RO recoveries (volume of product water per volume of feed water) range from 65 to 90%, depending on feed water salinity and composition, so that the concentrate typically represents 10 – 35% of the RO feed. In comparison, fresh water treatment plants have recoveries of greater than 99%. For brackish waters, the primary limitation to increasing RO recovery is salt precipitation on the membrane surface, which causes product flux decline or requires an increase in the hydrostatic feed pressure to maintain product flux. This type of membrane fouling, termed scaling, is caused by sparingly soluble salts such as calcium carbonate ($CaCO_3$), calcium sulfate ($CaSO_4$), barium sulfate ($BaSO_4$), strontium sulfate ($SrSO_4$), and silica. Membrane scaling can occur in the absence of precipitation in the bulk solution (Rahardianto, et al., 2006). In the worst case, scaling can permanently damage a membrane.

RO membrane scaling can be controlled using pH adjustment and the addition of scale inhibitors called antiscalants. Antiscalants are synthetic organic compounds that contain negatively charged groups such as carboxylic acid and phosphate. These compounds prevent or delay precipitation through association with surface cations of

nucleating precipitates (Yang, et al., 2001). Antiscalants disrupt the ordered lattice structure of the salt precipitates and prevent the growth stage of precipitation by blocking crystal growth sites (Lin and Singer, 2005). Often less thermodynamically stable forms of a precipitate are present. In the presence of antiscalant, calcium carbonate, for example, can remain as vaterite, rather than transform to the more stable calcite (Tang, et al., 2008; Yang, et al., 2001). In brackish water RO, antiscalants are often dosed in the RO feed, prior to membrane treatment, and are rejected by the RO membranes, therefore becoming part of the RO concentrate.

As RO recovery increases, the salt content of the concentrate increases, and eventually the antiscalant precipitation control is overcome; precipitation and membrane scaling can occur even in the presence of antiscalants. To decrease the concentrate volume produced and improve the economic feasibility of using brackish water RO desalination inland, increasing RO recovery within the membrane system must be accomplished. Previous studies have investigated various methods to reduce concentrate volume (Almulla, et al., 2002; Gilron, et al., 2005; Mickley, 2004; Rahardianto, et al., 2007; Williams, et al., 2002); one of the most promising general approaches is to treat the RO concentrate through a side-stream process of precipitation and solid/liquid separation (Rahardianto, et al., 2007) to remove scaling salts and return most of the water to a secondary RO system.

While salt precipitation can be achieved in the presence of antiscalants, the antiscalant may affect the precipitation and solid/liquid separation steps through changes in the extent of precipitation, precipitate particle morphology, and effectiveness of solid/liquid separation. The primary objective of this study was to determine the effect of antiscalants on calcium carbonate precipitation in a simplified brackish water RO concentrate. Several different antiscalants were used to study the effect of these

compounds on the extent of calcium carbonate precipitation, particle size distributions, particle morphology, and separation of the precipitated particles and water. The effects of antiscalant type, antiscalant concentration and pH on calcium precipitation were investigated through analysis of dissolved calcium, particle size distribution of precipitated calcium salts, scanning electron microscope (SEM) imaging, and microfiltration flux during solid/liquid separation.

EXPERIMENTAL METHODS

Materials

Reagents

All inorganic salts, acids, and bases used in experiments were ACS grade reagents obtained from Fisher Bioblock Scientific (France). Salts used to make synthetic test solutions included calcium chloride, sodium bicarbonate, and sodium chloride. Distilled water was used to make all test solutions. Solution pH adjustment was achieved using solutions of 5 N hydrochloric acid (HCl) (made from concentrated HCl) and 6 N sodium hydroxide (NaOH) (made from NaOH pellets).

Antiscalants

Two common classes of antiscalants are used in drinking water RO applications. Both are synthetic organic compounds, with one based on phosphonates alone and the other based on acrylic acid with or without blending with phosphonates. As shown in Figure 9, the four antiscalants used in this study included three phosphonates and one polymer. Each of these four antiscalants are often used in membrane drinking water applications (Knepper, 2003). The defining characteristic of phosphonates is a phosphorus-carbon (P-C) bond, and the antiscalants also have at least one tertiary amine

(nitrogen bonded to three carbons). The P-C bonds make phosphonates less susceptible to biodegradation, as compared to the simpler phosphate antiscalants used before synthetic phosphonates were developed.

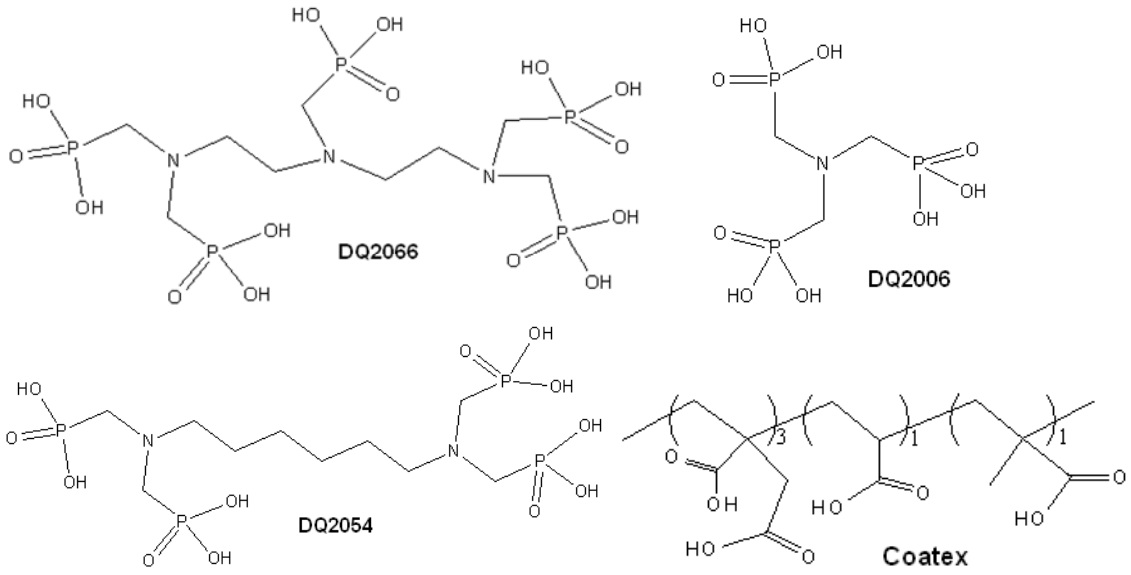

Figure 9. Chemical structures of phosphonate antiscalants DQ2006, DQ2066, (recommended for general metal ion control), DQ2054 (recommended for calcium sulfate control), and polymer antiscalant Coatex.

Phosphonate antiscalant samples were obtained from Dequest Water Management Additives, a subsidiary of Thermophos. The antiscalants included the penta-sodium salt of aminotri(methylene phosphonic acid), or ATMP, the hexa-potassium salt of hexamethylenediamine tetra(methylenephosphonic acid), or HDTMP, and the hepta-sodium salt diethylenetriamine penta(methylene phosphonic acid) or DTPMP. Dequest refers to ATMP as DQ2006, to HDTMP as DQ2054, and to DTPMP as DQ2066, and these commercial names are used throughout the rest of this article to indicate which

antiscalant was used. Dequest recommends DQ2006 and DQ2066 for general purpose metal ion control, while DQ2054 is specifically recommended for calcium sulfate precipitation control. The polymer antiscalant was obtained from Coatex S.A. (France) and is a proprietary polymer containing 19% acrylic acid, 20% methacrylic acid, and 61% itaconic acid. Proton nuclear magnetic resonance (NMR) spectroscopy was used to determine the composition of this polymer. Total organic carbon (TOC) and total solids analysis were used to determine the mass and organic carbon concentrations of all the antiscalants.

Synthetic RO Concentrates

The composition of the water used for precipitation experiments was based on that of a brackish groundwater in Maricopa County, Arizona, USA (Jurenka and Chapman-Wilbert, 1996). A simplified water data set that reflects the major ions in Maricopa water was chosen to make synthetic RO concentrate in the laboratory, based on an 80% assumed recovery of the feed water and an RO membrane ion rejection of 100%. These assumptions result in a concentrate that is five times as concentrated as the RO feed; the composition of this synthetic concentrate is shown in Table 5. To focus specifically on calcium carbonate precipitation, all ions were omitted except for calcium, carbonate, sodium, and chloride. The pH value shown in Table 1 was the natural starting pH of the synthetic concentrate; for all precipitation experiments, the pH was adjusted to the desired value with NaOH.

Table 5. Composition of the synthetic brackish water RO concentrate used in precipitation experiments.

Component	Mass Concentration (mg/L)	Molar Concentration (mM)
Na^+	1,556	67.7
Cl^-	4,168	117.6
Ca^{2+}	1,325	33.1
HCO_3^-	990	16.2
TDS	8,028	---
pH	7.8	---

Methods

Precipitation

Precipitation experiments were performed in a jar test apparatus (type 10008, Fisherbrand), with agitation by stainless steel paddles (2.5 cm wide and 7.5 cm in length). Each solution was rapid-mixed at the start while sodium bicarbonate and sodium hydroxide were added. Then the solution was mixed at 60 rpm for one hour. One liter beakers were used, and each measured 13 cm high with an internal diameter of 10 cm.

Precipitation experiments were performed at pH 10.5. When appropriate, antiscalant was added from a stock solution prior to carbonate addition and pH elevation. For most experiments, the antiscalant concentrations tested were 0, 0.1, 0.5, and 2.1 mg/L as dissolved organic carbon (DOC) in the hypothetical RO feed stream; therefore, actual antiscalant concentrations in the synthetic RO concentrate were 0, 0.5, 2.5, and 10.5

mg/L DOC. Additional antiscalant concentrations were tested for some experiments where additional data points were necessary. The order of addition of antiscalant and dissolved salts did not affect the precipitation results. To initiate precipitation, additional carbonate was added as $NaHCO_3$ (26 mM) in excess of the molar calcium concentration (to enable complete precipitation of calcium and stabilize the precipitation pH). A solution of 6 M NaOH was used to increase the pH.

The separation step was performed using 0.1 μm pore size Millipore nitrocellulose membranes in either a dead-end pressurized (0.5 bar) cell with a stir bar or using a Millipore glass filter holder assembly (47 mm diameter, 300 mL filter holder) under vacuum. The dead-end filtration cell was used with a digital mass balance to measure filtrate (permeate) flux as the precipitated solution was filtered. A stopwatch was used to record mass measurements every five to 10 seconds during filtration. The effect of antiscalant addition on flux was evaluated. Samples filtered with the vacuum assembly were analyzed for dissolved calcium.

Analytical Measurements

Dissolved calcium measurements were obtained through a standard titration with ethylenediaminetetraacetic acid (EDTA) (Eaton, et al., 2005). If necessary, samples were stored at 4 ^{o}C for no longer than 2 weeks before analysis.

All pH measurements were taken with a Thermo Electron Corp. pH meter (Orion 720 A+), calibrated with three buffers (pH 4, 7, and 10 standard buffers). The pH of a solution changes with ionic strength, due to a decrease in the hydrogen ion activity and ion interferences at the pH electrode surface (Baumann, 1973; Wiesner, et al., 2006). Therefore, 8 g/L sodium chloride (0.14 M) was added to each pH buffer to account for experimental solution ionic strength. Based on work by Wiesner, et al., (2006) the addition of 0.14 M NaCl causes the pH of the buffers to decrease by no more than 0.1 pH

units. Therefore the salted buffers were used to calibrate the pH meter at 4.0, 7.0, and 10.0, and no recalculation of pH was performed. The pH values presented in this work are reported as recorded based on the above procedure.

A light microscope (Lamp 12v/20W, B2 series, MOTIC, 50x magnification) and a LEO 1530 scanning electron microscope (SEM) were used to obtain images of the precipitates. Particle size distributions were obtained using a laser granulometer Mastersizer S (Malvern Instruments). The Mastersizer S is a static laser light scattering instrument. A polydisperse deconvolution algorithm and the Fraunhofer theory were used to translate the detected light scattering data (diffraction intensity with as a function of diffraction angle) into a best-fit particle size distribution. The SEM and particle size distribution results were obtained from samples of repeat experiments performed for the same experimental conditions and were used together to explain changes in particle morphology.

RESULTS AND DISCUSSION

Precipitation prevention by antiscalants

The primary potential precipitate (scale) in the synthetic concentrate was calcium carbonate, $CaCO_3$, which precipitates most easily in the mineral form of calcite. The driving force for precipitation is often expressed in terms of the saturation index, defined generally as the ratio of the ion activity product to the solubility product and specifically for calcium carbonate as follows:

$$SI_x = \frac{IAP}{K_{sp,x}} = \frac{\left\{Ca^{2+}\right\}\left\{CO_3^{2-}\right\}}{K_{sp,CaCO3}}$$

where the K_{sp} value for calcite is 3.311×10^{-9} (Stumm and Morgan, 1996). If *SI* is greater than one, precipitation is thermodynamically favorable. The precipitation of calcium carbonate (*i.e.*, the value of *SI*) is a strong function of pH because the carbonate species shifts from being dominated by bicarbonate (HCO_3^-) to being dominated by carbonate (CO_3^{2-}) as the pH goes from neutral to pH 11. Hence, in this research, it was critical to investigate the effectiveness of antiscalants in preventing calcium carbonate precipitation as a function of pH.

Precipitation experiments were performed with and without antiscalant at initial pH values of 8.0, 9.0, 10.5, and 11.0. To ensure that calcium precipitation was not limited by the stoichiometric requirement for carbonate, sodium bicarbonate ($NaHCO_3$) was added to bring the total carbonate concentrate to 42 mM, in excess of the calcium concentration in the synthetic concentrate, as shown in Table 5. The antiscalant used was DQ2006 at a dose of 85 mg/L (10.5 mg/L DOC). The pH was adjusted to the desired starting values with NaOH and precipitation was allowed to occur in stirred beakers for one hour. As the initial pH was increased, the saturation index for calcite for the initial conditions also increased from 880 at pH 8.0 to 27,000 at pH 10.5 and 28,000 at pH 11.0; the activity coefficients for calcium and carbonate were calculated using the Pitzer equations (Pitzer, 1991). After precipitation, the suspensions were filtered through 0.45 μm pore size filters, and the filtrate was analyzed for the soluble calcium concentration.

The results of these experiments are shown in Figure 10; the data are plotted against the final pH values, which were 0.1 to 0.3 units below the initial values because $CaCO_3$ precipitation reduces the pH. For the experiments without antiscalant, the precipitation was extensive in all cases, with lower remaining soluble calcium concentrations with increasing pH, as expected; these results were consistent with thermodynamic equilibrium calculations with the software program PHREEQC (Version

2.15). The experiments in the presence of antiscalant all had more soluble calcium remaining than the corresponding experiments without antiscalant, indicating some effectiveness of antiscalant regardless of pH. However, the antiscalant was highly successful only in the experiment at pH 8.0, where 91% of the calcium remained in solution despite the high saturation ratio; in contrast, only 5% remained in solution in the pH 11.0 experiment. Antiscalants have a certain maximum saturation index for each salt precipitate above which they are no longer effective. For calcium carbonate, the maximum recommended *SI* value is approximately 800 (Hydranautics, 2003). The results for all the experiments with antiscalant present were consistent with that recommendation and indicated that some precipitation may occur when the *SI* value approaches the recommended limit.

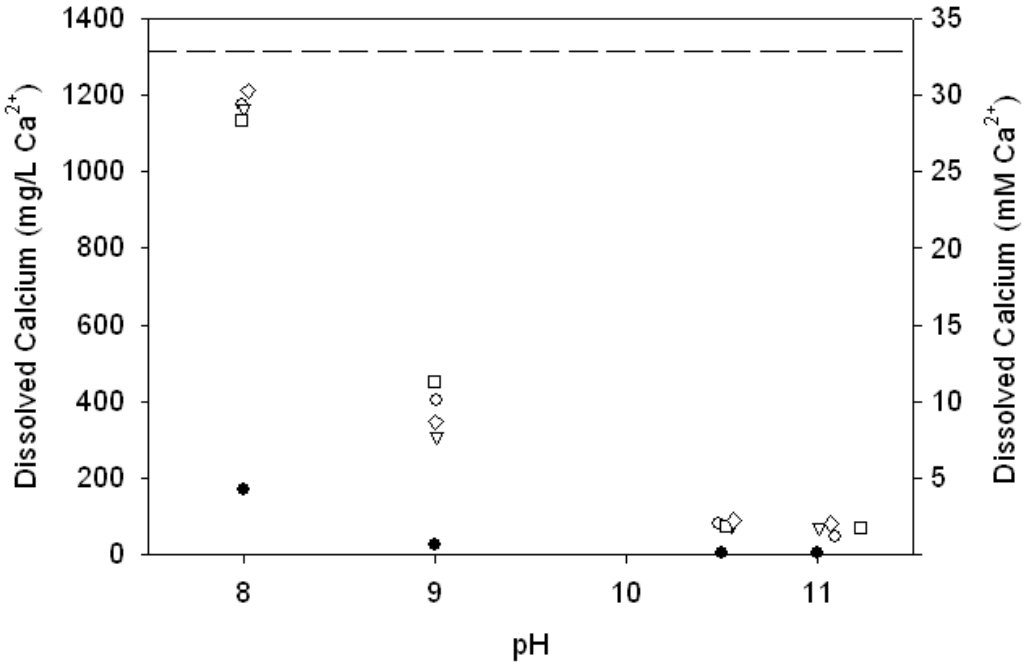

Figure 10. Comparison of calcium carbonate precipitation with and without antiscalant (85 mg/L DQ2006) for a final pH range of 8.0- 11.2. Open symbols represent four repeat experiments with antiscalant and closed symbols represent experiments without antiscalant. The initial calcium concentration before precipitation (1325 mg/L) is represented by the horizontal dotted line.

The four antiscalants were tested for their effectiveness in preventing $CaCO_3$ precipitation for the synthetic concentrate over a range of concentrations (2 – 100 mg/L) at a precipitation pH of 10.5; results are shown in Figure 11. In all cases, the dissolved calcium remaining in solution after precipitation increased as antiscalant concentration increased. The performance of three of the antiscalants, DQ2006, DQ2066, and the Coatex polymer, was similar, while DQ2054 was not effective at preventing precipitation. The DQ2054 antiscalant is recommended for calcium sulfate precipitation prevention by the manufacturer. Calcium sulfate, or gypsum, particles have a needle-like shape, and the elongated structure of DQ2054 is designed to adsorb well to nucleating

gypsum particles. However, calcium carbonate particles are typically spherical or rhombohedral in shape, and the more compact or more highly branched compounds (DQ2006, DQ2066, and Coatex) appear to be better suited for adsorption and prevention of calcium carbonate precipitation. For DQ2006, DQ2066, and Coatex, the increase in remaining dissolved calcium increases dramatically for lower antiscalant concentrations, but at higher antiscalant concentrations, an increase in antiscalant causes little to no increase in final dissolved calcium.

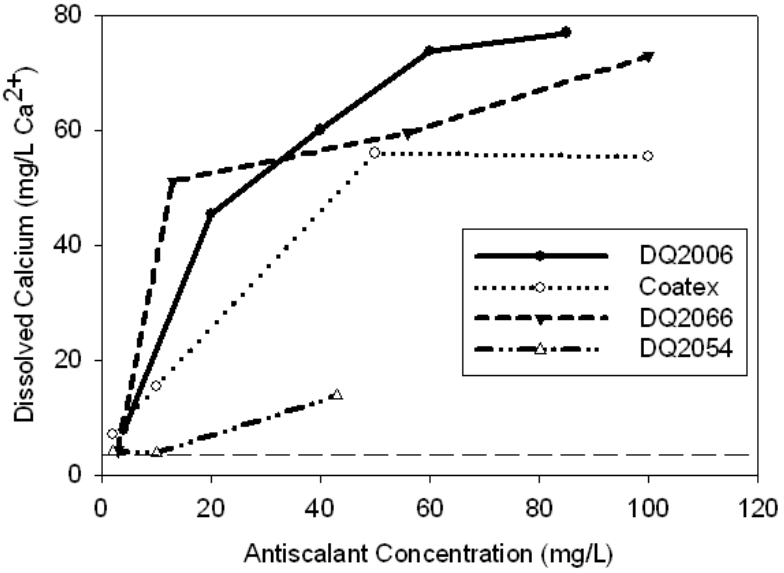

Figure 11. Variation of the final dissolved calcium concentration as a function of antiscalant type and concentration after precipitation (pH 10.5) and filtration. All DQ antiscalants are phosphonates, and Coatex is an acrylic acid polymer. The horizontal dotted line represents the final dissolved calcium concentration of an antiscalant-free precipitated solution.

The same precipitation experiment was performed for the same range of antiscalants (for DQ2006, DQ2054, and Coatex) at pH 8.0. The data (not shown) did not indicate a relationship between antiscalant type or concentration and calcium precipitation; all

antiscalant types and concentrations resulted in approximately the same dissolved calcium concentration after precipitation. For all antiscalant concentrations tested, an average 91% of the calcium remained in solution after one hour precipitation and subsequent filtration. The results at pH 8.0 indicate that even small doses of antiscalant can prevent precipitation if used within the recommended range for the precipitate Saturation Index.

Particle size distribution as a function of pH

The relationship between precipitate particle size and pH was investigated for an antiscalant dose of 85 mg/L DQ2006. Particle size distribution measurements based on an assumption of equivalent spherical particle diameter were obtained directly following one hour precipitation, and a pH range of 8.0 – 11.0 was tested. At all four pH values, the calculated particle volume distribution was bi-modal, with a larger peak in the 11 – 21 μm size range and a smaller peak in the sub-micron size range; the results are shown in Figure 12a. While there were no dramatic differences in these distributions, the results at pH 8.0 exhibited the most monodisperse distribution, perhaps because the driving force and amount of precipitation was the least at that pH. However, when the samples were measured again after two days (results shown in Figure 12b), the modal particle diameter of all four samples increased, and the particle size distribution became a function of pH; the modal diameter increased dramatically with increases in pH. The pH of the aged solutions did not vary significantly from the precipitation pH. At pH 8.0, the modal particle diameter increased from 15 μm to 33 μm in the two days after the precipitation experiment. For an increase in pH from 8.0 to 11.0, the modal particle diameter increased from 33 μm to 275 μm when particle size measurements were taken after two days.

In Figure 12a, the particle size distribution for all four pH values is bimodal, while in Figure 12b, the curves for most of the aged samples are monomodal. The bimodal distributions of Figure 12a result from the mechanism by which antiscalants generally prevent precipitation; antiscalants inhibit or slow crystal growth through adsorption onto nucleating crystals, causing the crystal growth sites to be blocked (Lin and Singer, 2005; Reddy and Hoch, 2001). The extent to which crystal growth and crystal structure are disrupted is dependent on where the antiscalant adsorbs on the surface and how strongly the antiscalant is bound to the surface (Yang, et al., 2001). Antiscalants may also inhibit crystal growth through coordination or chelation with lattice cations, such as calcium (Reddy and Hoch, 2001) and through particle dispersion (Gillard, et al., 1989; Tang, et al., 2008). A precipitating solution that contains antiscalant typically has more nucleated crystals but less fully grown precipitated particles than an antiscalant-free solution. In Figure 12a, the particles represented by the curves between 0.1 and 1 μm particle diameter are nucleated particles, while the curves in the larger size range represent fully grown crystals. The monomodal distributions in the aged samples resulted from a reduction in nucleated particles, most likely caused by crystal growth over the two days.

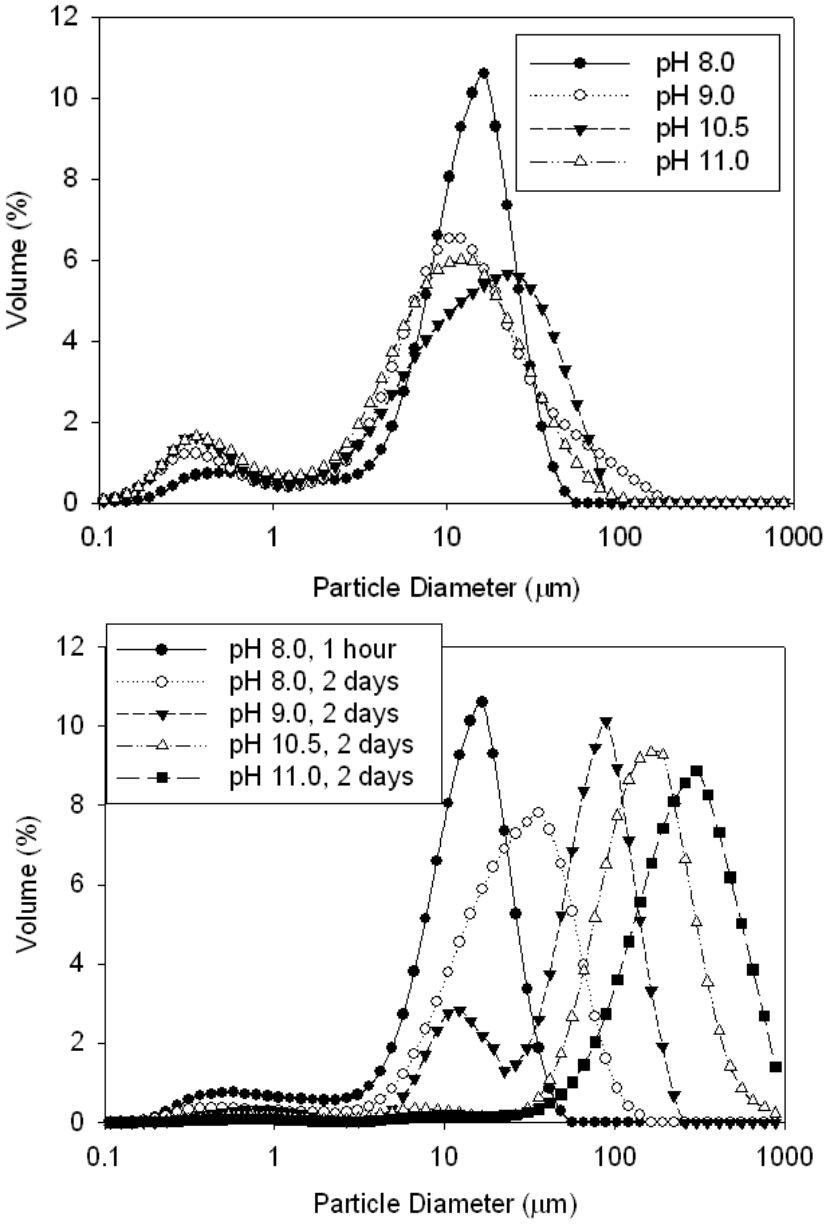

Figure 12. Calcium carbonate precipitate particle size distribution as a function of pH for measurements taken (a) directly following one hour precipitation and (b) two days after precipitation. Antiscalant concentration was 85 mg/L DQ2006.

Light microscope images, shown in Figure 13, were taken of calcium carbonate particles that were measured after two days. The particle images are consistent with the

particle size measurements obtained. The image for the pH 9.0 sample after two days shows the two particle size groups that are indicated by the two distinct peaks in the particle size distribution curve in Figure 12b. As the pH increases, the particles appear to have a more irregular shape and lose the regular rhombohedral structure seen for pH 9.0. The combination of particle size distribution measurements and microscopic imaging give a clearer picture of particle size.

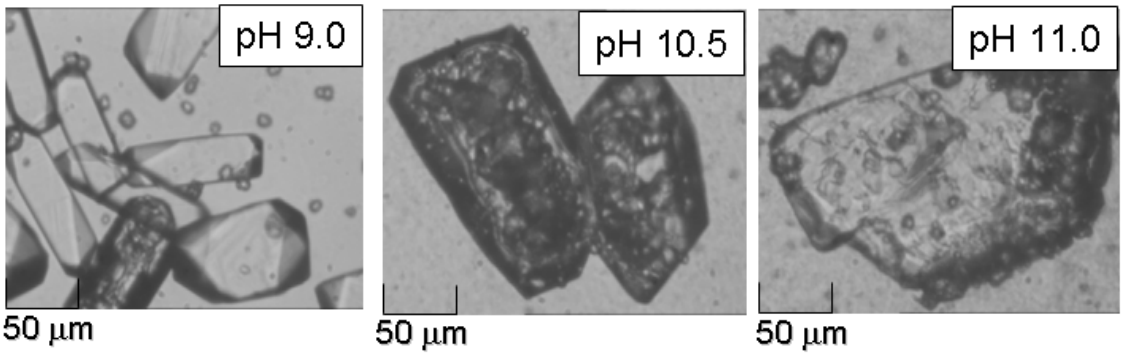

Figure 13. Light microscope images of calcium carbonate particle growth in the presence of phosphonate antiscalant DQ2006 (85 mg/L).

There are two possible explanations for the increase in modal particle diameter after two days; either additional precipitation occurred over the two days or the particles that were already precipitated combined and grew in size over the two days. The monomodal distributions for the aged samples, along with the unchanging pH values of the precipitated solutions and the microscope images (Figure 13), suggest that the increase in modal particle diameter resulted from flocculation, rather than additional precipitation. Previous research has suggested that at a Saturation Index of 2 or greater, calcium carbonate precipitation begins through the formation of crystal nuclei, and over time the nuclei coalesce together to form larger particles (Dove and Hochella, 1993;

Lebron and Suarez, 1996); Lebron and Suarez (1996) observed an increase in calcium carbonate particle size after 24 hours and SEM images confirmed the particles were clumps of smaller particles. In this study, additional precipitation would have caused the pH of the solution to decrease due to a loss of dissolved carbonate. The results of Figure 10 show more calcium carbonate precipitation as pH increased, and therefore more particles were available for flocculation and growth as pH increased. Previous work has shown that the dissolved ion concentrations can affect the rate of crystal growth and whether the growth is controlled by ion transport (convection and diffusion) or by the crystal surface (Nielsen and Toft, 1984). At low supersaturation, calcium carbonate precipitation is typically controlled by surface reactions, while at high supersaturation, which is the condition relevant to this study, precipitation is controlled by diffusion. When precipitation is controlled by diffusion, the crystal growth rate is primarily controlled by the lower ion concentration. As the pH increased from 8 to 11 (Figure 12), the initial carbonate concentration increased from 0.9 mM to 40 mM, while the initial calcium concentration was constant at 33 mM. The increase in the initial carbonate concentration may have contributed to the increase in particle size at longer times (2 days); while significant differences in particle size as a function of pH were not observed after one hour, it is possible that the solution was not at equilibrium after one hour, and particle growth continued to occur.

Another potential influence on particle size is the surface chemistry of the particles. Recent work and a compilation of data by Wolthers, et al., (2008) showed that the surface charge (zeta potential) of calcite (a polymorph of calcium carbonate) can vary dramatically with pH and under different experimental conditions at the same pH. In a discussion on varying zeta potential measurements for the same pH, Wolthers, et al., (2008) focused on the differences observed for washed versus unwashed calcite but did

not discuss calcite precipitated *in situ*, which would be the equivalent to the experiments performed in this study. However, the primary differences between washed and unwashed calcite were postulated to be small particles that rapidly dissolve, surface layers, and deposits present in unwashed calcite, but not in washed calcite. Calcite precipitated *in situ* from a simplified water composition as presented in Table 5 is most likely similar to the washed calcite samples, due to the absence of fine, rapidly-dissolving particles and surface deposits. Given this comparison, data presented by Wolthers, et al., (2008) for the change in zeta potential of washed calcite with changes in pH and excess dissolved calcium can be considered. For a calcite solution with no excess calcium, the zeta potential and calculated net surface charge of the particles is negative above a pH of 7. However, as the concentration of excess dissolved calcium was increased (1 and 10 mM), the researchers reported an increase in zeta potential and surface charge, and the point of zero charge of calcite increased from around pH 7 to around pH 9 (1 mM excess calcium) or pH 11.5 (10 mM excess calcium) (Wolthers, et al., 2008). For the present study, as pH increased from 8 to 11 and calcium precipitation increased (as shown in Figure 10), the excess calcium concentration decreased from 30 mM to 1.7 mM. The results presented by Wolthers, et al., (2008) suggest that the reduction in excess calcium from pH 8 to 11 may have lowered the point of zero charge to a pH similar to the experimental pH values (pH 10.5 – 11); the possible decrease in surface charge may have made the particles more amenable to agglomeration and growth since flocculation is typically the fastest at the point of zero charge.

Effect of antiscalant type and concentration on particle size and filtration flux

The effects of antiscalant type and antiscalant concentration were also investigated for the synthetic brackish water RO concentrate. All four antiscalants were tested, and results varied for each antiscalant. For antiscalants DQ2054 and Coatex, the

addition of antiscalant slightly decreased the modal particle diameter; an increase in DQ2054 concentration from 0 to 43 mg/L decreased the modal particle size from 53 μm to 35 μm, while an increase in Coatex concentration from 0 to 50 mg/L decreased the modal particle size to 40 μm. Microfiltration flux of the suspensions was not affected by the addition of DQ2054 or Coatex before precipitation. These results, along with the data shown in Figure 11, indicate that the phosphonate antiscalant DQ2054 (within the concentration range tested) does not arrest precipitate particle growth or significantly reduce calcium carbonate precipitation. However, for the polymer antiscalant Coatex, increasing the antiscalant concentration did decrease calcium precipitation, while the particle size distribution varied only slightly. Coatex appears to be as effective as DQ2006 and DQ2066 at preventing calcium carbonate precipitation but may have a weaker surface binding ability, resulting in the formation of larger particles. The chelating functional groups of Coatex are carboxylic acids, while the chelating groups of the phosphonates are phosphate groups; organo-phosphate moieties have a stronger calcium carbonate surface binding ability than carboxylic acids (Yang, et al., 2001).

More dramatic reductions in particle size were observed for the addition of antiscalants DQ2006 and DQ2066. For DQ2006 doses of 4 or 20 mg/L (0.5 or 2.5 mg/L DOC) (shown in Figure 14a), the particle size distribution shifted slightly from a modal particle diameter of 53 mm to 46 mm; for doses of 40, 60, and 85 mg/L (4.9, 7.4, and 10.5 mg/L DOC) (also shown in Figure 14a), the average particle diameter decreased to 12 μm. In addition, the particle size distribution for the higher DQ2006 concentrations becomes bimodal; the majority of the particles (on a number basis) formed are within the smaller particle size range (0.1 – 1 μm), as explained in the following section on SEM imaging. However, for DQ2066, the results are quite different, as shown in Figure 14b. The smallest dose, 3 mg/L (0.5 mg/L DOC), resulted in a significant decrease in modal

particle size diameter (37 μm), and concentrations of 13 and 56 mg/L (2.5 and 10.5 mg/L DOC) reduced the modal particle size diameter to 12 μm. These two concentrations also resulted in a bimodal particle size distribution. For the highest dose (i.e., 100 mg/L (18.8 mg/L DOC)), the average particle size increased to the same range of the control solution containing no antiscalant, at 53 μm; however, the particle size distribution curve indicates three groups of particle sizes, with two groups of smaller particles (0.1 – 1 μm and 1 μm – 10 μm).

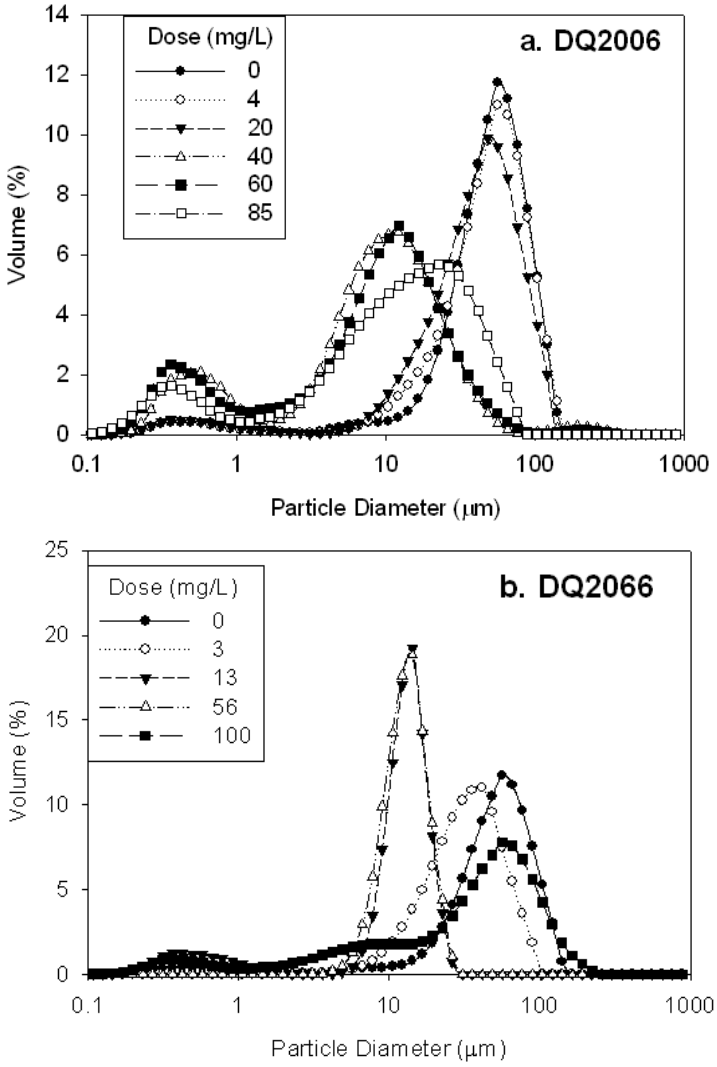

Figure 14. Variation in precipitated calcium carbonate particle size distributions and modality due to the presence of (a) DQ2006 and (b) DQ2066 antiscalant concentrations. Antiscalant doses are listed in the legend for each set of curves. Antiscalant added before precipitation, and precipitation performed at pH 10.5.

The subsequent microfiltration performance of the precipitated suspensions was affected by the changes in precipitate particle size. Microfiltration results for DQ2006, shown in Figure 15a, indicated how changes in precipitate particle size and morphology

influence filtration. The filtration results for a precipitated solution with no antiscalant and with 20 mg/L DQ2006 had similar flux performance; both experiments resulted in approximately 25% flux decline. However, the higher DQ2006 dose (85 mg/L) caused a greater flux decline (40%). The poorer flux performance of the experiment with 85 mg/L DQ2006 may be caused by increased particle fouling in the pores of the microfilter or changes to the filter cake caused by the presence of the antiscalant; in addition, SEM images (Figure 17c) indicate that the presence of higher concentrations of antiscalant cause the precipitated particles to stick together through web-like structures and form a denser cake on the membrane surface. The other two antiscalant doses (0 and 20 mg/L) resulted in larger particles that also formed a visible cake layer on the surface of the membrane. To verify that the additional flux decline is caused by the interaction of the antiscalant with the precipitate and not solely the antiscalant itself, filtration experiments were performed with solutions of deionized water and antiscalant. Flux results revealed little to no flux decline due to antiscalant addition.

All doses tested for DQ2066 caused changes to the microfiltration performance (results shown in Figure 15b). While a dose of 3 mg/L resulted in an improvement in flux performance, doses from 13 to 100 mg/L caused poorer flux performance, as compared to the precipitated solution containing no antiscalant. The intermediate doses of 13 and 56 mg/L resulted in the same particle size distribution, as well as the same flux decline during microfiltration. While the dose of 100 mg/L caused an increase in particle size for a portion of the precipitate, many smaller particles were still present, resulting in a greater flux decline than the precipitated solution with no antiscalant. The improvement in flux performance caused by a small antiscalant dose of 3 mg/L DQ2066 may be due to the decrease in precipitation and minimal change to particle morphology.

The same effect of small antiscalant dose on improved microfiltration performance was observed for 4 mg/L DQ2006.

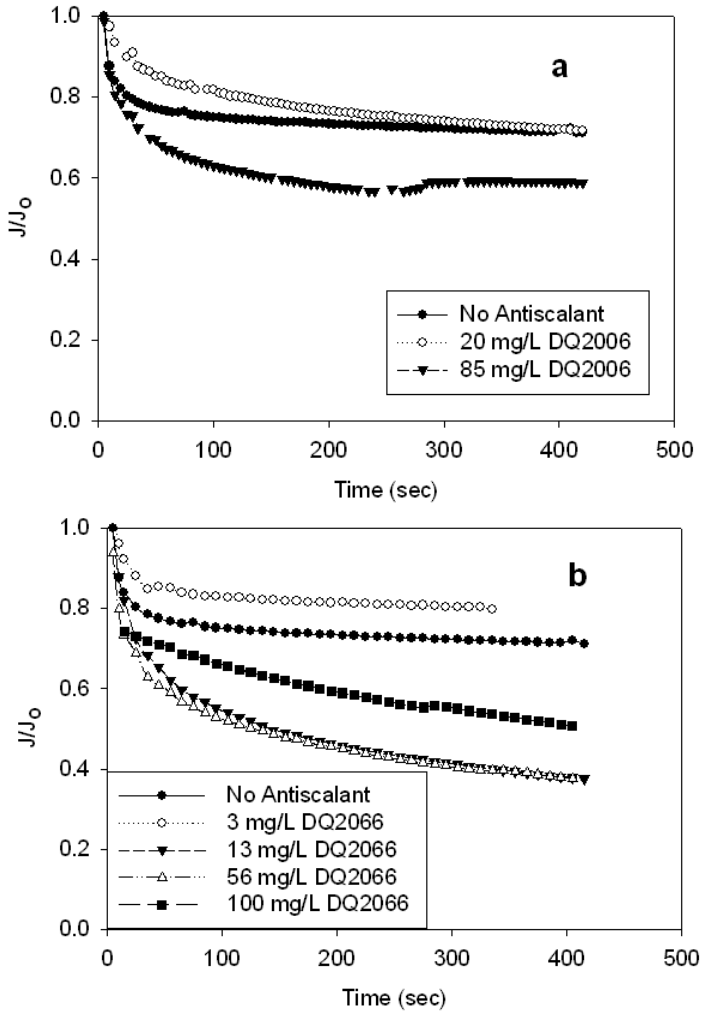

Figure 15. Microfiltration flux performance for antiscalant-free precipitated solutions and comparison to precipitated solutions with (a) DQ2006 and (b) DQ2066 antiscalant concentrations (0.1 μm pore size). Precipitation performed at pH 10.5 after addition of antiscalant.

Previous research on types of membrane fouling (Grenier, et al., 2008; Hermia, 1982; Wang and Tarabara, 2008) have illustrated several techniques to determine the

fouling category based on permeate mass data. Grenier, et al. (2008) used the first and second derivatives of time divided by volume to evaluate fouling; the relationship between t/V and fouling mechanism was first identified by Hermia (1982). However, an analysis of the data from this study using the derivatives method was not successful due to the sensitivity of the method to data scatter. Following the method used by Wang and Tarabara (2008), the microfiltration data were evaluated using the integrated forms of the equations developed by Hermia (1982) to categorize the fouling.

Hermia (1982) identified four possible types of fouling or pore blocking mechanisms, including complete blocking, intermediate blocking, standard blocking, and cake filtration. Complete blocking occurs when a particle has the same diameter and shape as the pore and completely blocks the pore opening at the surface of the membrane. Standard blocking occurs when particles are slightly smaller than the membrane pores and travel part way through the membrane, causing internal fouling. Intermediate blocking occurs at the membrane surface when each particle partially blocks a pore, effectively blocking the pore opening. Finally, cake filtration occurs when the particles form a dense layer of precipitate on the surface of the membrane that acts as an additional resistance to water permeation. Illustrations of the types of fouling can be found elsewhere (Grenier, et al., 2008; Wang and Tarabara, 2008). A complete analysis for both DQ2066 and DQ2006 can be found in the Supplementary Information (Appendix A), with an example of analysis shown in Figure 16 for antiscalant DQ2066 and complete blocking.

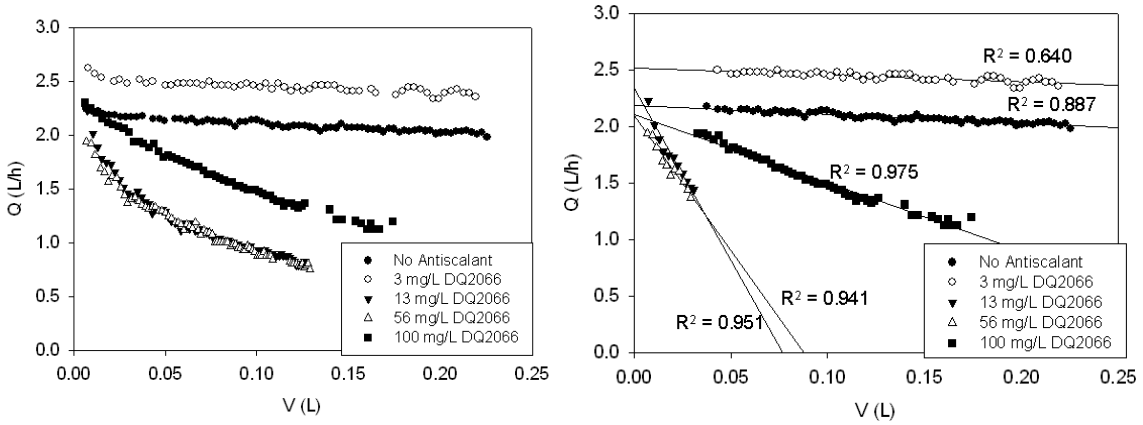

Figure 16. Analysis of DQ2066 microfiltration data for complete blocking.

A summary of the fouling mechanisms determined for each antiscalant over a range of concentrations is shown in Table 6. For most antiscalant concentrations, the data fit several of the blocking models, and the models predicted that the type of fouling changed during the course of microfiltration. For most samples, multiple fouling mechanisms were predicted to be operative at the same time. The blocking models identified to explain fouling were similar for antiscalant doses of 0 mg/L, 3 mg/L DQ2066, and 4 mg/L DQ2006, while larger antiscalant doses resulted in different combinations of fouling mechanisms. The results for 13 and 56 mg/L DQ2066 were similar. For these two antiscalant doses, the complete blocking model fit the flux data during the first minute of filtration; after one minute, intermediate blocking became the acting fouling mechanism. Complete blocking is primarily caused by total blockage within the pores, while intermediate blocking includes both pore blockage and a build-up of a fouling cake layer on the surface. The largest doses of 100 DQ2066 and 85 mg/L DQ2006 resulted in data that fit all four blocking models; however, for DQ2006, none of the fouling mechanism relationships resulted in a linear region during the first minute of

filtration, and it is unclear which mechanism(s) are responsible for initial fouling in this case.

Table 6. Summary of fouling mechanisms for antiscalants DQ2066 and DQ2006 during microfiltration (0.1 μm pore size) of the precipitated suspensions.

Antiscalant	**Dose (mg/L)**	**Fouling Mechanism**	**Start of Fouling (min)**
DQ2066	0, 3	Intermediate Blocking	0
DQ2006	4	Standard Blocking/Cake Filtration	1.4
DQ2066	13	Complete Blocking	0
		Intermediate Blocking	1
		Cake Filtration	1.5
		Standard Blocking	2
	56	Complete Blocking	0
		Intermediate Blocking/Cake Filtration	1
		Standard Blocking	1.4
	100	Intermediate Blocking/Standard Blocking/Cake Filtration	0
		Complete Blocking	1
DQ2006	20	Intermediate Blocking	0
		Standard Blocking/Cake Filtration	1.5
	85	Intermediate Blocking/Standard Blocking/Cake Filtration/Complete Blocking	1

For both antiscalants DQ2006 and DQ2066, the results suggest that the changes in particle size distribution caused by the addition of antiscalant affect the subsequent microfiltration flux performance. A decrease in particle size appears to allow complete blocking to become a fouling mechanism; this result is evident in the fouling study results for higher antiscalant concentrations. The antiscalant-free solution, along with solutions

containing 3 mg/L DQ2066, 4mg/L DQ2006, and 20 mg/L DQ2006, did not display complete blocking or a reduction in filtration flux. However, solutions containing higher antiscalant concentrations did have poorer flux performance and complete blocking as a fouling mechanism. In theory, complete blocking occurs when a particle fits into a pore and completely blocks solvent flow through the pore (Wang and Tarabara, 2008). In this study, the microfiltration nominal pore size was 0.1 μm, and the smaller particles formed at higher antiscalant concentrations could fit into the pores, while the larger particles would only collect on the surface and form a cake layer. In addition, the higher antiscalant concentrations may aid in particle agglomeration on the membrane surface, creating a more dense cake layer that is resistant to water flux. Both effects, smaller particle size and particle agglomeration, would cause the microfiltration flux to decrease more over time.

SEM images of calcium carbonate and DQ2006

SEM images of calcium carbonate precipitation in the presence and absence of antiscalant revealed changes in both the size and shape of the precipitate due to antiscalant addition. For the phosphonate antiscalant DQ2006, two concentrations (20 mg/L and 85 mg/L) were tested, along with a control experiment which included no antiscalant. The images, shown in Figure 17, compare the three cases at similar magnifications (1 - 3 μm), with an additional image of 85 mg/L DQ2006 at higher magnification (300 nm). Both the spherical vaterite and rhombohedral calcite phases of calcium carbonate are present in the precipitated solution with no antiscalant (Figure 17a).

In a typical aqueous system, calcium carbonate will first nucleate and precipitate as vaterite and will transition to a more stable phase (aragonite or calcite) with time (Chakraborty, et al., 1994). The solubility constants, K_{sp}, of vaterite, aragonite, and

calcite are $1.41x10^{-8}$, $4.61x^{-9}$, and $3.31x10^{-9}$, respectively. Chakraborty et al. (1994) extensively studied calcium carbonate precipitation for different molar ratios of calcium to carbonate and examined particle size and particle morphology. They found that, in a typical jar test, for low molar ratios of calcium to carbonate (0.8-1), scale quickly forms on the surfaces of the reactor; precipitation is initially heterogeneous, initiated at the reactor surfaces, and becomes homogeneous bulk precipitation once the reactive sites on the reactor walls are blocked. The change from heterogeneous to homogeneous precipitation is also accompanied by an increase in particle size; results showed the average particle size increased from 1 μm to 5 – 6 μm. In the present study, the molar ratio of calcium to carbonate was approximately 0.8 (after the addition of sodium bicarbonate before pH elevation to start precipitation), and the SEM images reveal particles within the range reported by Chakraborty et al. (1994).

Previous cryo-SEM results also showed that, for a calcium/carbonate molar ratio of 0.8, the precipitate formed both vaterite and calcite (Chakraborty, et al., 1994). The researchers only observed aragonite (needle-like shape) in off-line images taken after the precipitation experiment and attributed this formation of aragonite to nucleation on other surfaces (such as flasks or other sample containers) after the main experiment. The results from the present work for calcium carbonate in the absence of antiscalant are consistent with and confirmed by these previous results. No needle-like particles were observed in any of the samples tested; aragonite typically forms under conditions of high temperature (above 40 ^{o}C) (Chakraborty, et al., 1994).

When 21 mg/L DQ2006 was added to the synthetic brackish water RO concentrate, the resulting precipitate morphology was different (Figure 17b). The particle size of the precipitate did not significantly change, but the crystal structures of both the vaterite and calcite particles were less uniform. The vaterite particles appeared

slightly more globular, and some appeared partially formed and connected to other vaterite particles. The calcite particles still had the basic rhombohedral or cubic shape, but the particles had less well-defined edges and appeared to have a layered-like structure.

The change in particle morphology was more dramatic for the precipitated solution with 85 mg/L DQ2006 (Figure 17c & d). All of the particles in the sample were much smaller, on the order of 50 – 100 nm, and they were nearly spherical with rough edges and appeared to associate together in a large film on the membrane support. While calcite is the most stable form of calcium carbonate, previous research has shown that less thermodynamically stable forms can be stabilized by other ions or organic compounds in solution, including antiscalant-type organophosphonates (Yang, et al., 2001). The precipitated sample with 85 mg/L DQ2006 resulted in nucleated vaterite particles; the secondary or homogeneous precipitation step was completely prevented, even at the elevated precipitation pH (10.5), by the antiscalant. The web-like, small particle precipitate was responsible for the increase in microfiltration membrane fouling (and subsequent flux decline seen in Figure 15a) during the solid/liquid separation step. When the SEM images for 85 mg/L DQ2006 are compared to the particle size distribution results of Figure 14a, there were no individual particles larger than 100 – 200 nm. Therefore, the second mode of the bimodal curve (approximate particle size range from 3 to 100 μm) resulted from particle agglomeration. In contrast, the antiscalant-free and 21 mg/L DQ2006 samples both contained larger particles from the growth of nucleated crystals.

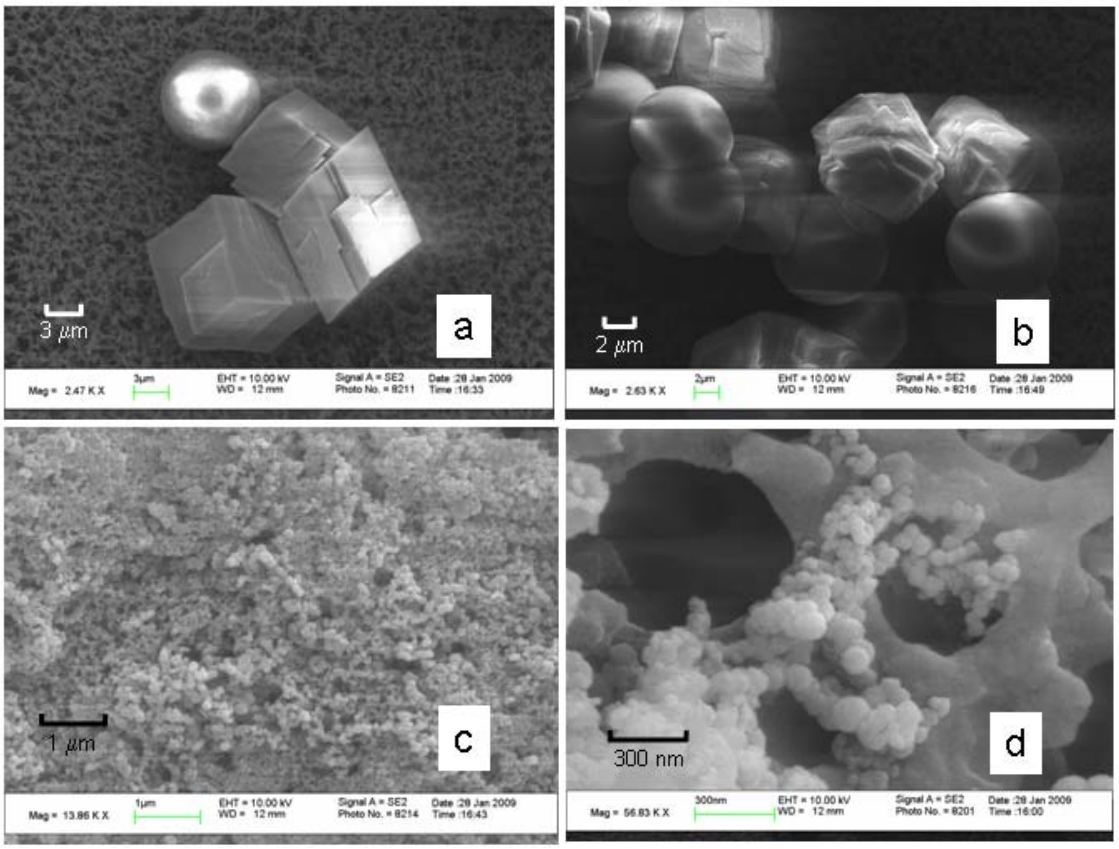

Figure 17. SEM images of precipitated calcium carbonate at pH 10.5: (a) no antiscalant; (b) 21 mg/L DQ2006; (c & d) 85 mg/L DQ2006. Particles were on a 0.22 μm Millipore nitrocellulose membrane support.

SEM images for the DQ2066 doses considered can be found in Supplementary Information (Appendix A). For the lowest dose, 3 mg/L, both vaterite and calcite were observed, and the presence of this small antiscalant dose did not greatly change the particle morphology. A dose of 13 mg/L resulted in irregular spherically-shaped particles, while a dose of 56 mg/L resulted in both spherical and rod-like particles. Finally, the largest dose of 100 mg/L resulted in a dense layer of precipitate on the membrane surface, with small particles (approximately 200 – 300 nm) distinguishable at higher magnification. The particles, similar to those formed for 85 mg/L DQ2006,

appear to be attached through web-like connections. As with 85 mg/L DQ2006, the 100 mg/L DQ2066 sample contained no large particles, and the second and third modes of the particle size distribution are a result of agglomerated particles measured as one larger particle.

While the particle size distribution and microfiltration flux data for DQ2066 are consistent, the results are not intuitive. Based on the presence of the smaller particles in the 100 mg/L sample (as observed in the particle size distribution data and confirmed by the SEM results), the flux of this sample could be expected to decline the most. However, the 13 and 56 mg/L samples resulted in the poorest flux performance. The formation of rod-like particles, along with particle agglomeration and the formation of a more dense cake layer due to the presence of antiscalant may have caused the increase in microfilter fouling. The rod-like particles may be more effective at blocking the membrane surface and decreasing water flux.

CONCLUSIONS

Increasing the recovery of a reverse osmosis system that treats inland brackish water requires a novel approach, such as side-stream concentrate treatment, to increase the overall recovery of the system and reduce concentrate waste volume. The treatment of RO concentrate to remove scaling precipitates could be a viable method of improving RO recovery. While the presence of antiscalants within the RO system helps prevent salt precipitation and membrane scaling, antiscalants may have a deleterious effect on the use of salt precipitation in concentrate treatment. Antiscalants not only prevent calcium precipitation, even at extremely high saturation indices, but can reduce precipitate particle size and cause increased fouling during filtration of the precipitated salts. Results from this study have shown that:

- An increase in pH causes an increase in calcium carbonate precipitation for solutions with and without antiscalants. Calcium carbonate precipitation typically occurs at pH values of 7 or higher, as the carbonate system speciation shifts from carbonic acid (H_2CO_3) to bicarbonate (HCO_3^-) and subsequently carbonate (CO_3^{2-}), and carbonate becomes the primary species. As pH increases from 8.0 to 11.0, the saturation index of calcium carbonate increases, and the difference between final dissolved calcium concentrations for antiscalant-dosed and antiscalant-free solutions diminishes. The larger the saturation index, the more the effect of the antiscalant is overcome, and more precipitation occurs. However, even at pH 11.0, the final calcium concentration of antiscalant-dosed samples remains higher than that of antiscalant-free samples.
- The addition of antiscalants to synthetic brackish water concentrate reduces the amount of calcium carbonate precipitated. At pH 8.0, addition of antiscalant caused 91% of the calcium to remain in solution, while in the antiscalant-free solution, 13% of the calcium remained.
- Increasing the antiscalant concentration from 0.5 to 10.5 mg/L DOC decreases the amount of calcium precipitated. For three of the four antiscalants tested, concentrations from 0.5 to 2.5 mg/L DOC caused a significant increase in the calcium remaining in solution after precipitation and filtration, while higher antiscalant concentrations resulted in little to no increase in final dissolved calcium. The antiscalant DQ2054 was not effective in preventing calcium carbonate precipitation, most likely due to poor adsorption of the antiscalant onto nucleating crystals.
- In the presence of antiscalants, precipitated calcium carbonate particles increase in particle size over time. Particle size is not a function of pH for measurements

taken directly following precipitation, but after two days, particle size increases with pH. Initially, the presence of antiscalants caused a bimodal particle size distribution, and over time, the smaller, nucleated particles combined and grew into larger particles. More precipitation occurs as pH increases, thus allowing larger particles to form in aged samples at higher pH.

- The presence of antiscalants during calcium carbonate precipitation can change the particle size and shape of the precipitate and affect subsequent microfiltration. For a simplified RO concentrate, addition of antiscalant tends to decrease precipitate particle size. In particular, high antiscalant (DQ2006 and DQ2066) concentrations completely prevent crystal growth, and only small (100-300 nm) particles form. These small particles cause complete pore blocking and may agglomerate, causing a denser cake layer on the membrane surface. Results indicate that both fouling mechanisms play a role in causing a decrease in filtration flux.

While significant calcium removal can be achieved in the presence of antiscalants when the saturation index is increased (through an increase in pH for calcium carbonate), the removal of antiscalants may increase calcium precipitation and the overall performance of the concentrate treatment process. An even greater removal of calcium would further reduce the precipitation potential of the filtered solution, allowing a greater recovery in the secondary RO stage. Increased calcium precipitation could be achieved by removing or deactivating the antiscalants prior to the precipitation step.

Chapter 5: Effect of antiscalants on precipitation of an RO concentrate: Metals precipitated and particle characteristics for several water compositions[2]

ABSTRACT

Inland brackish water reverse osmosis (RO) is economically and technically limited by the large volume of salty waste (concentrate) produced. The use of a controlled precipitation step, followed by solid/liquid separation (filtration), has emerged as a promising side-stream treatment process to treat reverse osmosis concentrate and increase overall system recovery. The addition of antiscalants to the RO feed prevents precipitation within the membrane system but may have a deleterious effect on a concentrate treatment process that uses precipitation to remove problematic precipitates. The effects of antiscalant type and concentration on salt precipitation and precipitate particle morphology were evaluated for several water compositions. The primary precipitate for the synthetic brackish waters tested was calcium carbonate; the presence of magnesium, sulfate, minor ions, and antiscalant compounds affected the amount of calcium precipitated, as well as the phases of calcium carbonate formed during precipitation. Addition of antiscalant decreased calcium precipitation but increased incorporation of magnesium and sulfate into precipitating calcium carbonate. Antiscalants prevented the growth of nucleated precipitates, resulting in the formation of small (100 – 200 nm diameter) particles, as well as larger (6 – 10 μm) particles. Elemental analysis revealed changes in composition and calcium carbonate polymorph with antiscalant addition and antiscalant type. Results indicate that the presence of antiscalants does reduce the extent of calcium precipitation and can worsen subsequent filtration performance.

[2] Manuscript to be submitted to the journal Water Research.

Key Words

Desalination

Antiscalants

Reverse osmosis

Concentrate treatment

Precipitation

Brackish water

Nomenclature

ATMP	Aminotri(methylene phosphonic acid)
DOC	Dissolved organic carbon
DTPA	Diethylenetriamine-pentaacetate
DTPMP	Diethylenetriamine penta(methylene phosphonic acid)
HDTMP	Hexamethylenediamine tetra(methylenephosphonic acid
IAP	Ion activity product
K_{sp}	Solubility constant
MSF	Multi-stage flash
NMR	Nuclear magnetic resonance
NOM	Natural organic matter
RO	Reverse osmosis
SI	Saturation index
TDS	Total dissolved solids concentration (mg/L)
TOC	Total organic carbon concentration (mg/L)
wt%	Weight percent (mass component/total mass*100%)

INTRODUCTION

Brackish water desalination has emerged as one of the key water treatment technologies to provide drinking water for communities and countries throughout the world. Traditional fresh water resources such as lakes and rivers are dwindling, and ground water aquifers are becoming increasingly saline (Service, 2006). In many countries, large natural brackish water aquifers are essentially untapped water resources that could supplement current fresh drinking water supplies (Sandia, 2003). Brackish water contains between 1 and 10 g/L total dissolved solids (TDS).

Reverse osmosis (RO) membranes are the primary choice in desalination technology; RO desalination requires much less energy than thermal desalination (evaporation) (1.5-2.5 kWh/m^3 for RO versus 15-25 kWh/m^3 for evaporation) (Service, 2006), and improvements in membranes and energy recovery have dropped the cost of RO desalination significantly.

The key limitation of the application of RO desalination to inland brackish water is the volume of the waste stream, or concentrate, produced. The recovery (ratio of the product volume to the feed volume) of a brackish water RO system is typically limited to 60-90%; in comparison, a typical fresh water treatment plant has recoveries above 99%. Such a large waste volume results in high disposal costs and is environmentally undesirable, thereby reducing the feasibility of using RO. Brackish water RO recovery is limited by certain sparingly soluble salts ($CaCO_3$, $CaSO_4$, $BaSO_4$, $SrSO_4$, silica) in the feed water that become supersaturated during RO desalination and can precipitate on the membrane surface. Such membrane fouling, called scaling, can sometimes be removed by chemical cleaning processes, but often the membranes are permanently fouled and require replacement.

Synthetic chemicals called antiscalants are dosed to the RO feed stream to prevent precipitation. As crystals nucleate, antiscalants adsorb onto growth sites and prevent further growth and precipitation. Antiscalants may also prevent precipitation through particle dispersion. However, antiscalants (and pH control) only enable RO systems to achieve the recovery range stated above; to further increase RO system recovery, alternative methods must be used.

One promising method is to treat the RO brackish water concentrate through a controlled precipitation step, followed by solid/liquid separation to remove precipitated salts (typically sedimentation and filtration). Concentrate treatment allows removal of the problematic sparingly soluble salts and enables a secondary RO system (following concentrate treatment) to operate at high recovery, increasing the overall system recovery and reducing the volume of concentrate to be disposed. Rahardianto, et al., (2007) showed that most (90-95%) of the calcium present can be removed, but greater calcium removal was achieved in synthetic RO concentrate (95%) than in the field water sample tested (90%) (Rahardianto, et al., 2007). The authors hypothesized that natural organic matter (NOM) and/or the antiscalant present (30 mg/L) were mostly likely responsible for the decrease in calcium precipitation in the field sample.

This paper focuses on the possibility that the antiscalants are responsible for the reduced precipitation. The objectives were to determine how antiscalant compounds in synthetic brackish water RO concentrate affect the precipitation and the subsequent solid/liquid separation. Four different antiscalants were investigated, and the role of several water components was evaluated through four different water compositions of increasing complexity. For the precipitation step, not only was the extent of calcium precipitated measured, but the precipitated particles were evaluated for differences in size distribution and particle morphology. For the solid/liquid separation step, the flux

through microfiltration membranes (0.1 μm pore size) was the primary measure of the effects of the antiscalants.

EXPERIMENTAL METHODS

Antiscalants

Phosphonate antiscalant samples were obtained from Dequest Water Management Additives, a subsidiary of Thermophos. The antiscalants included the penta-sodium salt of aminotri(methylene phosphonic acid), or ATMP, the hexa-potassium salt of hexamethylenediamine tetra(methylenephosphonic acid), or HDTMP, and the hepta-sodium salt diethylenetriamine penta(methylene phosphonic acid) or DTPMP. Dequest refers to ATMP as DQ2006, to HDTMP as DQ2054, and to DTPMP as DQ2066, and these commercial names are used throughout this article. The polymer antiscalant was obtained from Coatex S.A. (France) and is a proprietary polymer containing 19% acrylic acid, 20% methacrylic acid, and 61% itaconic acid, as determined by proton nuclear magnetic resonance (NMR) spectroscopy. The antiscalants chosen are recommended by the manufacturers for general scale control and are used in various systems, including boiler water treatment, reverse osmosis desalination, and cooling water treatment. Total organic carbon (TOC) and total solids analysis were used to determine the mass and organic carbon concentrations of all the antiscalants.

Water Data

The synthetic concentrates used for precipitation experiments were based on the chemical composition of a brackish groundwater in Maricopa County, Arizona, USA (Jurenka and Chapman-Wilbert, 1996). Four different water compositions, shown in Table 7, were tested to determine the effect of major ions such as magnesium and sulfate

on calcium precipitation and antiscalant performance. To isolate the impacts of magnesium and sulfate on precipitation, each was added to the Simplified Maricopa water composition; the fourth water composition included both magnesium and sulfate, as well as other minor ions. The data for the "complete" Maricopa water shown in Table 7 were determined based on a theoretical 80% recovery and 100% rejection of all ions. The simplification of assuming 100% rejection results in synthetic RO concentrate that is five times as concentrated as the feed. In an operating reverse osmosis system, the membranes can have rejections of greater than 99% for most ions. The initial pH of the synthetic concentrates was 7.8.

Table 7. Composition of waters used for precipitation experiments.

	Water Type and Composition (mg/L)			
Component	**Simplified Maricopa (SM)**	**Simplified Maricopa + Na_2SO_4**	**Simplified Maricopa + $MgCl_2$**	**Complete Maricopa**
Na^+	1,552	2,027	548	849
Ca^{2+}	1,330	1,330	1,330	1,330
Mg^{2+}	---	---	514	514
Ba^{2+}	---	---	---	2.0
Fe^{3+}	---	---	---	2.3
Cl^-	4,163	4,163	4,114	3,933
SO_4^{2-}	---	991	---	991
NO_3^-	---	---	---	89
Alkalinity (as $CaCO_3$)	780	780	780	780
Total Dissolved Solids (TDS)	8,037	9,503	7,499	8,790

Experimental Design

The thermodynamic equilibrium software, PHREEQC (version 2.15.0.2697), available through US Geological Survey, was used to calculate saturation indices and predict precipitates. This software was chosen over others due to the available database that uses the Pitzer equations for activity calculations (Pitzer, 1991) that are appropriate for high ionic strength conditions.

The precipitation experiments were all performed as 500 mL batch experiments in a jar test apparatus (Fisherbrand model 10008 or Phipps & Bird Stirrer model 7790-400). To start each precipitation experiment, synthetic concentrate was made in the laboratory by first adding antiscalant and then adding individual salts from stock solutions. Preliminary experiments were performed to determine the effect of the order of addition of antiscalant and salts on precipitation, and results showed no difference in the amount of calcium precipitated or changes in the precipitated particle size distributions. Before precipitation, the total carbonate was increased to from 16 mM to 42 mM HCO_3^- (2560 mg/L) so that calcium precipitation was not limited by the availability of carbonate and to provide excess carbonate to stabilize the pH during precipitation. Then the pH was increased to 10.5 with 6 M NaOH. Increasing the pH to 10.5 increased the degree of supersaturation to the extent that significant precipitation occurred even in the presence of antiscalants.

The separation step was performed using 0.1 μm pore size Millipore nitrocellulose membranes in either a dead-end pressurized (0.5 bar) cell with a stir bar or using a Millipore glass filter holder assembly (47 mm diameter, 300 mL filter holder) under vacuum. The dead-end filtration cell was used with a digital mass balance to measure filtrate (permeate) flux. Samples filtered with the vacuum assembly were analyzed for dissolved calcium.

Analytical Methods

Inductively coupled plasma atomic emission spectroscopy (ICP-AES) was used to analyze metal concentrations before and after precipitation experiments. A Spectro Ciros CCD Model (Spectro AI GmbH) was used with Smart Analyzer data acquisition software (version 3.2, 1995-2000). Samples were analyzed for calcium, magnesium, barium, and iron. Standards were made with appropriate sodium chloride additions to avoid ion

effects on ICP concentration results. Samples were prepared in 15 mL screw-cap polypropylene centrifuge tubes with concentrated nitric acid added for a final concentration of 1.5% (v/v). If necessary, samples were stored at 4 ^{o}C for no longer than 2 weeks before analysis. Some calcium and magnesium measurements were made using standard titrations for calcium and hardness with ethylenediaminetetraacetic acid (EDTA) (Eaton, et al., 2005).

All pH measurements were taken with a Thermo Electron Corp. pH meter (Orion 720 A+), calibrated with three buffers (pH 4, 7, and 10 standard buffers). The pH of a solution changes with ionic strength (Baumann, 1973; Wiesner, et al., 2006). Therefore, 0.14 M sodium chloride was added to each pH buffer to account for experimental solution ionic strength. Based on previous work (Wiesner, et al., 2006), 0.14 M NaCl causes a decrease in pH of no more than 0.1 pH units in the standard buffers, and therefore no recalculation of buffer pH was performed. pH values are reported as recorded based on pH meter calibration with the salted buffers.

Particle size distributions were obtained using a laser granulometer Mastersizer S (Malvern Instruments). The Mastersizer S js a static laser light scattering instrument with associated computer software to convert the data to a relative volume distribution based on equivalent spherical diameter. A polydisperse deconvolution algorithm and the Fraunhofer theory translate the detected light scattering data (diffraction intensity as a function of diffraction angle) into a best-fit particle size distribution.

An ion chromatography system (Metrohm 700 series, column Metrosep A Supp 5, 150/4.0 mm) was used to measure sulfate concentrations after precipitation and filtration. Some sulfate measurements were taken with a Hach Ratio/XR turbidimeter; the turbidimeter was used to measure barium sulfate turbidity and to ultimately obtain sulfate

concentrations in filtered precipitated samples (Standard Method 4500-SO_4^{2-} E) (Eaton, et al., 2005)..

Two different scanning electron microscopes (SEM), a LEO 1530 and a Hitachi S-5500, were used to obtain images of the precipitates. Both SEMs were equipped with energy dispersive x-ray (EDX) elemental analysis. Samples were mounted on adhesive carbon tabs; precipitates were placed directly onto the carbon tab or were on a nitrocellulose microfilter that was placed on the carbon tab. All samples were sputter coated with silver. Samples used for SEM analysis were taken from a set of repeat precipitation experiments performed under identical conditions as those performed to obtain particle size distribution measurements; SEM data and particle size distribution data were used together to explain changes caused by antiscalant addition.

RESULTS AND DISCUSSION

Calculation of saturation indices and precipitate prediction

To predict the potential for precipitation in a concentrate, the ratio of the ion activity product (IAP) to the solubility constant (K_{sp}) of a specific salt can be calculated; when this ratio, termed the saturation index (SI), has a value of one (log value of zero), the solution is saturated with the salt. Log SI values greater than zero indicate that the salt is supersaturated and may precipitate out of solution, while negative values indicate the solution is undersaturated. The log of the saturation indices (log (IAP/K_{sp})) for individual salt precipitates in the four waters presented in Table 7 were calculated using the thermodynamic modeling program PHREEQC Interactive (Version 2.15.0.2697) (Parkhurst and Appelo, 2008); results for predicted precipitation at pH 10.5 are presented

in Figure 18. Calculations include the additional bicarbonate added prior to precipitation to increase calcium removal.

Calcium carbonate is predicted to precipitate for all four water compositions, and the log SI for each of the three calcium carbonate phases (calcite, aragonite, and vaterite) changes only slightly between each water composition. While the calculations indicate that any of the three phases could form, only calcite is thermodynamically stable. Aragonite and vaterite are metastable and will eventually transform into calcite; both calcite and vaterite have been observed during precipitation at room temperature, while aragonite is typically only observed at higher temperatures (> 40^{o}C) (Chakraborty, et al., 1994). Vaterite typically has a spherical or disc-shaped morphology, while aragonite is needle-like, and calcite is cubic or rhombohedral. Thermodynamically, vaterite and aragonite should eventually transform into calcite; however, the presence of other ions or additives (such as antiscalants) can stabilize the less thermodynamically stable forms of calcium carbonate (Chakraborty, et al., 1994). In addition, vaterite can be the primary precipitated form of calcium carbonate when the solution has a high supersaturation value and a high yield of precipitate (Andreassen and Hounslow, 2004).

For both water compositions that contain sulfate, the primary sulfate precipitate, gypsum, is not predicted to precipitate; the log SI values are slightly negative for both Simplified Maricopa + Na_2SO_4 and Complete Maricopa. However, for the two water compositions that contain magnesium, positive log SI values were obtained for three magnesium precipitates, brucite, magnesite, and dolomite. For the Complete Maricopa water, both the barium and ferric iron are predicted to precipitate. The primary precipitate for barium is barium sulfate, or barite, while the primary precipitate for ferric iron is hematite.

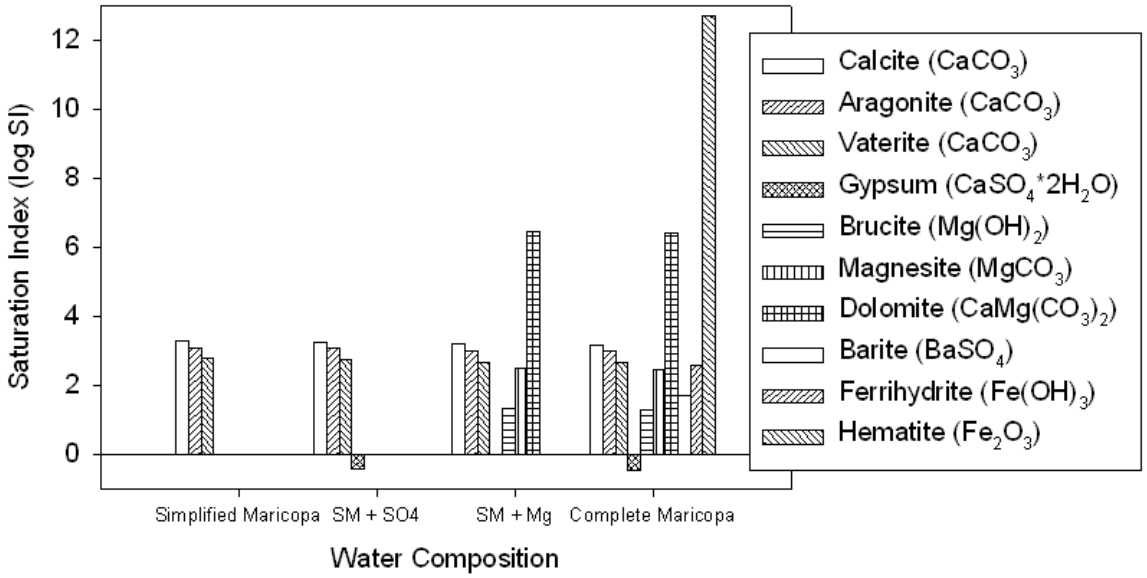

Figure 18. Saturation indices and salts that are predicted to precipitate for each of the four water compositions tested. SM = Simplified Maricopa. pH = 10.5.

SEM imaging and EDX analysis of precipitated particles without antiscalants

Scanning electron microscopy (SEM) images of the precipitates formed in the absence of antiscalants for the four water compositions are shown in Figure 19. The morphology of the precipitated particles is similar for the Simplified Maricopa and the Simplified Maricopa + Na_2SO_4 water compositions (Figure 19a & b). The precipitates from the Simplified Maricopa + $MgCl_2$ and Complete Maricopa water compositions (Figure 19c & d) are also quite similar to each other but considerably different from the first two. The addition of sulfate to the Simplified Maricopa water did not appear to significantly affect particle morphology, but the addition of magnesium changed and controlled morphology for both Simplified Maricopa + $MgCl_2$ and Complete Maricopa waters.

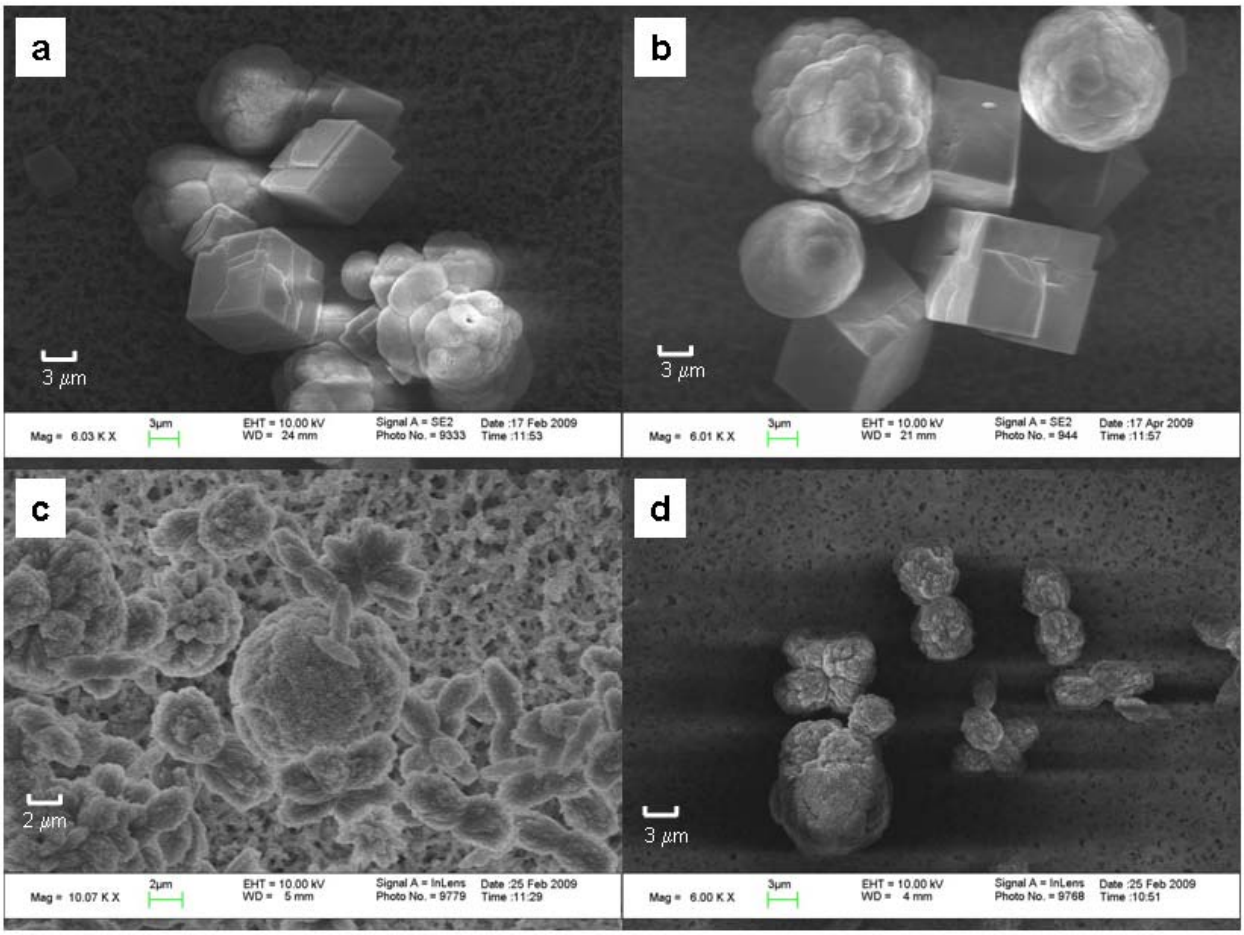

Figure 19. Comparison of four different water compositions tested without antiscalant present; (a) Simplified Maricopa, (b) Simplified Maricopa + Na_2SO_4, (c) Simplified Maricopa + $MgCl_2$, and (d) Complete Maricopa. Precipitation pH was 10.5.

Extensive work has been reported on the crystallization and morphology of calcium carbonate, both as a pure, saturated solution and with other additives, such as various cations and organic compounds (Brečević, et al., 1996; Brooks, et al., 1950; Clarkson, et al., 1992; Falini, et al., 2009; Lam, et al., 2007; Nancollas and Sawada, 1982; Nebel and Epple, 2008; Nebel, et al., 2008; Ogino, et al., 1987; Reddy and Wang, 1980; Sawada, 1997; Wada, et al., 1995; Westin and Rasmuson, 2005; Yang, et al.,

2001). The thermodynamically stable form of calcium carbonate is calcite, with aragonite and vaterite considered to be metastable forms that eventually form calcite. Calcite, aragonite, and vaterite are all anhydrous forms of calcium carbonate; three additional hydrated forms of calcium carbonate may also form during precipitation, including monohydrocalcite ($CaCO_3*H_2O$), ikaite ($CaCO_3*6H_2O$), and amorphous calcium carbonate (ACC) (Brečević, et al., 1996; Lam, et al., 2007).

Amorphous calcium carbonate has been shown to have a variable composition, and recent work has indicated that the internal structure of this carbonate can have the crystalline structure of the subsequent anhydrous calcium carbonate phase (Nebel, et al., 2008). ACC becomes more stable when magnesium, phosphate, or organic compounds are present. The influence of additives is thought to affect not only the solid crystalline forms of calcium carbonate but also the initially formed amorphous forms (Lam, et al., 2007). A molecular dynamics study of the solvation of dissolved calcium carbonate in water showed that the first hydration shell around an ionic bonded calcium carbonate pair is similar in structure to the polymorph ikaite (Bruneval, et al., 2007), and Lam et al. (2007) showed evidence that the formation of anhydrous phases results from the expulsion of water from the amorphous phase rather than dramatic changes in crystal structure.

At higher supersaturation conditions (greater than a log SI value of approximately 2.5 for calcite), the first calcium carbonate phase to form is amorphous calcium carbonate, while at lower supersaturation conditions (and in the absence of additives) calcite is the solid phase formed (Clarkson, et al., 1992). The experimental conditions tested in the present study, as well as the supersaturation conditions of most brackish water RO concentrates, can be considered to be high supersaturation conditions. When amorphous calcium carbonate is formed, subsequent forms can include ikaite (at

temperatures below 25 ^{o}C) and vaterite-calcite mixtures. Ikaite can also form when phosphate or organic additives are present.

The presence of magnesium changes the rhombohedral morphology of the calcium carbonate precipitates, while sulfate can cause calcite particles to form aggregates (Falini, et al., 2009). When magnesium is present in high concentrations relative to calcium (greater than 4:1 molar ratio) (Meldrum and Hyde, 2001), aragonite is formed instead of calcite (Falini, et al., 2009); at lower magnesium concentrations, calcite is the primary precipitate with a variable amount of incorporated magnesium (10 – 30 mole%). Organic compounds, including humic acids, polyacrylates, and organophosphorus compounds, have also been shown to change the distribution of calcium carbonate phases, delay or prevent precipitation, and influence the incorporation of ions such as magnesium into precipitating particles (Falini, et al., 2009; Tang, et al., 2008; Westin and Rasmuson, 2005; Yang, et al., 2001).

In this study, no additional clumping or aggregation of particles was observed when sulfate was present during calcium carbonate precipitation (Figure 19b), while the addition of magnesium did dramatically change the particle morphology (Figure 19c & d). The absence of particle aggregation by sulfate can be explained by the lower concentration of sulfate tested in this study (10 mM) than that tested by Falini, et al. (2009) (33 – 330 mM). Previous work has shown a positive correlation between increased sulfate concentration and increased calcium carbonate particle aggregation (Kralj, et al., 2004). Spherical vaterite and rhombohedral calcite are both observed for the Simplified Maricopa and the Simplified Maricopa + Na_2SO_4 water compositions. For the Simplified Maricopa + $MgCl_2$ and Complete Maricopa water compositions, the molar ratio of magnesium to calcium is approximately 0.6:1, and calcite with incorporated magnesium, known as magnesian calcite, is predicted to form rather than aragonite

(Falini, et al., 2009; Meldrum and Hyde, 2001). Both magnesium-containing waters display rough spherically-shaped particles as well as polycrystalline particles that have two or more branches emitting from a central point and radial symmetry. Previous work has shown similar magnesium-calcite particle morphologies (Loste, et al., 2003; Meldrum and Hyde, 2001).

Energy dispersive x-ray (EDX) analysis was performed on each of the precipitated water composition samples without antiscalant added. Both weight percent and atomic percent values were recorded for each element. The Simplified Maricopa water only contained calcium carbonate as a precipitate; calcium, oxygen, and carbon were included in the composition analysis. EDX analysis of the cubic or rhombohedral particles confirmed the presence of anhydrous calcium carbonate ($CaCO_3$). An analysis of the amorphous spheres indicated the elemental composition of monohydrocalcite with some anhydrous calcium carbonate. When magnesium was added to the Simplified Maricopa water, elemental analysis resulted in magnesium concentrations between 1.5 and 9.5% (wt.), and calcium carbonate polymorphs of anhydrous calcium carbonate and monohydrocalcite. Similar incorporated magnesium concentrations by weight were reported by Meldrum and Hyde (2001) and Loste et al. (2003).

Elemental analysis of the precipitates in Simplified Maricopa + Na_2SO_4 water revealed several calcium carbonate phases; the large amorphous spheres contained the elemental composition of ikaite, while the small smooth spheres appeared to be monohydrocalcite and the rhomboids had the elemental composition of anhydrous calcium carbonate. The sulfate anion is not known to stabilize metastable phases of anhydrous calcium carbonate (vaterite or aragonite), and calcite is typically formed (Falini, et al., 2009); therefore, the rhombohedral particles are predicted to be calcite. Even though sulfate was not predicted to precipitate (as gypsum), a small amount of

sulfur (0.21 – 0.43 wt% or 0.15 – 0.25 mole%) was present in the elemental composition of all particles analyzed. Compared to the drastic changes in particle morphology observed with the addition of magnesium, the addition of sulfate caused only minor changes to particle morphology.

Finally, an analysis of the Complete Maricopa water revealed both anhydrous and amorphous calcium carbonate phases. The larger spheres yielded elemental compositions for both phases when measurements were taken at different points on the same particle, while smaller spheres appeared to be primarily anhydrous calcium carbonate. Some particles with a rough rhombohedral shape were observed, and these particles were found to be anhydrous calcium carbonate. The magnesium content ranged between 0.34 and 3.44 wt%; the small spheres had a magnesium content of 0.34 – 0.48 wt%, while the bigger amorphous spheres and rhomboids had a magnesium content of 1.67 – 3.44 wt%. All measurements showed small amounts of sulfur, barium, and ferric iron in the particles; sulfur content ranged from 0.10 to 0.46 wt% (0.06 – 0.33 mole%), barium from 0.76 to 0.97 wt% (0.08 - 0.16 mole%), and ferric iron from 0.48 to 0.63 wt% (0.17 – 0.26 mole%).

SEM imaging and EDX analysis of precipitated particles in the presence of antiscalants

SEM images obtained for the Simplified Maricopa + Na_2SO_4 with several different antiscalant types and concentrations are shown in Figure 20; results obtained for the Simplified Maricopa water were similar. The higher concentrations of DQ2066 (56 mg/L) and DQ2006 85 mg/L) caused small particles to form, as well as some larger spherical particles, while most of the antiscalant types and concentrations tested did not significantly change the spherical and rhombohedral geometries observed for the antiscalant-free solution pictured in Figure 19b. No effect of antiscalant addition on

particle morphology was observed for Coatex (0.8 & 50 mg/L), 9 mg/L DQ2006, 5 mg/L DQ2066, or 4 mg/L DQ2054, while a slight distortion of the rhombohedral geometry was observed for 43 mg/L DQ2054 (Figure 20d).

The fully-formed precipitated particles that are approximately 6-10 μm in diameter are formed through heterogeneous precipitation. The first stage of precipitation is nucleation, and the second stage is particle growth; the small particles represent the first stage of crystallizing nuclei. Antiscalants act to both disperse particles and inhibit particle growth. Under conditions such as those studied in this paper, where the precipitation control of antiscalants is overcome, precipitation does occur but is largely arrested during the first stage as antiscalants adsorb onto crystal growth sites and prevent complete particle formation. Therefore, the number of large particles observed decreases, and the number of small particles increases dramatically, as is seen for DQ2066 and DQ2006 in Figure 20a-c. In the case of DQ2066, the small particles appear to attach to the larger particles that form, creating a rough surface on the normally smooth spheres. This is not the case for DQ2006 (Figure 20c), where the larger spherical particles appear to be unattached to the smaller particles. While the formation of larger particles was not observed when antiscalant was added to the Simplified Maricopa water, the result is different for the three other more complex waters; both small and larger particles are observed for several antiscalant types and concentrations.

EDX analysis of a sample of Simplified Maricopa with 85 mg/L DQ2006 indicated that calcium carbonate precipitated primarily as monohydrocalcite, with an average composition of 32.6 wt% calcium, 11.7 wt% carbon, and 55.5 wt% oxygen and a phosphorus content of 0.60 wt% (0.37 mole%). Similar results were obtained for Simplified Maricopa + Na_2SO_4; the primary precipitate phase was monohydrocalcite, with a decreased carbon content (average was 10.2 wt%) due to incorporation of some

sulfate anions into the calcium carbonate crystals (0.29 – 0.95 wt%). Results for 56 mg/L DQ2066 were different; the precipitate for both water compositions was primarily anhydrous calcium carbonate. However, the calcium content was slightly higher than that expected for the anhydrous phase, while the carbon content decreased. The average elemental composition was 46.2 wt% calcium, 6.6 wt% carbon, and 47.2 wt% oxygen; the expected elemental composition for anhydrous calcium carbonate is 40 wt% calcium, 12 wt% carbon, and 48 wt% oxygen. Previous work has shown that the anionic phosphate groups of phosphonate antiscalants can replace carbonate groups in the crystal lattice if the distance between phosphate groups within the phosphonate molecule is similar to that of the carbonate groups in the lattice structure (Nygren, et al., 1998). The incorporation of DQ2066 molecules into the crystal lattice reduced the carbon content and allowed recrystallization of amorphous calcium carbonate to an anhydrous polymorph. The distance between phosphate groups in DQ2066 is most likely quite similar to that of carbonate molecules in anhydrous calcium carbonate, while the phosphate groups of DQ2006 are apparently too close together to be incorporated into the crystal lattice. Such differences in antiscalant structure result in different calcium carbonate phases during precipitation.

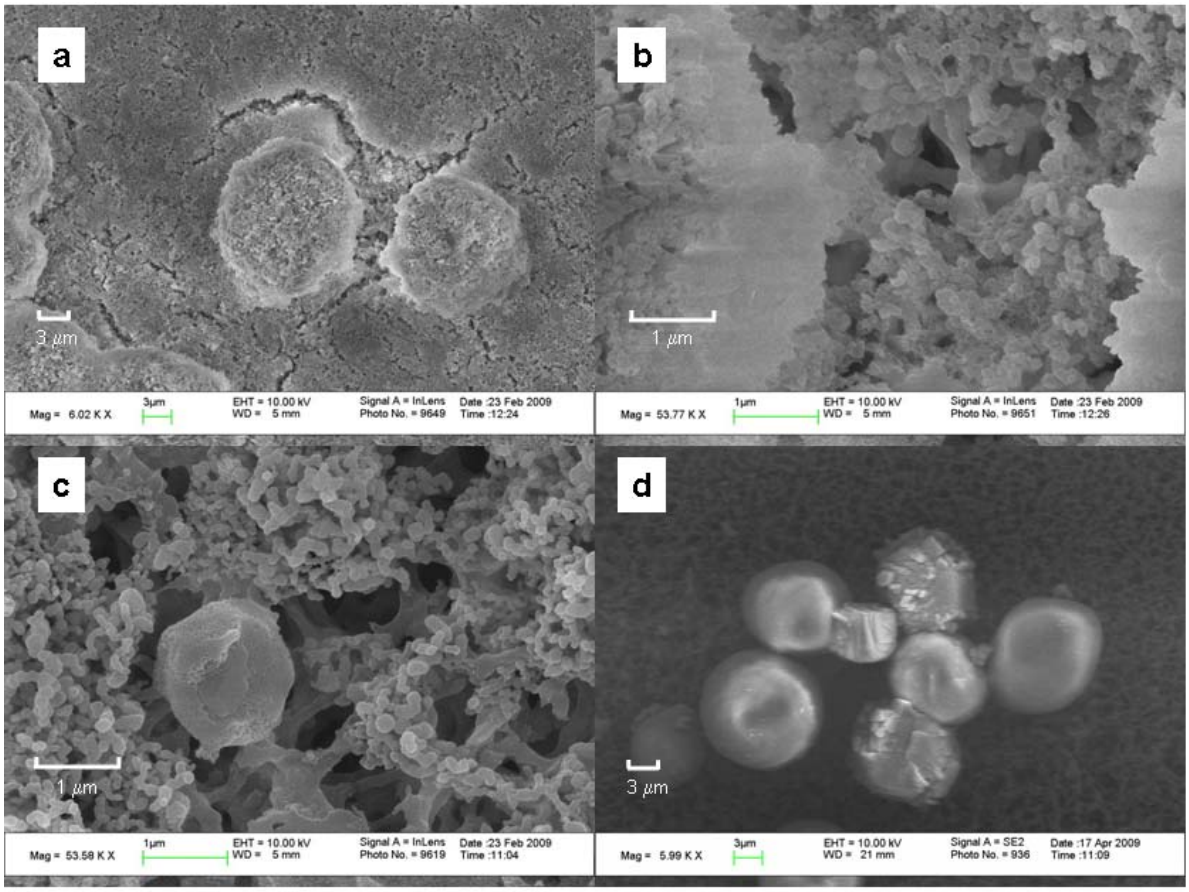

Figure 20. Precipitated solution of Simplified Maricopa + Na_2SO_4 with different antiscalants; (a, b) 56 mg/L DQ2066 at magnifications of 6,000 and 53,800 respectively, (c) 85 mg/L DQ2006, and (d) 43 mg/L DQ2054. Precipitation pH was 10.5.

SEM images of the Complete Maricopa water are shown in Figure 21. For the Complete Maricopa water, 9 mg/L DQ2006, 56 mg/L DQ2066, and 50 mg/L Coatex resulted in the formation of many small particles approximately 100 – 200 nm in diameter, as well as larger polycrystalline symmetrical crosses and rods. No change in particle morphology was observed for DQ2054 (4 & 43 mg/L), 5 mg/L DQ2066, and 0.8 mg/L Coatex. For 85 mg/L DQ2006, only the small particles were observed. Similar images were obtained for the Simplified Maricopa + $MgCl_2$ water composition; no effect of antiscalant on particle morphology was observed for 4 & 43 mg/L DQ2054 or 0.8

mg/L Coatex, but all other antiscalant types and concentrations resulted in formation of many small particles (100 - 200 nm) and some larger polycrystalline particles.

EDX analysis was performed on the Simplified Maricopa + $MgCl_2$ water composition with 56 mg/L DQ2066. Both the small and large particles were analyzed, and the elemental composition was significantly different between the two types of particles. The composition distribution for each particle type was averaged from four separate measurements taken on each type of particle. The small particles contained 1.8% (wt.) magnesium, 29.3% calcium, 60.4% oxygen, and 8.4% carbon, while the larger particles contained 3.4% magnesium, 41.2% calcium, 49.2% oxygen, and 6.2% carbon. The addition of antiscalant to the Simplified Maricopa + $MgCl_2$ water did not increase magnesium precipitation. The atomic ratio of calcium to oxygen of the small particles indicates that the small particles are amorphous calcium carbonate with at least one unit of hydration, while the ratio for the larger particles indicated that the particles are primarily anhydrous calcium carbonate. The magnesium content of the anhydrous calcium carbonate (larger particles) was higher, indicating a greater inclusion of magnesium as the amorphous calcium carbonate was transformed into a crystalline anhydrous form. Similarly, results from a sample of Simplified Maricopa + $MgCl_2$ with 85 mg/L DQ2006 showed both anhydrous and amorphous calcium carbonate. The DQ2006 sample contained a slightly higher average magnesium content (5.5 wt%). Phosphorus weight content ranged between 0.47 and 0.62 wt%; all phosphorus measurements for all samples and antiscalants were quite similar and within this range. The only source of phosphorus present in the synthetic solutions was antiscalant. Phosphonate antiscalants have been shown to adsorb onto and coprecipitate with anhydrous calcium carbonate (Jonasson, et al., 1996; Kan, et al., 2005; Nygren, et al., 1998). Antiscalant precipitation was observed for all four water compositions tested.

EDX analysis was also performed on a precipitated sample of Complete Maricopa with 85 mg/L DQ2006. Similar to the results obtained for Simplified Maricopa and Simplified Maricopa + Na_2SO_4, the primary phase of calcium carbonate was monohydrocalcite. Both magnesium and sulfur content increased over that observed for the antiscalant-free Complete Maricopa sample; the average particle composition for the DQ2006 sample was 4.9 wt% magnesium, 34.2 wt% calcium, 51.2 wt% oxygen, 6.6 wt% carbon, 0.8 wt% sulfur, 0.48 wt% barium, and 0.35 wt% ferric iron. The average particle composition for Complete Maricopa with 56 mg/L DQ2066 had a similar distribution as the sample with DQ2006. In contrast to the increased magnesium and sulfate precipitation, the barium and ferric iron content decreased slightly when antiscalant was added; the DQ2006 sample contained 0.05 – 0.12 mole% barium and 0.10 – 0.22 mole% ferric iron (down from 0.08 - 0.16 mole% and 0.17 – 0.26 mole%).

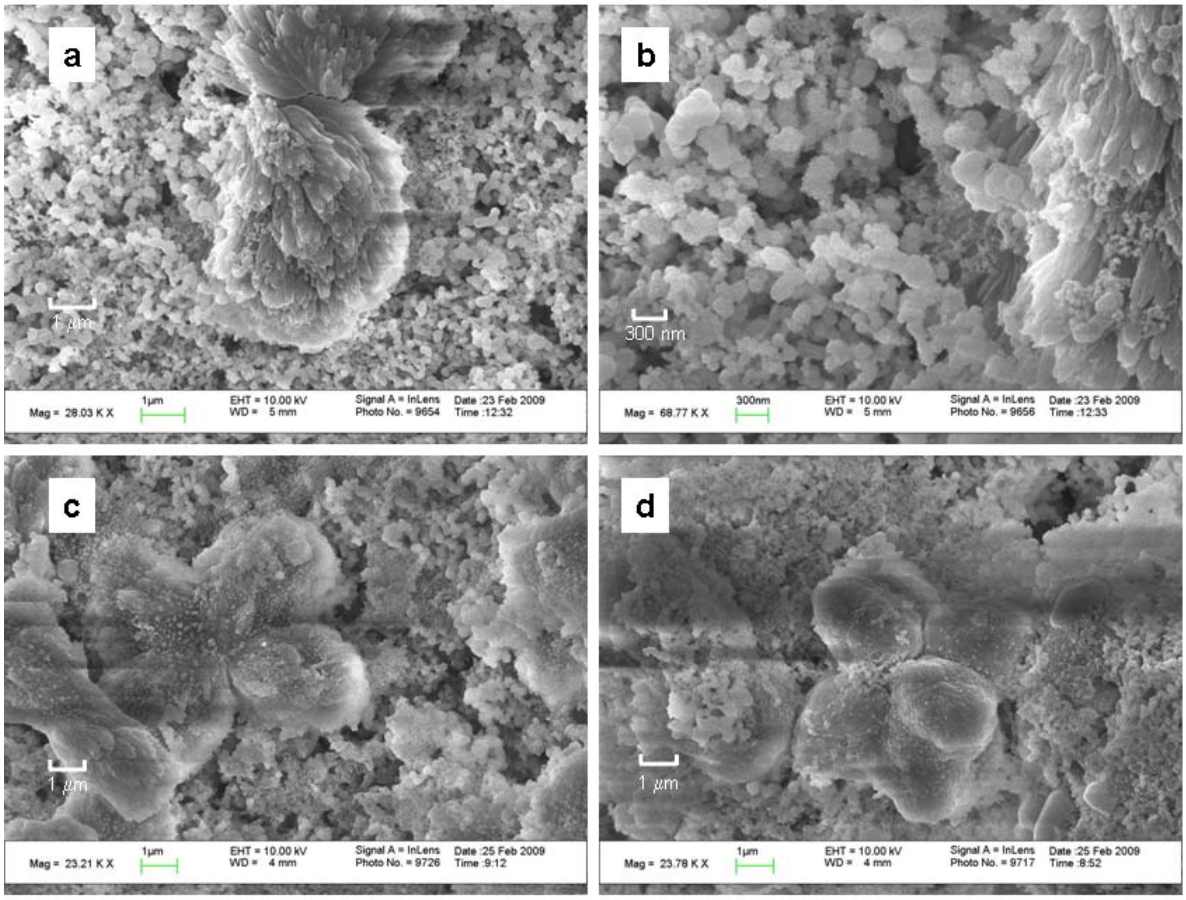

Figure 21. Precipitated solution of Complete Maricopa with different antiscalants; (a, b) 9 mg/L DQ2006 for magnifications of 28,000 and 68,800, respectively, (c) 56 mg/L DQ2066, and (d) 50 mg/L Coatex. Precipitation pH was 10.5.

Analysis of remaining dissolved ions after precipitation

An analysis of the ions remaining in solution after 30 min precipitation of the Complete Maricopa water data set also revealed an increase in magnesium precipitation with the addition of antiscalant; antiscalants DQ2006 (20 and 85 mg/L) and DQ2054 (43 mg/L) were tested. No significant difference in the amount of magnesium precipitated was observed for the two DQ2006 concentrations, and magnesium precipitation increased from 24% to 30% when antiscalant was present. For precipitation experiments allowed

to react for 60 minutes, solutions containing antiscalant DQ2006, DQ2066, or Coatex resulted in a similar increase in magnesium precipitation. The presence of DQ2054 resulted in the same amount of magnesium precipitation as the control solution, and in the Simplified Maricopa + $MgCl_2$ water, magnesium precipitation was equivalent for antiscalant-dosed and antiscalant-free solutions. This result for the Simplified Maricopa + $MgCl_2$ water is consistent with results obtained from EDX analysis of precipitated particles. A similar trend was observed for sulfate in the Complete Maricopa water; all antiscalant-dosed precipitated solutions resulted in lower final dissolved sulfate concentrations than the antiscalant-free solution. For the Maricopa + Na_2SO_4 water, the addition of antiscalant caused the sulfate precipitation to increase from 2% to 5%, and for the Complete Maricopa water, sulfate precipitation increased from 6% to 9%. The observed increase in magnesium and sulfate precipitation with antiscalant addition to the Complete Maricopa water is also consistent with EDX data obtained for precipitated particles.

The effects of antiscalant type and concentration on calcium precipitation were quite different than that seen for magnesium and sulfate. In general, the addition of antiscalant before precipitation caused a decrease in calcium precipitation, with higher antiscalant concentrations causing a greater decrease in calcium precipitation. For the 30 minute precipitation experiment with 85 mg/L DQ2006 and the Complete Maricopa water (pH 10.5), calcium precipitation decreased from 84 to 81% with the addition of antiscalant. Several concentrations of DQ2006 (4, 20, and 85 mg/L) and Coatex (2, 10, and 50 mg/L) were tested with the Complete Maricopa water data set for a precipitation time of 60 minutes, and the results for final dissolved calcium are shown in Figure 22. The remaining dissolved calcium increased with increased antiscalant concentration for both antiscalants. The lower antiscalant concentrations tested resulted in significantly

different results between the two antiscalant types; Coatex concentrations of 2 and 10 mg/L resulted in dissolved calcium concentrations of 49 and 73 mg/L, while DQ2006 concentrations of 4 and 20 mg/L resulted in 97 and 102 mg/L final dissolved calcium. This result illustrates the differences in precipitation control that can be found among antiscalant products (Plottu-Pecheux, et al., 2002; Semiat, et al., 2003; Shih, et al., 2006); antiscalant concentrations typically dosed into an RO feed are between 0.5 and 3 mg/L, resulting in concentrate antiscalant concentrations between 2.5 and 15 mg/L (for an 80% recovery).

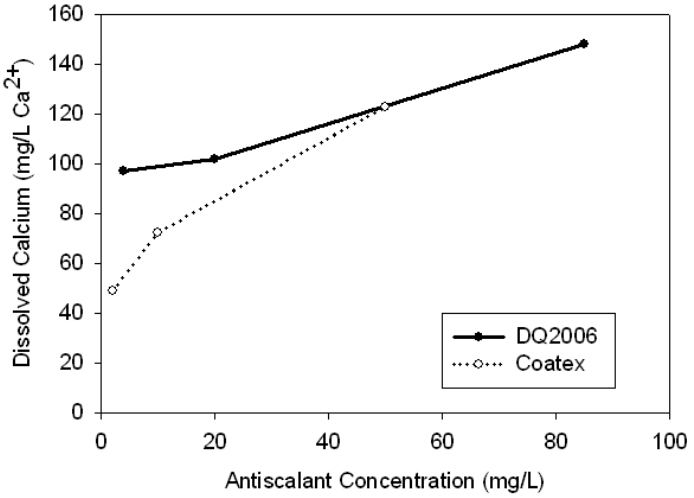

Figure 22. Increase in final dissolved calcium with increasing antiscalant concentration for antiscalants DQ2006 and Coatex and the Complete Maricopa water. Batch precipitation experiments performed at pH 10.5 for 60 minutes with excess total carbonate.

Kan et al. (2005) reported several relationships between dissolved antiscalant concentration and extent of coprecipitation of the antiscalant, depending on the concentration range of the antiscalant. For antiscalant concentrations less than approximately 0.1 – 0.3 mM, antiscalants adsorb onto calcite following a Langmuir-type isotherm (Kan, et al., 2005). The range of antiscalants tested in this research was 0.01 –

0.3 mM. Nygren et al. (1998) reported that phosphonate antiscalants adsorb onto calcite surfaces or steps in the crystal structure by replacing two carbonate molecules. In addition to the coprecipitation of antiscalant molecules, magnesium ions are known to incorporate into anhydrous calcium carbonate, and sulfate is a common coprecipitate to calcium carbonate (Falini, et al., 2009). However, a study on coprecipitation of calcium carbonate and calcium sulfate indicated that the solubility of a coprecipitating mixture follows the solubility of calcium sulfate rather than calcium carbonate (Sudmalis and Sheikholeslami, 2000), and Meldrum and Hyde (2001) showed that there was no correlation between increased magnesium incorporation and organic additive addition for malic and citric acid.

The results presented here are contradictory to some of the previous work mentioned above. The antiscalant concentration range tested lies within the range expected to have a Langmuir adsorption behavior; the antiscalants adsorb onto crystal growth sites and prevent or slow further precipitation and crystal growth. However, the precipitation of calcium did not follow the solubility of calcium sulfate, which is not predicted to precipitate, but followed the supersaturation level of calcium carbonate. This result may indicate incorporation of sulfate anions into the already existing calcium carbonate precipitating crystals, instead of coprecipitation of individual crystals of calcium carbonate and gypsum, and is due to the low sulfate concentration in the synthetic concentrate. The SEM images for the Simplified Maricopa + Na_2SO_4 and Complete Maricopa water compositions support this conclusion; no needle-like particles were observed in antiscalant-dosed precipitated solutions (Figure 20 and Figure 21), while Sudmalis and Sheikholeslami (2000) reported the presence of both needle-like $CaSO_4$ and rhombohedral $CaCO_3$. The magnesium ion has a smaller ionic radius than calcium (86 picometers versus 114 pm for a six-coordinate octahedral configuration of

calcium) and holds onto its hydration shell more strongly. The hydration shell must be removed before magnesium can be incorporated into the calcium carbonate crystal lattice and therefore represents an energy barrier to precipitation. The adsorption of a phosphonate antiscalant, which typically coordinates more strongly to divalent cations than similar compounds containing carboxylic acid moieties (such as malic and citric acid), may allow more magnesium and sulfate to be incorporated into the precipitating calcium carbonate. The antiscalant may coordinate with magnesium and lower the energy barrier to removal of the hydration shell, as well as free anion positions within the calcium carbonate lattice for sulfate ions as some carbonate anions are replaced by the adsorbing phosphonate.

Additional experiments were performed for a 60 minute precipitation time for all four antiscalants and water compositions, and the results for final dissolved calcium are shown in Table 8. Calculated values (calculations performed in PHREEQC) are shown for the log saturation index (log SI) of calcite. The first row of data displays the effect of sulfate and magnesium ions on calcium carbonate precipitation; the addition of these two ions to the Simplified Maricopa water composition caused a decrease in calcium precipitation. The effect appears to be additive as calcium precipitation decreased further when both ions were present in the Complete Maricopa water. While other minor ions present in the Complete Maricopa may have had a small effect on reducing calcium precipitation, sulfate and magnesium were the major ions present and had the largest effect on precipitation. The log SI increased consistently from the left to the right of most of the rows in Table 8. In some cases, the log SI decreased slightly for the Simplified Maricopa + $MgCl_2$ even though calcium precipitation decreased; this trend may be caused by the effect of magnesium on the calculated activity coefficients for calcium and carbonate in PHREEQC. Magnesium has been shown to significantly affect

calcium carbonate precipitation by changing lattice structure and adsorbing onto crystal growth sites (Chakraborty, et al., 1994); the presence of magnesium increases calcium carbonate solubility and thus would decrease the activity coefficients of the ionic components in solution. Previous work has shown that the addition of magnesium to a supersaturated calcium carbonate solution effectively increases the solubility of calcium carbonate through growth site blockage by the large hydrated magnesium ions (Falini, et al., 2009). As mentioned previously, this creates an energetic barrier to further growth of the calcium carbonate crystal (Loste, et al., 2003). The decrease in calcium precipitation in the Complete Maricopa water was most likely caused by other cations such as barium and ferric iron that also block calcium carbonate growth sites. Falini et al. (2009) also showed that the addition of sulfate, along with other ions such as sodium and potassium, decreases calcium precipitation; however, while the addition of magnesium also shifts the distribution of calcium carbonate phases that form, the presence of sulfate only affects the extent of precipitation, not phase formation; this finding is consistent with particle morphology observations of this study.

The subsequent rows in Table 8 show the effect of the four different antiscalants on calcium precipitation. In general, the remaining dissolved calcium increased with increasing water complexity, following the trend for solutions with no antiscalant. However, there was significant variation in remaining dissolved calcium between the four antiscalants, and two antiscalants (DQ2066 and Coatex) performed worse in the Complete Maricopa water than for several other water compositions. The presence of antiscalants DQ2054 and DQ2006 increased the log SI for calcium carbonate from 0.63 to 1.23-1.98 for the Simplified Maricopa water; similar increases were observed for the other three water compositions. For antiscalant DQ2006, the calcite ion activity product (the product of the activity of calcium and the activity of carbonate in solution) in the

Simplified Maricopa water increased by a factor of 20 over the antiscalant-free solution. The phosphonate antiscalant DQ2006 appeared to outperform the other antiscalants for both the Simplified Maricopa and Complete Maricopa water compositions, while Coatex prevented the most calcium precipitation for the other two water compositions. DQ2054 appears to have a minor effect on calcium precipitation, while DQ2066 was not effective at preventing precipitation in the Complete Maricopa water.

Table 8. Remaining dissolved calcium (mg/L) in solution and calculated saturation index for calcite ($CaCO_3$) after precipitation and filtration. Precipitation performed at pH 10.5 for 60 minutes.

	Dissolved Calcium (mg/L)/Calcite SI			
Water Composition/ Antiscalant	**Simplified Maricopa**	**Simplified Maricopa + Na_2SO_4**	**Simplified Maricopa + $MgCl_2$**	**Complete Maricopa**
No Antiscalant	3.5/0.63	14/1.14	67/1.70	81/1.77
DQ2006 (85 mg/L)	77/1.98	95/2.00	109/1.93	148/2.07
DQ2066 (56 mg/L)	73/1.96	65/1.83	108/1.90	36/1.41
DQ2054 (43 mg/L)	14/1.23	79/1.92	74/1.75	83/1.78
Coatex (50 mg/L)	55/1.83	105/2.05	137/2.06	123/1.99

Particle size distributions of precipitated solutions

A comparison of measured particle size distributions for two water compositions, Simplified Maricopa + Na_2SO_4 and Complete Maricopa, and the four antiscalants is shown in Figure 23. Most of the curves obtained were bimodal, with some trimodal distributions. Only two water compositions are shown because the relationship between antiscalant type and particle size distribution was the same for the Simplified Maricopa and the Simplified Maricopa + $MgCl_2$ water compositions and for the Simplified Maricopa + Na_2SO_4 and Complete Maricopa water compositions. For both groups of water types, antiscalants DQ2054 and Coatex had particle size distributions similar to the antiscalant-free precipitated solution, while antiscalants DQ2006 and DQ2066 caused the particle size distributions to shift. For the Simplified Maricopa + Na_2SO_4 water (Figure 23a), DQ2006 and DQ2066 caused a decrease in modal particle diameter for the mode with the largest relative volume (%). In addition, there was an increase in the relative volume of small particles between 0.1 and 1 μm for DQ2006, indicating a large increase in the number of small particles formed. As was confirmed through SEM imaging, the addition of DQ2006 or DQ2066 to the Simplified Maricopa + Na_2SO_4 water caused the formation of particles that were primarily between 100 and 200 nm in diameter, with some larger particles (~10-15 μm in diameter) observed. The modal particle diameter for the largest mode of the DQ2006 and DQ2066 curves in Figure 23a is slightly greater than the particles observed by SEM. This discrepancy might be due to smaller particles adhering to the larger particles, making the measured particle diameter slightly larger than the actual particle diameter. Another possible interpretation is the light scattering theory is based on spherical particles, and the SEM images make it obvious that the particles are not spherical. The presence of DQ2054 or Coatex did not cause the

formation of these small, nanometer scale particles, and therefore the particle size distributions for these two antiscalants were largely unaffected.

Antiscalants DQ2006 and DQ2066 caused an increase in the modal particle diameter in the Complete Maricopa water (Figure 23b), and antiscalants DQ2006, DQ2066, and Coatex caused the formation of small particles (100-200 nm). The curve for the antiscalant-free sample also indicated the presence of small particles, but SEM images showed no particles in the sub-micron range. This discrepancy is most likely due to the algorithm used to deconvolute the static light scattering data, and the particles are best represented by a monodisperse particle size distribution. No shift in the particle size distribution was observed for Coatex, although the relative volume of small particles (first mode) increased above that observed for DQ2054 or antiscalant-free samples. The increase in modal particle diameter for DQ2006 and DQ2066 appears to be caused by the attachment of many small particles to the larger rod- or cross-shaped symmetrical particles. While small particles are observed in the Coatex sample, the surfaces of the larger particles are smooth and relatively no small particle attachment was observed. This lack of small particle attachment in the Coatex sample may also explain the increase in relative volume of the small particle mode, which is not observed for DQ2006 or DQ2066; more small particles were actually measured during analysis of the Coatex sample than for the other two antiscalants. The addition of DQ2054 resulted in no change in the modal particle diameter.

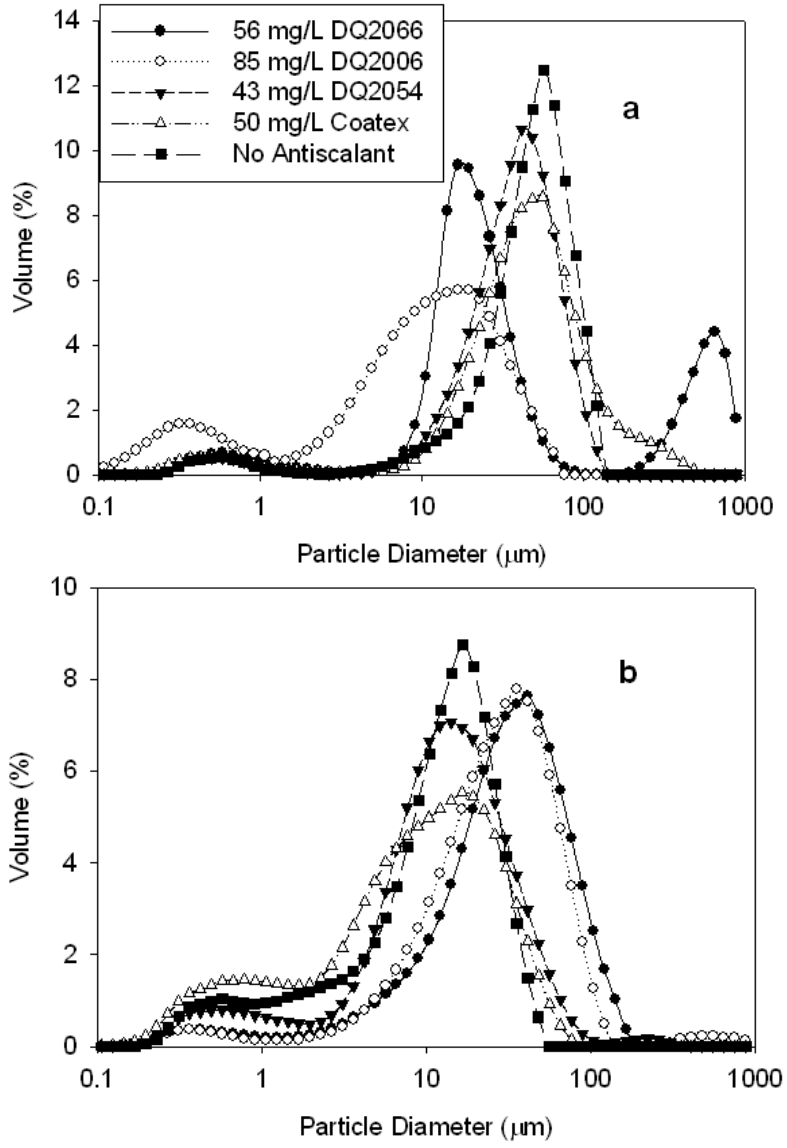

Figure 23. Variation in particle size distribution with antiscalant type for (a) Simplified Maricopa + Na_2SO_4 water composition and (b) Complete Maricopa water composition. Precipitation pH was 10.5.

The effect of antiscalant concentration on particle size diameter is shown in Figure 24 for antiscalant DQ2006 and the Complete Maricopa water composition. All particle size distributions were bimodal; as antiscalant concentration increased, the modal

particle diameter of the second mode increased, and the relative volume of the first mode decreased. The sample with no antiscalant did not show two distinct modes but rather two modal diameters within a connected particle size distribution. SEM imaging of the antiscalant-free Complete Maricopa water (Figure 19d) showed a range of particle sizes and shapes, while the addition of antiscalant DQ2006 resulted in many small spherical particles and some larger particles shaped as a symmetrical figure eight. An increase in antiscalant concentration caused an increase in the formation of small particles, which attach to the larger particles and increase the measured modal particle diameter of the second mode. The decrease in the relative volume of the first mode as antiscalant concentration increases is most likely due to an increased attachment of smaller particles to the larger particles, reducing the volume of small particles measured.

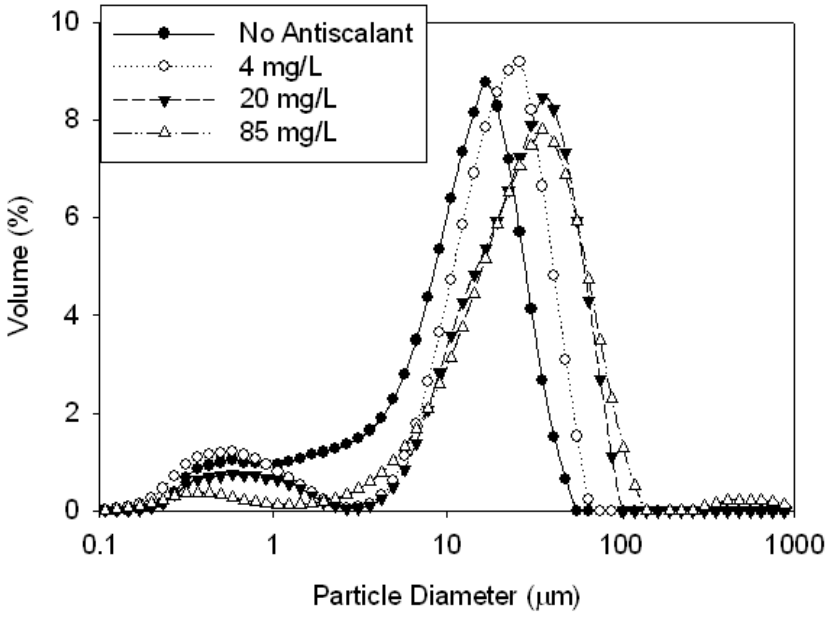

Figure 24. Effect of DQ2006 antiscalant concentration on particle size distribution for the Complete Maricopa water composition. pH 10.5.

Microfiltration of precipitated solutions

Microfiltration (0.1 μm) was used to separate the precipitated salts from the remaining dissolved ions in the brackish water RO concentrate; a comparison of the flux decline for the four water compositions is shown in Figure 25 for Coatex and DQ2066. For all four water compositions, the microfiltration flux for antiscalant-free solutions showed the same or slightly less flux decline than the samples with antiscalant. The antiscalant-free solutions of Simplified Maricopa and Simplified Maricopa + Na_2SO_4 resulted in approximately 20% flux decline over seven minutes, while the flux decreased approximately 10% for Simplified Maricopa + $MgCl_2$ and Complete Maricopa waters. The presence of antiscalant during precipitation caused at least a small increase in flux decline for all samples. A greater loss of microfiltration flux was observed for the Simplified Maricopa and the Simplified Maricopa + Na_2SO_4 water compositions for all four antiscalants. The presence of the Coatex antiscalant caused the greatest flux decline for the Simplified Maricopa + Na_2SO_4 water; approximately 70% of the flux was lost within 6.7 minutes. A smaller loss in flux occurred for the three other water compositions. For the DQ2066 antiscalant (Figure 25b), the flux decline for the Simplified Maricopa and the Simplified Maricopa + Na_2SO_4 water compositions was identical, as was the flux decline for two the magnesium-containing water compositions. The flux decline for the former curve was approximately 45%, while the flux decline for the latter was 20%. The addition of antiscalant to deionized water did not cause a decrease in water flux; therefore the flux decline observed for precipitated solutions with antiscalant was not caused by adsorption of the antiscalant to the membrane, but the changes in particle morphology and particle coadhesion caused by the antiscalant.

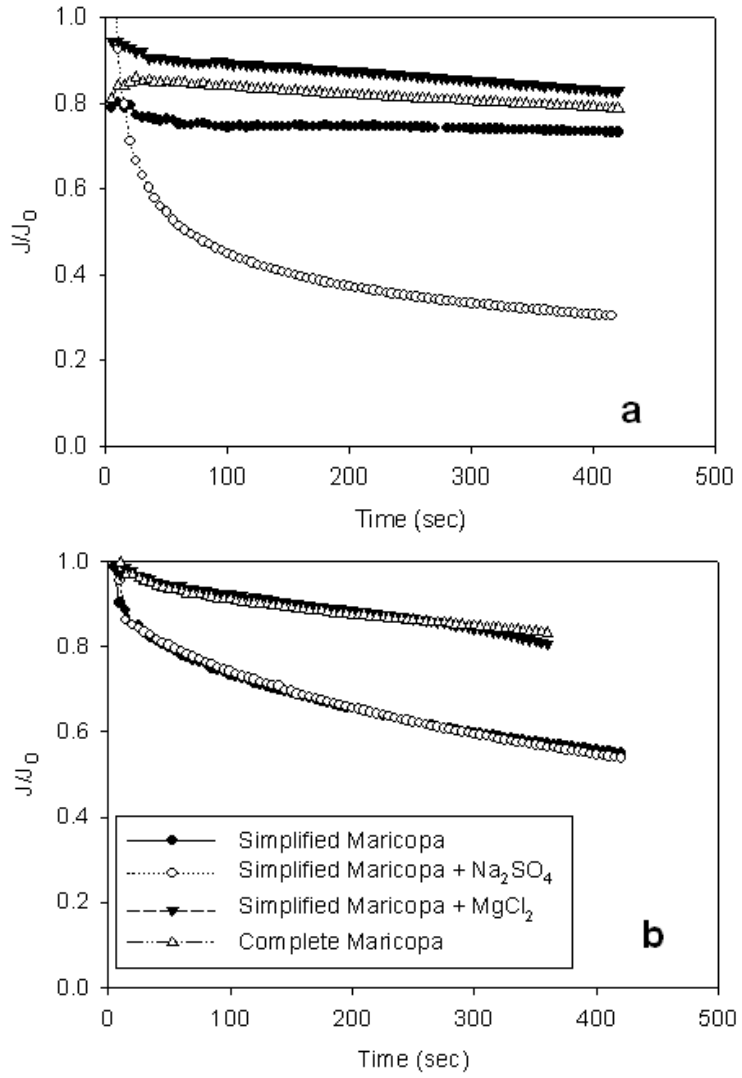

Figure 25. Microfiltration (0.1 μm pore size) of precipitated solutions containing antiscalants (a) 50 mg/L Coatex and (b) 56 mg/L DQ2066.

An analysis of the flux data for fouling mechanisms (Wang and Tarabara, 2008) indicated that, for the Coatex antiscalant, initial fouling for the Simplified Maricopa + $MgCl_2$ and Complete Maricopa waters occurred through both complete and intermediate blocking (inner pore blockage and partial surface and pore blockage, respectively), while

filtration of the precipitated Simplified Maricopa water resulted in initial fouling through intermediate blocking and filtration of the precipitated Simplified Maricopa + Na_2SO_4 water showed primarily complete blocking. The fouling mechanism for all four water compositions shifted to a combination of standard blocking (inner membrane fouling through partial pore blockage) and cake filtration (build up of a foulant layer on the membrane surface) after approximately 100 and 200 seconds, respectively.

CONCLUSIONS

The antiscalants studied increased the saturation index of calcite to different degrees for different water compositions and different antiscalants; optimal precipitation prevention may be attained by choosing the appropriate antiscalant for a specific water composition. Antiscalants DQ2006 and Coatex displayed the best precipitation control for the four water compositions studied. In the synthetic water compositions tested, the primary precipitate was calcium carbonate, and incorporation of magnesium and sulfate into precipitating calcium carbonate was observed. Addition of antiscalants caused an increase in magnesium and sulfate precipitation and a decrease in calcium precipitation.

In addition to affecting the amount of precipitation, the presence of antiscalants changed the precipitate particle size distribution, particle morphology, and calcium carbonate phases formed. SEM imaging revealed the formation of small (100 – 200 nm) particles with certain antiscalant types and concentrations, and EDX analysis showed antiscalant type-dependent calcium carbonate phase formation. Microfiltration performance was highly dependent on water composition, and the Complete Maricopa water resulted in the smallest flux decline; antiscalant-free precipitated solutions had the same or better flux performance than antiscalant-dosed samples.

The results presented indicate that the presence of antiscalant in an RO concentrate could significantly affect a concentrate treatment process based on precipitation and solid/liquid separation (filtration). The antiscalant would be concentrated along with the dissolved salts and could reduce calcium removal efficiency, as well as affect the solid/liquid separation process. Even small antiscalant concentrations can reduce the amount of calcium precipitated and will adsorb onto precipitating particles. The development of an RO concentrate treatment process must include tests with antiscalants to determine the effect of the antiscalant on the treatment process; for the concentrate treatment process and water composition considered, removal of the antiscalants prior to salt precipitation would allow optimal precipitation and filtration of a concentrate.

Chapter 6: Ozonation of phosphonate antiscalants used for reverse osmosis desalination: Parameter effects on the extent of oxidation[3]

ABSTRACT

The application of reverse osmosis (RO) to inland brackish water requires an increase in recovery, and RO concentrate treatment is necessary to achieve higher overall recoveries. A concentrate treatment that includes antiscalant oxidation prior to precipitation and solid/liquid separation steps may allow increased precipitation through deactivation of the antiscalant compounds. Ozone and hydrogen peroxide were used to oxidize phosphonate-type antiscalants. Parameters such as water composition, pH, ozone dose, antiscalant type, and antiscalant concentration were evaluated; orthophosphate is a phosphonate oxidation product and was used as a measure of the extent of oxidation. Antiscalant oxidation increases with ozone dose and in the presence of calcium. The addition of hydrogen peroxide to the ozone system causes only minor increases in antiscalant oxidation. The extent of oxidation varies with pH as a function of metal-ligand speciation, with the doubly-protonated metal-ligand species dominating the reactivity of the antiscalant. In the presence of calcium, the primary oxidation pathway is through direct reaction with ozone, while when calcium is removed, the oxidation pathway shifts to reaction with hydroxyl radicals.

Brief

Phosphonate antiscalants used in reverse osmosis desalination are ozonated, and the effects of parameters (pH, water composition, antiscalant type and concentration) on oxidation are evaluated.

[3] Manuscript to be submitted to the journal Environmental Science & Technology.

Nomenclature

ATMP	Aminotri(methylene phosphonic acid)
DOC	Dissolved organic carbon
DTPA	Diethylenetriamine-pentaacetate
DTPMP	Diethylenetriamine penta(methylene phosphonic acid)
HDTMP	Hexamethylenediamine tetra(methylenephosphonic acid)
K	Formation (protonation) constant
NOM	Natural organic matter
RO	Reverse osmosis
t-BuOH	Tert-butanol
TDS	Total dissolved solids
TOC	Total organic carbon

INTRODUCTION

Antiscalants, or scale inhibitors, are used in many different applications, such as cooling water treatment, boiler water treatment, oil field applications, and reverse osmosis desalination, to prevent salt precipitation (Knepper, 2003). A primary target precipitate is calcium carbonate ($CaCO_3$); however, several other precipitates of calcium, barium, and strontium can become problematic. Several types of precipitates can occur during reverse osmosis membrane desalination of brackish water (between 1 and 10 g/L total dissolved solids, TDS) (Ghafour, 2002), and salt precipitation can occur on the membrane surface even if no bulk precipitation occurs (Rahardianto, et al., 2006).

Antiscalants allow higher recovery in a reverse osmosis system; recovery is the ratio of the volume of permeate (product) to the volume of the feed. However, even with

antiscalants, brackish water reverse osmosis recovery is limited to 60 – 90%. Inland brackish water sources will become an important alternative water resource as traditional fresh water resources continue to diminish. The application of brackish water reverse osmosis inland is currently limited by the cost and technical feasibility of concentrate (reverse osmosis waste stream) disposal (Mickley, 2001) and requires an alternative approach to further increase recovery above 90%.

Current research has focused on using side-stream treatment of the concentrate with the goal of recovering more of the water that is typically disposed in the waste stream (Rahardianto, et al., 2007). The primary approach to water recovery in the concentrate stream is to perform a controlled precipitation step and remove salts that are likely to precipitate within the membrane system, followed by a solid/liquid separation step (typically microfiltration) and secondary reverse osmosis treatment. The product of concentrate treatment is a highly saline, but low scaling propensity water that can be desalinated, resulting in a smaller concentrate volume and more product (drinking) water.

Antiscalants that are dosed to a reverse osmosis feed water are concentrated in the concentrate and are present during subsequent concentrate treatment; these compounds are desired to prevent precipitation within the membrane system and therefore are likely to hinder a concentrate treatment process that uses salt precipitation to remove scaling potential. If antiscalants in the concentrate could be degraded prior to precipitation, more precipitation might occur, which would further lower the scaling propensity of the concentrate and enable even higher overall system recoveries. Many antiscalants are phosphonate-based synthetics that are not easily degraded; a strong oxidant is needed to deactivate these compounds.

In this study, ozone and hydrogen peroxide were used to oxidize phosphonate antiscalants. Specific parameters were examined, including pH, water composition,

antiscalant type and concentration, ozone dose, and hydrogen peroxide concentration. In particular, this paper focuses on the effect of specific cations typically present in brackish water on antiscalant oxidation and on the relative importance of reactions with ozone and with hydroxyl radicals in that oxidation.

MATERIALS AND METHODS

All inorganic salts, acids, and bases used in experiments were ACS grade reagents obtained from VWR International (West Chester, PA, USA). Unstabilized hydrogen peroxide (30%) was obtained from Sigma-Aldrich Co. (St. Louis, MO, USA). Stabilized hydrogen peroxide contains different types of additives to prevent chemical decomposition, often including organophosphonate compounds. Therefore, the unstabilized version was required to avoid false results due to antiscalant-like compounds in the hydrogen peroxide. 0.1 N potassium permanganate ($KMnO_4$) was used to confirm hydrogen peroxide concentration (Klassen, et al., 1994).

The ozone generator (OzoneLab™ Model OL80W/FM100VT) used for experiments was obtained from Ozone Services, a division of Yanco Industries, Ltd. (Burton, British Columbia, Canada). The oxygen flow to the ozone generator was controlled by a digital mass flow meter and controller (Mass Flo© Model 1179A-01522CS1BV), obtained from MKS Instruments (Wilmington, MA, USA). The flow meter was calibrated by MKS for oxygen flow at room temperature (20 ^oC) and was powered by a single channel power supply (15 pin Model 246C). The ozone offgased was captured by two catalytic ozone destructors. All experiments were performed using an aliquot of ozone stock solution to add ozone and start the experiment (Acero and von Gunten, 2000). The stock solution typically had an ozone concentration between 1.25 mM (60 mg/L) and 1.66 mM (80 mg/L). Ozone concentrations used in experiments included 1, 5, and 10 mg/L O_3. For experiments containing hydrogen peroxide (H_2O_2),

the H_2O_2 was added from the working solution of 1,000 mg/L to the experiment before ozone was dosed.

Two common classes of antiscalants, phosphonates and polymers, are used in drinking water RO applications. Both classes are synthetic organic compounds designed to adsorb onto nucleating crystals, effectively blocking the crystal growth sites and preventing particle growth. The three antiscalants used in this study, shown in Figure 26, included three phosphonates that are often used in membrane drinking water applications (Knepper, 2003).

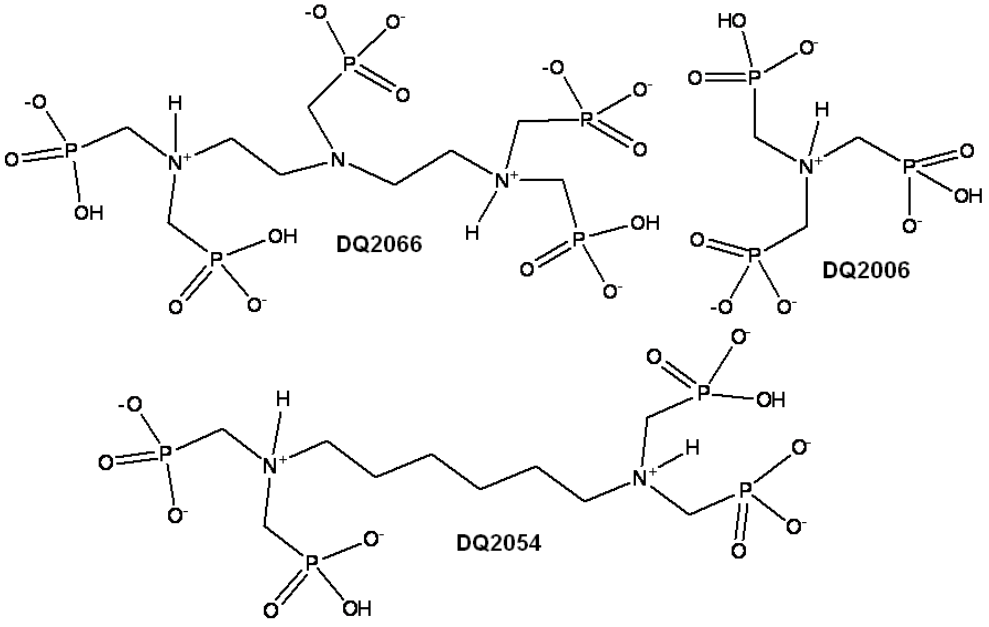

Figure 26. Phosphonate antiscalants in appropriate protonated form at pH 6.0.

Phosphonate antiscalant samples were obtained from Dequest Water Management Additives, a subsidiary of Thermophos. The antiscalants included the penta-sodium salt of aminotri(methylene phosphonic acid), or ATMP, the hexa-potassium salt of hexamethylenediamine tetra(methylenephosphonic acid), or HDTMP, and the hepta-sodium salt diethylenetriamine penta(methylene phosphonic acid) or DTPMP. Dequest refers to ATMP as DQ2006, to HDTMP as DQ2054, and to DTPMP as DQ2066, and

these commercial names are used throughout this article. Total organic carbon (TOC) and total solids analysis were used to determine the organic carbon and mass concentrations of all the antiscalants.

A summary of the water data used is shown in Table 9. The water composition is based on a brackish ground water in Arizona (Jurenka and Chapman-Wilbert, 1996) that has been evaluated in previous work as a potential feed water for a desalination facility. Several simplified versions of the water data set, as well as the complete water data set, were used to determine the effect of different water components on antiscalant oxidation.

Table 9. Water composition of the synthetic RO concentrates used in experiments.

	Water Type and Composition (mg/L)			
Component	**Simplified Maricopa**	**Simplified Maricopa + Na_2SO_4**	**Simplified Maricopa + $MgCl_2$**	**Complete Maricopa**
Na^+	1,552	2,027	474	849 (37)*
Ca^{2+}	1,002	1,002	1,002	1,030 (26)
Mg^{2+}	---	---	514	514 (21)
Ba^{2+}	---	---	---	2.0 (0.01)
Fe^{3+}	---	---	---	2.3 (0.04)
Cl^-	3,588	3,588	3,424	3,277 (92)
SO_4^{-2}	---	991	---	991 (10)
NO_3^-	---	---	---	89 (1.3)
Total Carbonate (as HCO_3^-)	998	998	998	998 (16)
Total Dissolved Solids (TDS)	7,137	8,603	6,409	7,749

*Component concentrations in mM are shown in parentheses for the Complete Maricopa column.

All pH measurements were taken with a Thermo Electron Corp. pH meter (Orion 720 A+), calibrated with three buffers (pH 4, 7, and 10 standard buffers). The pH of a solution changes with ionic strength (Baumann, 1973; Wiesner, et al., 2006). Therefore, 0.14 M sodium chloride was added to each pH buffer; buffer pH decreased by no more than 0.1, and no recalculation of pH was performed.

Standard method 4500-P E (Ascorbic Acid Method) was used to measure orthophosphate in aqueous solutions (Eaton, et al., 2005). A UV/visible spectrophotometer (Agilent model 8453) was used to measure reacted orthophosphate in test samples. A new calibration curve from known phosphate concentrations was made for each set of samples tested. Phosphate samples were taken from the initial solution and after ozonation.

RESULTS AND DISCUSSION

Antiscalant Concentration

A range of concentrations was tested for each antiscalant to study the effect of antiscalant concentration on the extent of oxidation. Results for the antiscalant DQ2006 in the Simplified Maricopa water are shown in Figure 27 as the fractional orthophosphate produced as a function of the O_3 dose; orthophosphate is a primary oxidation product of phosphonates. This fraction is the ratio of the mass of the phosphorus contained in the orthophosphate in solution after ozonation to the mass of phosphorus available in the un-oxidized antiscalant. This measure was used throughout the study to indicate the extent of oxidation accomplished. For each antiscalant concentration, fractional orthophosphate production increased with increasing ozone concentration. Concentrations of 4, 20, and 85 mg/L DQ2006 were compared, and the fractional orthophosphate production increased as the concentration of antiscalant decreased. The same trend was observed for the two other phosphonate antiscalants, DQ2054 (2, 10, and 43 mg/L) and DQ2066 (3, 13, and 56 mg/L), tested in this study (not shown). These results indicate that for most of the ozone and antiscalant concentrations tested, the extent of antiscalant oxidation is sensitive to changes in ozone dose (mg O_3/mg DOC), and antiscalant oxidation increases

with increasing ozone dose. Very little (0.13 – 0.23) of the organophosphorus is oxidized for a concentration of 85 mg/L, while the higher ozone doses result in 0.40 and 0.70 fractional organophosphorus oxidation for 20 and 4 mg/L antiscalant, respectively. Although the data suggest that the fractional orthophosphate produced for a DQ2006 concentration of 4 mg/L was less at the ozone dose 10 mg/L O_3 than at 5 mg/L, these two values are considered to be the same, based on the variation in data observed.

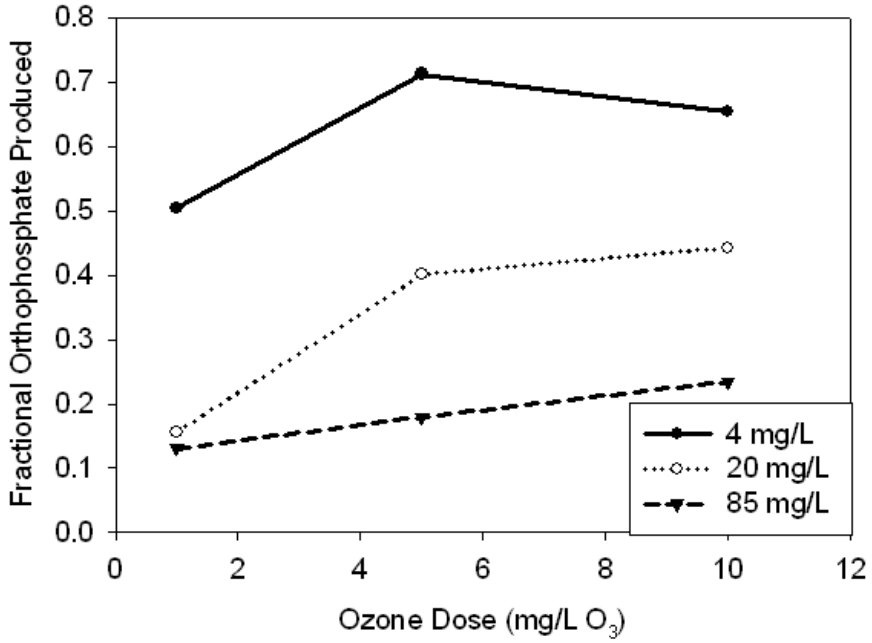

Figure 27. Increasing fractional phosphate production with decreasing DQ2006 antiscalant concentration. Orthophosphate concentrations adjusted for initial orthophosphate. pH for all experiments was 6.0.

For the highest antiscalant concentration (85 mg/L), the relationship between ozone dose and fractional orthophosphate is linear, and higher ozone doses would most likely lead to an increase in fractional orthophosphate produced. However, for 4 and 20 mg/L DQ2006, ozone doses greater than 5 mg/L O_3 cause little to no increase in fractional orthophosphate. Thus for a given antiscalant concentration, there appears to be

a limit to the extent of oxidation, and even for 4 mg/L DQ2006 and 10 mg/L O_3, complete oxidation is not achieved. For this concentration, approximately 30% of the phosphorus initially in the antiscalant compound remains as organophosphorus within what are most likely partial oxidation products. Several experimental solutions were tested with gas chromatography-mass spectrometry, and no measurable whole antiscalant (DQ2006) was detected after ozonation, which indicates that, while all antiscalant molecules undergo some oxidation, 30% to 85% of the organophosphorus is only partially oxidized.

Equivalent Antiscalant Concentration: Phosphorus and Carbon

The three phosphonate antiscalants were tested at equivalent concentrations of dissolved organic carbon (DOC) and phosphorus contained within each antiscalant. These experiments allowed the same dose of ozone for either the amount of carbon or phosphorus of each compound. The Simplified Maricopa water data set was used for most of these experiments, and concentrations of 10.5 mg/L DOC, 27 mg/L Phosphorus (P), and 2 mg/L P were tested. For the first two concentrations, an additional set of experiments was performed with the calcium removed from the Simplified Maricopa recipe. Results for 2 and 27 mg/L P are shown in Figure 28. The results for 10.5 mg/L DOC had the same trends as the results shown for 27 mg/L P.

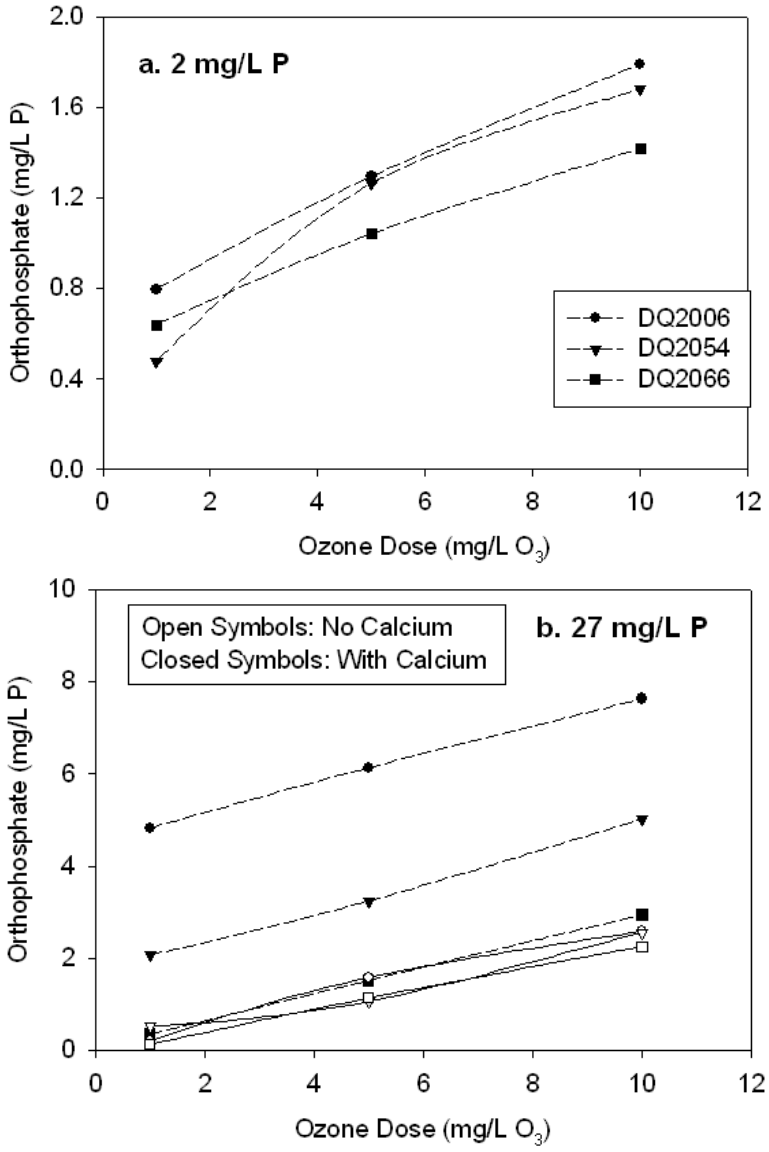

Figure 28. Comparison of three phosphonate antiscalants for the same ratio of ozone to phosphate available in the antiscalant (mg O_3/mg P) for (a) 2 mg/L P and (b) 27 mg/L P. Antiscalant concentrations were (a) 6.3 mg/L DQ2006, 7.9 mg/L DQ2054, and 7.4 mg/L DQ2066 and (b) 85 mg/L DQ2006, 107 mg/L DQ2054, and 100 mg/L DQ2066. DQ2006 is represented by circles, DQ2054 is represented by triangles, and DQ2066 is represented by squares. Closed symbols and dotted lines represent Simplified Maricopa water (with calcium), and open symbols and solid lines represent Simplified Maricopa water with no calcium present. The initial concentration of phosphate in solution was subtracted from the phosphate measured after ozonation and solution pH was 6.0 for all experiments.

In Figure 28a, a general trend existed in the order of antiscalants and the extent of oxidation; DQ2066 results in the least oxidation, while ozonation of DQ2006 resulted in the most oxidation for ozone doses of 5 and 10 mg/L ozone. This same trend is observed in Figure 28b for the samples with calcium present; the antiscalants in order of increasing oxidation are DQ2066, DQ2054, and DQ2006. The trend is more obvious for the higher phosphorus concentration; however, even at a low concentration of 2 mg/L P for each antiscalant, the extent of oxidation is different for each compound. In addition, for both phosphorus concentrations, the relationship between ozone dose and orthophosphate produced is nearly linear, indicating that even at 10 mg/L ozone and 2 mg/L P, ozone is still the limiting reactant for antiscalant oxidation, and higher ozone doses would likely result in higher orthophosphate concentrations. The ozone doses tested resulted in a greater fractional oxidation of the organophosphorus for 2 mg/L P than for 27 mg/L P, which is consistent with the results shown in Figure 27.

In Figure 28b, when calcium was removed from the experimental solution for 27 mg/L P, the three curves collapse onto each other, and ozonation of each antiscalant resulted in the approximately the same amount of orthophosphate produced. These results suggest that the complexation of phosphonate antiscalants with calcium, and resulting changes in stereochemistry, can have a significant impact on how much of the antiscalant is oxidized. When calcium was present, an ozone dose of 1 mg/L was apparently sufficient for all of the sterically-receptive calcium-antiscalant complexes to be attacked and oxidized by ozone; this conclusion is evidenced by the presence of the same linear slope for all experiments and the significant increase in orthophosphate production at 1 mg/L O_3. Although other interpretations might be possible, the fact that all of the lines have the same slope suggest that the higher ozone doses (5 and 10 mg/L)

were utilized similarly for all conditions, in that higher range, the ozone apparently oxidized sterically-hindered calcium-antiscalant complexes.

Previous work has shown that the presence of metals can increase or decrease the organic ligand oxidation for both direct reaction with ozone and reaction with hydroxyl radicals (Gilbert and Hoffmann-Glewe, 1990; Lati and Meyerstein, 1978; Stemmler, et al., 2001). In this work, the concentration of total carbonate in the experiments is quite high (16 mM); carbonate and bicarbonate are both hydroxyl radical scavengers and play an important role in the inhibition of ozone decomposition through radical chain reaction (Acero and von Gunten, 2000; Elovitz, et al., 2000). Therefore, ozone most likely reacts directly with the antiscalant molecules themselves. However, typically only the free amine in solution can react with ozone (Munoz and von Sonntag, 2000). Protonated amines have a low reactivity with ozone due to the presence of the hydrogen atom and the electrophilicity of the ozone molecule. An unprotonated amine can donate the lone pair of electrons to the ozone molecule, and protonation reduces the nucleophilicity of the amine and its ability to react with ozone. The primary reaction pathway for tertiary amines and ozone is through electrophilic addition and subsequent decomposition to an amino-oxyl radical and a superoxide molecule (O_2^{*-}) (von Gunten, 2003).

In this study, the tertiary amines of DQ2006 and DQ2054 are protonated at pH 6, and for DQ2066, only the middle amine is deprotonated. Based on the protonation of the amines in the phosphonate antiscalants and previous work showing a reduction in reaction rate constants with protonation (Munoz and von Sonntag, 2000), it was predicted that the primary pathway for antiscalant oxidation would be through reaction with hydroxyl radicals; however results from experiments with a hydroxyl radical scavenger, tert-butanol, suggest that the primary pathway for antiscalant oxidation is in fact through direct reaction with ozone. Based on these results (discussed below and shown in Figure

30 and Figure 31), and the fact that phosphonate molecules have been predicted to share the hydrogen(s) that protonate the tertiary amine group(s) between the nitrogen(s) and the organophosphate groups (Ichikawa and Sawada, 1997), the presence of calcium most likely increases antiscalant oxidation by making the amine nitrogen more available for reaction with ozone through changes in stereochemistry.

When a calcium ion is coordinated with an antiscalant molecule, the phosphate groups shift to wrap around the calcium and coordinate; protonated amines are not involved in the metal coordination (Sawada, et al., 1987). For DQ2006, one oxygen atom from each of the three phosphate groups forms a coordination bond with the metal (Sawada, et al., 1987). The amine nitrogen may or may not coordinate with the calcium ion, depending on whether the amine is protonated, and this protonation equilibrium has been predicted to be slow (Sawada, et al., 1987). Previous work has suggested that at least three to four electron donating atoms coordinate with a metal cation in the ligand-metal complex for aminophosphonate-type compounds (Duan, et al., 1999; Sawada, et al., 1987; Sawada, et al., 1993). Molecular modeling of the antiscalant-calcium complex with CS Chem3D Pro (Version 7.0.0) revealed that the amine nitrogen becomes more exposed when the molecule is coordinated with a calcium cation, reducing the steric hindrance of the phosphate groups to the reaction between the amine and an ozone molecule. The reduction in steric hindrance appears to be most dramatic for DQ2006, followed by DQ2054 and then DQ2066; the same antiscalant order was observed in Figure 28b with calcium present in solution. Both the reduction in steric hindrance and the amine protonation equilibrium may play a role in the increase in orthophosphate observed in the presence of calcium and ozone doses as small as 1 mg/L. Images of the molecular modeling performed are shown in the Supporting Information (Appendix B, Figure 61 - Figure 63).

Water Composition

Carbonate

At the experimental pH (6.0), the carbonate system is present as carbonic acid (H_2CO_3) and bicarbonate (HCO_3^-), with very little carbonate (CO_3^{2-}); the carbonate system dissociation constants of 6.35 and 10.33 decrease to 6.1 and 9.7 due to the ionic strength of the system (calculations performed using the Pitzer equations) (Pitzer, 1991). As the total carbonate concentration increased from 0 to 30 mM, antiscalant oxidation remained constant, with orthophosphate production between 5 and 6 mg/L as P. A typical reverse osmosis concentrate would have a total carbonate concentration of at least 10 mM; within the range of relevant carbonate concentrations, no effect of carbonate concentration on antiscalant oxidation would be expected for the antiscalant concentration tested. Ozone oxidation systems can be sensitive to carbonate concentration when the primary oxidation pathway is through reaction with hydroxyl radicals; the lack of dependence of antiscalant oxidation on carbonate concentration indicates that the antiscalants were oxidized through direct reaction with ozone. The effect of total carbonate concentration on antiscalant oxidation is shown in Figure 64 for DQ2006 in the Supporting Information (Appendix B).

Cations

Several experiments were performed with antiscalant DQ2006 (0.29 mM) to test the effect of individual cation types and concentrations. The data (shown in Figure 29) indicate that for calcium concentrations below 0.5 mM, the presence of calcium does not increase antiscalant oxidation; however for larger calcium concentrations (5-50 mM), the presence of calcium resulted in orthophosphate concentrations similar to those shown for pH 6.0 in Figure 64 (Appendix B, Supporting Information). Increasing the magnesium

concentration from 0.05 mM up to 50 mM did not affect antiscalant oxidation; a similar result was observed for barium at concentrations of 0.05 and 0.5 mM. Ferric iron appeared to slightly increase antiscalant oxidation at concentrations of 0.05 and 0.5 mM, but completely prevented oxidation at concentrations of 5 and 50 mM. In addition, at 5 and 50 mM, the iron also appeared to coordinate with available orthophosphate that was present in the initial solution (initial P concentration was 1.3 mg/L and orthophosphate concentration after ozonation was 0 mg/L P). Solubility calculations for ferric iron precipitates (ferrihydrite, $Fe(OH)_3$, goethite, FeOOH, and hematite, Fe_2O_3) indicate that the iron was supersaturated over the concentration range 0.05 – 50 mM at pH 5.85. The presence of phosphate has been shown to delay the transformation of amorphous ferrihydrite into crystalline particles by adsorbing onto ferrihydrite (Arai and Sparks, 2001; Khare, et al., 2005; Paige, et al., 1996), and crystallization is typically prevented at phosphorus to iron ratios greater than 0.025 (Gálvez, et al., 1999). In Figure 29, the ratio of phosphorus (as orthophosphate) to iron decreased below 0.025 at iron concentrations of 5 and 50 mM, and the phosphate coprecipitated with the iron. Therefore, the orthophosphate concentration measured after ozonation dropped below the initial orthophosphate concentration, for iron concentrations of 5 and 50 mM, due to complete precipitation of the phosphate with iron oxides. At concentrations relevant to a reverse osmosis concentrate (data given in Table 9), calcium appears to be the only cation that increases antiscalant oxidation; the three other cations did not significantly increase antiscalant oxidation.

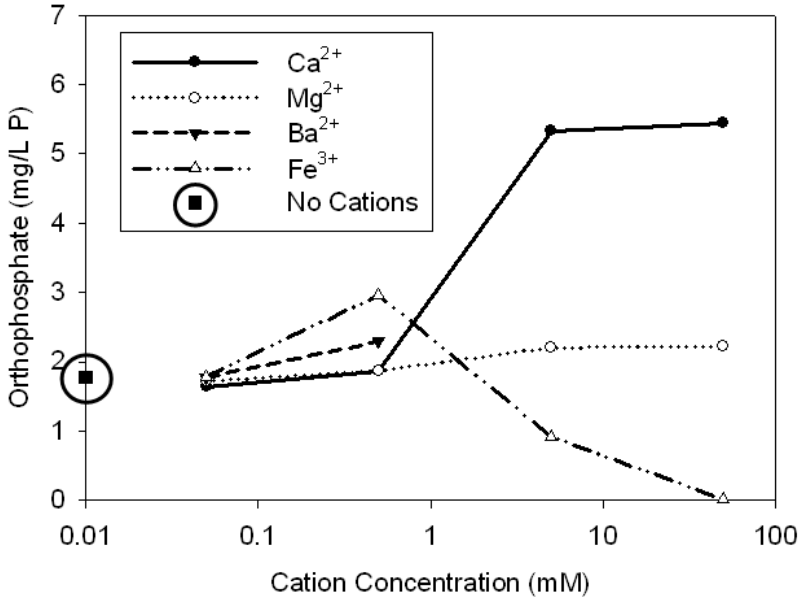

Figure 29. Effect of cation concentration on antiscalant oxidation for 85 mg/L DQ2006 (0.29 mM, 27 mg/L P), pH 6.0, 5 mg/L O_3. All experiments contained 16 mM HCO_3^-. Initial orthophosphate in solution was 1.3 mg/L P.

Simplified and Complete Water Compositions

Ten different water compositions were tested with DQ2006, including those described in Table 9, and several others, and the results are shown in Figure 30. In particular, the Simplified Maricopa data set was broken down into a water containing only calcium and sodium chloride (NaCl) and a water containing only carbonate and NaCl. Experiments with borate as a buffer in place of carbonate showed the effect of the carbonate system on oxidation. In addition, the effects of sulfate (SO_4^{2-}) and ferric iron (Fe^{3+}) were verified with the Simplified Maricopa containing, as addition components, sulfate and magnesium or sulfate, magnesium, and ferric iron. Several experiments were performed with the addition of tert-butanol (10 mM) added as a radical scavenger; these results (denoted in Figure 30 as x, closed circle, and cross symbols encircled by dotted or

solid lines) are discussed in a subsequent section on the addition of an *OH scavenger. For all water compositions tested, the addition of hydrogen peroxide (0.2 – 0.8 mole/mole O_3) caused a slight increase in antiscalant oxidation; however, the influence of individual water components and ozone concentration (Figure 28b) on antiscalant oxidation is much greater. This weak dependence of oxidation on hydrogen peroxide concentration is one indication that, for most water compositions, the antiscalant is primarily oxidized through direct reaction with ozone.

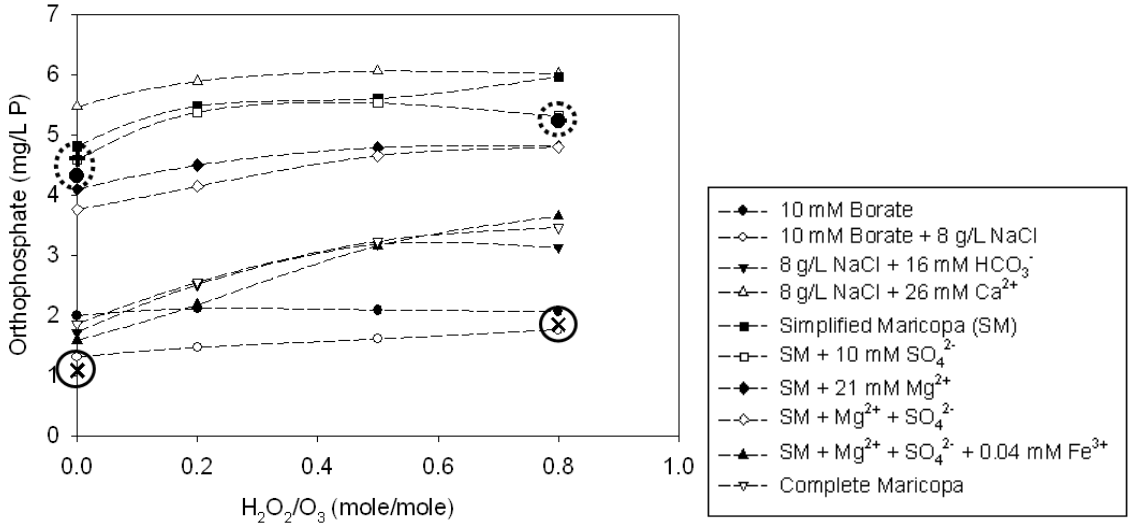

Figure 30. Antiscalant oxidation as a function of water composition for 85 mg/L DQ2006 (27 mg/L P), pH 6.0, and 5 mg/L O_3. X symbols located inside the solid line circles represent experiments performed with 10 mM tert-butanol added to the 8 g/L NaCl + 16 mM HCO_3^- water, closed circles inside dotted circles represent experiments with 10 mM tert-butanol added to the 8 g/L NaCl + 26 mM Ca^{2+} water, and plus symbols inside dotted circles represent experiments performed with 10 mM tert-butanol added to the Simplified Maricopa (SM) water. Initial orthophosphate in solution was 1.3 mg/L P.

The results shown in Figure 30 are explained in the following discussion for each water composition, beginning at the top of the legend with the most simplified water. Closed circles denote experiments with deionized water and 10 mM borate with 85 mg/L DQ2006. Borate is a buffer that does not interact with the dissolved ozone

decomposition or oxidation reactions; therefore, the results for 10 mM Borate indicate the extent of antiscalant oxidation that occurred when no water components affected the antiscalant or the ozone system. In the presence of 10 mM borate, approximately 0.7 mg/L P was produced during ozonation, but when NaCl was added to the 10 mM borate water (second entry in the legend, denoted by open circles), little to no antiscalant oxidation occurs. Previous research on how specific dissolved ions affect ozone decomposition showed that the addition of NaCl increases ozone decomposition in water (Sotelo, et al., 1989); the shorter lifetime of the dissolved ozone decreases the amount of antiscalant oxidation through direct reaction with ozone. The antiscalant oxidation that occurred for these two water compositions was most likely caused by reactions with radicals.

The replacement of 10 mM borate with 16 mM carbonate as the buffer (closed inverted triangles) had no effect on antiscalant oxidation for a H_2O_2/O_3 ratio of 0 but caused an increase in oxidation for ratios of 0.2, 0.5, and 0.8; the shape of the curve is quite different than for samples containing calcium and no ferric iron. Similar to the borate samples described above, some antiscalant oxidation may occur through reaction with hydroxyl radicals, particularly when calcium is not present to coordinate with the ligand and make the stereochemistry more favorable for reaction with ozone, or when ferric iron is available for chelation. The presence of carbonate causes the regeneration of hydroxyl radical molecules through reaction between carbonate radicals and H_2O_2 (Acero and von Gunten, 2000) and therefore increases the amount of radicals available for antiscalant oxidation. The same dependence on H_2O_2/O_3 ratio (and the same curve shape) was observed for the two water compositions containing ferric iron; as explained below, the iron tightly binds to the antiscalant preventing most of the oxidation that is achieved in samples that contain calcium.

The addition of 26 mM calcium (with no carbonate present, denoted by open triangles) caused a significant increase in antiscalant oxidation for all H_2O_2/O_3 ratios, and the presence of both calcium and carbonate (in the Simplified Maricopa water, denoted by closed squares) resulted in no further increase in antiscalant oxidation above that seen for calcium-only experiments. The calcium cations are present in excess of the DQ2006 molecules (present at 0.29 mM) and coordinate with the antiscalant, while the presence of carbonate does not appear to aid in antiscalant oxidation. Sulfate addition (open squares and open diamonds) had no effect on antiscalant oxidation, while the addition of magnesium to the Simplified Maricopa water (closed diamonds) caused a decrease in antiscalant oxidation. A more dramatic decrease in antiscalant oxidation was observed when a small concentration of ferric iron (0.04 mM) was added to the water composition (denoted by closed triangles). While several additional ions are present in the Complete Maricopa water (open inverted triangles), the results for ferric iron addition indicate that the decrease in antiscalant oxidation in the Complete Maricopa water is caused by ferric iron and not the other minor ions (Ba^{2+}, NO_3^-). The addition of ferric iron reduced antiscalant oxidation to the same amount observed for experiments containing no calcium, completely negating the positive effect of calcium on phosphonate oxidation.

Both divalent and trivalent cations have been previously reported to cause decreases in organic ligand oxidation by ozone or hydroxyl radicals (Gilbert and Hoffmann-Glewe, 1990; Lati and Meyerstein, 1978; Munoz and von Sonntag, 2000; Stemmler, et al., 2001). The strength of the coordination between the metal cation and the ligand, as well as the speciation of the metal-ligand complex, have a strong influence on the reactivity of the organic compound (Stemmler, et al., 2001). Ferric iron has been shown to form strong metal-ligand complexes with no coordination water or hydrogen bonding (on the amine ligand) and up to seven coordinating atoms within one ligand,

while cations such as calcium and zinc have been reported to form complexes with amino-organics where the amine is protonated. Following previous research, the formation (or protonation) constants, K, can be used to describe a similar expected trend for antiscalant DQ2006 and Fe^{3+}, Ca^{2+}, and Mg^{2+} (Martell, et al., 2004). The log K for Fe(III)$DQ2006^{3-}$ is 21.1 (Martell, et al., 2004), while the log K for $CaDQ2006^{4-}$ is 7.86 and the log K for $MgDQ2006^{4-}$ is 7.54 (Sawada, et al., 1993). Other values have been reported for the calcium-DQ2006 and magnesium-DQ2006 complexes (Martell, et al., 2004), but the same trend is observed; the ferric iron-DQ2006 complex has a much higher log K than either of the calcium or magnesium complexes, as well as the protonated Fe(III)DQ2006 complexes (log K for Fe(III)$HDQ2006^{2-}$ is 7.0 and log K for Fe(III)$H_2DQ2006^{-}$ is 4.8). The reduction in DQ2006 reactivity with the addition of ferric iron is most likely due to the strong un-protonated complex formed between the iron cation and the amine group, as well as several oxygen atoms, of the phosphonate. This coordination of the amine with ferric iron reduces the nucleophilicity of the nitrogen atom and makes the amine much less reactive towards ozone.

Coordination of calcium or magnesium with DQ2006 drastically changes the protonation log K values. With no metal cations present, the first protonation constant (log K) of DQ2006 is 14.2 (Popov, et al., 1999), and this log K represents the protonation of the single amine nitrogen. Therefore, at pH 6.0, the experimental pH for all data in Figure 30, essentially all DQ2006 molecules would be protonated at the amine and be relatively unreactive towards ozone; this prediction is observed in the low orthophosphate production for bivalent cation-free experiments. The log K values for calcium-protonated-DQ2006 complexes are 4.0 (M+HL, metal plus protonated ligand) and 8.85 (ML+H, protonated metal-ligand complex) (Popov, et al., 2001). Similar log K values are observed for magnesium-protonated-DQ2006 (4.3 and 9.42) (Popov, et al., 2001).

The first log K represents an amine-protonated ligand that complexes with calcium and the second log K represents a calcium-ligand complex that is protonated. While the second pKa value for a metal-free solution of DQ2006 is 7.25, indicating that the calcium-ligand log K of 8.85 represents protonation on the amine and not on one of the phosphate groups, the protonation equilibrium of the calcium-ligand complex is slow (Sawada, et al., 1987). Work by Sawada et al. (1987) suggested that amine protonation of the metal- (calcium or magnesium) ligand complex (for DQ2006) causes the metal-nitrogen bond to break, and the metal is subsequently loosely held by three oxygen-calcium ionic bonds. The unprotonated metal-ligand complex is tetrahedral and the metal is held much more tightly. The effect of calcium or magnesium on DQ2006 protonation and stereochemistry appears to play a part in the increase in oxidation observed in Figure 30; both cations allow an increase in antiscalant oxidation above that observed for 8 g/L NaCl + 16 mM HCO_3^- (closed inverted triangles).

The addition of magnesium to the Simplified Maricopa water caused a slight decrease in antiscalant oxidation as compared to results for Simplified Maricopa alone. As reported above, the log K for Mg-DQ2006+H is greater than that of the calcium complex; more of the metal-ligand complex is protonated for magnesium than for calcium, causing a decrease in antiscalant reactivity with ozone.

Effect of pH and Multiple Ozone Doses on Antiscalant Oxidation

All of the results reported thus far were obtained at pH 6.0, and in the following sections, the relationship between antiscalant oxidation and pH is discussed. Several successive ozone doses of 5 mg/L each were added to Simplified Maricopa water with DQ2006 (85 mg/L); results are shown in Figure 31 as a function of pH and H_2O_2/O_3 ratio. Samples were taken three minutes after each ozone dose was added, the second and third doses were added immediately after sampling, and a final sample (data not

shown) was taken 30 minutes after the third ozone dose; orthophosphate concentrations were the same for samples taken three minutes and 30 minutes after the third ozone dose. This result indicates that all of the antiscalant oxidation occurs very quickly, within the first three minutes after ozone is added. For both experiments with and without H_2O_2, the second and third additions of ozone caused an increase in antiscalant oxidation above that observed for the prior dose. In addition, the shape of the curve between pH 5.0 and pH 8.0 remained the same with the addition of the second and third ozone doses, and for each dose, the experiments containing H_2O_2 resulted in more antiscalant oxidation than those with no H_2O_2. While ozone decomposition to hydroxyl radicals through reaction with the deprotonated form of H_2O_2 is expected to play a minor role in antiscalant oxidation (pKa of H_2O_2 is 11.6) (Acero and von Gunten, 2000), carbonate radicals can react with H_2O_2 to form superoxide (O_2^{*-}), which can then react with ozone, forming hydroxyl radicals. Carbonate radicals are likely formed during ozonation due to the high total carbonate concentration and radical species formed from reaction between organoamines and ozone (von Gunten, 2003). Based on results from experiments with tert-butanol (shown in Figure 30 and Figure 32, and discussed below), the oxidation system appears to have a minor contribution of antiscalant oxidation from hydroxyl radicals.

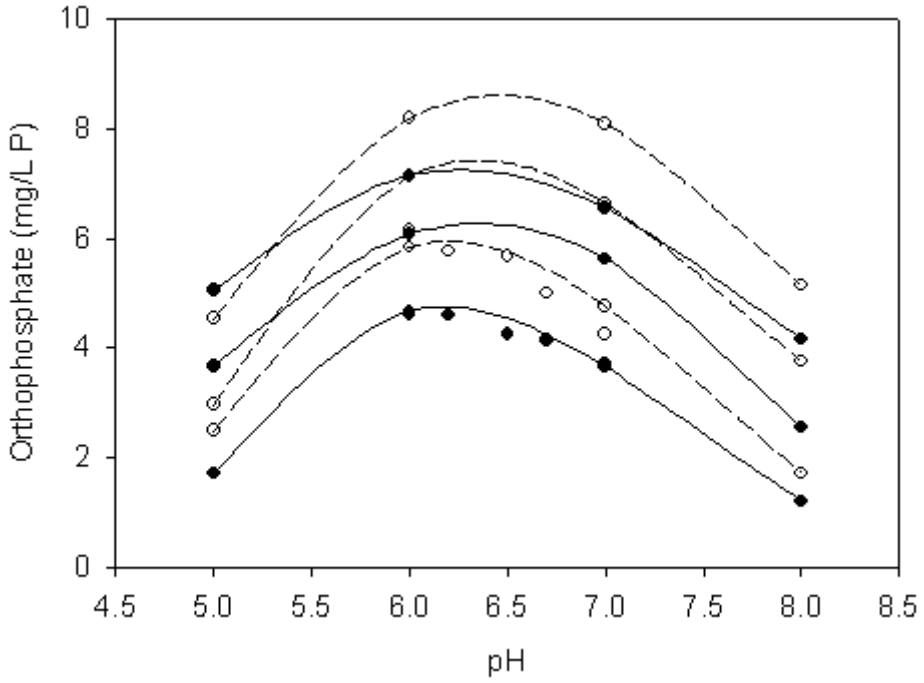

Figure 31. DQ2006 (85 mg/L) antiscalant oxidation as a function of pH and ozone dose. Solid lines and closed circles represent three successive ozone stock solution doses (5 mg/L O_3 per dose added) for experiments without hydrogen peroxide, and dashed lines and open circles represent three successive ozone doses for experiments with a ratio of 0.8 H_2O_2/O_3 (mole/mole), or 2.8 mg/L H_2O_2. The first dose resulted in the bottom curve (smallest orthophosphate concentrations) for both open and closed circles, and the second and third doses are the two curves above the first. All experiments performed in Simplified Maricopa water. Initial orthophosphate in solution was 1.3 mg/L P.

A range of pH values from 5.0 to 8.0 was tested for 85 mg/L DQ2006 (0.29 mM) and three water compositions (Simplified Maricopa, 8 g/L NaCl + 16 mM HCO_3^-, and 8 g/L NaCl + 26 mM Ca^{2+}); results are shown in Figure 32. Similar trends were obtained for experiments performed with the Simplified Maricopa water and either 43 mg/L DQ2054 or 56 mg/L D2066. For the Simplified Maricopa (Figure 31 and Figure 32, circles) and 8 g/L NaCl + 26 mM Ca^{2+} (Figure 32, closed triangles) waters, the amount of orthophosphate production was similar. Antiscalant oxidation increased from pH 5.0 to

6.0, and then decreased for pH values greater than 6.0 for both ratios of H_2O_2/O_3 tested (0 and 0.8 mole/mole). For the calcium-free water (Figure 32, open triangles), orthophosphate production increases slightly with pH; this small increase is due to an increase in ozone decomposition to hydroxyl radicals as more hydroxide ions (OH^-) are available. When calcium is not present, antiscalant oxidation occurs through reactions with hydroxyl radicals.

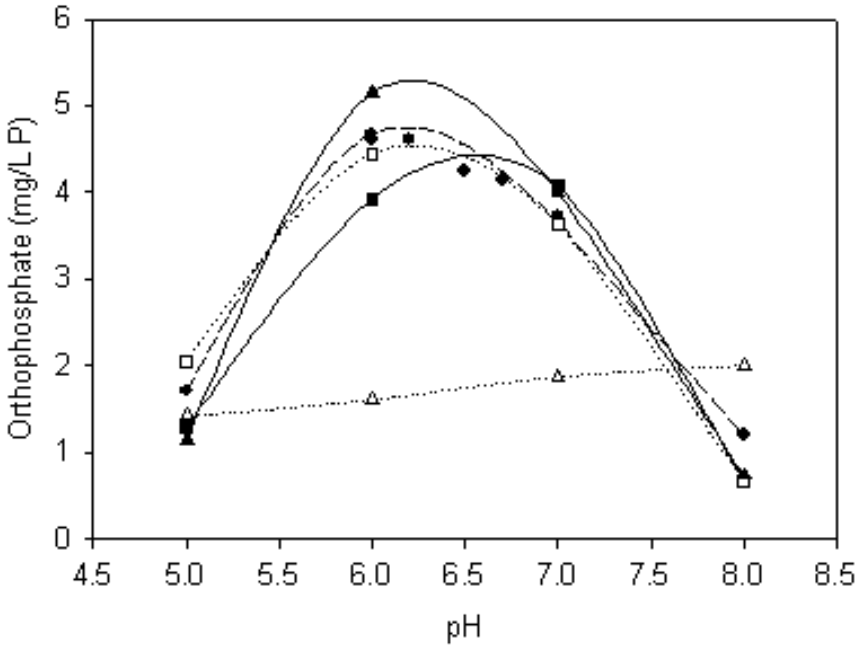

Figure 32. DQ2006 (85 mg/L) oxidation as a function of pH and water composition. Closed circles are the first dose of ozone shown in Figure 31 for no H_2O_2. Open and closed squares represent experiments containing 10 mM tert-butanol for no H_2O_2 and 0.8 H_2O_2/O_3, respectively. Open and closed triangles represent experiments with 8 g/L NaCl + 16 mM HCO_3^- and 8 g/L NaCl + 26 mM Ca^{2+}, respectively. Initial orthophosphate in solution was 1.3 mg/L P. Ozone concentration was 5 mg/L.

The dependence of antiscalant oxidation on pH results from changes in calcium-DQ2006 speciation as the pH increases from 5.0 to 8.0. A graph of calcium-DQ2006 speciation is shown in the Supporting Information (Figure 65); speciation calculations

were performed using ChemEQL (Version 3.0) (Mueller, 1996). ChemEQL is a general thermodynamic equilibrium calculation software and has been previously used to predict metal ion-ligand speciation (Stemmler, et al., 2001). The trend in oxidation as a function of pH appears to primarily follow the presence of $CaH_2DQ2006^{2-}$, with some oxidation occurring with $CaHDQ2006^{3-}$. The 2-proton form increases in concentration from pH 5 to 6 and then decreases in concentration above pH 6, while the 3-proton form increases in pH over the entire pH range tested. The 2-proton form would have a protonated amine and a proton shared between oxygen atoms of the phosphate groups.

Stemmler et al. (2001) showed dependence of zinc- and ferric iron-ligand complex oxidation (with diethylenetriamine-pentaacetate, DTPA) on pH and found that the primary species responsible for reaction with ozone were the unprotonated metal complexes. The results for DQ2006 indicate that the trend may be different for phosphonate-type compounds; the primary reactant with ozone is a protonated metal-ligand form. Within the pH range tested in this study, the unprotonated species is a minor component, while for DTPA, the unprotonated species are major species within pH 5 – 8. However, if DQ2006 had the same trend as DTPA, antiscalant oxidation should increase from pH 6.85 to 7.85 as the relative concentration of the unprotonated form increases, and the data clearly do not suggest this trend. Phosphonate compounds are known to chelate cations such as calcium more strongly than similar compounds containing carboxylic acid groups (Buglyó, et al., 1997), and protonation of the CaDQ2006 complex must affect charge distribution and complex stereochemistry so as to increase antiscalant reactivity towards ozone.

Interestingly, the same pH range was studied for an antiscalant concentration of 9 mg/L DQ2006 (0.03 mM, 1.1 mg/L DOC) and the Simplified Maricopa water, and no dependence on pH or on the presence of H_2O_2 was observed. For pH 5.0 – 8.0 and

H_2O_2/O_3 ratios of 0 and 0.8, the orthophosphate production was 1.5 – 1.8 mg/L P (of 2.9 mg/L P available in the initial antiscalant molecules). It appears that at the smaller antiscalant concentration, the shift in calcium-antiscalant speciation does not significantly affect antiscalant oxidation. This insensitivity may be due to the low DOC concentration; changes in organic carbon concentration can affect the ozone oxidation system.

Previous research has shown that ozonation of waters with high organic carbon content (>3 mg/L DOC) is not sensitive to the addition of H_2O_2 and can be considered an advanced oxidation process without the addition of H_2O_2 (Acero and von Gunten, 2001; Buffle, et al., 2006a). The ozone/H_2O_2 system is an advanced oxidation process because the primary oxidant is the hydroxyl radical; in the presence of high DOC concentration, ozone reacts with specific moieties (such as amine groups), producing radicals, including the hydroxyl radical. For experiments with 85 mg/L DQ2006, the ozone system is most likely an advanced oxidation process, with radical production and oxidation occurring through direct reaction with ozone. At 9 mg/L DQ2006, the ozone system is not likely to be an advanced oxidation process; however, the presence of calcium caused oxidation to occur through reactions with ozone and not *OH. This can be concluded because the addition of H_2O_2 had no effect on antiscalant oxidation. Experiments with calcium have shown that calcium coordination increases antiscalant oxidation and shifts the primary oxidation pathway to reaction with ozone (Figure 29 and Figure 32, explained in the following section). It appears that for low DOC concentrations and therefore minimal *OH production, phosphonate antiscalant oxidation is not sensitive to pH, while at high DOC concentrations (and increased radical production) this system is quite sensitive to pH. The difference is likely due to how calcium coordination affects antiscalant oxidation after initial reaction with the ozone molecule for low DOC versus high DOC conditions.

Addition of an *OH Scavenger

Several experiments were performed with 85 mg/L DQ2006 (10.5 mg/L DOC) and 10 mM of tert-butanol added as a hydroxyl radical scavenger to determine the primary pathway for ozone decomposition. The results for an abbreviated water composition study and a pH study performed with tert-butanol in the Simplified Maricopa water are shown in Figure 30 and Figure 32, respectively. Based on previous work (Benner, et al., 2008; Buffle, et al., 2006a; Elovitz, et al., 2000), tert-butanol was chosen as a hydroxyl radical scavenger that does not react directly with ozone; the presence of tert-butanol prevents ozone decomposition through radical chain reaction (Acero and von Gunten, 2000; Buffle, et al., 2006a). Due to the high concentration of DOC, the presence of amine groups in the antiscalants, and the weak dependence of phosphonate antiscalant oxidation on the addition of hydrogen peroxide (shown previously in Figure 30), the addition of tert-butanol was expected to have little to no effect on antiscalant oxidation. The addition of hydrogen peroxide typically increases ozone decomposition through radical chain reaction to the hydroxyl radical; if hydroxyl radicals were primarily responsible for antiscalant oxidation, the addition of hydrogen peroxide should significantly increase oxidation. However, little to no increase in antiscalant oxidation was observed with the addition of hydrogen peroxide, and ozone reacted directly with the amine groups present in the antiscalants. In addition, previous work (Buffle, et al., 2006b) has shown that in waters with high NOM concentrations (i.e., greater than 3-4 mg/L DOC), the addition of hydrogen peroxide has little effect on increasing ozone decomposition, and ozone alone may act as an advanced oxidation process through reactions with specific functional groups (phenols, amines, and olefins) of natural organic matter.

If ozone decomposition is controlled by radical chain reaction, then the addition of tert-butanol should greatly decrease antiscalant oxidation, while if ozone decomposition is controlled by direct reaction with the dissolved organic compounds, the addition of tert-butanol should have little to no effect on oxidation. The pH experiments performed with tert-butanol with or without H_2O_2 (open and closed squares in Figure 31b) resulted in an orthophosphate production similar to that of experiments performed without tert-butanol; ozone decomposition appears to be primarily controlled by direct reaction with antiscalant for the pH range tested and the Simplified Maricopa water, and antiscalant oxidation occurs primarily through direct reaction with ozone and not through reaction with hydroxyl radicals.

In Figure 32, experiments for tert-butanol added to Simplified Maricopa water with or without H_2O_2 are compared with data for the Simplified Maricopa water and no H_2O_2. Both tert-butanol experiments resulted in the same amount of orthophosphate production as that of the Simplified Maricopa water with no H_2O_2. The slight increase in antiscalant oxidation with the addition of H_2O_2 to Simplified Maricopa water, shown in Figure 31, is prevented through the addition of tert-butanol, but no further decrease in antiscalant oxidation is observed for all pH values tested (5.0 – 8.0). These results clearly indicate that the primary pathway for antiscalant oxidation in waters with high concentrations of calcium and carbonate is through direct reaction with ozone.

The water composition study with tert-butanol (Figure 30) included tests with three water compositions: 8 g/L NaCl + 16 mM HCO_3^-, 8 g/L NaCl + 26 mM Ca^{2+}, and Simplified Maricopa for H_2O_2/O_3 ratios of 0 and 0.8. For the first water, the presence of tert-butanol completely prevented antiscalant oxidation (initial orthophosphate in solution before oxidation was measured at 1.3 mg/L P), while the experiments with the 8 g/L NaCl + 26 mM Ca^{2+} and Simplified Maricopa waters resulted in little to no decrease in

antiscalant oxidation. The results indicate that, while direct reaction with ozone is most likely the oxidation pathway for DQ2006 antiscalant in the second two waters in which calcium was present, reaction with hydroxyl radical is the oxidation pathway when only carbonate is present. In the absence of calcium, the amine nitrogen is protonated and antiscalant stereochemistry is not optimal for direct reaction with ozone. When both calcium is present, the oxidation pathway shifts to ozone and calcium contributes through changes in protonation and stereochemistry.

SUPPORTING INFORMATION AVAILABLE

Figure 61. Molecular model of antiscalant DQ2006 alone and coordinated to a calcium ion.

Figure 62. Molecular model of antiscalant DQ2054 alone and coordinated to a calcium ion.

Figure 63. Molecular model of antiscalant DQ2066 alone and coordinated to a calcium ion.

Figure 64. The effect of carbonate concentration on DQ2006 oxidation.

Figure 65. Speciation of calcium with DQ2006 for a pH range of 5 to 8.

Chapter 7: Side-stream treatment of brackish water reverse osmosis concentrate: Effect of antiscalant degradation on salt precipitation and solid/liquid separation[4]

ABSTRACT

The key limitation to the application of brackish water reverse osmosis (RO) desalination on inland water resources is concentrate disposal. Due to salt precipitation of sparingly soluble salts ($CaCO_3$, $CaSO_4$, $BaSO_4$, $SrSO_4$), RO membrane recovery cannot be increased further; thus, other strategies must be investigated. Antiscalants are often added to RO feed water to help prevent precipitation and increase RO recovery, but in concentrate treatment, antiscalants may prevent precipitation of problematic constituents. A 3-stage process to treat brackish water RO concentrate was investigated; the stages include oxidation of antiscalants with ozone and hydrogen peroxide, precipitation at elevated pH, and solid/liquid separation. A model water concentrate was used to perform laboratory scale experiments for each treatment stage. Experimental results showed that the advanced oxidation process (AOP) of ozonation and hydrogen peroxide allowed increased calcium precipitation as compared to precipitation without prior ozonation. The AOP also removed the effect of antiscalant on precipitate particle size distribution and particle morphology. In some cases, the AOP also improved microfiltration performance for the solid/liquid separation stage. The concentrate treatment could increase overall recovery from 80% to 96%. In comparison, precipitation without oxidation allows a calculated increase in overall recovery from 80% to 94%.

Keywords

[4] Manuscript to be submitted to the Journal of Membrane Science.

Desalination

Antiscalant

Precipitation

Concentrate

Ozone

Nomenclature

ACC	Amorphous calcium carbonate
AOP	Advanced oxidation process
APS	Accelerated precipitation softening
ATMP	Aminotri(methylene phosphonic acid)
CF	Concentration factor
DOC	Dissolved organic carbon
DTPA	Diethylenetriamine-pentaacetate
DTPMP	Diethylenetriamine penta(methylene phosphonic acid)
ED	Electrodialysis
EDX	Energy dispersive x-ray
G_m	Gibb's free energy
HDTMP	Hexamethylenediamine tetra(methylenephosphonic acid
IAP	Ion activity product
IC	Ion chromatography
ICP-AES	Inductively coupled plasma atomic emission spectroscopy
K_{sp}	Solubility constant
LSI	Langlier saturation index
MF	Microfiltration

NF	Nanofiltration
NOM	Natural organic matter
RO	Reverse osmosis
R_w	Recovery
R_s	Salt rejection
S	Saturation ratio
SEM	Scanning electron microscopy
SI	Saturation index
TDS	Total dissolved solids
UV	Ultraviolet

INTRODUCTION

Reverse osmosis (RO) membrane technology has advanced dramatically over the past 40 years to become the primary technology choice for new desalination plant installations (Frenkel, 2000; Fritzmann, et al., 2007; Glueckstern, 2000; Glueckstern, et al., 2001; Graber, 2006; Lee, et al., 2003; Magara, et al., 2000; Sandia, 2003; Wilf and Klinko, 2001). RO membrane desalination for drinking water uses either seawater or brackish water. Both seawater and brackish water plants must dispose of the RO waste stream (concentrate); the concentrate volumetric flow is much larger for seawater RO plants, but most plants are coastally located and return the concentrate to the same seawater source. Brackish water RO plants have a much smaller concentrate volume, but compared to conventional fresh water treatment plants (>99% recovery (the fraction of feed water that becomes product water)), concentrate disposal remains one of the most difficult challenges faced during new plant development. Options for RO concentrate disposal include combined sewer disposal, evaporation ponds, deep well injection,

irrigation, and surface water disposal (Bloetscher, et al., 2006; Mickley, 2004). However, each option has drawbacks and can be costly to implement; surface water disposal is the least expensive choice but is often impossible due to deleterious environmental effects. Therefore, concentrate disposal remains a key limiting factor for brackish water RO plants, particularly those built inland.

To reduce the RO concentrate volume and increase recovery, the concentrate can be treated to remove problematic precipitates and most of the concentrate water can be returned to the RO system for further desalination. Accordingly, this study focuses on the development of a novel 3-stage concentrate treatment process (shown in Figure 33): antiscalant degradation, salt precipitation, and solid/liquid separation. Following concentrate treatment, the recovered water would be treated by a secondary RO or nanofiltration (NF) step, and the overall recovery of the system would be the combined recovery of the original RO stages and the secondary membrane treatment. The key objective of this research was to evaluate the effect of antiscalant degradation on salt precipitation and solid/liquid separation (filtration). Data were obtained for the change in concentration of specific ions in solution, particle size distributions of precipitates, particle morphology, elemental content of precipitates, and microfiltration of precipitated solutions. The advanced oxidation process (AOP) of ozone (O_3) and hydrogen peroxide (H_2O_2), often called peroxone, was used to degrade organophosphonate antiscalants; the effects of several parameters, including ozonation time, antiscalant type, water composition, ratio of H_2O_2 to O_3, and ozone dose (mg O_3/mg DOC), on antiscalant oxidation were evaluated. The results obtained from the combined ozonation-precipitation-separation experiments were used to calculate the increase in predicted overall RO recovery.

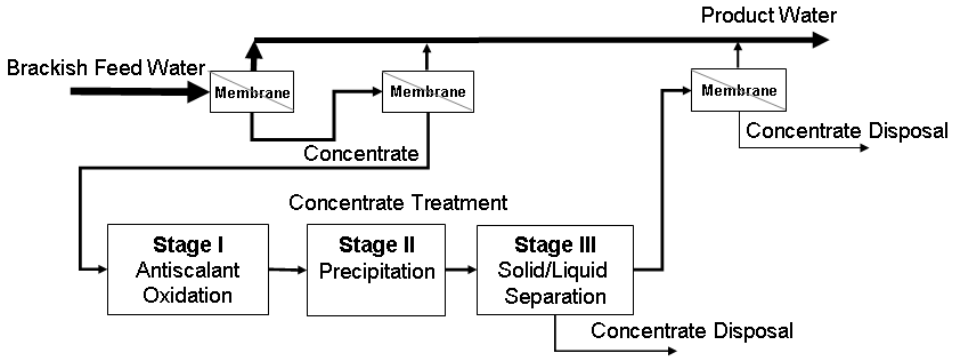

Figure 33. Flow diagram of proposed concentrate treatment process.

BACKGROUND

Seawater sources have a total dissolved solids (TDS) content between 30,000 and 45,000 mg/L, while the TDS of most brackish waters ranges from 1,000 to 10,000 mg/L (Mickley, 2001). This difference in salt content limits the recovery for seawater RO systems to around 50%, while brackish water systems can achieve between 75% and 90% recovery. Today, the need for inland desalination is continuously increasing (Afonso, et al., 2004; Allam, et al., 2002; Masson, et al., 2005; Sandia, 2003; Walha, et al., 2007); fresh water aquifers are being depleted or slowly becoming saline due to activities such as overuse, farming, oil and gas drilling, and seawater infiltration. In addition, naturally saline aquifers remain a largely untapped water resource (Sandia, 2003). Brackish water RO membrane recovery is primarily limited by sparingly soluble salts that precipitate and deposit on the membrane surface, creating an impermeable layer of scale. Low-solubility salts include calcium carbonate ($CaCO_3$), calcium sulfate ($CaSO_4$), barium sulfate ($BaSO_4$), strontium sulfate ($SrSO_4$), and silicates. When each salt reaches its respective solubility limit during RO treatment, precipitation occurs, and irreversible membrane scaling causes either decreased permeate flow or increased feed pressure. Salt

precipitation can be controlled using a combination of pH and chemical addition; chemicals called antiscalants are often used to limit precipitation (Plottu-Pecheux, et al., 2002; Rahardianto, et al., 2006; Semiat, et al., 2003). While antiscalants allow RO recovery to increase above the point of salt saturation, antiscalants do not completely prevent precipitation, and at high recoveries (>90%), precipitation will occur even in the presence of antiscalants. As a result, novel RO concentrate treatment is necessary to achieve increased RO recovery and decreased concentrate volume.

Various alternative strategies to conventional concentrate disposal have been investigated, including coupled membrane technology (RO combined with ultrafiltration or concentrate treated by seawater RO membranes), evaporation combined with salt production, and pre- or inter-stage treatment through salt precipitation (Almulla, et al., 2002; Gilron, et al., 2005; M'nif, et al., 2007; Mickley, 2004; Rahardianto, et al., 2007; Ravizky and Nadav, 2007). All of these options increase brackish water RO membrane recovery and significantly decrease the concentrate volume to be disposed. In particular, concentrate treatment through accelerated salt precipitation (termed accelerated precipitation softening, APS) between brackish water RO stages in series has been studied (Gabelich, et al., 2007; Rahardianto, et al., 2007; Williams, et al., 2002). The work on interstage salt precipitation has shown that a large portion of target ions (Ca^{2+}) can be removed from the concentrate, enabling further RO treatment of the concentrate and increased overall recovery (from 90% to 97% for Colorado River water) (Rahardianto, et al., 2007). However, the effect of antiscalants on the precipitation process has not been evaluated; although precipitation can be achieved when antiscalants are present, the chemicals are expected to have an influence on the salt precipitation.

Antiscalants prevent precipitation by disrupting one or more aspects of the crystallization stages. Antiscalants are effective in increasing the ion concentration

threshold required for clustering, as well as disrupting the nuclei ordering and crystal structure (Darton, 2000). Some antiscalants also can adsorb onto crystal surfaces and repel other ions in solution or fully chelate with dissolved ions (Darton, 2000). Of all of the possible actions between antiscalants and ions, only the chelation mechanism requires equimolar amounts of ion and antiscalant. Therefore, typical antiscalant concentrations in the RO feed do not exceed 35 mg/L and are more often less than 10 mg/L (Boffardi, 1997; Hasson, et al., 2001; Hydranautics, 2003; Rahardianto, et al., 2006; Shih, et al., 2004; Vrouwenvelder, et al., 2000).

Two common classes of antiscalants are used in drinking water RO applications. Both are synthetic organic polymers, with one based on phosphonates alone and the other based on acrylic acid with or without phosphonate blending. The four antiscalants used in this study, shown in Figure 34, were chosen because they are often used in drinking water applications (Knepper, 2003). The defining characteristic of phosphonates is a phosphorus-carbon (P-C) bond, and the antiscalants also have at least one fully-substituted amino group (nitrogen bonded to three carbons). The P-C bonds make the phosphonates much less susceptible to biodegradation, as compared to the original phosphate antiscalants.

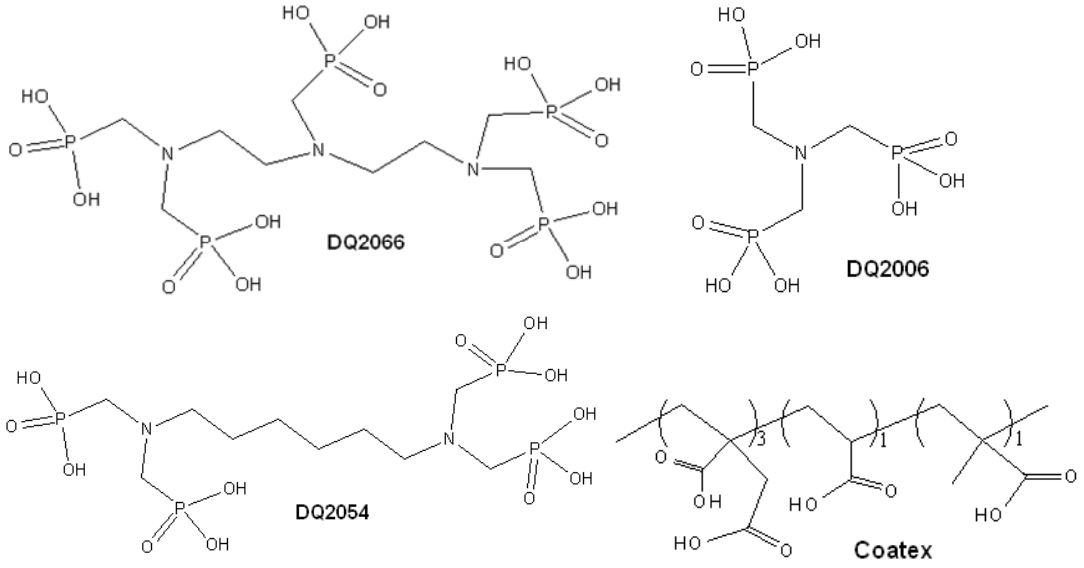

Figure 34. Chemical structures of antiscalants DQ2066, DQ2006 (recommended for general metal ion control), DQ2054 (recommended for calcium sulfate control), and Coatex.

Little research has been done on the oxidation of antiscalant compounds (Yang, et al., 2004). Yang *et al*. used the Fenton process (Munter, et al., 2001) to degrade antiscalants. This process was successful in degrading antiscalants but would not be easily applied in municipal drinking water treatment systems. After a review of available advanced oxidation processes (Andreozzi, et al., 1999; Guzzella, et al., 2002; Suty, et al., 2004), the AOP using ozone (O_3) and hydrogen peroxide (H_2O_2) was chosen for antiscalant degradation. This AOP, often termed peroxone, is the most common AOP used today in drinking water treatment (Acero and von Gunten, 2000). Ozone, alone, is used for disinfection in many conventional drinking water treatment facilities, and the extension of an ozone treatment system to peroxone would require minor system modifications; the application of peroxone treatment in a desalination facility could be implemented on a full-scale basis using current knowledge of ozone installations.

Aqueous ozone naturally decomposes into the hydroxyl radical molecule, *OH, a powerful, nonspecific oxidant. Oxidation with ozone occurs both through reactions with the ozone molecule itself and with the hydroxyl radicals produced through decomposition (von Gunten, 2003). Ozone is the desired and useful molecule in disinfection, but the hydroxyl radical is often the desired oxidant for organic compound degradation in water and wastewater (Acero and von Gunten, 2001). The system of major chemical reactions that describe ozone decomposition in water has been extensively studied (Buffle, et al., 2006b; Elovitz and von Gunten, 1999; Elovitz, et al., 2000; Gurol and Singer, 1982; von Gunten, 2003), and similar reactions for the peroxone system have also been determined (Acero and von Gunten, 2000; Acero and von Gunten, 2001).

Several parameters can be used to describe the state of an RO concentrate in relation to the feed water and the precipitation potential. The concentration factor (CF) can be calculated through a mass balance relationship with the variables recovery (R_w) and salt rejection (R_s) (Le Gouellec and Elimelech, 2002; Rahardianto, et al., 2007; Rahardianto, et al., 2006):

$$CF = \left(\frac{1}{1 - R_W} \right) \left[1 - R_W \left(1 - R_S \right) \right] \qquad (1)$$

Recovery is the volume fraction of permeate to feed, and salt rejection is the fraction of dissolved ions retained by the membrane on the feed/concentrate side. All experiments in this research were performed on synthetic RO concentrate with an assumed recovery of 80% and a salt rejection of 100%, giving a CF value of 5.

Recovery and CF values are specific to the feed water and vary depending on the feed water TDS and specific composition. The recovery and CF are often restricted by solubility limits of typical precipitates, including calcium carbonate ($CaCO_3$), calcium

sulfate ($CaSO_4$), barium sulfate ($BaSO_4$), strontium sulfate ($SrSO_4$), and silicates. Thus, it is helpful to describe the a concentrate in terms of the precipitation potential of each component. Saturation indices, SI, are often used in RO membrane research (Hydranautics, 2001; Rahardianto, et al., 2006; Shih, et al., 2004) to describe the precipitation potential of a particular salt. The general relationship is as follows:

$$SI_x = \frac{IAP}{K_{sp,x}} \tag{2}$$

where the IAP, or ion activity product, is the activity product of the individual ion components in solution, and the K_{sp} is the solubility constant of the salt precipitate. If the SI for a particular precipitate increases above 1, precipitation may occur (kinetics affects the extent of precipitation during RO treatment). Another relationship is often used in precipitation literature to describe the thermodynamic potential of a salt to precipitate. For a general reaction $A_xB_y(s) = xA^{y+} + yB^{x-}$, the saturation ratio, S, is given by:

$$S = \left(\frac{IAP}{K_{sp}} \right)^{1/(x+y)} \tag{3}$$

S can be directly connected to the thermodynamic driving force for salt crystallization, the increase in Gibb's free energy, ΔG_m (Nielsen, 1984). While the details of crystallization growth were not studied in this work, the use of *S* as a comparison parameter allows future possible thermodynamic and kinetic study of experimental results.

The successful use of antiscalants is limited at high saturation ratios. The limits for several problematic precipitates according to a membrane manufacturer are shown in Table 10. At a recovery of 80% and pH 6.0, the synthetic concentrate used in this study (called Maricopa) has S values of 12.2 for barium sulfate, 1.05 for calcium sulfate, 0.97

for calcium carbonate (calcite), and 0.45 for magnesium hydroxide. As the recovery is increased, the S values increase; the relationship between the Maricopa concentrate and the saturation ratio (at pH 6.0) is shown in Figure 35. Activity calculations were performed using the equations developed by Pitzer (Pitzer, 1991). The Pitzer equations for mixed electrolytes were used, and all terms were employed except for uncharged species terms. The Pitzer equations are based on the Debye-Huckel and Guggenheim models and can be used for solutions of up to 6 M ionic strength, due to inclusion of terms that account for short-range forces and higher-order electrostatic terms (Pitzer, 1973; Pitzer, 1975; Pitzer and Mayorga, 1973). Reported activity coefficient values for ions in seawater (Pitzer, 1991), as well as the Davies model (valid for ionic strength < 0.5 M), were used to check Pitzer equation results.

As the theoretical recovery increases from 80% to 98%, the saturation ratio of each precipitate increases, as shown in Figure 35. At 80% recovery, both gypsum ($CaSO_4$) and calcite ($CaCO_3$) have S values around 1 (1.05 and 0.97, respectively). At this recovery, gypsum and calcite precipitation would be largely avoided during RO treatment. However, barium sulfate is supersaturated, and the S value is above the recommended S limit for antiscalant application. Although the barium concentration in the model water is low compared to the calcium concentration, the precipitate can still cause scaling and limit the RO recovery. A recovery increase would cause all three precipitates to be supersaturated; therefore, increasing the RO recovery alone is not a viable strategy for concentrate volume reduction. The concentrate treatment scheme of ozonation, precipitation, and solid/liquid separation is one potential strategy for concentrate management and increased recovery.

Table 10. Concentration limit (as SI or S) of antiscalant use for several sparingly soluble salts [29].

Salt Precipitate	**SI**	**S**
$BaSO_4$	80	8.9
$CaSO_4$	4	2.0
$SrSO_4$	12	3.5
$CaCO_3$*	$10^{2.9}$ (LSI = 2.9)	28
Silica (SiO_2)	1.6	1.2

*The SI for calcium carbonate is typically presented as the log SI (LSI, Langlier Saturation Index).

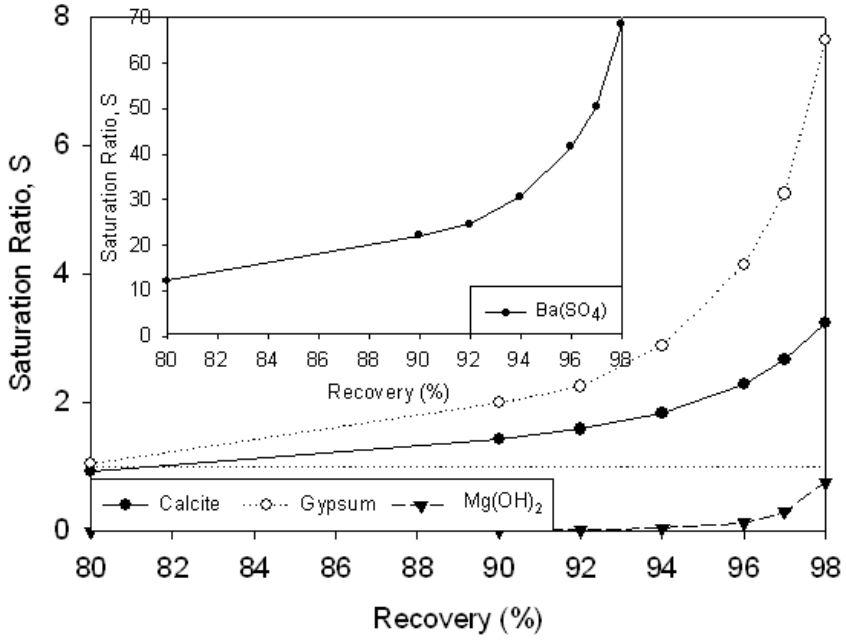

Figure 35. Saturation ratios increase as recovery increases for the model Maricopa County water. Calculations performed at pH 6.

Although ozone decomposition increases as pH increases, the pH for combined ozonation-precipitation experiments was chosen based on calcite scale control. While the

saturation ratios of most precipitates remain relatively constant with pH, the saturation ratio of calcite changes drastically (Rahardianto, et al., 2007), and pH control through acid dosing is often used during RO treatment to control calcite scaling. At pH values above 6, the saturation ratio for calcite increases as the proportion of carbonate available increases. The carbonate system is controlled by the reactions:

$$H_2CO_3^* \leftrightarrow H^+ + HCO_3^-, (K_1) \quad (4)$$

$$HCO_3^- \leftrightarrow H^+ + CO_3^{2-}, (K_2) \quad (5)$$

where $pK_1 = 6.1$ and $pK_2 = 9.7$ (for the Maricopa concentrate at 80% recovery, calculations based on Pitzer equations) (Pitzer, 1991). At pH 6, the carbonate ion concentration is negligible but increases with pH. For the Maricopa County water, at a pH of 7.5, the calculated saturation ratio for calcite at 80% recovery is 8.1.

The carbonate system also becomes important during precipitation, where calcium carbonate, or calcite, is a major precipitate. In addition to calcite, the precipitate magnesium hydroxide is highly sensitive to pH changes. Although the calcite precipitate is solidly packed and settles easily, the magnesium hydroxide precipitate retains water and does not settle easily. Therefore, the choice of precipitation pH is important to maximize calcite precipitation and avoid excessive magnesium hydroxide precipitation. The bases typically used in precipitation softening include sodium hydroxide (NaOH), calcium hydroxide ($Ca(OH)_2$), and sodium carbonate (Na_2CO_3).

EXPERIMENTAL

Materials

All inorganic salts, acids, and bases used in experiments were obtained from VWR International (West Chester, PA, USA) and were all ACS grade reagents. Salts used to make synthetic test solutions included calcium chloride dihydrate, barium

chloride dihydrate, sodium bicarbonate, sodium chloride, sodium sulfate, magnesium chloride hexahydrate, calcium nitrate tetrahydrate, and ferric chloride hexahydrate. Deionized water was used to make all test solutions. Solution pH adjustment was achieved using solutions of 5 N hydrochloric acid (HCl) (made from concentrated HCl) and 6 N sodium hydroxide (NaOH) (made from NaOH pellets). A combination of sodium carbonate ($NaHCO_3$) and NaOH were used to change the pH and add carbonate at the beginning of each precipitation experiment. Potassium iodide (KI) was used in ozone traps and to measure the ozone offgased during ozonation experiments. Sodium thiosulfate (0.01 N $Na_2S_2O_3$) and a stabilized starch solution (0.5%) were used to titrate reacted KI solution; both solutions were obtained from VWR International. 10% Nitric acid was used to soak all glassware in contact with organic compounds following a typical laboratory washing procedure. Standard pH buffers (4, 7, and 10) were obtained from VWR International.

Unstabilized hydrogen peroxide (30%) was obtained from Sigma-Aldrich Co. (St. Louis, MO, USA). Stabilized hydrogen peroxide contains different types of additives to prevent chemical decomposition, often including organophosphonate compounds. Therefore, the unstabilized version was required to avoid false results due to antiscalant-like compounds in the hydrogen peroxide. Hydrogen peroxide can react with heavy metals and water and is more reactive in light. The stock solution was kept in its original container in the dark, and all experiments were completed using a working solution of 10,000 mg/L. 0.1 N potassium permanganate ($KMnO_4$) was obtained from VWR International and was used to titrate hydrogen peroxide solutions (Klassen, et al., 1994) and check for chemical degradation. Titrations with $KMnO_4$ showed that the original solution did not significantly degrade over one year, but the more dilute working solutions needed to be replaced every month.

Three antiscalant samples were obtained from Dequest Water Management Additives, a subsidiary of Thermophos. The antiscalants included the penta-sodium salt of aminotri(methylene phosphonic acid), or ATMP, the hexa-potassium salt of hexamethylenediamine tetra(methylenephosphonic acid), or HDTMP, and the hepta-sodium salt diethylenetriamine penta(methylene phosphonic acid) or DTPMP. Dequest refers to ATMP as DQ2006, to HDTMP as DQ2054, and to DTPMP as DQ2066, and these names are used throughout the article. A polymer antiscalant sample was obtained from Coatex S.A. (France) and is a proprietary polymer containing 19% acrylic acid, 20% methacrylic acid, and 61% itaconic acid.

The water data set used for ozonation and ozonation-precipitation-separation experiments was based on a brackish groundwater in Maricopa County, Arizona, USA (Jurenka and Chapman-Wilbert, 1996). The water source has been considered for desalination due to high levels of nitrate, chloride, and TDS; the 1996 study considered electrodialysis (ED), reverse osmosis (RO), and nanofiltration (NF) and concluded that RO was the most successful at reducing the inorganic contaminants of concern.

An operating pH of 6.0 was chosen for the ozonation step of the ozonation-precipitation-separation experiments presented in this work. This choice was based on knowledge of typical RO concentrate pH (Bloetscher, et al., 2006; Martin and Goodman, 2003; Wilf, 1997). For precipitation, the operating pH was 10.5 and was chosen based on the saturation ratios of calcite (87) and magnesium hydroxide (2.7). Some magnesium precipitation was expected at this pH value.

All experiments were performed on synthetic RO concentrate assuming an RO recovery of 80% and a salt rejection of 100%. The complete water data set (termed Complete Maricopa) used for the synthetic RO concentrate is shown in Table 11. The pH of the RO feed water was reported as 7.5 (Jurenka and Chapman-Wilbert, 1996), and the

natural pH of the synthetic RO concentrate solution was 7.8. In addition to the complete water data set, several simplified water compositions were tested. The simplified waters contained additional sodium and chloride to achieve a similar ionic strength as the full data set. The water composition of Simplified Maricopa is shown in Table 12. Simplified Maricopa + Na_2SO_4 included the sulfate concentration, and Simplified Maricopa + $MgCl_2$ included the magnesium concentration (shown in Table 11). To make the synthetic waters, stock solutions of each individual salt were made; stock solutions of sodium bicarbonate were made fresh at least once every week to minimize the change in carbonate concentration as carbon dioxide slowly offgased from the solution.

Table 11. Complete Maricopa water components concentrations at a calcium carbonate saturation ratio of S = 8 and an RO recovery = 80%.

Component	Concentration (mg/L)	Concentration (mM)
Ba^{2+}	2	0.01
Ca^{2+}	1,030	25.7
Fe^{3+}	2.25	0.04
Mg^{2+}	515	21.1
Na^{+}	661	36.9
SO_4^{2-}	991	16.3
Cl^{-}	3,346	92.5
NO_3^{-}	87	1.4
Alkalinity (as $CaCO_3$)	780	
TDS	7,580	
Natural Starting pH	7.8	

Table 12. Simplified Maricopa water used for preliminary ozonation-precipitation combined experiments. Salts used: NaCl, $NaHCO_3$, $CaCl_2$. Natural pH = 7.8 and ozonation pH = 6.0.

Component	Concentration (mg/L)	Concentration (mM)
Na^+	1,537	66.8
Cl^-	3,649	102.8
Ca^{2+}	1,030	25.8
*C_T added as HCO_3^-	950	15.6
Alkalinity (as $CaCO_3$)	780	
TDS	7,166	

*C_T = Total Carbonate

Equipment

The ozone generator (OzoneLab™ Model OL80W/FM100VT) used for experiments was obtained from Ozone Services, a division of Yanco Industries, Ltd. (Burton, British Columbia, Canada). The oxygen flow to the ozone generator was controlled by a digital mass flow meter and controller (Mass Flo© Model 1179A-01522CS1BV), obtained from MKS Instruments (Wilmington, MA, USA). The flow meter was calibrated by MKS for oxygen flow at room temperature (20 ^oC). The flow meter was powered by a single channel power supply (15 pin Model 246C). The ozone generator was used to apply gaseous ozone directly to an aqueous experiment or make an ozone stock solution (60 – 70 mg/L O_3) from which aliquots were taken and dosed to an experiment as dissolved aqueous ozone.

Precipitation experiments were performed in a jar test apparatus (Fisherbrand model 10008 or Phipps & Bird Stirrer model 7790-400) in 1 L beakers, each agitated by a stainless steel paddle.

Inductively coupled plasma atomic emission spectroscopy (ICP-AES) was used to analyze metal concentrations before and after precipitation experiments. A Spectro Ciros CCD Model was used from Spectro AI GmbH, with Smart Analyzer data acquisition software (version 3.2, 1995-2000). Samples were analyzed for magnesium, calcium, barium, and iron. Standards were made with appropriate sodium chloride additions to avoid ion effects on ICP concentration results. Samples were prepared in 15 mL screw-cap polypropylene centrifuge tubes with concentrated nitric acid added for a final concentration of 1.5% (v/v). If necessary, samples were stored at 4 ^{o}C for no longer than 2 weeks before analysis. Some calcium and magnesium measurements were made using standard titrations for calcium and hardness with ethylenediaminetetraacetic acid (EDTA) (Eaton, et al., 2005).

Two different scanning electron microscopes (SEM), a LEO 1530 and a Hitachi S-5500, were used to obtain images of the precipitates. Both SEMs were equipped with energy dispersive x-ray (EDX) elemental analysis. Samples were mounted on adhesive carbon tabs; precipitates were placed directly onto the carbon tab or were on a nitrocellulose microfilter that was placed on the carbon tab. All samples were sputter coated with silver.

All pH measurements were taken with a Thermo Electron Corp. pH meter (Orion 720 A+), calibrated with three buffers (pH 4, 7, and 10 standard buffers). The pH of a solution changes with ionic strength, due to changes in hydrogen ion activity and interferences at the electrode surface caused by other ions (Baumann, 1973; Wiesner, et al., 2006). Therefore, 8 g/L sodium chloride was added to each pH buffer to account for

experimental solution ionic strength. The addition of NaCl to the standard buffer solutions causes a decrease in the pH of the buffer; however, based on previous work by Wiesner, et al., (2006), 8 g/L NaCl causes no more than a 0.1 unit change in pH to each buffer solution. Therefore, no recalculation of the buffer pH values was performed, and the pH values are reported as recorded based on pH meter calibration with the salted buffers.

An ion chromatography system (Metrohm 700 series, column Metrosep A Supp 5, 150/4.0 mm) was used to measure sulfate concentrations after precipitation and filtration. Some sulfate measurements were taken with a Hach Ratio/XR turbidimeter; the turbidimeter was used to measure barium sulfate turbidity and to ultimately obtain sulfate concentrations in filtered precipitated samples.

Filtration of precipitated samples was performed using either a dead-end pressurized (0.5 bar) cell with a stir bar or a Millipore glass filter holder assembly (47 mm diameter, 300 mL filter holder), with funnel, fritted base, rubber stopper, and clamp. Millipore nitrocellulose filters (0.1 μm pore size) were used. The dead-end filtration cell was used with a digital mass balance to measure filtrate (permeate) flux. Samples filtered with the vacuum assembly were analyzed for dissolved calcium.

Particle size distributions were obtained using a laser granulometer Mastersizer S (Malvern Instruments). The Mastersizer S is a static laser light scattering instrument. A polydisperse deconvolution algorithm and the Fraunhofer theory were used to translate the detected light scattering data (diffraction intensity with as a function of diffraction angle) into a best-fit particle size distribution.

Orthophosphate is a major oxidation product of phosphonate-type compounds (Klinger, et al., 1998). Standard method 4500-P E (Ascorbic Acid Method) was used to measure orthophosphate in aqueous solutions (Eaton, et al., 2005). A UV/visible

spectrophotometer (Agilent model 8453) was used to measure reacted orthophosphate in test samples. A new calibration curve from known phosphate concentrations was made for each set of samples tested. Phosphate samples were taken from the initial solution and after ozonation.

Ozonation Experimental Setup

The ozone generator setup is shown in Figure 36. The ozone generator was first calibrated through a series of flow measurements with 20 g/L KI solution. Then generator settings were chosen based on the optimal operating range for the generator and the desired ozone mass flow rate. For most experiments, an ozone flow rate of 3 mg/min was used. This ozone flow allowed operation within the typical ozone dose range (0.4 – 2 mg O_3/mg DOC) used in ozone disinfection processes (Chang and Singer, 1991; Speitel Jr., et al., 1993). Operation within the applicable ozone dose range was achieved by varying ozone mass flow and ozonation time based on the antiscalant concentrations chosen. Ozonation times of 1, 10, and 30 minutes were tested.

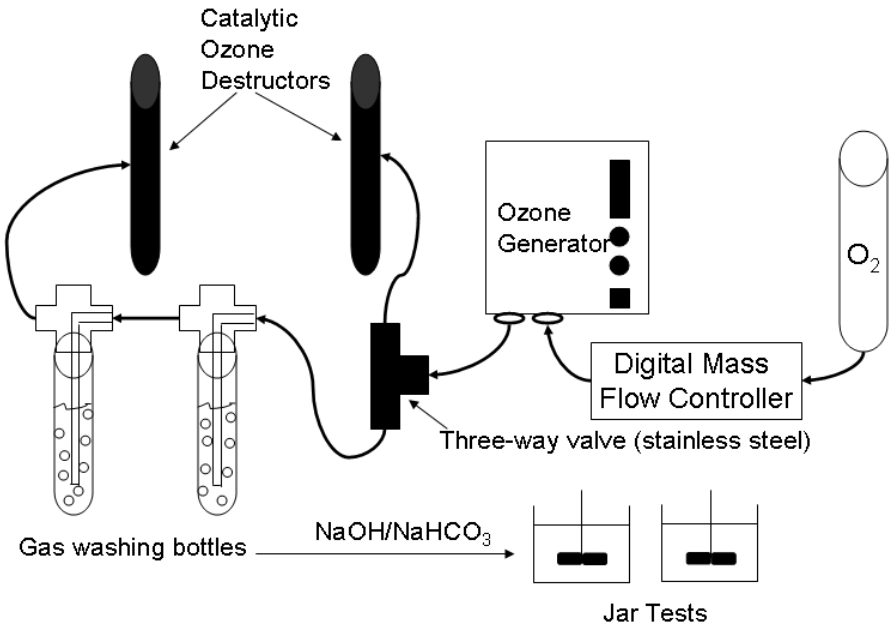

Figure 36. Ozone generator experimental setup. Gas washing bottles contained either 20 g/L KI for ozone capture and measurement or test solutions (500 mL each).

For experiments performed with gaseous ozone, a series of tests on the model Maricopa water containing antiscalant allowed calculation of the ozone transferred to the solution. The first gas washing bottle in series contained the test solution and the second gas washing bottle contained 20 g/L KI. The ozone transferred was calculated as the difference between the known applied ozone mass flow and the ozone captured by the KI solution during the test. Initially, estimates were used for ozone transfer, based on previous research on ozone transfer efficiency (Wanielista, 1997). Wanielista found a 35% ozone transfer efficiency for a 20-L carboy and a 45% ozone transfer efficiency for a 45-L carboy (experiments performed at pH 7). For the peroxone system, transfer efficiencies were expected to be higher even at lower pH because of the presence of hydrogen peroxide. Ozone transfer is affected by both mass transfer properties and the aqueous reactions; the aqueous ozone decomposition is faster in the presence of hydrogen

peroxide and reduces the ozone concentration in water. Therefore, the driving force for ozone transfer from gas to water would increase, increasing the ozone transfer. An initial guess of 75% was used to calculate the appropriate hydrogen peroxide dose for the ozonation time chosen; ozone transfer efficiencies were found to be between 75% and 100% (no measurable ozone captured in KI offgas trap) for ozonation times between 1 and 10 minutes. Longer ozonation times were not tested for ozone transfer efficiency. Assuming an average ozone transfer efficiency of 85%, the equivalent applied ozone concentrations are shown in Table 13.

Table 13. Ozonation times and corresponding transfered ozone concentrations.

Ozonation Time (min)	**Transferred Ozone Concentration (mg/L)**
1	5
10	50
30	150

Each 500 mL reaction solution was made through appropriate volume additions from stock solutions of each salt and the chosen antiscalant. The pH was adjusted using 6 M NaOH and 5 N HCl. Hydrogen peroxide was added directly to the gas washing bottle, and then the test solution was added. For each new experiment, the ozone generator was run at the chosen settings for ozone production for at least 10 minutes to allow the generator to warm up and reach maximum ozone production capacity. Samples for orthophosphate were taken from each initial solution. After each ozonation test, pure oxygen was bubbled through the test solution to remove any residual ozone and samples were taken for orthophosphate. The final pH of each test solution was recorded.

Combination Ozone-Precipitation-Separation Experiments

Most of the combined ozone-precipitation-separation experiments were performed by bubbling gaseous ozone through the experimental solution, located in the first gas washing bottle in series in Figure 36. Samples were taken from the initial solution for dissolved ion measurement. After ozonation and oxygen bubbling to remove residual ozone, the solution was transferred to a jar test vessel. Agitation was started, and NaOH and Na_2CO_3 were added. The Maricopa water initially has a calcium concentration of 25.7 mM and a total carbonate concentration of 16.4 mM. To maximize calcium precipitation, additional carbonate was added (20 mM $NaHCO_3$). While in a real treatment system, only enough carbonate would be added to be equimolar to calcium, it was found that at the equimolar condition, the pH dropped during the agitation period. To maintain a stable pH throughout the precipitation step, additional $NaHCO_3$ was used, and the total carbonate for all precipitation results presented was 36 mM. Precipitation experiments were operated at a pH of 10.5.

After 30 or 60 minutes, the agitation was stopped, and a water sample was filtered either under vacuum or with a dead-end pressurized (0.5 bar) filtration cell using a 0.1 μm filter. The final pH of the precipitated solution was taken. Samples were taken from the filtrate for dissolved ion analysis. All starting pH values were between 10.5 and 10.55 and all final pH values were between 10.35 and 10.54, unless noted.

Activity Calculations

The system of equations developed by Pitzer (1991) for activity coefficient calculation of high ionic strength solutions was used to obtain individual ion activities and the pKa values for the carbonate system, as well as the carbonate system distribution at a specific pH. For the Maricopa County data set at 80% recovery and pH 6.0, all of the ions had activity coefficients less than one. The results for both the Pitzer equations and

the Davies equation are shown in Table 14. The carbonate system pKa values ($pK_1 = 6.1$, $pK_2 = 9.7$) are lower than the standard values ($pK_1 = 6.35$, $pK_2 = 10.33$) and reflect the activity calculations of the system.

Table 14. Activity coefficients for Maricopa water components at pH 6.0 and 80% recovery (CF = 5).

Component	Pitzer Activity Coefficient	Davies Activity Coefficient
Ba^{2+}	0.320	0.323
Ca^{2+}	0.330	0.323
Mg^{2+}	0.350	0.323
Fe^{3+}	0.041	0.078
Na^{+}	0.822	0.754
Cl^{-}	0.849	0.754
HCO_3^{-}	0.818	0.754
CO_3^{2-}	0.257	0.323
SO_4^{2-}	0.334	0.323
OH^{-}	0.699	0.754

RESULTS AND DISCUSSION

Fate of Orthophosphate

Antiscalant oxidation conditions, based on optimization studies, were chosen to be: H_2O_2:O_3 ratio = 0.8, pH 6.0, ozone mass flow = 3 mg/min. Ozonation times ranged from 1 – 30 minutes, giving an ozone dose range of 0.6 – 14 mg O_3/mg DOC.

Orthophosphate is a major oxidation product of the three phosphonate antiscalants and is undesirable in a treatment system because it will promote bacterial growth. The orthophosphate concentration was followed through the 3-stage process, and the results are shown in Figure 37, for ozonation times of 1 – 30 minutes and a precipitation time of 30 minutes. Little phosphate was present in all initial solutions tested, and phosphate was produced during ozonation through oxidation of the phosphonate molecule. Phosphate production increased with ozonation time, leveling off at longer ozonation times. All of the phosphate produced during ozonation was subsequently precipitated within 30 minutes of precipitation at pH 10.5. Based on thermodynamic calculations with the program Visual Minteq (Version 2.50) (Gustafsson, 2006), 100% of the phosphate produced during ozonation was predicted to precipitate as hydroxyapatite ($Ca_5(PO_4)_3OH$). Predicted and experimental results were consistent in all experiments performed.

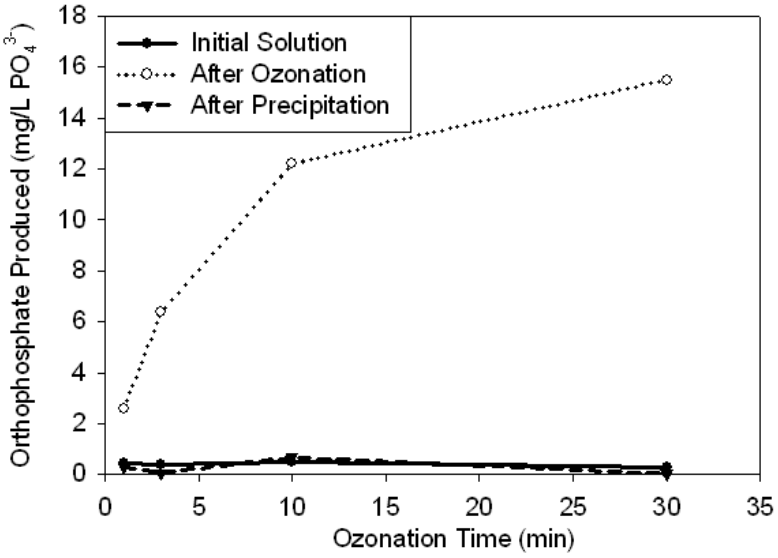

Figure 37. Aqueous orthophosphate as a function of ozonation time and process step. Experimental conditions: Simplified Maricopa water at 80% recovery, DQ2006 = 85 mg/L = 27 mg/L as P, H_2O_2:O_3 = 0.8, ozonation at pH 6, precipitation at pH 10.5.

Effect of Antiscalant Oxidation on Calcium Precipitation

Several precipitation experiments were performed at pH 10.5 without prior ozonation on both the Simplified and Complete Maricopa waters. For the Simplified Maricopa water with no antiscalant added, average calcium removal after 30 minutes agitation was 99.7%, while when DQ2006 was added (85 mg/L), average calcium removal dropped to 90.0%. In comparison, results from ozonation and then precipitation of Simplified Maricopa water with 85 mg/L DQ2006 showed an average calcium precipitation of 95.5%. Ozonation allowed an increase in calcium precipitation above that obtained for the non-ozonated samples. Results for ozonation times of 1, 10, and 30 minutes (equivalent to ozone doses of 3.8, 48, and 134 mg/L ozone) and the Simplified Maricopa water with DQ2006 = 85 mg/L are shown in Figure 38. At longer ozonation times, the fractional calcium precipitation increased slightly, but even with one minute of ozonation, the calcium precipitation was higher than that of a solution with no ozone treatment. However, none of the ozonated samples increased calcium precipitation to the amount observed in the antiscalant-free solution.

For the Complete Maricopa water, and 30 minutes precipitation, average calcium removal for antiscalant-free solutions was 84.9%. Several antiscalant concentrations were tested with the Complete Maricopa water (DQ2006 = 4, 20, and 85 mg/L and DQ2054 = 2, 10, and 43 mg/L) without ozone treatment. For both antiscalants, calcium precipitation decreased with increasing antiscalant concentration, as expected. At DQ2006 = 4 mg/L, the calcium removal was 82.4%, and at DQ2054 = 2 mg/L, the calcium removal was 88.7%. Average calcium removals of 80.8% and 84% were found for non-ozonated samples with DQ2006 and DQ2054, respectively. All of the ozonated samples tested in the same set of experiments had greater calcium removals than the non-

ozonated samples. The average calcium removals for ozonated samples (10 min ozone) were 87% and 88%, for DQ2006 and DQ2054, respectively. Results from the combined ozonation-precipitation-separation experiments show that ozonation increases calcium precipitation above that observed for the same solution with no antiscalant added (and no ozonation). Solutions with antiscalant and no ozonation had the least amount of calcium precipitation, and as with the simplified Maricopa water results, an ozonation time of one minute was adequate to increase calcium precipitation above that of non-ozonated solutions.

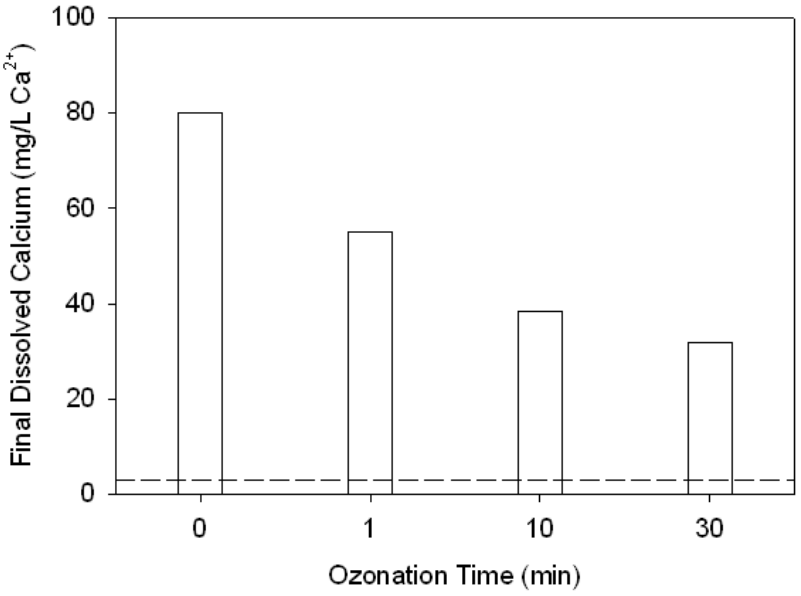

Figure 38. The effect of ozonation time on subsequent calcium precipitation for the Simplified Maricopa water. DQ2006 = 85 mg/L, 30 min precipitation at pH 10.5. The dotted line represents the final dissolved calcium of the antiscalant-free precipitated solution.

Subsequent experiments also at pH 10.5 were performed for 60 minutes of precipitation time; results for the Simplified Maricopa and Complete Maricopa waters and the four antiscalants are shown in Figure 39. The effectivemess of the antiscalants,

even at this high pH, is shown by the results at zero ozonation time; in all six cases shown, the presence of antiscalants limited the precipitation. With ozonation times as low as one minute, however, calcium precipitation increased beyond that observed for the antiscalant-dosed precipitated solutions; this results is similar to results presented above for the Complete Maricopa water. In addition, 60 minutes precipitation allowed the same trend for two of the antiscalants (DQ2006 and DQ2054) used with the Simplified Maricopa water composition. For DQ2066 and Coatex, the two larger antiscalant compounds, the longer ozonation times of 10 and 30 minutes were sufficient to increase calcium precipitation to match that of the antiscalant-free solution, but calcium precipitation for one minute of ozone was slightly less than that obtained for the antiscalant-free solution. The final dissolved calcium concentration for 30 minutes ozonation was quite similar to that obtained for 10 minutes ozonation for all antiscalants, and the data for 30 minutes are not shown in Figure 39. Ozonation of the different antiscalant compounds resulted in quite similar amounts of calcium precipitation; while different antiscalants can prevent calcium precipitation to different degrees, oxidation by ozone appears to deactivate the different compounds, creating essentially the same conditions for precipitation and making precipitation independent of the type of antiscalant present. Interestingly, for precipitation times of both 30 and 60 minutes and the Complete Maricopa water, ozonation increased calcium precipitation above that observed for the antiscalant-free solution. Experiments were repeated several times to confirm this result; the increase in precipitation may result from an increase in surfaces for heterogeneous precipitation or create partial oxidation products that aid in precipitation for the Complete Maricopa water composition. In addition, the orthophosphate produced during ozonation caused additional calcium precipitation in the form of hydroxyapatite. However, the maximum orthophosphate concentration produced

was approximately 0.15 mM, and ozonation caused an increase of 0.4 mM calcium to precipitate. Therefore, the production of orthophosphate during ozonation and its subsequent precipitation is not solely responsible for the additional calcium precipitation observed.

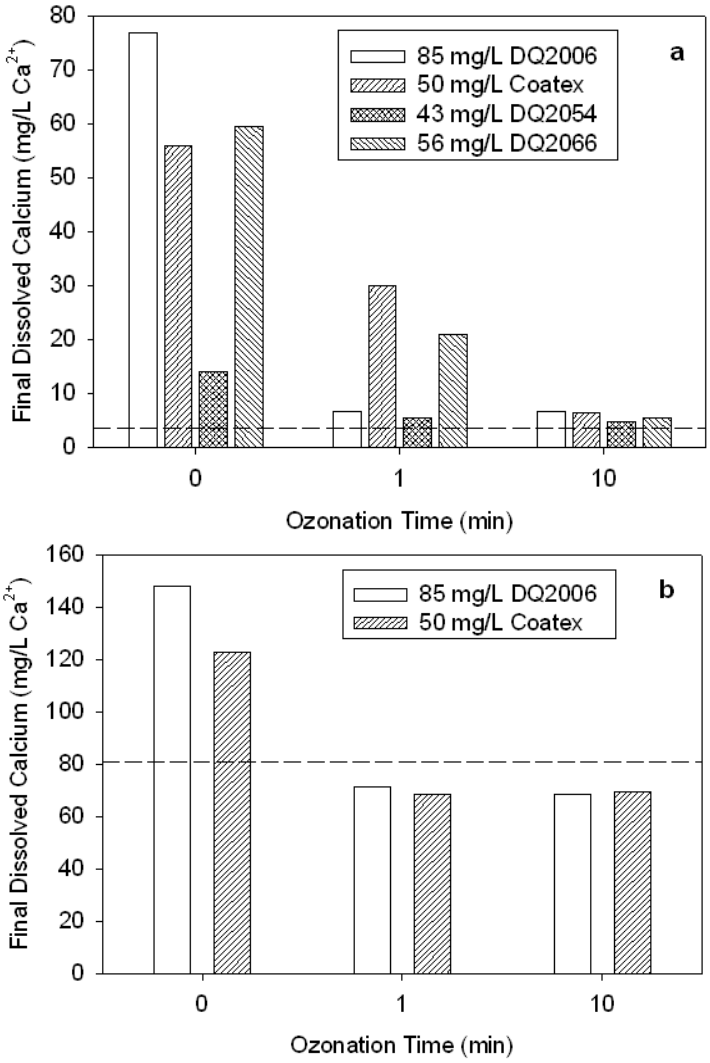

Figure 39. Calcium precipitation for the (a) Simplified Maricopa and (b) Complete Maricopa waters compositions and several antiscalant concentrations after ozonation times of 0, 1, and 10 minutes. Precipitation conditions: 60 minutes, pH 10.5. The horizontal dotted line in both charts represents the final dissolved calcium concentration for a precipitated solution with no antiscalant and no ozone.

Effect of Antiscalant Oxidation on Magnesium and Sulfate Precipitation

Magnesium and sulfate precipitation were also followed during experiments with the complete Maricopa water. The initial concentrations of each component were 515

mg/L (21.2 mM) and 991 mg/L (10.3 mM), respectively. In antiscalant-free, non-ozonated samples of Complete Maricopa, approximately 24% of the magnesium and 6% of the sulfate precipitated. Sulfate most likely precipitates as barium sulfate and gypsum; ICP results showed no measurable barium (or iron) in the precipitated and filtered samples, so most or all of the barium precipitated. However, the sulfate that precipitated with barium represents less than 0.2% of the sulfate available. The saturation ratio for gypsum is slightly below one; calculations with the thermodynamic equilibrium software, PHREEQC, confirmed this prediction of saturation (Parkhurst and Appelo, 2008). Therefore, gypsum is not predicted to precipitate, but some precipitation did occur, most likely due to inclusion into calcium carbonate crystals. At the precipitation pH of 10.5, some magnesium is predicted to precipitate as $Mg(OH)_2$ and some will also co-precipitate with calcium carbonate in forming magnesian calcite.

When any one of the four antiscalants was added to Complete Maricopa, sulfate precipitation increased to approximately 9%, and magnesium precipitation increased to 30%, while the calcium precipitation decreased. Two antiscalants, DQ2006 and Coatex, were tested with ozonation and the Complete Maricopa water composition. Several trends were observed for DQ2006; 10 minutes of ozonation with an antiscalant concentration of 4 mg/L resulted in 22% magnesium precipitation, while the same ozonation time for 20 and 85 mg/L resulted in 28% and 29% magnesium precipitation, respectively. A magnesium precipitation of 24% was obtained for 85 mg/L and 30 minutes of ozonation. Therefore, an increase in ozonation time or a decrease in DQ2006 concentration decreased magnesium precipitation in the Complete Maricopa water. For Coatex, the lowest concentration (2 mg/L) and 10 minutes of ozonation resulted in 27% magnesium precipitation, but for 10 and 50 mg/L and 10 minutes of ozonation, 32% magnesium precipitation was observed. An increase in ozonation time to 30 minutes for

the 50 mg/L sample decreased the magnesium precipitation to 28%. For sulfate precipitation, no dependence on antiscalant concentration or type was observed, but ozonation did cause a slight decrease in precipitation to approximately 8%. Previous research has shown that antiscalants can adsorb onto nucleating calcium carbonate crystals by replacing several carbonate anions (Nygren, et al., 1998); it is possible that the adsorption of antiscalants and incorporation into the calcium carbonate crystal lattice structure allows sulfate precipitation to increase. The adsorbed antiscalants may also lower the energy barrier to magnesium precipitation by coordinating with magnesium cations and preventing the normal tightly-bound hydration shell that surrounds magnesium ions in solution (Loste, et al., 2003). Ozonation appeared to at least partially prevent this increase in magnesium or sulfate precipitation through antiscalant degradation and deactivation.

Effect of Antiscalant Oxidation on Particle Size and Solid/liquid Separation

Particle size distribution measurements were taken for all four antiscalants and all four water compositions for ozonated and non-ozonated samples. Particle size measurements were compared to microfiltration flux data to correlate changes in particle size with filtration performance. Results for antiscalant DQ2066 and Simplified Maricopa are shown in Figure 40. The results shown for Simplified Maricopa were similar to results obtained for Simplified Maricopa + Na_2SO_4. For these two water compositions, addition of antiscalant caused a decrease in the modal particle diameter, with a resulting poorer microfiltration performance. Scanning electron microscope (SEM) images of antiscalant-free and antiscalant dosed-samples revealed the formation of many small (100-200 nm) particles with the addition of antiscalant. Antiscalants adsorb onto nucleating crystals, preventing complete particle growth; the small particles represent the initial nucleation phase of precipitation. Some larger particles (~10 μm in

diameter) were also formed when DQ2066 was present during precipitation; however, the particle size distribution measured indicates that there were particles greater than 10 μm in diameter. The discrepancy between the particle size ranges observed through SEM analysis and the modal particle diameter measured for Simplified Maricopa + 56 mg/L DQ2066 (shown in Figure 40a) is most likely due to particle agglomeration; the particles measured between approximately 10 and 30 μm were most likely clumps of smaller particles or smaller particles that adhered to larger particles, making the large particles appear even larger during measurement. The difference in light scattering between the assumed spheres and actual particles can also lead to some error in particle sizing.

With ozonation (one or 10 minutes) prior to precipitation, the modal particle diameter returned to a value similar to the antiscalant-free sample. Treatment with ozone, even for small times such as one minute, decomposed the antiscalant molecules enough so that the precipitation step was largely unaffected by the presence of antiscalant. Orthophosphate measurements indicated that the antiscalant molecules were not completely oxidized, but the partial oxidation products formed did not seem to affect the precipitation step in the same manner as the whole antiscalant molecules. When the ozonated, precipitated solutions were then filtered, the loss in flux was recovered; ozonated samples resulted in the same flux decline as the sample with no antiscalant. These results for particle size distribution and microfiltration are consistent with the data obtained for dissolved calcium; ozonation allows the system to precipitate as if no antiscalant compound was present in solution. The DQ2006 antiscalant (85 mg/L) performed similarly to 56 mg/L DQ2066 in both the Simplified Maricopa and Simplified Maricopa + Na_2SO_4 water compositions. Smaller DQ2006 antiscalant concentrations tested (4 and 20 mg/L) did not result in significant differences in particle size distribution or microfiltration performance for ozonated versus non-ozonated samples. In addition,

the Coatex and DQ2054 antiscalants did not decrease the particle size distribution for these two waters; therefore, no effect of ozonation on precipitation morphology or microfiltration performance was observed.

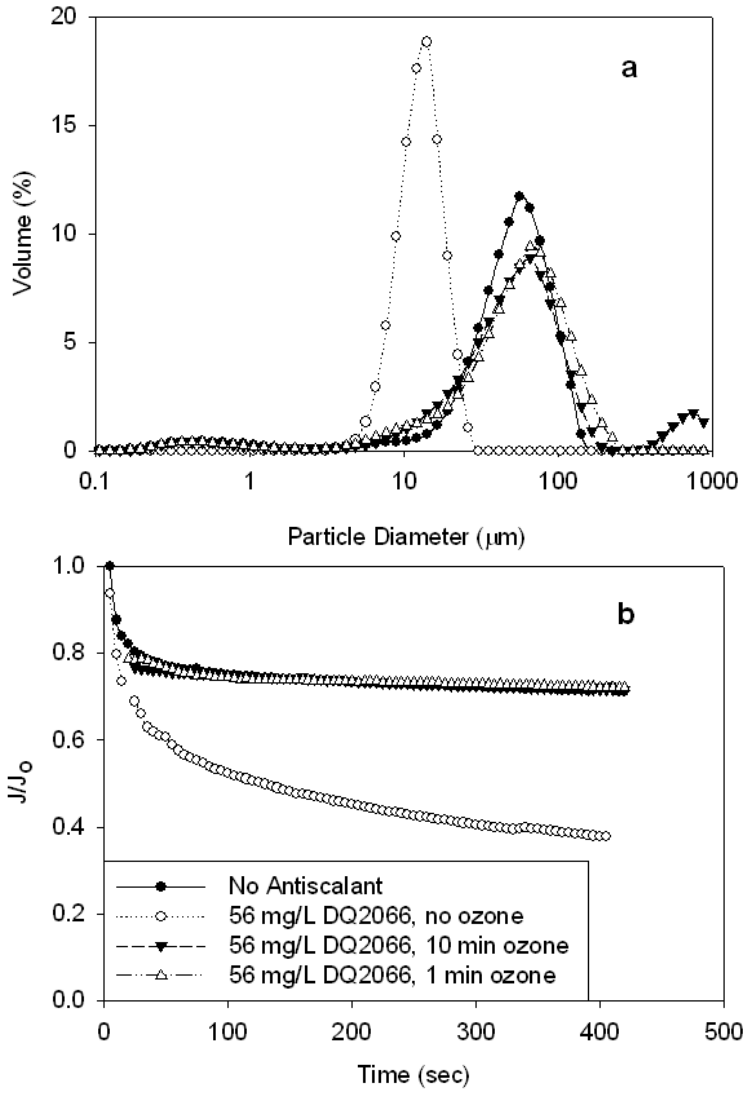

Figure 40. Effect of antiscalant ozonation prior to precipitation on (a) particle size distribution and (b) microfiltration for the Simplified Maricopa water and DQ2066. Precipitation conditions were pH 10.5 and 60 minutes.

The effect of antiscalant oxidation on particle size distribution was evaluated for both the Simplified Maricopa + $MgCl_2$ and Complete Maricopa water compositions. The trends observed for Simplified Maricopa + $MgCl_2$ were similar to those observed for Complete Maricopa. Results for the former water composition with Coatex and DQ2066 are shown in Figure 41. The ozonated samples of Coatex and DQ2066 had the same modal particle diameter, indicating that ozonation of different types of antiscalants results in the same particle size distribution, even though the effect of a specific antiscalant on particle size distribution may be different. For Coatex, addition of the antiscalant also caused a relative increase in the first mode volume contribution, indicating an increase in the volume of small particles formed. SEM imaging confirmed the presence of small particles for DQ2006, DQ2066, and Coatex in these two water compositions. The increase in modal particle diameter with the addition of DQ2066 or DQ2006 appears to be caused by the adsorption of these small particles onto the larger particles that are also formed; small particle adsorption does not appear to occur for Coatex samples. The decrease in modal particle diameter for Coatex resulted from actual smaller particles formed, as compared to an antiscalant-free solution. Results for DQ2006 followed the same trend as DQ2066, but results for DQ2054 showed no effect of antiscalant on particle morphology. The influence of antiscalant addition on particle size distribution was opposite for DQ2006/DQ2066 and Coatex; addition of either DQ2066 or DQ2006 caused the modal particle diameter to increase, while addition of Coatex caused the modal particle diameter to decrease. In both cases, 10 minutes of ozone degraded the antiscalant compound and returned the particle size distribution to that of the antiscalant-free precipitated solution.

Microfiltration of Simplified Maricopa + $MgCl_2$ and Complete Maricopa water compositions did not drastically change when antiscalants were present. Therefore, no

impact on microfiltration flux was observed when samples were ozonated prior to precipitation and solid/liquid separation.

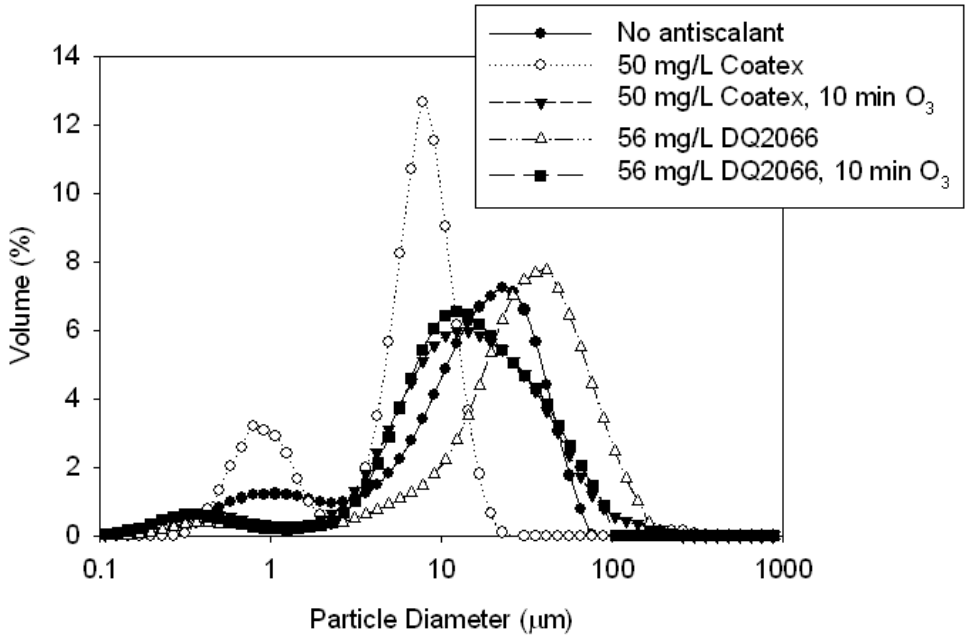

Figure 41. Influence of antiscalant ozonation on particle size distribution for the Simplified Maricopa + $MgCl_2$ water composition. Precipitation pH was 10.5.

Effect of Antiscalant Oxidation on Particle Morphology and Composition

SEM imaging and elemental analysis were used to evaluate how precipitate morphology changed with antiscalant ozonation for each of the four water compositions. Energy dispersive x-ray (EDX) analysis was performed for both DQ2006 and DQ2066 and the Simplified Maricopa water composition, while only DQ2006 was tested for the remaining three water compositions. The effect of antiscalant oxidation on particle morphology is shown in Figure 42 for 85 mg/L DQ2006 and Simplified Maricopa water. When DQ2006 is added before precipitation, the typical spherical or rhombohedral

particles (~10 μm, Figure 42a) are not observed; only small spherical particles (100 – 200 nm) are formed (Figure 42b).

SEM samples of ozonated solutions were obtained after ozonation, precipitation, and microfiltration; however, ozonation was performed using a stock solution of ozone (~60-70 mg/L O_3), while all other data reported in this paper was obtained in experiments where gaseous ozone was bubbled through the experiment. Therefore, ozone concentrations are reported in this section, while ozone mass flows and times were used in previous sections. Ozone concentrations of 1, 5, and 10 mg/L O_3 were used; these concentrations correspond to ozone doses of 0.005, 0.026, and 0.05 mM. Ozone times of 1, 10, and 30 minutes (at 3 mg/min) result in ozone doses of 0.08, 1.0, and 2.8 mM ozone. As indicated in Figure 39, ozonation times of one minute were sufficient for most samples to allow calcium precipitation similar to the antiscalant-free samples, and while larger ozone doses would be needed to approach complete oxidation, such small doses are sufficient to arrest the precipitation control of the antiscalants. In addition, aliquots of dissolved ozone appeared to be more efficient at degrading antiscalants; an ozone dose of 5 mg/L O_3 resulted in 4-5 mg/L P as PO_4^{3-}, while a gaseous ozone dose of 1 minute resulted in 2.5 mg/L P as PO_4^{3-} for the same initial antiscalant concentration (85 mg/L DQ2006). This result indicated that the ozone doses of 5 and 10 mg/L O_3 would overlap the lower range of gaseous ozone times tested with respect to antiscalant oxidation and orthophosphate production, and most likely, particle morphology. Therefore, an ozone stock solution was used to dose small ozone concentrations and determine if such small ozone doses could cause changes in particle morphology.

When 1 mg/L O_3 was added (Figure 42c) the majority of particles formed were the small nanometer-scale nucleated crystals. However, some larger (2 – 4 μm) spherical particles were observed, and many of the smaller particles were adhered to the larger

spheres. Less abundant than the spherical particles were some cubic particles with rounded edges and an amorphous appearance. When 5 or 10 mg/L O_3 was used to ozonated DQ2006 (Figure 42d & e, respectively), the small particles were largely eliminated from the precipitated solution, and spherical particles with a diameter range of approximately 5 – 10 μm were observed. Most of the spheres had a rough surface and some particles appeared to be attached to each other. The SEM images for 5 and 10 mg/L O_3 indicate that most of the effect that antiscalants have on calcium carbonate precipitation was removed with ozonation. However, the images indicate some residual organic content remained that prevented formation of rhombohedral calcite and caused the vaterite spheres to appear rough and, at times, somewhat amorphous in shape.

EDX analysis of the sample with 5 mg/L ozone, pictured in Figure 42d, revealed the presence of anhydrous calcium carbonate, with some amorphous calcium carbonate (ACC). The elemental distribution of anhydrous calcium carbonate is 40% (wt.) calcium, 12% carbon, and 48% oxygen, while ACC can contain a variable amount of hydration (Nebel and Epple, 2008; Nebel, et al., 2008), with calcium content typically between 34 and 35%. In comparison, a non-ozonated sample of Simplified Maricopa with 85 mg/L DQ2006 had an average elemental composition that indicated the primary phase of calcium carbonate present was monohydrocalcite ($CaCO_3*H_2O$). The elemental composition of antiscalant-free samples was anhydrous calcium carbonate. Similarly for ozonated samples of 56 mg/L DQ2066 and Simplified Maricopa, the primary phase appeared to be anhydrous calcium carbonate.

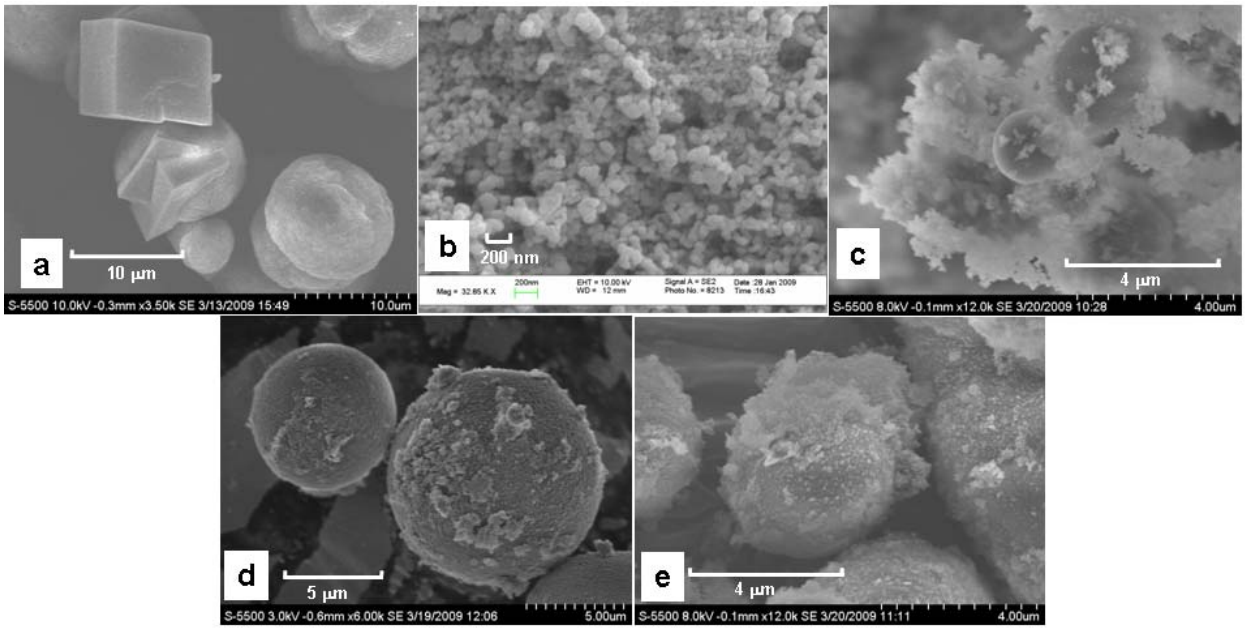

Figure 42. Effect of ozonation on particle morphology for Simplified Maricopa with 85 mg/L DQ2006: (a) No antiscalant and no ozone, (b) 85 mg/L DQ2006 and no ozone, (c) 85 mg/L DQ2006 and 1 mg/L ozone, (d) 85 mg/L DQ2006 and 5 mg/L ozone, and (e) 85 mg/L DQ2006 and 10 mg/L ozone. Precipitation at pH 10.5 for 60 min.

Ozonated samples with DQ2006 and each of three more complex water compositions (Simplified Maricopa + Na_2SO_4, Simplified Maricopa + $MgCl_2$, and Complete Maricopa) are shown in Figure 43, with a comparison to an antiscalant-free precipitated solution of Complete Maricopa. The antiscalant-free precipitated solution of Simplified Maricopa + $MgCl_2$ resembled the Complete Maricopa sample shown in Figure 43a, and the antiscalant-free precipitated solution of Simplified Maricopa + Na_2SO_4 contained the same particle morphology as the Simplified Maricopa sample in Figure 43a. The ozonated sample of Simplified Maricopa + Na_2SO_4 with 85 mg/L DQ2006 (Figure 43b) contained spherical particles similar to those observed for ozonated samples in Figure 42d & e; spherical particles between 5 and 10 μm in diameter had rough

surfaces and some residual smaller particles attached to the surface. In contrast to the symmetrical rods, crosses, and spheres formed in the antiscalant-free Simplified Maricopa + $MgCl_2$ and Complete Maricopa water samples, the ozonated samples shown in Figure 43c & d contained large (10 – 15 μm) round amorphous particles with cracks running around many of the particles and some smaller particles adhering to the larger particles. The antiscalant-dosed samples of these two water compositions contained some of the rods and crosses visible in the antiscalant-free sample, as well as many of the small particles observed in Figure 42b. As with the Simplified Maricopa water, antiscalant ozonation greatly reduced the nano-size particles formed, but the remaining organic partial oxidation products still affected the particle morphology. The orthophosphate produced during ozonation may have also affected the particle morphology; no orthophosphate was present in non-ozonated samples.

EDX analysis of the larger particles in the Simplified Maricopa + $MgCl_2$ water with 85 mg/L DQ2006 and an ozone dose of 5 mg/L (Figure 43c) resulted in an elemental composition of 33 – 35% calcium, 49 - 56% oxygen, 6 - 11% carbon, and 3 – 5% magnesium. In comparison, an antiscalant-dosed sample contained small particles with an average magnesium content of 1.8% (wt.) and large particles with 3.4% magnesium. The ozonation treatment resulted in particles with a magnesium content similar to the larger particles of the non-ozonated sample, as well as to the particles formed in the antiscalant-free sample. The calcium and oxygen content of the ozonated samples indicated that the phases present were most likely ACC and monohydrocalcite. The residual organics present, as well as the orthophosphate produced and magnesium present, allowed the metastable, hydrated phases of calcium carbonate to remain in solution instead of transitioning to anhydrous calcium carbonate (Brečević, et al., 1996; Loste, et al., 2003; Meldrum and Hyde, 2001).

EDX analysis of the Complete Maricopa water with 85 mg/L DQ2006 and 5 mg/L ozone (Figure 43d) resulted in a magnesium content (1.9 – 3.5% (wt.)) similar to the antiscalant-free sample; the antiscalant-dosed sample contained an increased (~5%) magnesium content. Similarly, the sulfur content (average 0.14%) of the ozonated samples was lower than the non-ozonated samples (average 0.80%), and the barium and ferric iron (0.60 and 0.46%, respectively) were both higher than the non-ozonated samples. All of these components followed the trend of having weight percent values similar to the antiscalant-free sample. However, the calcium and oxygen content did not indicate the presence of anhydrous calcium carbonate, as was observed for the antiscalant-free sample; the calcium content ranged from 25 to 35%, and the oxygen content ranged from 57 to 61%, indicating variable amounts of hydration and most likely a combination of ACC and monohydrocalcite.

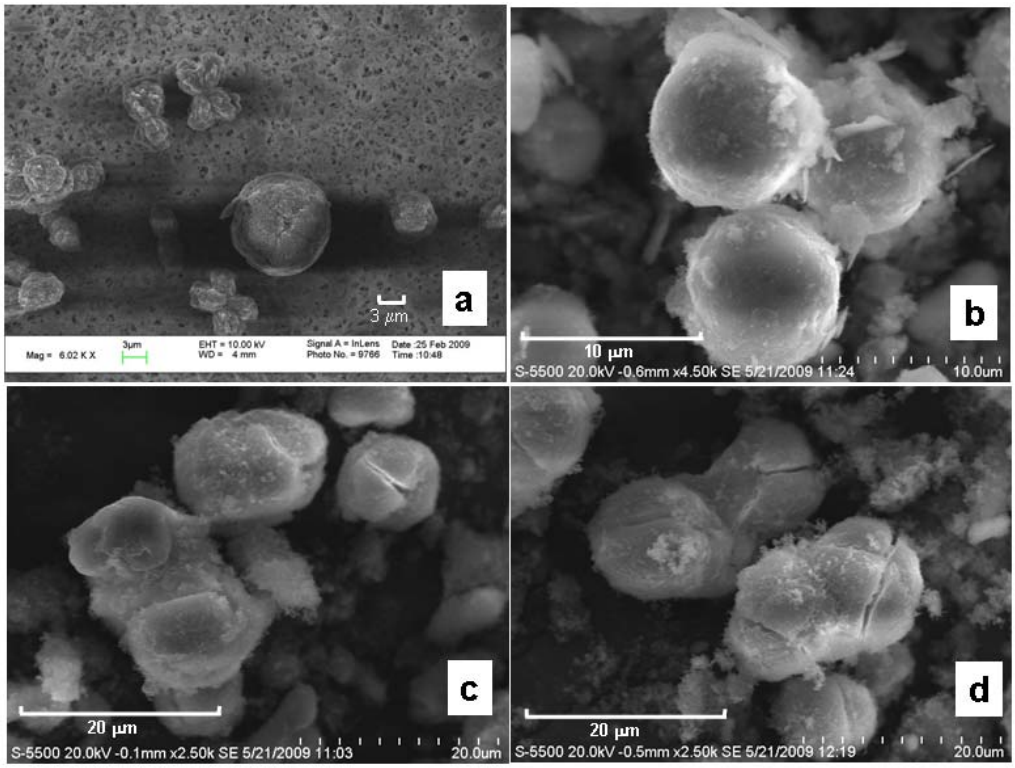

Figure 43. Effect of antiscalant oxidation for three complex water compositions: (a) Complete Maricopa with no antiscalant and no ozone, (b) Simplified Maricopa + Na_2SO_4 with 85 mg/L DQ2006 and 5 mg/L ozone, (c) Simplified Maricopa + $MgCl_2$ with 85 mg/L DQ2006 and 5 mg/L ozone, and (d) Complete Maricopa with 85 mg/L DQ2006 and 5 mg/L ozone. Precipitation at pH 10.5 for 60 min.

Estimation of Overall Recovery

To estimate the potential overall recovery achievable with an RO treatment system combined with the three-stage concentrate treatment (RO-concentrate treatment-RO/NF), saturation ratios were calculated for representative results with and without the ozonation step. The overall recovery is the combined recovery of the original RO treatment system (model Maricopa water at 80% recovery), and the recovery achievable on the treated concentrate. Saturation ratios for the treated model concentrate of the

complete Maricopa water were calculated for calcite, gypsum, and magnesium hydroxide. The calcite values were calculated with a total carbonate of 10 mM remaining after concentrate treatment and for a secondary RO feed at pH 6.0, with the assumption that *S* must be less than one (undersaturated). This assumption is conservative because the bulk feed solution to an RO membrane module can be slightly supersaturated, and precipitation may not occur. Saturation ratio calculations show that during the secondary RO or NF treatment of the treated concentrate, gypsum would be the limiting precipitate. In addition, ozonation would allow a greater overall recovery when performed before precipitation for the model Maricopa water containing antiscalant. Saturation ratios calculated for an overall recovery range of 80 – 98% (secondary recovery of 0 – 90%) are shown in Figure 44 for calcite and gypsum. Magnesium hydroxide S values are not shown and were all less than 0.01. The three-stage concentrate treatment, with ozonation, precipitation, and solid/liquid separation, could achieve a greater overall recovery than concentrate treatment with only precipitation and solid/liquid separation. With antiscalant addition to control gypsum, the maximum predicted recovery for concentrate treatment without ozonation would be approximately 94%; with ozonation the maximum predicted recovery increases to 96% (based on the saturation ratios of calcite). More importantly, the concentrate volume would decrease from 6% to 4% of the feed volume; this reduction represents a significant decrease in the associated costs of concentrate disposal.

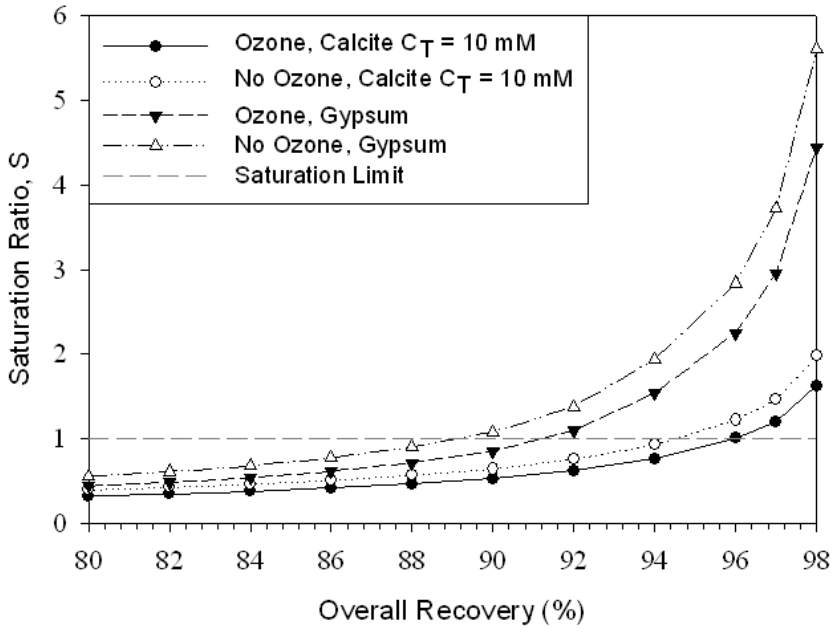

Figure 44. Saturation ratio calculations for calcite and gypsum in the treated concentrate as a function of overall recovery and ozonation treatment step during concentrate treatment. pH of secondary RO assumed to be 6.0.

CONCLUSIONS

The application of a side-stream RO concentrate treatment process could significantly increase the overall recovery achieved for the RO-concentrate treatment system. The concentrate treatment scheme investigated consisted of ozonation, precipitation, and filtration steps. Results from a synthetic RO concentrate indicated that recovery could increase from 80% to 94-96%, greatly reducing the concentrate volume and the associated disposal costs. The ozonation step influenced not only the amount of calcium and other ions that precipitated, but the particle size distribution, particle morphology, and filtration performance. Ozonation times as low as one minute allowed an increase in calcium precipitation above that observed for antiscalant-dosed samples, and ozonation doses of 5 – 10 mg/L O_3 were effective in removing the particle

morphology changes caused by antiscalants. Any orthophosphate produced during ozonation of phosphonate antiscalants was removed during the precipitation and filtration steps. Results indicated that a concentrate treatment process that uses precipitation to remove problematic precipitates may be affected by the presence of antiscalant, and removal of the antiscalant could enhance the concentrate treatment efficiency and the overall system recovery.

Chapter 8: Concentrate treatment between membrane stages: A pilot BWRO study[5]

ABSTRACT

A two-stage pilot reverse osmosis (RO) membrane system with interstage concentrate treatment was investigated with a water sample from a brackish karstic spring. Concentrate treatment consisted of precipitation and filtration or ozonation, precipitation, and filtration. A synthetic concentrate was made in the laboratory and used as a comparison to the real water sample during concentrate treatment. Results from the pilot system indicated that concentrate treatment can significantly increase overall RO recovery. Differences in calcium precipitated, particle size distribution, and filtration for the real and synthetic water samples were most likely due to the presence of natural organic matter. Ozonation caused an increase in calcium precipitation but a decrease in magnesium and sulfate precipitation.

INTRODUCTION

Brackish water sources are now considered to be a critical future resource for desalination and drinking water needs; the desalination market has grown exponentially over the past 50 years, with 50% of current desalination production capacity and 80% of the total number of plants using membrane processes (Frenkel, 2000; Gleick, 2006). The primary membrane desalination technology of choice today is reverse osmosis (RO). RO membranes are able to achieve salt rejections of 97% to greater than 99%, producing a fresh water product and a highly saline waste stream, termed the concentrate. During RO desalination, the process is limited by several factors including salinity (for seawater, 30

[5] Manuscript to be submitted to the Journal of Membrane Science.

– 45 g/L total dissolved solids (TDS)) and salt precipitation (for brackish water, 1 – 10 g/L TDS) (Greenlee, et al., 2009). Due to these limitations, RO membrane recovery, the ratio of the permeate volume to the feed volume, for seawater is typically 50%, while the brackish water RO recovery has a range of 60 – 90%. Hence, the concentrate waste volume can be a significant portion of the RO feed volume, and concentrate disposal remains a critical financial and technological challenge of desalination facility design.

While seawater desalination facilities are typically located on a coast, many brackish water sources are located inland. Coastal plants typically dispose of the concentrate back into the adjacent ocean or sea; surface water disposal is the most cost effective method of concentrate disposal (Mickley, 2004). However, inland brackish water desalination plants cannot typically use surface disposal due to the lack of an appropriate saline receiving water body, and all other concentrate disposal options are significantly more costly to implement.

During brackish water RO desalination, salts become concentrated on the feed side of the membrane; as the recovery is increased, salt concentrations increase, and eventually specific sparingly soluble salts ($CaCO_3$, $CaSO_4$, $BaSO_4$, $SrSO_4$, silica) become supersaturated and precipitate on the surface of the membrane. While chemical cleaning processes are often used, precipitation causes membrane flux decline, and eventually the membranes must be replaced. Chemical addition and pH adjustment are used to control salt precipitation. Chemicals called antiscalants are dosed to the RO feed stream and prevent precipitation by adsorbing onto crystal growth sites and raising the effective saturation limit (Tang, et al., 2008; Yang, et al., 2001). However, as the recovery increases and the salt content of the concentrate increases, eventually precipitation control by antiscalants is overcome and precipitation occurs.

While the recovery for brackish water RO plants is typically much higher than that of seawater plants, the concentrate volume is still significant compared to a fresh water treatment plant (recovery is often greater than 99%). Widespread application of inland brackish water RO requires an alternative approach to increase RO system recovery due to limitations caused by salt precipitation and because of the high cost and technical infeasibility of concentrate disposal.

In this study, a three-stage side-stream concentrate treatment process was investigated. Concentrate treatment can reduce the volume of wastewater produced by removing sparingly soluble salts in a controlled precipitation step and returning most of the water in the concentrate to the RO system for further desalination. The concentrate treatment process, shown as a schematic in Figure 45, consists of three stages: (I) antiscalant deactivation, (II) salt precipitation, and (III) solid/liquid separation. Antiscalants are deactivated through oxidation by ozone, and subsequent precipitation and solid/liquid separation (by microfiltration) remove the problematic sparingly soluble salts. The concentrate treatment effectively removes the primary limitation to increasing recovery within the RO system, salt precipitation, and allows the secondary RO system to operate at high recoveries (>70%). Previous research has shown that a concentrate system consisting of Stages II and III (precipitation and solid/liquid separation) alone can effectively remove a large portion of the precipitating salts (primarily calcium carbonate and calcium sulfate) (Rahardianto, et al., 2007). However, both antiscalants and natural organic matter (NOM) are present in the concentrate and may affect the individual stages of the concentrate treatment process, as well as the overall achievable system recovery.

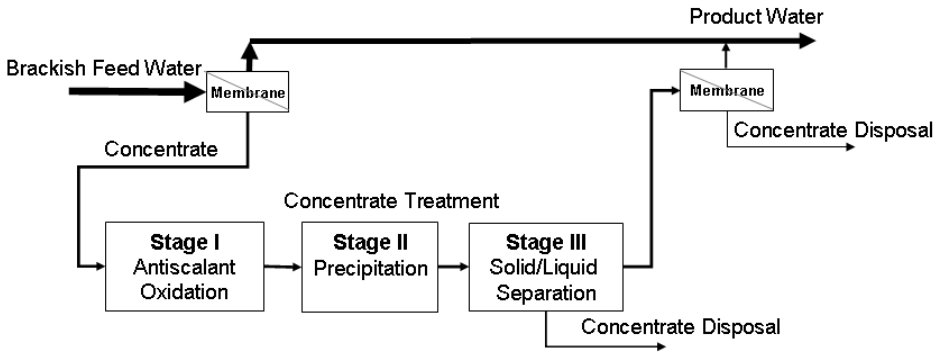

Figure 45. Schematic of the concentrate treatment as a side-stream process to a brackish water reverse osmosis (RO) system.

A low-pressure RO module was used as the first or primary RO stage, and the concentrate produced during the primary RO stage was divided into one of three cases:

- Case I – No concentrate treatment.
- Case II – Precipitation and solid/liquid separation.
- Case III – Ozonation, precipitation, and solid/liquid separation.

The objectives of this study were two-fold: to compare concentrate treatment of a real brackish water sample to a synthetic water (with the same ionic composition) made in the laboratory and to compare the proposed three-stage concentrate treatment process (Case III) with both an untreated concentrate (Case I) and a concentrate treated by only Stages II and III, precipitation and solid/liquid separation (Case II). Two spiral wound RO membrane modules were used to treat a real brackish water sample.

A high-pressure RO module was used as the secondary RO stage that treated the concentrate from the first RO stage for each of the three Cases listed above. The overall system performance (including both primary and secondary RO stages, and concentrate treatment, if applicable) was evaluated; individual RO stage recoveries, total system recovery, and secondary RO stage permeate flux were compared for Case I, II and III.

To determine if the effects of concentrate treatment on RO concentrate properties can be accurately predicted through the use of a synthetic water, a synthetic concentrate was made directly in the laboratory and treated by Case II or Case III. Results were obtained for extent of precipitation, precipitate particle size distribution, and microfiltration flux.

EXPERIMENTAL METHODS

Phosphonate antiscalant samples were obtained from Dequest Water Management Additives, a subsidiary of Thermophos. The antiscalant tested was the penta-sodium salt of aminotri(methylene phosphonic acid), or ATMP, the hexa-potassium salt of hexamethylenediamine tetra(methylenephosphonic acid). Throughout this study, the antiscalant is referred to as DQ2006. Total organic carbon (TOC) and total solids analysis were used to determine the mass and organic carbon concentrations of the antiscalant.

Two spiral wound membrane models were used during this study. The first RO treatment stage was performed using a Koch Ultra Low Pressure (ULP) RO membrane (Model# 2540ULP). The secondary RO treatment stage was performed using a Koch high pressure SWRO membrane (Fluid Systems TFC, part number 8254004, Model 2540 SW). The average permeability for the ULP model was 1.20 L/m^2-h-bar, and the average permeability for the SWRO module was 1.38 L/m^2-h-bar. The pilot membrane system was operated in either permeate recycle mode or permeate withdrawal mode. For the permeate recycle mode, the permeate line was fed back into the feed tank, and all of the permeate was recycled; the salt concentration in the feed tank was assumed constant. For the permeate withdrawal mode, permeate was collected in a separate tank that was placed on a digital balance to record accumulated mass, and the concentration of the feed tank increased during the experiment. For both modes of operation, the concentrate line was recycled back into the feed tank; therefore, in permeate withdrawal mode, the salt

concentration of the feed/concentrate steadily increased throughout the test. For all experiments, the feed/concentrate flow rate was approximately 230 L/hr. The pilot system feed tank was temperature controlled by a set of metal coils; a water bath was set at the desired temperature, and water was sent through the coils to control the feed tank temperature. However, the temperature still increased over time when the pilot system was operated in permeate withdrawal mode due to the decreasing volume of the feed and the orientation of the coils. The temperature varied between 18 and 22 ^{o}C during operation of the ULP module. The variation of the viscosity with water temperature was taken into account for this temperature range. Each module was rinsed before and after each test run with distilled water in recycle mode until the initial permeability (measured before each test) was recovered. If the initial permeability was not achieved, a chemical wash was performed to clean the membrane module.

A water sample was obtained from a natural karstic spring in Marseille, France. The water was analyzed for dissolved calcium, magnesium, sulfate, carbonate, turbidity, and conductivity. Sodium and chloride concentrations were estimated from the conductivity and from previous measurements taken on a similar karstic spring in southern France (Blavoux, et al., 2004). A summary of the composition for the water sample obtained is shown in Table 15. While the water composition has a salinity typical of a brackish water (1 – 10 g/L total dissolved solids (TDS)), the water sample is atypical of many brackish water sources, primarily due to the high sulfate and magnesium concentrations. In addition, a typical brackish groundwater will have a higher alkalinity (Jurenka and Chapman-Wilbert, 1996). The natural pH of the water sample was 7.6. The pH was adjusted to 6.5 prior to primary RO treatment with the ULP RO module. A synthetic version of the water sample was made in the laboratory; the synthetic water was made as RO concentrate, based on the recovery (67%) and concentration factor (~3)

calculated from primary RO treatment of the real water sample. The RO concentrate treatment process was evaluated with the synthetic concentrate, and results were compared to data obtained from concentrate treatment of the real water RO concentrate.

Table 15. Composition of water sample obtained from a karstic spring in Marseille, France.

Component	**Concentration**	**Units**
Sodium (Na^+)	2,500 – 2,800	mg/L
Chloride (Cl^-)	5,200 – 5,900	mg/L
Calcium (Ca^{2+})	173	mg/L
Magnesium (Mg^{2+})	387	mg/L
Bicarbonate (HCO_3^-)	65	mg/L
Sulfate (SO_4^{2-})	787	mg/L
Alkalinity	1	meq/L
Turbidity	0.19	NTU*
Conductivity	15	mS/cm at 20^{o}C

*NTU = Nephelometric Turbidity Units

The ozone generator (OzoneLab^{TM} Model OL80W/FM100VT) used for experiments was obtained from Ozone Services, a division of Yanco Industries, Ltd. (Burton, British Columbia, Canada). The oxygen flow to the ozone generator was controlled by a digital mass flow meter and controller (Mass Flo© Model 1179A-01522CS1BV), obtained from MKS Instruments (Wilmington, MA, USA). The flow

meter was calibrated by MKS for oxygen flow at room temperature (20 ^{o}C). The flow meter was powered by a single channel power supply (15 pin Model 246C).

The precipitation experiments were all performed as 1 L batch experiments in a jar test apparatus (Fisherbrand model 10008). To start each precipitation experiment, either a sample of the primary RO concentrate of the real water sample was aliquoted or the synthetic concentrate was made by first adding antiscalant and then adding individual salts from stock solutions. The concentration factor of the primary RO concentrate was approximately three and the initial antiscalant dose to the RO feed was 4 mg/L DQ2006; therefore, the synthetic RO concentrate contained 12 mg/L DQ2006. Before precipitation, 19 mM carbonate (as $NaHCO_3$) was added to account for the higher initial calcium concentration and to provide excess carbonate to stabilize the pH during precipitation. Then the pH was increased to 10.4 with 6 M NaOH.

The separation step was performed using Millipore 0.1 μm pore size nitrocellulose membranes in a dead-end pressurized (0.5 bar) cell with a stir bar. The dead-end filtration cell was used with a digital mass balance to measure filtrate (permeate) flux.

Calcium and magnesium measurements were made using standard titrations for calcium and hardness with ethylenediaminetetraacetic acid (EDTA) (Eaton, et al., 2005). Sulfate measurements were taken with a Hach Ratio/XR turbidimeter; the turbidimeter was used to measure barium sulfate turbidity and to ultimately obtain sulfate concentrations in filtered precipitated samples. Carbonate was measured through alkalinity titrations with 0.36 M hydrochloric acid (HCl).

All pH measurements were taken with a Thermo Electron Corp. pH meter (Orion 720 A+), calibrated with three buffers (pH 4, 7, and 10 standard buffers). The pH of a solution changes with ionic strength (Baumann, 1973; Wiesner, et al., 2006). Therefore,

sodium chloride was added to each pH buffer to account for experimental solution ionic strength. The addition of NaCl to the standard buffer solutions causes a decrease in the pH of the buffer; however, based on previous work by Wiesner, et al., (2006), 8 g/L NaCl causes no more than a 0.1 unit change in pH to each buffer solution. Therefore, no recalculation of the buffer pH values was performed, and the pH values are reported as recorded based on pH meter calibration with the salted buffers.

Particle size distributions were obtained using a laser granulometer Mastersizer S (Malvern Instruments). The Mastersizer S is a static laser light scattering instrument that uses laser light scattering data to obtain a relative volume size distribution. A polydisperse deconvolution algorithm and the Fraunhofer theory were used to translate the detected light scattering data (diffraction intensity with as a function of diffraction angle) into a best-fit particle size distribution.

RESULTS & DISCUSSION

Effect of concentrate treatment on calcium, magnesium, and sulfate precipitation.

Measurements for calcium, magnesium, and sulfate were taken for Case II and Case III after concentrate treatment; results and a comparison to the untreated concentrate are shown in Table 16. All data shown are for the real water sample with 4 mg/L DQ2006 antiscalant added to the primary RO feed water; the primary RO concentrate contained approximately 12 mg/L DQ2006. In Case II, 93% of the calcium was removed, while 96% of the calcium was removed in Case III. Magnesium precipitation decreased slightly from 6.6% to 5.3% when ozonation was performed prior to precipitation and microfiltration, and sulfate precipitation also decreased from 15% to 7.5% with the addition of the ozonation step. Previous work has shown that phosphonate

antiscalant will coprecipitate with calcium carbonate, and the phosphate groups within the antiscalant molecule can replace some of the carbonate ions within the crystal structure (Nygren, et al., 1998). Both magnesium and sulfate have been shown to coprecipitate with calcium carbonate (Loste, et al., 2003; Meldrum and Hyde, 2001; Sudmalis and Sheikholeslami, 2000); however, even though the magnesium ion is smaller than the calcium ion, magnesium does not become incorporated into aragonite, a particularly dense form of anhydrous calcium carbonate. Researchers have postulated that the magnesium ions in solution have a tightly bound hydration shell that serves as a significant energy barrier to incorporation into the anhydrous calcium carbonate lattice structure (Falini, et al., 2009). In this study, the presence of antiscalant appears to decrease that energy barrier, and more magnesium precipitates. The same effect of phosphonate antiscalant on sulfate incorporation may occur; the ability of phosphonate antiscalants to coprecipitate with calcium carbonate by replacing some of the carbonate anions may allow sulfate anions to more easily incorporate into the calcium carbonate lattice structure. It is also possible that the sulfate that precipitated for Case III was primarily in the form of $CaSO_4$, and the additional sulfate that precipitated for Case II was primarily sulfate anion incorporated into $CaCO_3$.

As a control experiment, a sample of the real water was concentrated without antiscalant and the precipitation and microfiltration steps were performed. The control experiment resulted in a lower calcium removal than that of Case III. The results suggest that ozonation may not only deactivate the antiscalant compound but may oxidize other organic compounds within NOM that affect calcium precipitation.

Table 16. Remaining dissolved ion concentrations for untreated and treated primary reverse osmosis (RO) concentrate. RO feed water was the real water sample obtained from the karstic spring in Marseille, France. The data in the far right column are for a sample of the real water with no antiscalant added.

	Case I: Untreated RO Concentrate	**Case II: Precipitation and Filtration**	**Case III: Ozonation, Precipitation and Filtration**	**No Antiscalant: Precipitation and Filtration**
Component	***Concentration (mg/L)***			
Ca^{2+}	448	195	83	175
Mg^{2+}	975	911	923	935
SO_4^{2-}	2,000	1,700	1,850	1,990

RO membrane module performance.

During RO desalination of the real water sample, both RO modules were operated in permeate withdrawal mode. For the primary (first) RO stage, the initial pH of the feed water was 6.5; during RO membrane treatment, the pH of the permeate after 10 minutes was approximately 5.7, while the pH of the concentrate increased slowly (pH 6.8 after 1 hour and 36 min of operation). Over five hours of operation, the pH of both streams increased; the final pH of the permeate was 6.8, and the final pH of the concentrate was 7.2. Several batches of 25 L RO feed water were treated in the primary RO membrane module to produce RO concentrate; the RO concentrate was then treated in the secondary RO membrane module with or without intermediary concentrate treatment.

The dissolved organic carbon (DOC) concentration was measured during primary RO membrane treatment. The primary RO feed water contained approximately 1.0 mg/L

DOC (0.5 mg/L from DQ2006 addition and 0.5 mg/L from natural organic matter (NOM)), while the permeate contained approximately 0 mg/L DOC, and the concentrate had 3.0 mg/L DOC. While a small portion of the DOC (below the detection limit) may have passed through the RO membranes, the results indicate that most of the DOC was retained by the membranes and concentrated in the RO concentrate. The DOC results are consistent with a measured concentration factor of 3; the concentration factor was estimated from dissolved calcium measurements in the feed and concentrate.

During operation of the primary RO desalination stage measurements were taken for the instantaneous values of calcium, conductivity, pH, and temperature in both the RO permeate and concentrate. At the end of pilot system operation, final measurements were taken to obtain the average values for calcium, magnesium, sulfate, carbonate, temperature, conductivity, and turbidity. During operation, the instantaneous calcium concentration and conductivity of the permeate and concentrate increased; the increase in instantaneous calcium concentration in the permeate with the increase in total permeate collected is shown in Figure 46. While the instantaneous permeate concentration increased to greater than 80 mg/L during operation, the average concentration of the permeate was 31 mg/L. A similar trend was observed for the conductivity; initial instantaneous conductivity was 1.4 mS/cm and increased to 14.6 mS/cm, but the average conductivity of the permeate volume was 5.9 mS/cm. The average magnesium concentration in the permeate was 70 mg/L, the sulfate concentration was 143 mg/L, and the turbidity was 0.07 NTU. The final primary RO concentrate conductivity was 31 mS/cm, with a magnesium concentration of 975 mg/L, a calcium concentration of 448 mg/L, a sulfate concentration of 2,000 mg/L, and a turbidity of 0.5 NTU. The initial temperature was 18 ^{o}C and the final temperature was 20 ^{o}C. While the primary RO stage successfully decreased the conductivity and the divalent ion concentrations (calcium,

magnesium, and sulfate), a secondary RO stage is necessary to further decrease salinity, hardness (calcium and magnesium), and sulfate.

A mass balance on the measured dissolved ions in the primary RO feed, permeate, and concentrate resulted a discrepancy of 2 – 11%. For all three ions (calcium, magnesium, and sulfate) the mass in the permeate and concentrate was less than that measured in the feed. It is possible that some of the ions remained in the RO membrane and caused a decrease in the measured mass of ions in the permeate and concentrate as compared to the feed.

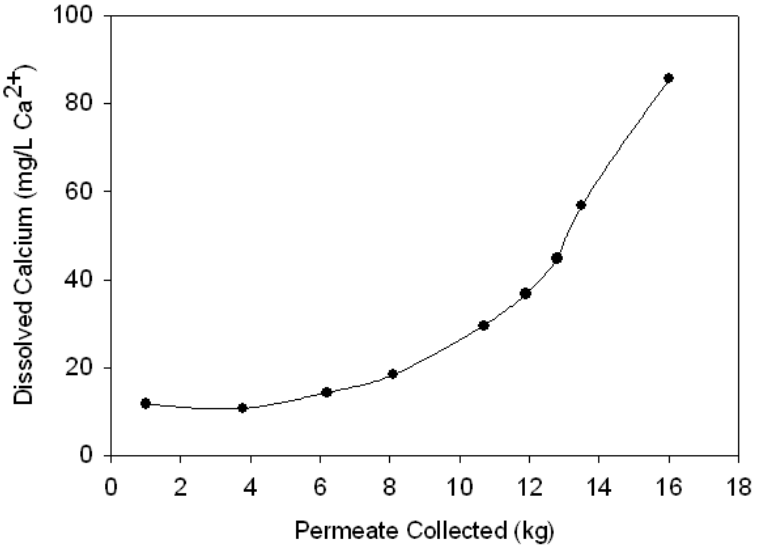

Figure 46. Instantaneous dissolved calcium concentration measurements in the primary reverse osmosis (RO) permeate. 4 mg/L DQ2006 antiscalant added to RO feed, initial feed pH was 6.5, initial volume of the RO feed was 25 L and permeate volume was 17 L.

For Case I, the concentrate produced during the primary RO stage was recovered and treated directly in the secondary RO stage; the treatment scheme, individual RO stage recoveries, and the overall system recovery are shown in Figure 47. The recovery of the

primary RO stage was 67% and was the same value for all three Cases studied. The recovery of the second stage was 62% for Case I. For each RO stage, the saturation index (SI) was calculated for both calcium carbonate ($CaCO_3$) and calcium sulfate ($CaSO_4$); the saturation index is defined as the logarithm of the ratio of the ion activity product (IAP) to the solubility constant (K_{sp}) ($\log(IAP/K_{sp})$) for a particular precipitate. When the IAP is greater than the K_{sp}, the solution is supersaturated with respect to the specific precipitate; $\log(IAP/K_{sp})$ values greater than zero indicate supersaturation. After the primary RO stage, the SI for $CaCO_3$ was 0.03 and the SI for $CaSO_4$ was 0.4. For Case I, after the secondary RO stage, the SI in the concentrate for $CaCO_3$ increased to 0.7, and the SI for $CaSO_4$ increased to 1.6; the recovery of the secondary RO stage was limited by supersaturation of calcium sulfate, and if recovery was increased further, calcium sulfate could precipitate on the membrane surface. The system for Case I is theoretically limited to an overall recovery of 90%, based on the upper saturation limit of precipitation control; antiscalants are able to keep calcium sulfate in solution up to an SI of 2.3 - 4.0 (Hydranautics, 2003). The secondary RO concentrate for Case I contained 912 mg/L calcium, 1,973 mg/L magnesium, 4,215 mg/L sulfate, and a conductivity of 67 mS/cm. The secondary RO permeate for Case I contained 14 mg/L calcium, 29 mg/L magnesium, and 47 mg/L sulfate, with a conductivity of 2.3 mS/cm.

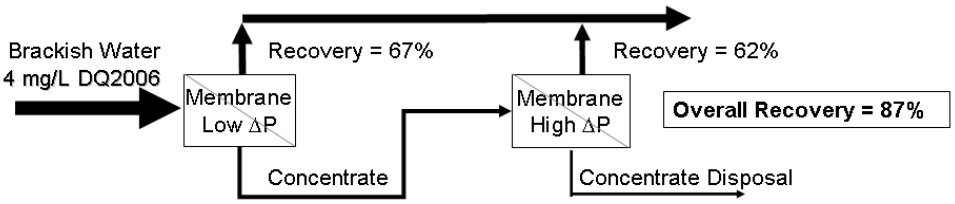

Figure 47. Pilot reverse osmosis (RO) membrane treatment scheme and recovery achieved (%) when no concentrate treatment was used. The primary RO module was operated at low pressure (10 bar), and the secondary RO module was operated at high pressure (50 bar).

The treatment scheme and recoveries achieved for Case III are shown in Figure 48. The treatment scheme for Case II is similar, except Stage I (Antiscalant Oxidation) is not included as part of the side-stream concentrate treatment. The theoretical recoveries for Case II and Case III are 96% and 97%, respectively, based on the supersaturation of calcium sulfate and the limit of antiscalant control of precipitation. In this study, in both Case II and Case III, the secondary RO stage was operated at 73% recovery, for an overall recovery of 91%. For Case II, this operation resulted in a concentrate SI value of -0.6 for calcium carbonate and a value of 0.5 for calcium sulfate. For Case III, the SI values were -0.7 and 0.4 for $CaCO_3$ and $CaSO_4$, respectively. Hence, the inclusion of ozonation prior to precipitation and filtration of the primary RO concentrate increased calcium removal slightly over that observed for Case II. The secondary RO concentrate contained 192 mg/L calcium for Case II and 160 mg/L calcium for Case III. The permeate from the secondary RO stage contained 4.4 mg/L calcium for Case II and 3.6 mg/L calcium for Case III. Slight decreases in magnesium, sulfate, and conductivity were observed for both Cases.

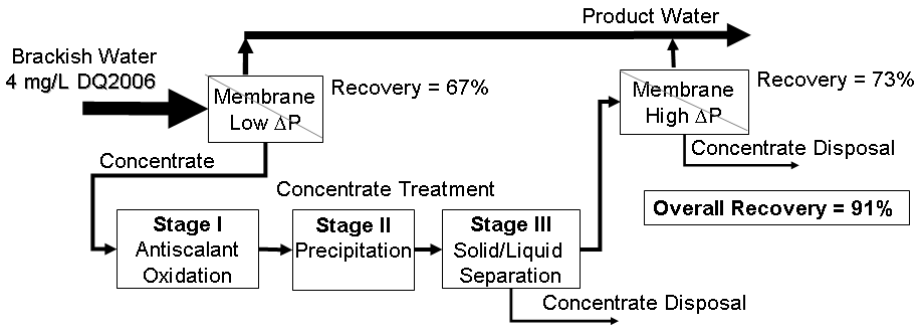

Figure 48. Pilot RO membrane scheme with concentrate treatment between the first and second (low pressure and high pressure) RO stages. Recoveries for each RO stage and the total system are shown as percentages. Case II does not include antiscalant oxidation (Stage I, ozonation), while Case III does include ozonation as the antiscalant oxidation step.

A comparison of the secondary RO permeate flux for Cases I-III is shown in Figure 49. The permeate flux decreased dramatically due to the operation mode (permeate withdrawal) and the resulting increase in salinity on the feed/concentrate side of the RO membrane. As the salinity increases, the osmotic pressure of the feed-side solution increases, and at constant operating hydrostatic pressure (50 bar), the driving force for water flow through the membrane (difference between the hydrostatic and osmotic pressures) decreases, and the water flux decreases. A slight increase in flux occurred with concentrate treatment, and a slight increase for Case III (ozone-precipitation-filtration) over Case II (precipitation-filtration) was observed. This increase in permeate flux is primarily due to the removal of a portion of the dissolved ions during concentrate treatment and a resulting decrease in the osmotic pressure. The osmotic pressure can be calculated by multiplying the molar concentration of dissolved species by the ideal gas constant (R = 0.08206 L-atm/mol-K) and the temperature of the solution. Therefore, the osmotic pressure has a direct relationship with changes in dissolved ion concentrations. The difference in permeate flux for Case I versus Case II or Case III may

have been even greater, but the temperature of the secondary pilot RO system was difficult to control for Case II and Case III; the final temperature for Case I was 22 ^{o}C, whereas the final temperature for Cases II and III was 31 ^{o}C. This increase in temperature would have effectively increased the osmotic pressure and masked some of the effect of concentrate treatment on decreasing the osmotic pressure and increasing the permeate flux.

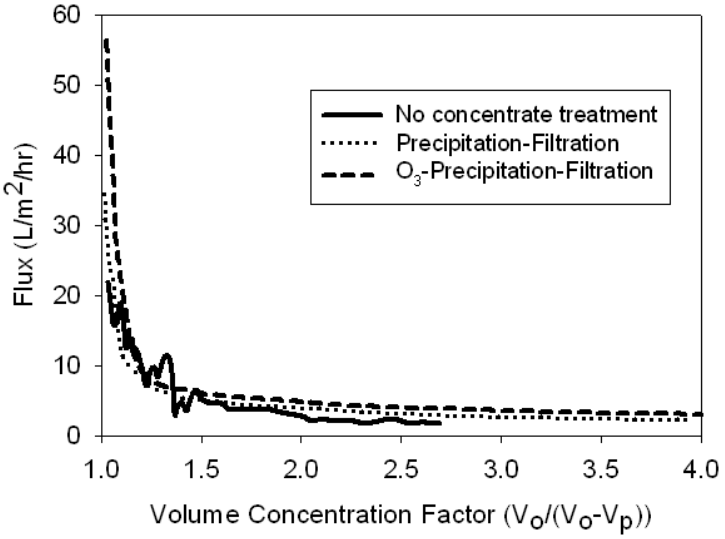

Figure 49. Secondary RO permeate flux for the three cases tested: no concentrate treatment, concentrate treatment by precipitation and filtration, and concentrate treatment by ozonation, precipitation and filtration. The RO membrane module used was the SWRO high pressure module.

Finally, the silt density index (SDI) (ASTM Standard Test Method D4189) is often used as an indication of the fouling capability of an RO feed water (Bu-Rashid and Czolkoss, 2007; Kremen and Tanner, 1998; Petry, et al., 2007; Reverberi and Gorenflo, 2007; Sanz, et al., 2007). The SDI was measured for each concentrate for Case I, Case II, and Case III. The SDI for a 15 minute filtration time (0.45 μm dead-end filtration) for

the untreated primary RO concentrate was 6.0, while the SDI for both the ozonated and non-ozonated treated concentrates was 5.5. The decrease in SDI indicates that the concentrate treatment decreased the fouling propensity of the RO concentrate, possibly by removing particular and organic contaminants.

Comparison between Case II and Case III for real and synthetic RO concentrate.

The real and synthetic RO concentrate samples were tested for Case II (concentrate treatment by precipitation and filtration) and Case III (concentrate treatment by ozonation, precipitation, and filtration). The primary difference between Case II and Case III was the antiscalant present in the RO concentrate was partially degraded by ozonation (in Case III). Phosphonate antiscalants, such as the DQ2006 antiscalant used in this study, contain organo-phosphorus groups that are oxidized to orthophosphate (PO_4^{3-}) during ozonation. The effect of ozonation time on fractional orthophosphate production is shown in Figure 50 for an antiscalant concentration of 85 mg/L DQ2006 (27 mg/L P). Fractional orthophosphate is the ratio of the orthophosphate produced during ozonation to the phosphate available in the original antiscalant molecule. Even for an ozonation time of 30 minutes, only 0.6 of the phosphate available was oxidized to orthophosphate, indicating that complete oxidation does not occur, and some partial oxidation products were present in the RO concentrate. However, ozonation times between one and 10 minutes are sufficient to inactivate the antiscalant and arrest the ability of the antiscalant to prevent precipitation.

The synthetic RO concentrate was analyzed for calcium, magnesium, and sulfate before and after concentrate treatment. Again, a control experiment was performed on a sample of synthetic concentrate with no addition of antiscalant; results indicated an increase in precipitation for all three ions in the synthetic water concentrate as compared to the real water RO concentrate. The same trend was observed for synthetic concentrate

containing 12 mg/L DQ2006 and treated for Case II; calcium precipitation decreased as compared to the synthetic control and increased as compared to the real water sample. However, for Case III treatment, while calcium precipitation increased as compared to Case II, calcium precipitation decreased in comparison to the ozonated real water sample. This last result was unexpected and may be due to the presence and oxidation of natural organic matter.

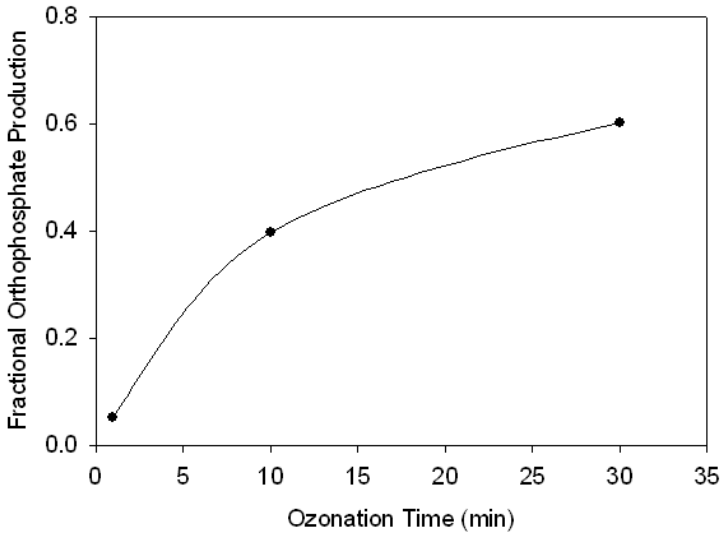

Figure 50. Effect ozonation time on fractional orthophosphate production for an initial antiscalant concentration of 27 mg/L P. Ozonation performed at pH 6.0, with an ozone mass flow of 3 mg/min.

Particle size distribution measurements were taken on the precipitated solutions for both the synthetic and real water RO concentrates, for both Case II and Case III. The control for both water types was a precipitated sample with no antiscalant and no ozone treatment; results are shown in Figure 51a & b for the real and synthetic water samples, respectively. Several differences existed between the two water types. The first is that the synthetic water samples were all multi-modal, and in particular, the non-ozonated

samples (with and without antiscalant) had three to four modes, while the ozonated sample had a primary modal particle diameter of approximately 10 μm, with a non-distinct mode between 0.1 and 3 μm. Repeat experiments performed in this study resulted in the same multi-modal shape for the synthetic water. The addition of antiscalant to the synthetic water (Figure 51b) appeared to increase the modal particle diameter of the mode with the largest relative volume, while ozonation returned this modal value to that of the control (no antiscalant, no ozone). The opposite effect of antiscalant addition was observed for the real water sample (Figure 51a); the addition of antiscalant caused the modal particle diameter to decrease and ozonation caused the modal particle diameter to increase back to that of the control sample. In addition, while the real samples were multi-modal as well, the curves did not have as many modes and each mode was distinct, whereas most of the modes for the synthetic water samples were connected over several orders of magnitude of particle diameter.

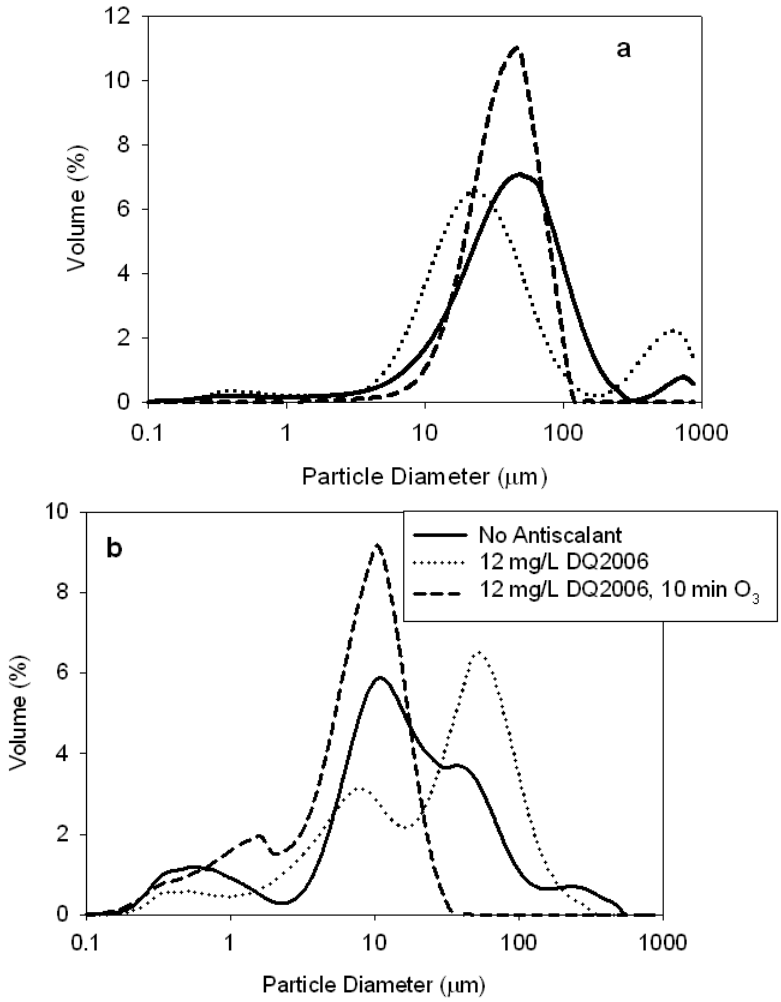

Figure 51. Particle size distributions for the (a) real and (b) synthetic precipitated reverse osmosis (RO) concentrates. Precipitation performed at pH 10.5 for 1 hour with addition of $NaHCO_3$ and NaOH.

High sulfate concentrations have been shown to cause particle agglomeration, and particle agglomeration increases with sulfate concentration (Falini, et al., 2009). The molar ratio of sulfate to calcium was 2 in this study; Falini et al. (2009) studied sulfate to calcium molar ratios between 1 and 10. Other research has shown that sulfate to calcium ratios as low as 0.5 – 1.5 can cause particle clumping (Kralj, et al., 2004). Both water types have modes or portions of the particle size distribution that are much larger than

typical calcium carbonate precipitated particles (5 – 10 μm), and particle agglomeration is most likely the source of the larger particles measured. The addition of antiscalant can also cause changes in particle morphology and particle agglomeration (Dove and Hochella, 1993; Kan, et al., 2005; Tang, et al., 2008); however, the shapes of the particle size distributions were different between the two water types independent of the presence or absence of antiscalant.

The real water contained several ions that were not included in the synthetic water, such as potassium and nitrate; potassium has been shown to affect the distribution of calcium carbonate phases formed (Falini, et al., 2009), while nitrate (in the presence of magnesium) changes the morphology of calcite (anhydrous calcium carbonate) crystals from rhombohedral to dumbbell-shaped but has a minor impact on changes to the crystal lattice structure (Kralj, et al., 2004). Neither potassium nor nitrate has been reported to cause particle clumping.

The real water sample also contained a small amount (0.5 mg/L DOC) of natural organic matter. Research on portions of natural organic matter (NOM) has shown that NOM prevents particle growth by adsorbing onto crystal nuclei (Falini, et al., 2009). In addition, NOM can prevent the conversion of less thermodynamically stable phases of calcium carbonate, such as vaterite, to calcite (the most stable form) by adsorbing onto vaterite crystals and preventing the dissolution-precipitation process during which calcite is formed. Falini et al. (2009) showed that the presence of humic acids caused the precipitation of vaterite, but in the presence of sulfate or sodium ions, only calcite was formed. Humic acids also caused increased aggregation in the presence of all ions typically found in seawater. Since humic acids are thought to adsorb onto calcium carbonate crystals through strong electrostatic interactions, preventing such phase transformations as vaterite to calcite, the presence of certain ions (sulfate or sodium)

appeared to reduce these interactions. The electrostatic interactions between humic acid and crystals were most likely precluded by strong interactions between humic acid and sulfate (or sodium); the results presented by Falini et al. (2009) suggest that, for the present study, the natural organic matter in the real water sample formed interactions with the sulfate ions and prevented the extensive aggregation and clumping observed in the particle size distributions of the synthetic water samples (Figure 51b). Some aggregation still occurred, as indicated by the mode shifting from 100 μm to greater than 1000 μm in Figure 51a, for both the control sample and the sample with antiscalant added. However, the particle size distribution curves for the real water were more uniform in shape; the aggregation that did occur in the real water is most likely primarily controlled by the NOM, while the aggregation in the synthetic water samples is most likely due to the high sulfate to calcium molar ratio. The presence of NOM in the real water sample may also have caused the difference in changes to the modal particle diameter with the addition and ozonation of antiscalant.

The addition of antiscalant to the real water sample also caused a group of smaller particles between 0.1 and 1 μm to form; on a volume basis (as shown in Figure 7), the difference between the samples with and without antiscalant is not great, but the small volume increase represents a far larger number concentration increase than is apparent. Antiscalants prevent precipitation by blocking crystal lattice growth sites (Yang, et al., 2001), and a higher number of small nucleated particles are formed during precipitation, while the number of fully grown particles tends to decrease. Ozonation of the real water sample made the particle size distribution mono-modal, with no smaller nucleated particles or larger agglomerated particle groups. Ozonation of the antiscalant allowed particle growth, and very few small particles were present after one hour of precipitation. Ozonation also caused partial oxidation of the NOM, and arrested the ability of NOM to

cause particle aggregation. However, the remaining organic matter in solution appeared to still control sulfate interactions and prevent sulfate from causing particle agglomeration.

Addition of antiscalant to the synthetic water did not appear to reduce the extent of particle agglomeration, based on the multiple modes present for both the control and antiscalant addition samples. Ozonation of the synthetic water with antiscalant present inhibited the formation of particles larger than approximately 30 – 40 μm, indicating that ozonation prevented particle clumping. However, small particles between approximately 0.2 and 2 μm were measured even with ozonation. It is unclear why both the control and ozonated samples both had a mode within this particle size range, but it is possible that some of the vaterite was undergoing transformation to calcite, and small nucleating crystals of calcite were present and measured.

The precipitated samples of Figure 51a & b were subsequently filtered using 0.1 μm pore size Millipore nitrocellulose microfilters; a comparison of the permeate flux data is shown in Figure 52a & b. The permeate flux is shown as a function of the volume concentration factor (VCF), the ratio of the initial volume (V_o) to the difference between the initial volume and the permeate volume (V_p). For both water types, the addition of antiscalant causes a decline in permeate flux; ozonation of the antiscalant prior to precipitation causes a partial recovery of the flux lost due to antiscalant addition for the real water sample and complete recovery of the flux for the synthetic water sample. As mentioned above, the addition of antiscalant causes the formation of many small nucleated particles that do not grow into full-size particles. The increase in the number of small particles may have caused increased pore blockage and fouling during microfiltration, which caused a greater decline in the permeate flux. Ozonation of the antiscalant allowed particle growth and precipitation, and the larger particles caused only

a small decline in permeate flux. Ozonation of the real water sample did not allow full recovery of the flux lost due to antiscalant addition, and the real water control sample without antiscalant had a lower permeate flux than the synthetic water control sample. Both of these results indicate that the natural organic matter in the real water sample also played a role in microfiltration permeate flux decline, and the presence of NOM appeared to negatively impact microfiltration of the precipitated solutions. Ozonation of antiscalant in the presence of NOM was not completely effective in removing the effect of antiscalant on microfiltration; ozonation in the presence of NOM may cause a smaller fraction of the antiscalant to be oxidized or create partial oxidation products from the antiscalant or organic compounds of NOM that negatively impact filtration.

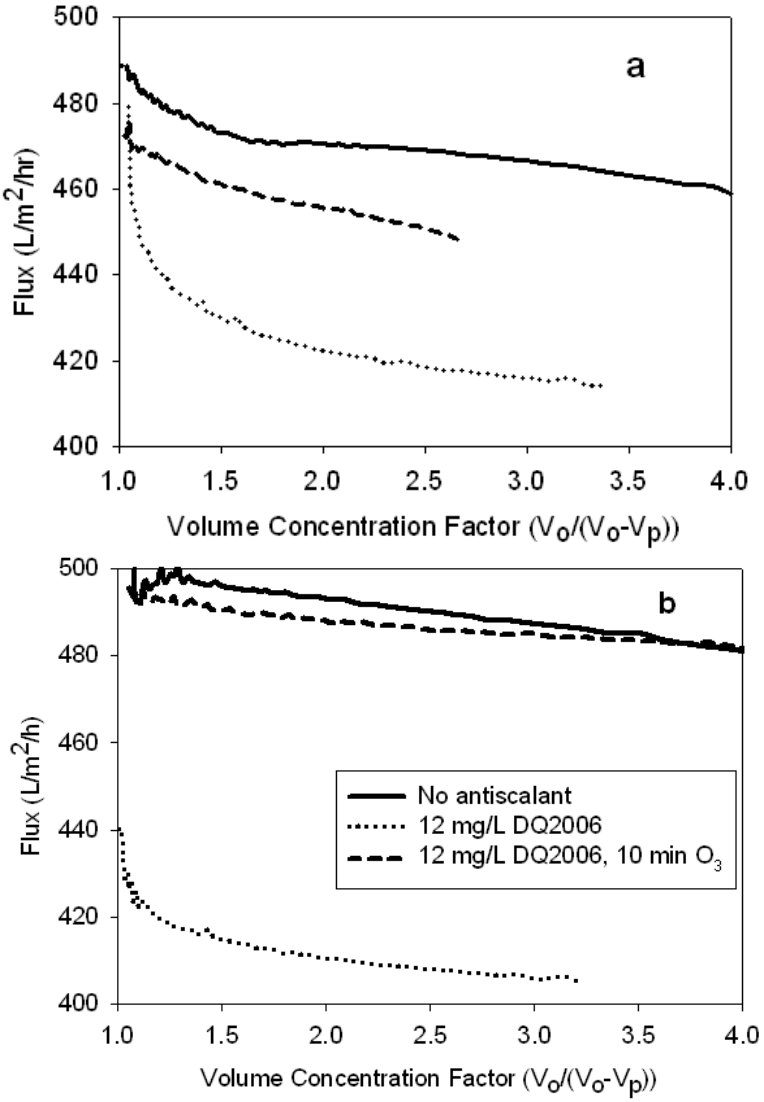

Figure 52. Microfiltration permeate flux performance of the precipitated reverse osmosis (RO) concentrates for (a) the real water sample and (b) the synthetic RO concentrate. Microfilter pore size was 0.1 μm and filtered volume was 300 mL.

CONCLUSIONS

A water sample from a brackish karstic spring in southern France was used with two reverse osmosis membrane modules to test intermediary concentrate treatment. The

concentrate treatment consisted of precipitation and filtration (Case II) or ozonation, precipitation, and filtration (Case III). The ozonation step was used to oxidize antiscalants and potentially increase precipitation. Both types of concentrate treatment removed a significant portion of the calcium, as well as some magnesium and sulfate. Ozonation allowed increased calcium precipitation but decreased the amount of magnesium and sulfate that precipitated. Results show that concentrate treatment can significantly reduce the precipitation potential of the concentrate and allow increases in recovery above those typically seen for a brackish water reverse osmosis membrane system. A comparison of real and synthetic water samples indicated that natural organic matter played an important role in the extent of calcium precipitated, the particle size distribution of precipitated samples, and microfiltration of precipitated solutions. While tests with synthetic water can indicate how a real water might behave during concentrate treatment, this study clearly shows the importance of ultimately testing with the real water to be used in treatment. Results from this study indicate that concentrate treatment can significantly increase the overall recovery of a brackish water RO system and enable inland brackish water RO to be a more viable solution to diminishing fresh water resources.

Chapter 9: Conclusions

SUMMARY

The primary objective of this research was to develop a side-stream treatment process to treat a brackish RO concentrate, with the goals of reducing concentrate volume and increasing overall RO system recovery. The concentrate treatment process consisted of three stages: antiscalant oxidation, salt precipitation, and solid/liquid separation. The research focused on experimental investigation with the aid of thermodynamic equilibrium software. Four different antiscalant compounds were tested, including three phosphonates and one acrylic acid polymer. The antiscalants were chosen for their ability to reduce or eliminate calcium precipitation (as calcium carbonate or calcium sulfate). Several synthetic brackish RO concentrate water compositions, as well as a natural water sample, were tested to determine the role of specific water components on the three-stage process. Ozone with and without hydrogen peroxide was investigated as the oxidation system, and key parameters that affect antiscalant oxidation were identified and evaluated. The primary oxidation pathway was determined for phosphonate antiscalants and the ozone/hydrogen peroxide system under specific experimental conditions. The effects of antiscalants on salt precipitation and microfiltration (solid/liquid separation) were investigated; the precipitation step was evaluated through measurements of particle size distribution, particle morphology, particle composition, and dissolved ionic species. These measurements showed how the presence and oxidation of antiscalants caused changes to the morphology and composition of precipitating particles. Changes in microfiltration flux were related to the addition of specific antiscalant compounds and concentrations. Small doses of ozone prior to precipitation allowed

antiscalant deactivation and largely prevented the antiscalant from impacting the precipitation and separation steps. While results indicated that not all of the antiscalant molecules were completely oxidized, an evaluation of the precipitation and separation stages indicated that the partial oxidation products did not act in the same manner as whole antiscalant molecules. Ozonated samples resulted in similar particle characteristics and filtration flux as the control samples containing no antiscalant. The three-stage concentrate treatment was evaluated as an integrated process for its effect on system recovery; the effect of antiscalant oxidation on salt precipitation and microfiltration was studied, and a pilot RO system study was performed to determine the potential increase in overall RO recovery with concentrate treatment.

CONCLUSIONS

Based on experimental results, the following conclusions can be drawn from the research on precipitation and solid/liquid separation without any oxidation of the antiscalant, are reported in Chapters 4 and 5:

1) The presence of antiscalants during precipitation decreases calcium precipitation but increases magnesium and sulfate precipitation.
2) The extent of calcium precipitation varies with antiscalant type and water composition; the presence of magnesium and sulfate cause a decrease in calcium precipitation for the water composition used in this study. Both magnesium and sulfate increase the solubility of calcium carbonate through adsorption onto crystal growth sites, changes in crystal lattice structure, and incorporation into the crystal lattice.
3) Calcium carbonate precipitate particle morphology and composition are affected by the presence of antiscalant and the presence of specific water components, including magnesium and sulfate. The presence of antiscalants during calcium

carbonate precipitation can cause the formation of sub-micron spherical particles (100 - 200 nm) and prevent full growth of the nucleated crystals. In a concentrate with a simplified water composition (only $CaCl_2$ and $NaHCO_3$), higher antiscalant concentrations (40 – 85 mg/L) are more likely to cause the formation of these small particles. In more complex water compositions (with magnesium, sulfate, ferric iron, barium, and nitrate), lower antiscalant concentrations (9 mg/L) cause the formation of sub-micron particles.

4) The presence of antiscalant during precipitation can cause a decrease in permeate flux during subsequent microfiltration. This negative impact on flux is caused by interactions between the antiscalant and the precipitated particles and not through adsorption of antiscalant onto the microfiltration membrane.

The following conclusions can be drawn from the research on the oxidation of antiscalants, as reported in Chapter 6:

1) Phosphonate oxidation by ozone is primarily controlled by cation coordination, pH, and the number of ozone doses (or total mass of ozone applied). The effect of pH on phosphonate oxidation is caused by changes in calcium-antiscalant speciation, with the optimal conditions occurring when the calcium-antiscalant compound is partially protonated. In the case of DQ2006, the species controlling oxidation is $CaH_2DQ2006^{2-}$.
2) In the presence of calcium, the extent of oxidation varied considerably between the three phosphonate antiscalants tested; the extent of oxidation by ozone is significantly affected by conformational changes of the phosphonate molecule caused by calcium-phosphonate coordination.
3) Phosphonate oxidation by ozone is not affected by the carbonate system in the presence of calcium; in the absence of cation coordination, the presence of

carbonate causes increased oxidation as the molar ratio of H_2O_2 to O_3 is increased (0 – 0.8 H_2O_2/O_3).

4) When calcium is present, the primary pathway for oxidation of phosphonates is through direct reaction with ozone. In the absence of cations, such as calcium, magnesium, or iron, that will complex with phosphonate antiscalants, the primary pathway for oxidation of phosphonates is through reactions with hydroxyl radicals.
5) The fraction of original antiscalant that is oxidized increases with an increase in ozone concentration (1 - 10 mg/L) and with a decrease in antiscalant concentration.

The following conclusions can be drawn based on the research reported in Chapter 7 on the bench scale experiments with the complete three-stage treatment system:

1) Ozonation of phosphonate or acrylic acid-based polymer antiscalants can deactivate the antiscalant, allowing increased calcium precipitation in a brackish RO concentrate.
2) Ozonation of antiscalant prior to precipitation and filtration causes an increase in calcium precipitation, a decrease in magnesium and sulfate precipitation, and at least partially removes the effect of the antiscalant on precipitate particle morphology and microfiltration flux.
3) Ozonation does not completely oxidize phosphonate antiscalants, even with a long ozonation time of 30 minutes (3 mg/L O_3). A primary oxidation product of phosphonate antiscalants is orthophosphate, and all orthophosphate produced during ozonation is removed during precipitation.

The following conclusion can be drawn based on bench-scale (Chapter 7) and pilot system-scale (Chapter 8) results:

1) Concentrate treatment of a brackish RO concentrate by the three stage process investigated in this research can remove most of the calcium in the concentrate, reduce the scaling propensity of the concentrate, and significantly increase the overall system recovery.

SIGNIFICANCE

Research in the area of concentrate treatment and volume reduction has received increased interest as reverse osmosis desalination becomes a more widespread technology and as more inland communities face water shortages. Current research ranges from basic experimental research to large-scale pilot system studies, and a common concern is the effects of specific concentrate constituents, such as antiscalants and NOM, on a concentrate treatment process. Most concentrate treatment processes use a controlled precipitation step to remove scaling salts. Hence, this research focuses on a relevant and critical aspect of RO concentrate treatment.

While the broad objective of the study was to develop an overall concentrate treatment process, the experiments resulted in a more detailed understanding of antiscalant oxidation and the effects of antiscalants on precipitation and filtration. As is evidenced by current pilot system studies and previous research, RO concentrate treatment can be performed without a complete understanding of the effects of individual water components. Ultimately, however, delineating the details of the specific water chemistry is crucial to optimal treatment. The results of this study provide a greater understanding of antiscalant chemistry within the framework of an applicable brackish RO concentrate treatment scheme.

Furthermore, phosphonate compounds are used not only as antiscalants for RO desalination, but as dispersion and scale inhibitor chemicals in many industrial and

research applications. The ozonation results from this research provide insight into oxidation pathways, the influence of various cations (including calcium) on antiscalant chemistry, and the effects of operational parameters on phosphonate oxidation. Calcium is a ubiquitous component of natural waters and thus is the major ion involved in most scaling problems or precipitation events. Hence, the results of this research could allow advances not only in RO desalination but in other unrelated fields.

The pilot RO system study performed in this research suggested that, in addition to antiscalant, the presence of NOM, even in small amounts, can affect RO concentrate treatment. This result could be critical because most brackish waters will have at least some NOM, and the NOM becomes concentrated in the RO concentrate. Differences between the real and synthetic RO concentrates illustrate the importance of testing real water samples and indicate that results from a synthetic sample can both underestimate and overestimate expected results from the real water. While a more detailed study of antiscalant and NOM interactions is necessary, it is clear that NOM plays an important role in precipitation-based RO concentrate treatment.

RECOMMENDATIONS FOR FUTURE WORK

This research has resulted in the development of a RO concentrate treatment process (tested at bench-scale) and has delineated several details of phosphonate oxidation by ozone. Research results have also shown how four specific antiscalants affect calcium carbonate precipitation and filtration in several different water compositions. However, most of the results are based on synthetic RO concentrates, and further study and understanding of several aspects of the research is recommended. A prioritized list of specific recommendations follow.

1) Based on work in Chapters 6 and 7, the antiscalants are not completely oxidized during ozonation, and partial oxidation products are formed. A recommended area of research is to determine the partial oxidation products of antiscalant ozonation and their fate in the RO concentrate treatment process. Results from the work described in this dissertation clearly indicate that the organophosphate compounds are not completely oxidized, and partial oxidation products may be returned to the RO system with the recovered water. Furthermore, partial oxidation products may be formed from NOM, and known oxidation products such as bromate may be a concern.
2) To continue the work in Chapter 6 on the details of antiscalant oxidation by ozone, further research is recommended to perform a kinetics study on antiscalant oxidation by measuring the concentrations of antiscalant, ozone, and hydroxyl radical over time for both short time steps (< 30 seconds) and longer time steps (>1 min). A radical scavenger, such as tert-butanol, would be used to isolate the ozone reaction system, and a non-ozone source of hydroxyl radicals, such as ultraviolet irradiation, would be used to isolate the radical reaction system. Recommended parameters to vary include water composition (in particular, cation type and concentration), pH, antiscalant type and concentration, and ozone dose/radical dose applied. In addition, experimental conditions that include both low carbonate and low calcium concentrations should be examined to determine any differences in antiscalant oxidation.
3) Based on the work done in Chapters 4 and 5, further research is recommended to understand antiscalant-precipitate particle interactions. A recommended research project is to perform a study on the adsorption and coprecipitation of antiscalants during salt precipitation. Little work has been done specifically on the

coprecipitation of specific antiscalants in the presence of different precipitates (e.g., calcium carbonate versus calcium sulfate). This study would quantify how much antiscalant precipitates with the salt and what experimental parameters affect adsorption and coprecipitation. A particular parameter of interest is particle surface charge; this parameter was not studied in the research presented but is an important parameter that can affect adsorption and precipitation.

4) Based on the results in Chapter 8, further research is recommended on natural water samples and RO concentrate treatment. A possible research project is to perform additional pilot RO studies on several different natural water samples to determine how results change with water source and natural water composition. Important parameters to study would be NOM concentration and composition, ionic species composition, and antiscalant type. Results from water samples could be compared based on total organic carbon in the concentrate, orthophosphate produced during antiscalant oxidation, amount of base and carbonate added for precipitation, amount of calcium precipitated, precipitation of other species (magnesium, sulfate, silica), differences in surface charge, and filtration flux performance. Develop a continuous flow RO concentrate treatment experimental setup.
5) Futher research is recommended on RO concentrate treatment when polymer antiscalants are used. This research primarily focused on phosphonate antiscalants, but polymer antiscalants are often used in water treatment and RO desalination and contain different functional groups. NMR techniques can be used to determine polymer composition, and the effect of ozonation on polymer antiscalants could be studied.

6) Results from Chapter 4 indicate that significant precipitation can occur at lower pH values (7.85 – 8.85). Further research is suggested with antiscalants and precipitation (with and without ozone) at different pH values and saturation ratios to further study and optimize concentrate treatment and antiscalant dose. Study additional antiscalant types and relate antiscalant choice to specific water components and efficient RO concentrate treatment. Determine whether antiscalant choice can be based primarily on successful RO concentrate treatment, rather than on RO membrane performance.
7) Results from Chapters 4 and 5 indicated the presence of multiple particle sizes, while some of the SEM images showed only one particle size. Further research is recommended to perform a particle size study with other size measurement instruments, such as the Coulter Counter (which measures the actual solid volume of each particle) to compare size distribution results and better determine the specific causes of changes in particle size distribution. This study would further explain if changes in measured particle size are caused by events such as particle agglomeration, the adsorption of small particles onto larger particles, and the formation of sub-micron particles. Using other instruments could also help explain or determine errors in the data deconvolution algorithms used by the laser light scattering instrument in this research.

Appendix A: Supporting Information for Chapter 4

ANALYSIS OF FILTRATION DATA TO DETERMINE FOULING MECHANISMS FOR ANTISCALANT DQ2066

The results for DQ2066 microfiltration data analysis to determine the fouling mechanisms for each experiment are shown in Figures S1 – S4. The results for DQ2006 microfiltration data analysis are shown in Figures S5 – S8. For each figure, the entire data set for each antiscalant concentration is shown in the left figure and the linear regions that were analyzed in a linear regression are shown in the right figure, with the associated R^2 values. Due to scatter in the data, R^2 values of greater than 0.90 were accepted as an indication of the specific type of fouling.

The linear relationships for each type of fouling are as follows (Wang and Tarabara, 2008):

Complete blocking $$Q = Q_0 - K_b V$$

Intermediate blocking $$\frac{1}{Q} = \frac{1}{Q_0} + K_i t$$

Standard blocking $$\frac{t}{V} = \frac{K_s t}{2} + \frac{1}{Q_0}$$

Cake filtration $$\frac{2t}{V} = K_c V + \frac{2}{Q_0}$$

where Q_0 is the initial volumetric flow rate and K with any subscript is a constant for that blocking mechanism.

SEM images of the DQ2066 concentrations tested are shown in Figure S9.

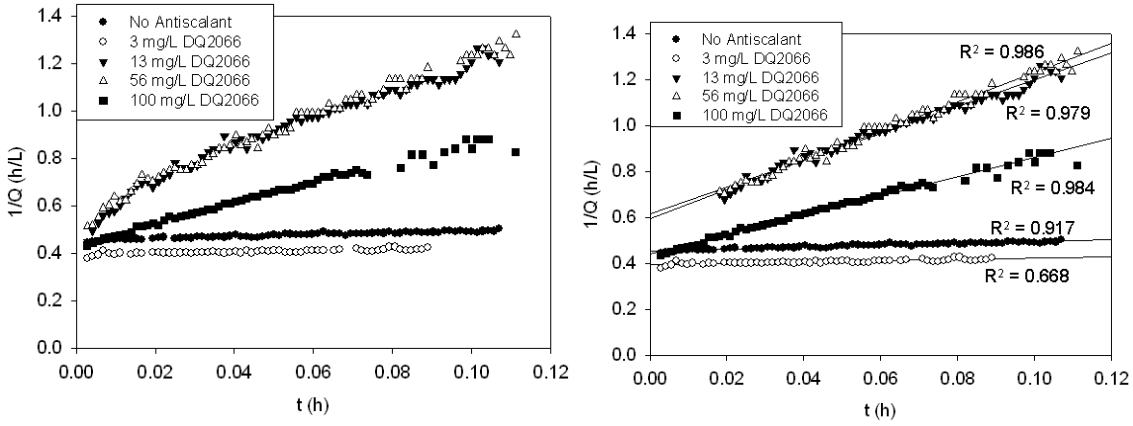

Figure 53. Analysis of DQ2066 microfiltration data for intermediate blocking.

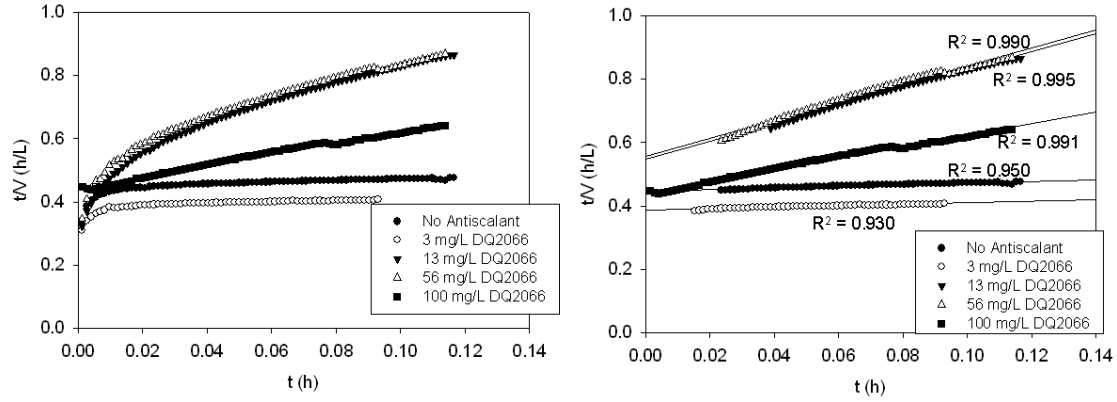

Figure 54. Analysis of DQ2066 microfiltration data for standard blocking.

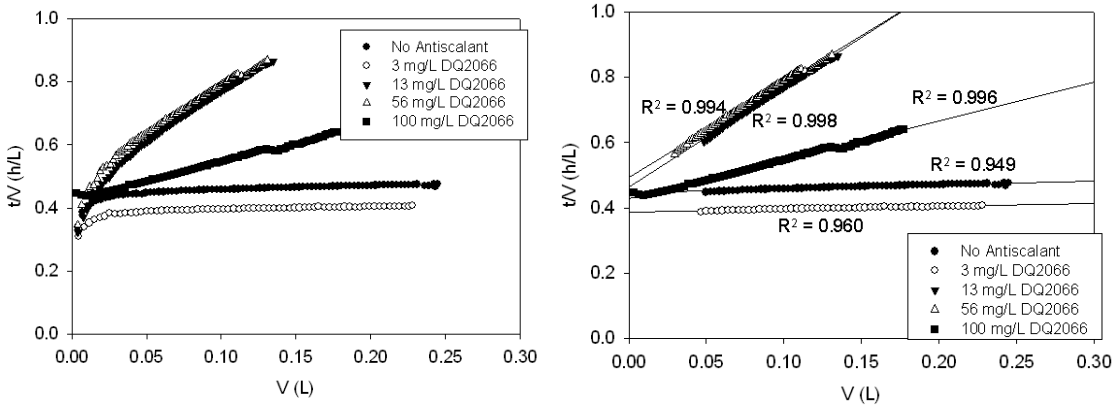

Figure 55. Analysis of DQ2066 microfiltration data for cake filtration.

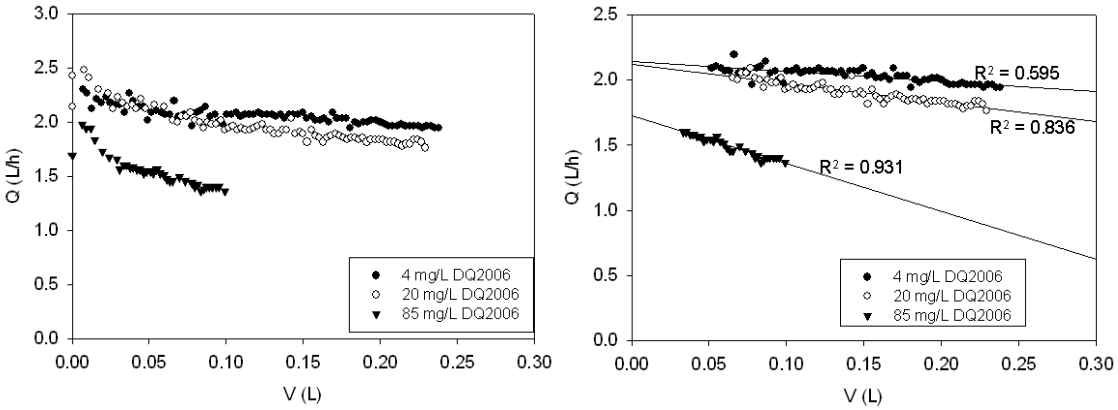

Figure 56. Analysis of DQ2006 microfiltration for complete blocking.

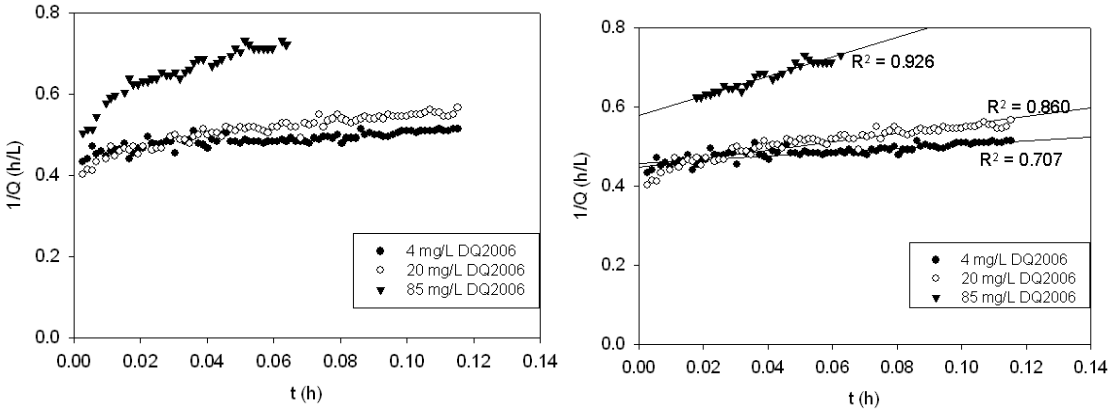

Figure 57. Analysis of DQ2006 microfiltration for intermediate blocking.

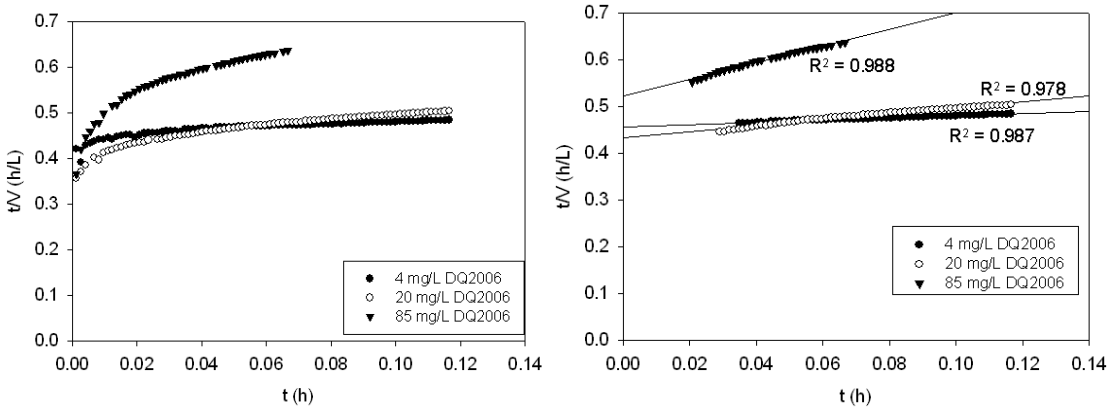

Figure 58. Analysis of DQ2006 microfiltration for standard blocking.

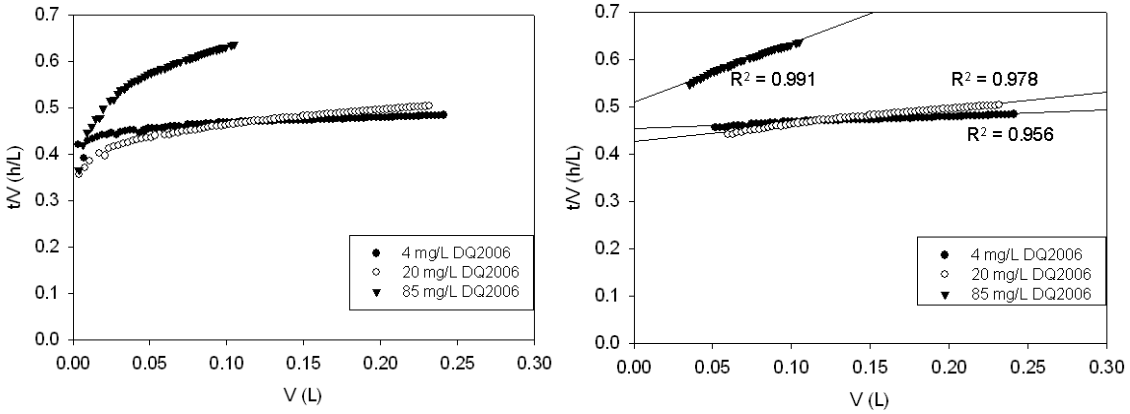

Figure 59. Analysis of DQ2006 microfiltration for cake filtration.

SEM IMAGES OF DQ2066

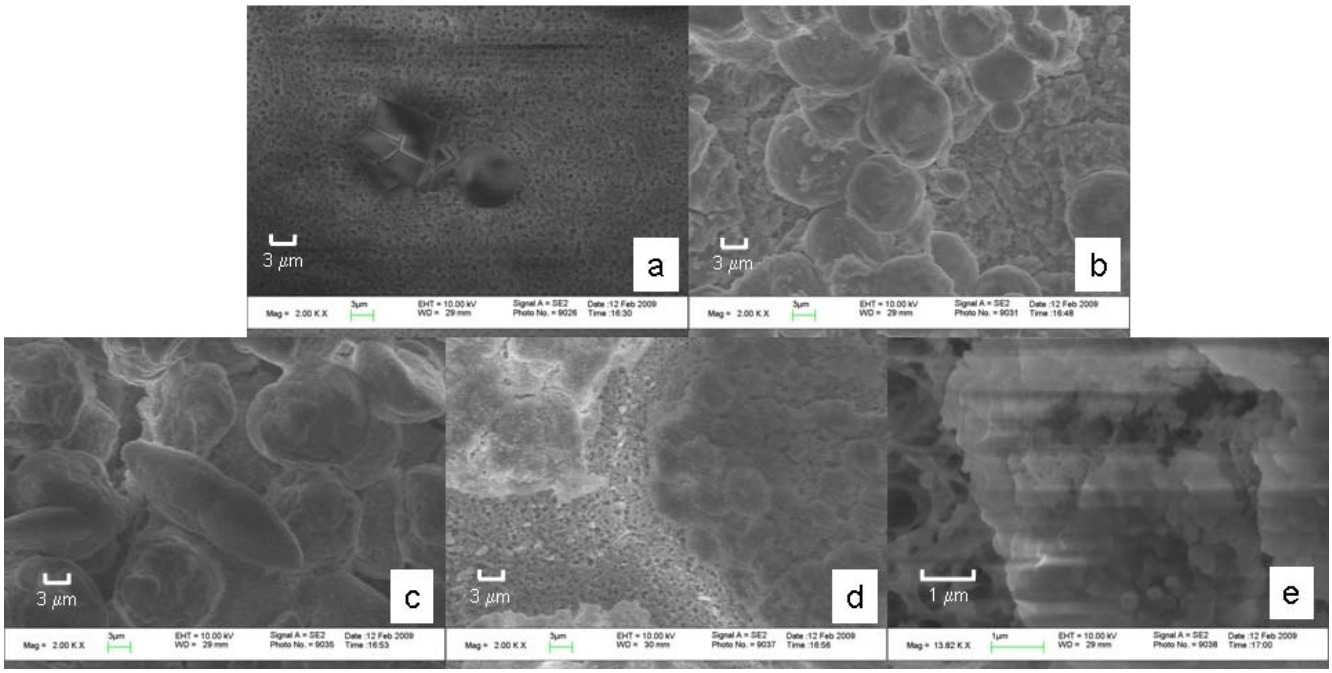

Figure 60. SEM images of calcium carbonate precipitation at pH 10.5 with doses of DQ2066: (a) 3 mg/L, (b) 13 mg/L, (c) 56 mg/L, (d & e) 100 mg/L.

Appendix B: Supporting Information for Chapter 6

MOLECULAR MODELING FOR PHOSPHONATE ANTISCALANTS WITH AND WITHOUT CALCIUM COORDINATED

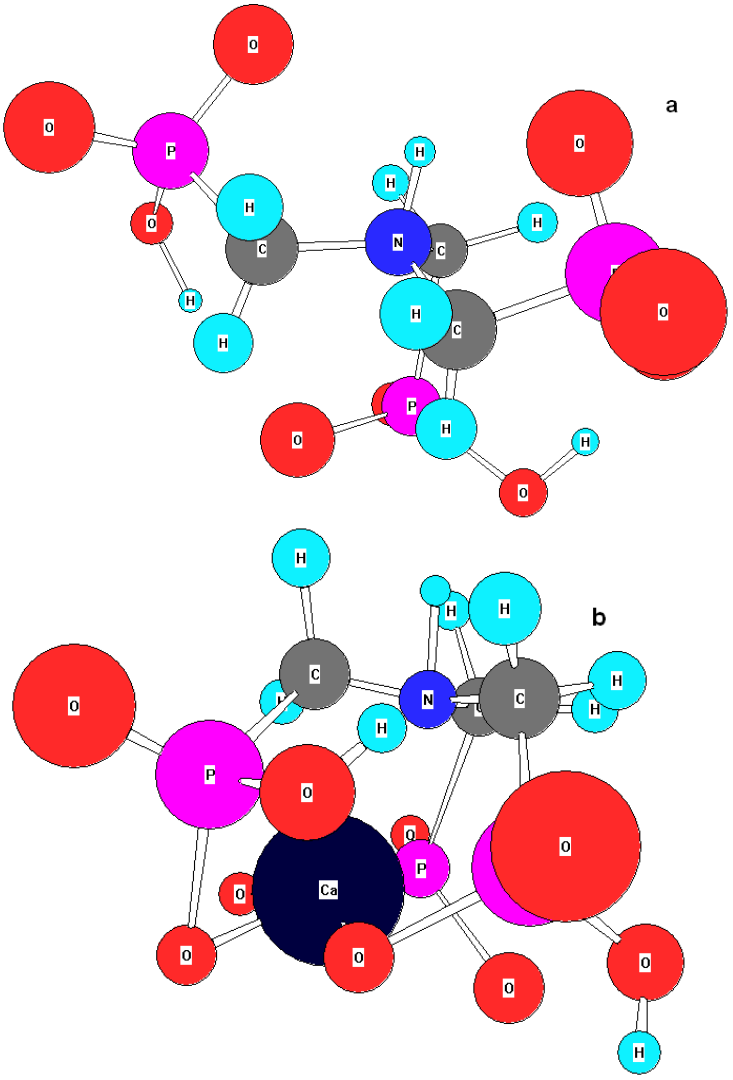

Figure 61. Molecular models of antiscalant DQ2006 (a) without and (b) with calcium coordinated to the ligand.

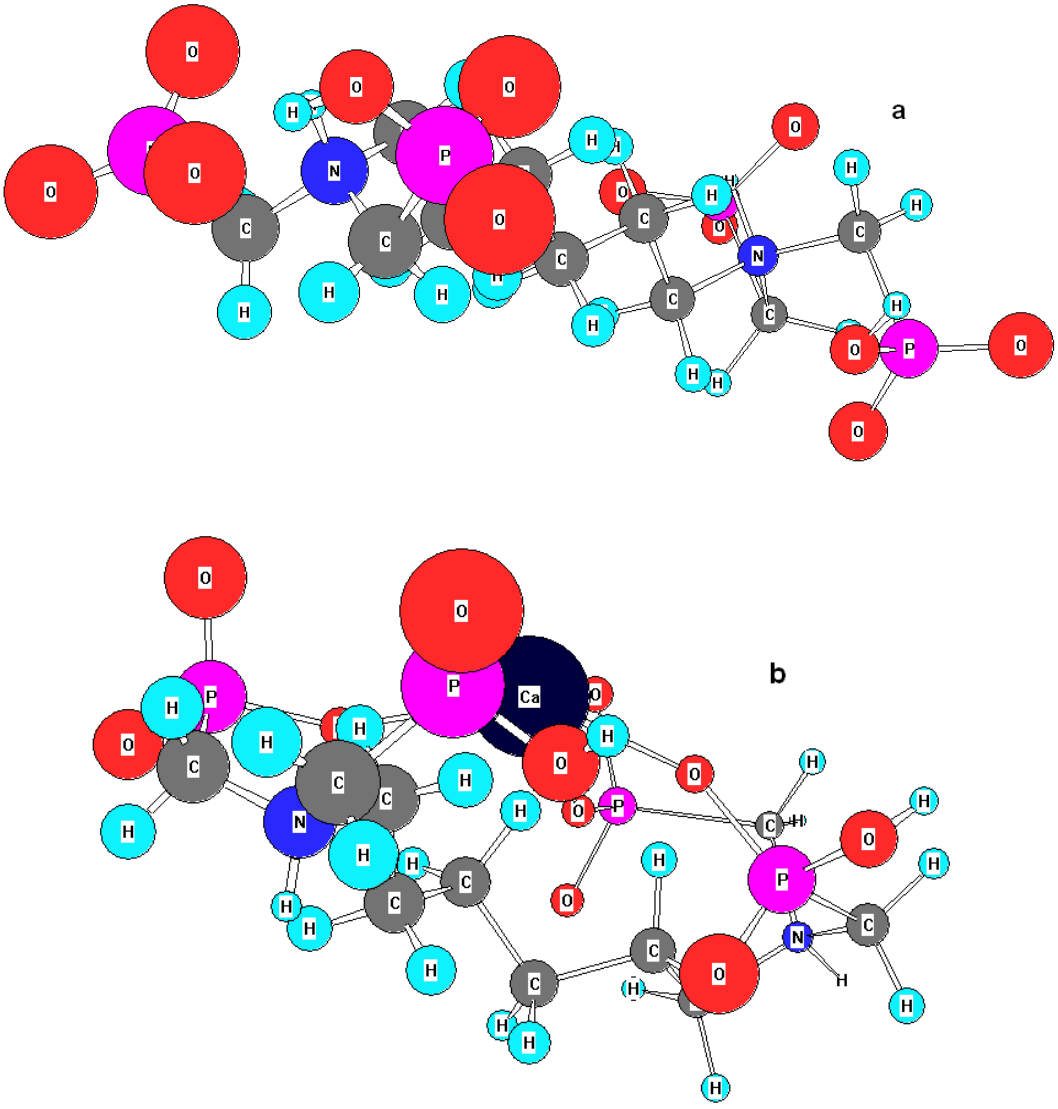

Figure 62. Molecular models of antiscalant DQ2054 (a) without and (b) with calcium coordinated to the ligand.

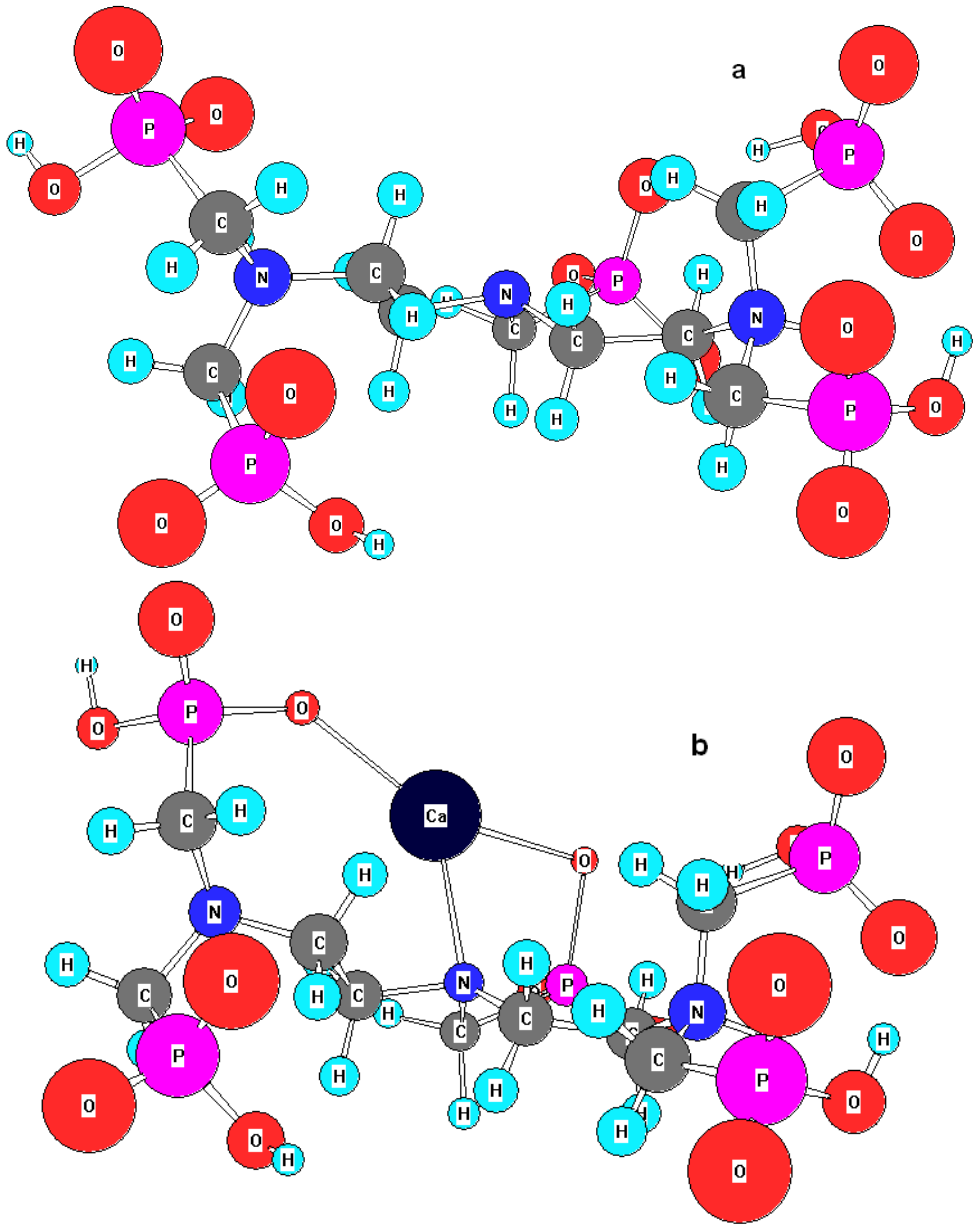

Figure 63. Molecular models of antiscalant DQ2066 (a) without and (b) with calcium coordinated to the ligand.

EFFECT OF CARBONATE ON PHOSPHONATE ANTISCALANT OXIDATION

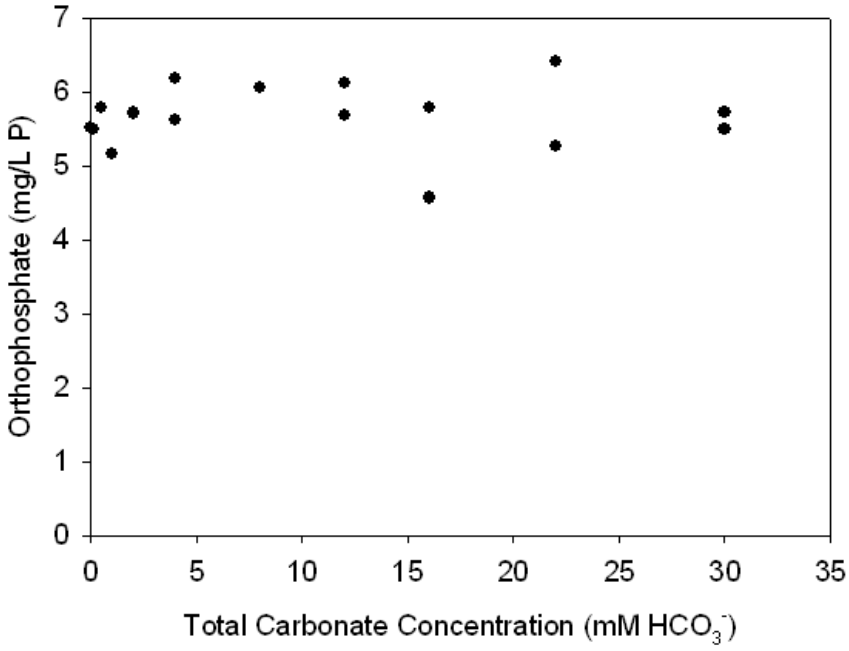

Figure 64. Effect of the carbonate concentration on antiscalant oxidation. All experiments contained 26 mM Ca^{2+} and were performed at pH 6.0. Initial orthophosphate in solution was 1.3 mg/L P.

CALCIUM-DQ2006 SPECIATION AS A FUNCTION OF PH

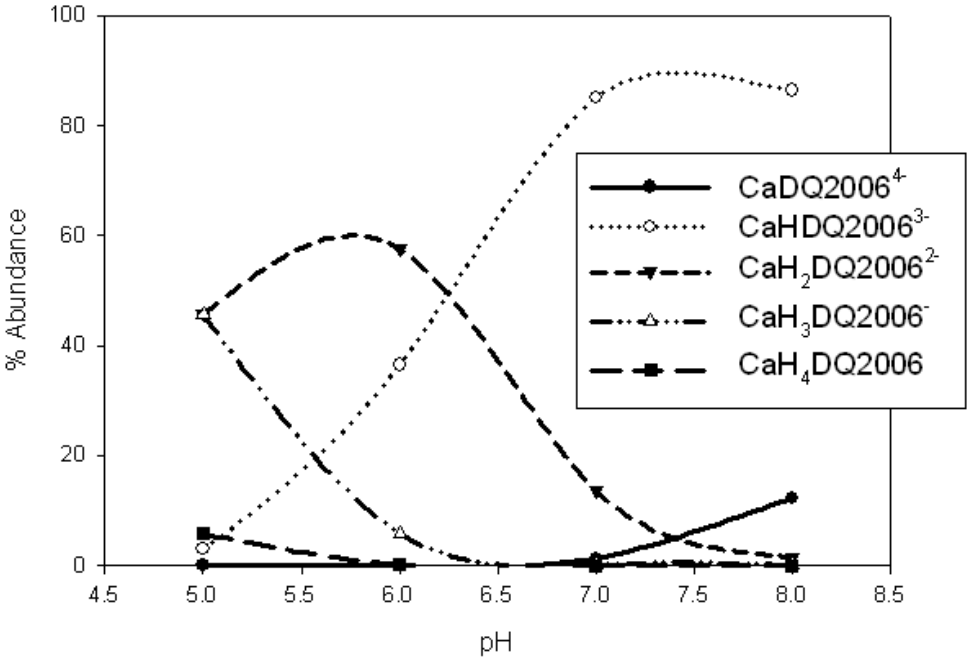

Figure 65. Speciation of calcium complexes with antiscalant DQ2006.

Appendix C: Supporting Information for Chapter 7

CARBONATE LOST DURING OZONATION

To determine the amount of carbonate lost during ozonation, carbonate titrations were performed. One liter of initial solution was tested twice, once with the typical ozone/oxygen mix used during ozonation and once with oxygen only. For both tests, the gases were bubbled for 10 minutes. Carbonate titrations for the initial solution, initial solution at pH 6.0, and gas-treated solutions (shown in Figure 66) enabled a comparison between non-ozonated and ozonated solutions. For both gases tested, titrations revealed that approximately 7 mM of the total carbonate is lost due to carbon dioxide degassing. The initial solution at pH 7.8 was found to have a total carbonate concentration of 16.7 mM, and at pH 6.0 the carbonate titrated was 13.9 mM, indicating a shift in the carbonate system distribution (more H_2CO_3 at lower pH). The ozone/oxygen-treated solution had a final pH of 6.9 after 10 minutes of gas treatment and a total carbonate concentration of 7.0 mM. The oxygen-treated solution had a final pH of 6.7 and a total carbonate concentration of 7.6 mM. Additional tests showed similar results, and the average total carbonate after gas treatment was approximately 7.5 mM. This value was used to calculate the addition of $NaHCO_3$ at the start of each precipitation experiment that was performed after gaseous ozone treatment.

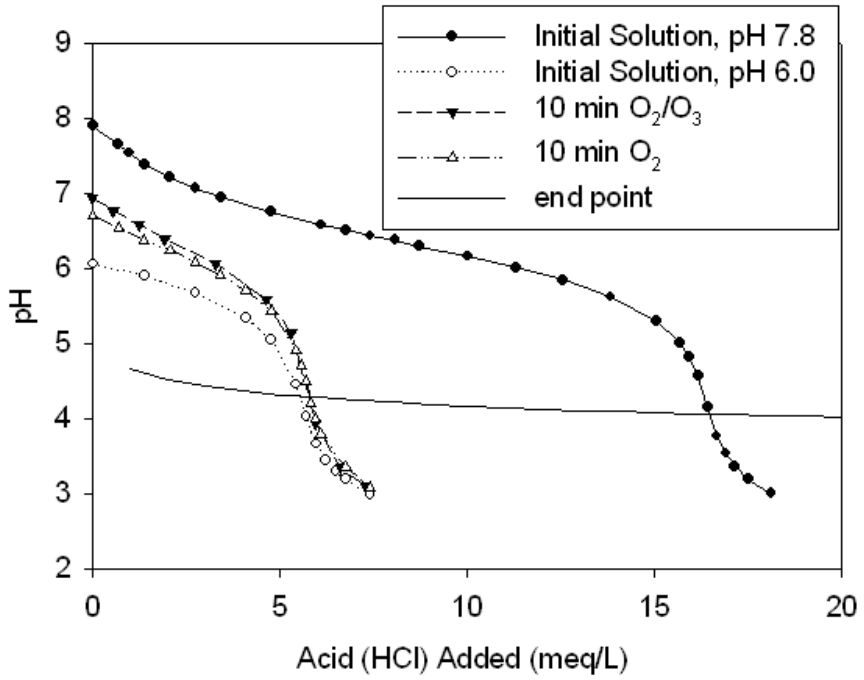

Figure 66. Effect of gas bubbling through Maricopa water on total carbonate reduction.

Appendix D: Proton NMR of the Polymer Antiscalant

The Coatex polymer was evaluated by proton NMR, and the composition was determined to be 61% itaconic acid, 20% acrylic acid, and 19% methacrylic acid or 3:1:1 (itaconic:acrylic:methacrylic). A 5 mL sample of the polymer in aqueous solution was rotovapped at room temperature (22 ^{o}C) to remove all water and redissolved in D_2O for NMR analysis. The NMR analysis was performed at 15 ^{o}C. The spectra were taken on a Varian Unity 300 spectrometer. For 1H spectra, the frequency was 300 MHz. All spectra were taken in D_2O (deuterium oxide) and were referenced to the residual protio solvent (delta = 4.78 ppm), relative to TMS. The results from the NMR study are shown in Figure 67 and Figure 68. There were two non-equivalent groups of protons within the three monomer compounds that were used to determine the polymer composition. The two groups are shown in Figure 69 in the itaconic and methacrylic acid molecules (enclosed in dotted squares). The peak at 2.330 ppm was determined to be the itaconic acid monomer, while the doublet set of peaks at 1.397 and 1.319 ppm was the methacrylic acid monomer. The doublet may have been caused by some of the methyl group protons becoming unsymmetrical due to adjacent itaconic or acrylic acid molecules within the polymer. The large combined peak between 2.0 and 1.5 ppm represents the rest of the protons on the backbone of the polymer. No individual peak assignments can be made from this group of peaks. The peak assignments for the itaconic and methacrylic protons were determined based on known NMR data for the individual monomers, and peak heights were used to calculate the polymer composition. The clearly defined itaconic and methacrylic acid peaks suggest that the polymer may be a block copolymer,

rather than a random copolymer. However, further experimental investigation is necessary to confirm this suggestion.

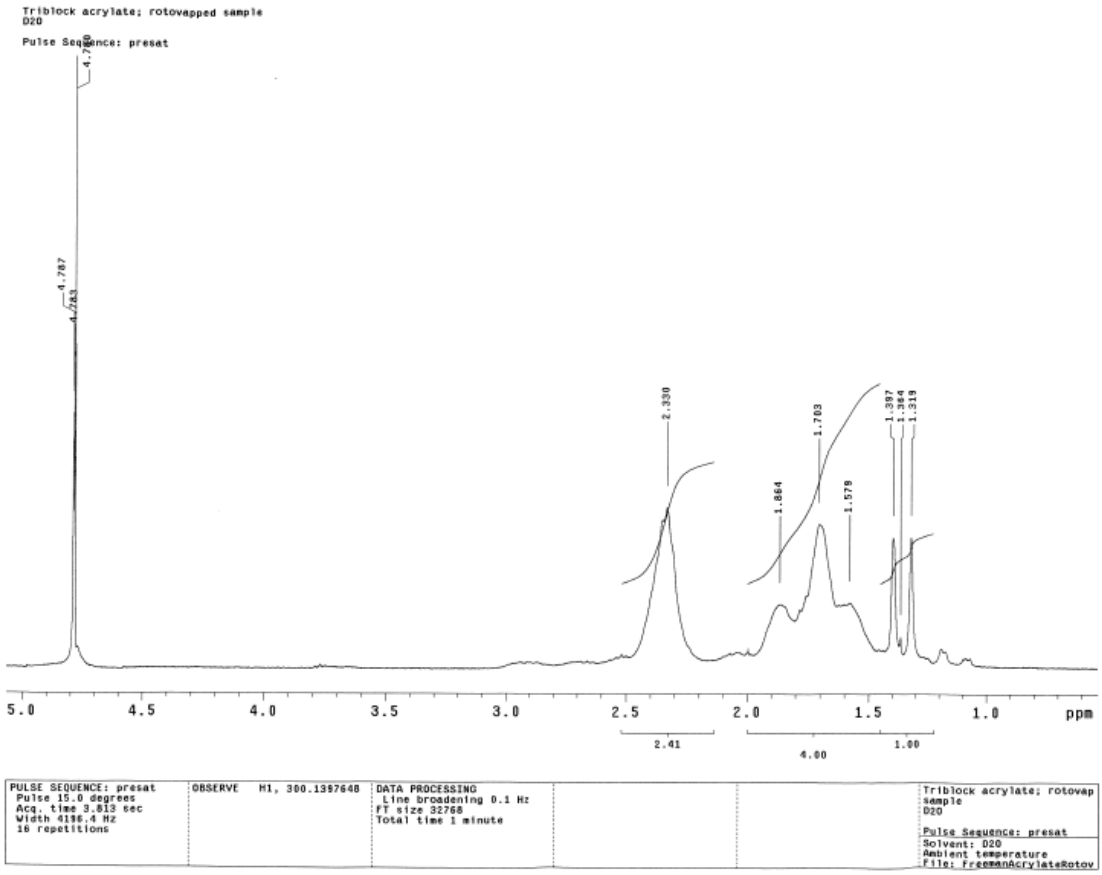

Figure 67. Proton NMR result for the polymer antiscalant, Coatex.

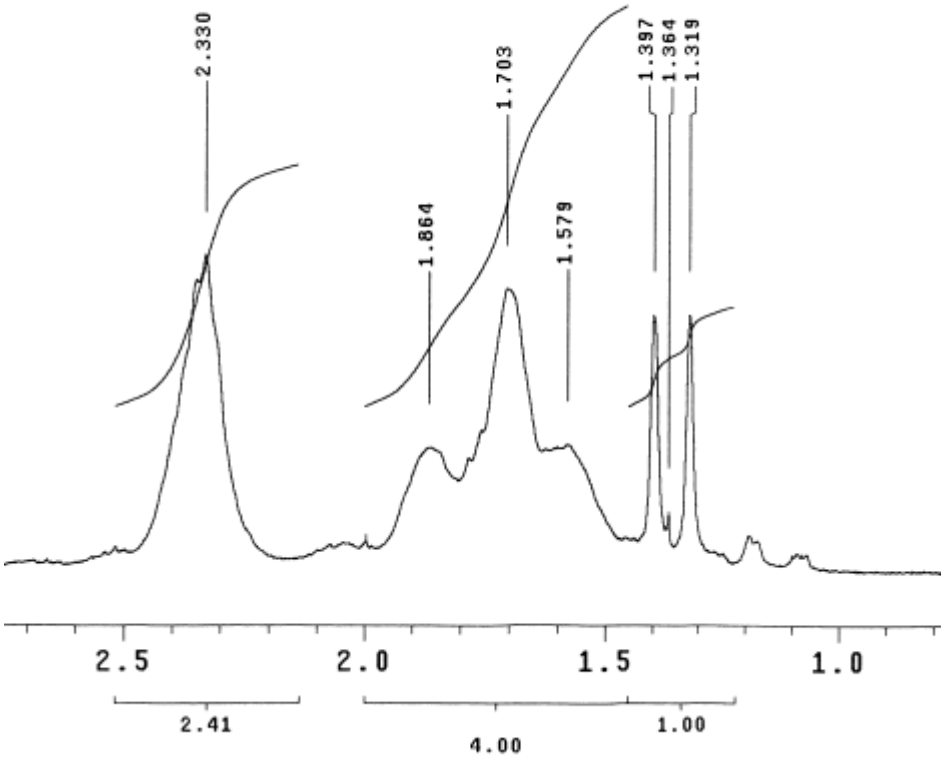

Figure 68. Zoom view of the proton NMR peaks obtained for the polymer antiscalant, Coatex.

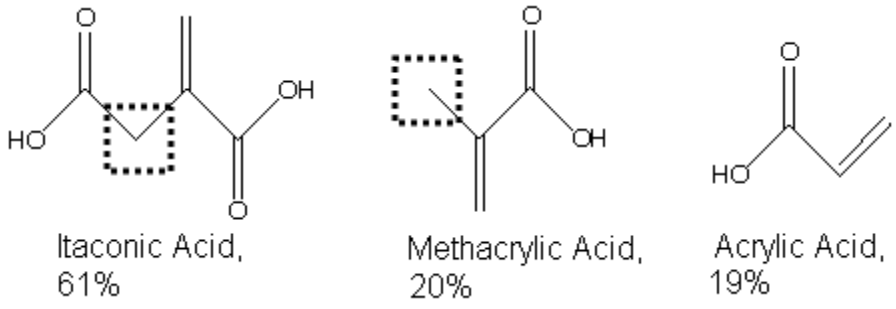

Figure 69. Individual monomers that make up the polymer antiscalant. Carbon groups located inside dotted squares are the two non-equivalent groups of protons within the polymer that form individual peaks at 2.330 ppm and 1.397/1.319 ppm.

References

Acero, J.L. and von Gunten, U. (2000) Influence of carbonate on the ozone/hydrogen peroxide based advanced oxidation process for drinking water treatment. Ozone Science & Engineering 22, 305-328.

Acero, J.L. and von Gunten, U. (2001) Characterization of oxidation processes: Ozonation and the AOP O_3/H_2O_2. Journal American Water Works Association 93(10), 90-100.

Afonso, M.D., Jaber, J.O. and Mohsen, M.S. (2004) Brackish groundwater treatment by reverse osmosis in Jordan. Desalination 164, 157-171.

Allam, A.R., Saaf, E.-J. and Dawoud, M.A. (2002) Desalination of brackish groundwater in Egypt. Desalination 152, 19-26.

Almulla, A., Eid, M., Coté, P. and Coburn, J. (2002) Developments in high recovery brackish water desalination plants as part of the solution to water quantity problems. Desalination 153, 237-243.

Andreassen, J.P. and Hounslow, M.J. (2004) Growth and aggregation of vaterite in seeded-batch experiments. AIChE Journal 50(11), 2772-2782.

Andreozzi, R., Caprio, V., Insola, A. and Marotta, R. (1999) Advanced oxidation processes (AOP) for water purification and recovery. Catalysis Today 53, 51-59.

Arai, Y. and Sparks, D.L. (2001) ATR-FTIR spectroscopic investigation on phosphate adsorption mechanisms at the ferrihydrite-water interface. Journal of Colloid and Interface Science 241, 317-326.

Baker, R.W. (2004) Membrane Technology and Applications. John Wiley & Sons, Ltd., Chichester.

Baumann, E.W. (1973) Determination of pH in concentrated salt solutions. Analytica Chimica Acta 64, 284-288.

Benner, J., Salhi, E., Ternes, T. and von Gunten, U. (2008) Ozonation of reverse osmosis concentrate: Kinetics and efficiency of beta blocker oxidation. Water Research 42, 3003-3012.

Bird, R.B., Stewart, W.E. and Lightfoot, E.N. (2002) Transport Phenomena. John Wiley & Sons, Inc., New York.

Blavoux, B., Gilli, É. and Rousset, C. (2004) Feed and salinity origin of the marine spring of Port-Miou (Marseille-Cassis). Principal emergence of a karstic network originating from the Messinian age (original language: French). Comptes rendus Geoscience 336, 523-533.

Bloetscher, F., Meeroff, D.E., Wright, M.E., Yang, D., Rojas, R., Polar, J., Laas, M., Bieler, B., Sakura-Lemessy, D.-M., Aziz, S.A. and Fiekle, C. (2006) Defining the concentrate disposal problem and identifying potential solutions. Florida Water Resources Journal 58(4), 25-30.

Boffardi, B.P. (1997) Scale and deposit control for reverse osmosis systems. Membrane Technology Conference, American Water Works Association: New Orleans, LA, February 23-26, 681-693.

Bonné, P.A.C., Hofman, J.A.M.H. and Hoek, J.P.v.d. (2000) Scaling control of RO membranes and direct treatment of surface water. Desalination 132, 109-119.

Bowers, A.R., Gaddipati, P., Jr., W.W.E. and Monsen, R.M. (1989) Treatment of toxic or refractory wastewaters with hydrogen peroxide. Water Science and Technology 21(6-7), 477-486.

Brečević, L., Nöthig-Laslo, V., Kralj, D. and Popović, S. (1996) Effect of divalent cations on the formation and structure of calcium carbonate polymorphs. Journal of the Chemical Society-Faraday Transactions 92(6), 1017-1022.

Brooks, R., Clark, L.M. and Thurston, E.F. (1950) Calcium carbonate and its hydrates. Philosophical Transactions of the Royal Society of London. Series A, Mathematical and Physical Sciences 243(861), 145-167.

Bruneval, F., Donadio, D. and Parrinello, M. (2007) Molecular dynamics study of the solvation of calcium carbonate in water. Journal of Physical Chemistry B 111(42), 12219-12227.

Bu-Rashid, K.A. and Czolkoss, W. (2007) Pilot tests of multibore UF membrane at Addur SWRO desalination plant, Bahrain. Desalination 203, 229-242.

Buffle, M.-O., Schumacher, J., Meylan, S., Jekel, M. and von Gunten, U. (2006a) Ozonation and advanced oxidation of wastewater: Effect of O_3 dose, pH, DOM, and HO*-scavengers on ozone decomposition and HO* generation. Ozone: Science & Engineering 28, 247-259.

Buffle, M.-O., Schumacher, J., Salhi, E., Jekel, M. and von Gunten, U. (2006b) Measurement of the initial phase of ozone decomposition in water and wastewater by means of a continuous quench-flow system: Application to disinfection and pharmaceutical oxidation. Water Research 40, 1884-1894.

Buglyó, P., Kiss, T., Dyba, M., Jezowska-Bojczuk, M., Kozlowski, H. and Bouhsina, S. (1997) Complexes of aminophosphonates - 10. Copper(II) complexes of phosphonic derivatives of iminodiacetate and nitrilotriacetate. Polyhedron 16(19), 3447-3454.

Chakraborty, D., Agarwal, V.K., Bhatia, S.K. and Bellare, J. (1994) Steady-state transitions and polymorph transformations in continuous precipitation of calcium carbonate. Industrial & Engineering Chemistry Research 33(9), 2187-2197.

Chang, S.D. and Singer, P.C. (1991) The impact of ozonation on particle stability and the removal of TOC and THM precursors. Journal American Water Works Association 3, 71-79.

Clarkson, J.R., Price, T.J. and Adams, C.J. (1992) Role of metastable phases in the spontaneous precipitation of calcium carbonate. Journal of the Chemical Society-Faraday Transactions 88(2), 243-249.

Darton, E.G. (2000) Membrane chemical research: Centuries apart. Desalination 132, 121-131.

Dequest (2006) Phosphonates based antiscalants, dispersants, corrosion inhibitors and chelants. Solutia, Inc. St. Louis, http://www.dequest.com/pages/phosphonates.asp.

Dove, P.M. and Hochella, M.F. (1993) Calcite precipitation mechanisms and inhibition by orthophosphate - In situ observations by Scanning Force Microscopy. Geochimica et Cosmochimica Acta 57(3), 705-714.

Duan, W.B., Oota, H. and Sawada, K. (1999) Stability and structure of ethylenedinitrilopoly(methylphosphonate) complexes of the alkaline-earth metal ions in aqueous solution. Journal of the Chemical Society-Dalton Transactions (17), 3075-3080.

Eaton, A.D., Clesceri, L.S., Rice, E.W. and Greenberg, A.E., (Ed.) (2005) Standard methods for the examination of water and wastewater. American Public Health Association, American Water Works Association, Water Environment Federation, Washington, D.C.

Elliot, A.J. and Mccracken, D.R. (1989) Effect of temperature on O_3^- reactions and equilibria: a pulse radiolysis study. Radia. Phys. Chem. 33, 69-74.

Elovitz, M.S. and von Gunten, U. (1999) Hydroxyl radical/ozone ratios during ozonation processes. I. The R_{ct} concept. Ozone Science & Engineering 21, 239-260.

Elovitz, M.S., von Gunten, U. and Kaiser, H.-P. (2000) Hydroxyl radical/ozone ratios during ozonation processes. II. The effect of temperature, pH, alkalinity, and DOM properties. Ozone Science & Engineering 22, 123-150.

Fahmi, Nishijima, W. and Okada, M. (2003) Improvement of DOC removal by multi-stage AOP-biological treatment. Chemosphere 50, 1043-1048.

Falini, G., Fermani, S., Tosi, G. and Dinelli, E. (2009) Calcium carbonate morphology and structure in the presence of seawater ions and humic acids. Crystal Growth & Design 9(5), 2065-2072.

Frenkel, V. (2000) Desalination Methods, Technology, and Economics. Kennedy/Jenks Consultants http://www.idswater.com/Common/Paper/Paper_90/Desalination%20Methods,%20Technology,%20and%20Economics1.htm. December 13, 2007.

Fritzmann, C., Löwenberg, J., Wintgens, T. and Melin, T. (2007) State-of-the-art of reverse osmosis desalination. Desalination 216, 1-76.

Frost, J.W., Loo, S., Cordeiro, M.L. and Li, D. (1987) Radical-based dephosphorylation and organophosphonate biodegradation. Journal of the American Chemical Society 109, 2166-2171.

Gabelich, C., Williams, M.D., Rahardianto, A., Franklin, J.C. and Cohen, Y. (2007) High-recovery reverse osmosis desalination using intermediate chemical demineralization. Journal of Membrane Science 301, 131-141.

Gabelich, C.J., Gerringer, F.W., Franklin, J.C., Gao, J., Cohen, Y. and Suffet, I.H. (2004) Reverse osmosis pretreatment: Challenges with conventional treatment. Proceedings - Annual Conference, American Water Works Association.

Gálvez, N., Barrón, V. and Torrent, J. (1999) Effect of phosphate on the crystallization of hematite, goethite, and lepidocrocite from ferrihydrite. Clays and Clay Minerals 47(3), 304-311.

Ghafour, E.E.A. (2002) Enhancing RO system performance utilizing antiscalants. Desalination 153, 149-153.

Gilbert, E. and Hoffmann-Glewe, S. (1990) Ozonation of ethylenediaminetetraacetic acid (EDTA) in aqueous solution: Influence of pH value and metal ions. Water Research 24(1), 39-44.

Gillard, R.D., Newman, P.D. and Collins, J.D. (1989) Speciation in aqueous solutions of di-ethylenetriamine-N,N,N',N",N"-pentamethylenephosphonic acid and some metal complexes. Polyhedron 8(16), 2077-2086.

Gilron, J., Daltrophe, N., Waissman, M. and Oren, Y. (2005) Comparison between Compact Accelerated Precipitation Softening (CAPS) and conventional pretreatment in operation of brackish water reverse osmosis (BWRO). Industrial & Engineering Chemistry Research 44, 5465-5471.

Gleick, P.H. (1996) *Water Resources* in Encyclopedia of Climate and Weather. S. H. Schneider, (Ed.), University Press, New York, Vol. 2, 817-823.

Gleick, P.H. (2006) The World's Water 2006-2007, The Biennial Report on Freshwater Resources. Island Press, Chicago.

Glueckstern, P. (2000) Desalination: Current situation and future prospects. http://www.biu.ac.il/Besa/waterarticle1.html. October 31, 2007.

Glueckstern, P., Thoma, A. and Priel, M. (2001) The impact of R&D on new technologies, novel design concepts and advanced operating procedures on the cost of water desalination. Desalination 139, 217-228.

Graber, C. (2006) Desalination in Spain, Technology Review. Massachusetts Institute of Technology (MIT) http://www.technologyreview.com/microsites/spain/water/index.aspx. December 13, 2007.

Greenlee, L.F., Lawler, D.F., Freeman, B.D., Marrot, B. and Moulin, P. (2009) Reverse osmosis desalination: Water sources, technology, and today's challenges. Water Research 43(9), 2317-2348.

Grenier, A., Meireles, M., Aimar, P. and Carvin, P. (2008) Analysing flux decline in dead-end filtration. Chemical Engineering Research & Design 86(11A), 1281-1293.

Gurol, M.D. and Singer, P.C. (1982) Kinetics of ozone decomposition: A dynamic approach. Environmental Science & Technology 16(7), 377-383.

Gustafsson, J.P. (2006) Visual MINTEQ. KTH, Dept. of Land and Water Resources Engineering, Stockholm, Sweden.

Guzzella, L., Feretti, D. and Monarca, S. (2002) Advanced oxidation and adsorption technologies for organic micropollutant removal from lake water used as drinking-water supply. Water Research 36, 4307-4318.

Hasson, D., Drak, A. and Semiat, R. (2001) Inception of $CaSO_4$ scaling on RO membranes at various water recovery levels. Desalination 139, 73-81.

Hayes, V.E.A., Ternan, N.G. and McMullan, G. (2000) Organophosphonate metabolism by a moderately halophilic bacterial isolate. FEMS Microbiology Letters 186, 171-175.

Hermia, J. (1982) Constant pressure blocking filtration laws - Application to power-law non-Newtonian fluids. Transactions of The Institution of Chemical Engineers 60(3), 183-187.

Hoigné, J. (1998) *Chemistry of aqueous ozone and transformation of pollutants by ozonation and advanced oxidation processes* in The Handbook of Environmental Chemistry: Quality and Treatment of Drinking Water II. J. Hrubec, (Ed.), Springer-Verlag, Berlin, Vol. 5, Part C, 83-142.

Hoigné, J., Bader, H., Haag, W.R. and Staehelin, J. (1985) Rate constants of reactions of ozone with organic and inorganic compounds in water - III Inorganic compounds and radicals. Water Research 19, 993-1004.

Huntington (2006) Worldwide Seawater Desalination Capabilities. Huntington Beach Water Desalination Facility/Poseidon Resources Corporation www.hbfreshwater.com/desalinationhistory.asp.

Hydranautics (2001) Design parameters affecting performance. http://www.membranes.com/docs/trc/desparam.pdf. March 9, 2008.

Hydranautics (2003) Chemical pretreatment for RO and NF, Technical Application Bulletin No. 111, Rev. B. http://www.membranes.com/docs/tab/TAB111.pdf. May 17, 2008.

Ichikawa, T. and Sawada, K. (1997) Protonation behavior and intramolecular interactions of alpha,omega-alkanediaminepolymethylenepolyphosphonates. Bulletin of the Chemical Society of Japan 70(4), 829-835.

Ikehata, K. and El-Din, M.G. (2004) Degradation of recalcitrant surfactants in wastewater by ozonation and advanced oxidation processes: A review. Ozone: Science & Engineering 26, 327-343.

Ito, K., Jian, W., Nishijima, W., Baes, A.U., Shoto, E. and Okada, M. (1998) Comparison of ozonation and AOPs combined with biodegradation for removal of THM precursors in treated sewage effluents. Water Science and Technology 38(7), 179-186.

Jonasson, R.G., Rispler, K., Wiwchar, B. and Gunter, W.D. (1996) Effect of phosphonate inhibitors on calcite nucleation kinetics as a function of temperature using light scattering in an autoclave. Chemical Geology 132(1-4), 215-225.

Jurenka, R.A. and Chapman-Wilbert, M. (1996) Maricopa groundwater treatment study. Water Treatment Technology Program Report No. 15, U.S. Department of the Interior, Bureau of Reclamation.

Kan, A.T., Fu, G.M. and Tomson, M.B. (2005) Adsorption and precipitation of an aminoalkylphosphonate onto calcite. Journal of Colloid and Interface Science 281(2), 275-284.

Khare, N., Hesterberg, D. and Martin, J.D. (2005) XANES investigation of phosphate sorption in single and binary systems of iron and aluminum oxide minerals. Environ. Sci. Technol. 39, 2152-2160.

Kim, S. and Hoek, E.M.V. (2005) Modeling concentration polarization in reverse osmosis processes. Desalination 186, 111-128.

Klassen, N.V., Marchington, D. and McGowan, H.C.E. (1994) H_2O_2 determination by the I_3^- method and by $KMnO_4$ titration. Analytical Chemistry 66(18), 2921-2925.

Klinger, J., Lang, M., Sacher, F., Brauch, H.-J., Maier, D. and Worch, E. (1998) Formation of glyphosate and AMPA during ozonation of waters containing ethylenediaminetetra(methylenephosphonic acid). Ozone Science & Engineering 20, 99-110.

Knepper, T.P. (2003) Synthetic chelating agents and compounds exhibiting complexing properties in the aquatic environment. Trends in Analytical Chemistry 22(10), 708-724.

Kralj, D., Kontrec, J., Brečević, L., Falini, G. and Nöthig-Laslo, V. (2004) Effect of inorganic anions on the morphology and structure of magnesium calcite. Chemistry-A European Journal 10(7), 1647-1656.

Kremen, S.S. and Tanner, M. (1998) Silt density indices (SDI), percent plugging factor (%PF): their relation to actual foulant deposition. Desalination 119, 259-262.

Krzysko-Lupicka, T., Strof, W., Kubs, K., Skorupa, M., Weiczorek, P., Lejczak, B. and Kafarski, P. (1997) The ability of soil-borne fungi to degrade organophosphonate carbon-to-phosphorus bonds. Applied Microbiology and Biotechnology 48, 549-552.

Lam, R.S.K., Charnock, J.M., Lennie, A. and Meldrum, F.C. (2007) Synthesis-dependant structural variations in amorphous calcium carbonate. CrystEngComm 9(12), 1226-1236.

Lati, J. and Meyerstein, D. (1978) Oxidation of 1st-row bivalent transition metal complexes containing ethylenediaminetetraacetate and nitrilotriacetate ligands by free-radicals - Pulse-radiolysis study. Journal of the Chemical Society-Dalton Transactions (9), 1105-1118.

Le Gouellec, Y.A. and Elimelech, M. (2002) Calcium sulfate (gypsum) scaling in nanofiltration of agricultural drainage water. Journal of Membrane Science 205, 279-291.

Lebron, I. and Suarez, D.L. (1996) Calcite nucleation and precipitation kinetics as affected by dissolved organic matter at 25 ^{o}C and pH >7.5. Geochimica et Cosmochimica Acta 60(15), 2765-2776.

Ledakowicz, S. and Solecka, M. (2001) Influence of ozone and advanced oxidation processes on biological treatment of textile wastewater. Ozone: Science & Engineering 23, 327-332.

Lee, R.-W., Glater, J., Cohen, Y., Martin, C., Kovac, J., Milobar, M.N. and Bartel, D.W. (2003) Low-pressure RO membrane desalination of agricultural drainage water. Desalination 155, 109-120.

Lin, Y.P. and Singer, P.C. (2005) Inhibition of calcite crystal growth by polyphosphates. Water Research 39(19), 4835-4843.

Loeb, S. and Sourirajan, S. (1963) Seawater dimineralization by means of an osmotic membrane. Advances in Chemistry Series 38, 117-132.

Lonsdale, H.K., Merten, U. and Riley, R.L. (1965) Transport properties of cellulose acetate osmotic membranes. Journal of Applied Polymer Science 9, 1341-1362.

Loste, E., Wilson, R.M., Seshadri, R. and Meldrum, F.C. (2003) The role of magnesium in stabilising amorphous calcium carbonate and controlling calcite morphologies. Journal of Crystal Growth 254(1-2), 206-218.

Luu, C.A. (1994) Improved chelators and sequestrants for Army Reverse Osmosis Water Purification Units (ROWPUs). Desalination 97, 165-170.

M'nif, A., Bouguecha, S., Hamrouni, B. and Dhahbi, M. (2007) Coupling of membrane processes for brackish water desalination. Desalination 203, 331-336.

Magara, Y., Kawasaki, M., Sekino, M. and Yamamura, H. (2000) Development of reverse osmosis seawater desalination in Japan. Water Science and Technology 41(10-11), 1-8.

Martell, A.E., Smith, R.M. and Motekaitis, R.J. (2004) NIST critically selected stability constants of metal complexes, Version 8. Texas A&M University.

Martin, C.J. and Goodman, A.E. (2003) Desalination demonstration report for Buena Vista Water Storage District. State of California, Dept. of Water Resources.

Masson, L., Richards, B.S. and Schaefer, A.I. (2005) System design and performance testing of a hybrid membrane-photovoltaic desalination system. Desalination 179, 51-59.

Meldrum, F.C. and Hyde, S.T. (2001) Morphological influence of magnesium and organic additives on the precipitation of calcite. Journal of Crystal Growth 231(4), 544-558.

Merten, U. (1963) Flow relationships in reverse osmosis. Industrial and Engineering Chemistry Fundamentals 2(3), 229-232.

Mickley, M.C. (2001) Membrane concentrate disposal: Practices and regulation. U.S. Department of the Interior, Bureau of Reclamation, Mickley & Associates.

Mickley, M.C. (2004) Review of concentrate management options, Ground Water Report 363: The Future of Desalination in Texas Volume II: Technical Papers, Case Studies and Desalination Technology Resources. Texas Water Development Board http://www.twdb.state.tx.us/iwt/desal/docs/Volume2Main.asp. May 21, 2008.

Morel, F.M.M. and Hering, J. (1993) Principles and Applications of Aquatic Chemistry. John Wiley & Sons, Inc.

Mueller, B. (1996) ChemEQL, a program to calculate chemical speciation, Internal Report, Limnological Research Center. Swiss Federal Institute of Environmental Science and Technology, CH-6047 Kastanienbaum, Switzerland.

Munoz, F. and von Sonntag, C. (2000) The reactions of ozone with tertiary amines including the complexing agents nitrilotriacetic acid (NTA) and ethylenediaminetetraacetic acid (EDTA) in aqueous solution. Journal of the Chemical Society, Perkin Transactions 2, 2029-2033.

Munter, R., Preis, S., Kallas, J., Trapido, M. and Veressinina, Y. (2001) Advanced oxidation processes (AOPs): Water treatment technology for the twenty-first century. Kemia-Kemi 28(5), 354-362.

Nancollas, G.H. and Sawada, K. (1982) Formation of scales of calcium carbonate polymorphs - The influence of magnesium ion and inhibitors. Journal of Petroleum Technology 34(3), 645-652.

Nebel, H. and Epple, M. (2008) Continuous preparation of calcite, aragonite and vaterite, and of magnesium-substituted amorphous calcium carbonate (Mg-ACC). Zeitschrift fur Anorganische und Allgemeine Chemie 634(8), 1439-1443.

Nebel, H., Neumann, M., Mayer, C. and Epple, M. (2008) On the structure of amorphous calcium carbonate - A detailed study by solid-state NMR spectroscopy. Inorganic Chemistry 47(17), 7874-7879.

Nicot, J.P. and Chowdhury, A.H. (2005) Disposal of brackish water concentrate into depleted oil and gas fields: a Texas study. Desalination 181, 61-74.

Nielsen, A.E. (1984) Electrolyte crystal growth mechanisms. Journal of Crystal Growth 67(2), 289-310.

Nielsen, A.E. and Toft, J.M. (1984) Electrolyte crystal growth kinetics. Journal of Crystal Growth 67(2), 278-288.

Nowack, B. and Stone, A.T. (2000) Degradation of nitrilotris(methylenephosphonic acid) and related (amino)phosphonate chelating agents in the presence of manganese and molecular oxygen. Environmental Science & Technology 34, 4759-4765.

Nygren, M.A., Gay, D.H., Catlow, C.R.A., Wilson, M.P. and Rohl, A.L. (1998) Incorporation of growth-inhibiting diphosphates into steps on the calcite cleavage plane surface. Journal of the Chemical Society-Faraday Transactions 94(24), 3685-3693.

Ogino, T., Suzuki, T. and Sawada, K. (1987) The formation and transformation mechanism of calcium carbonate in water. Geochimica et Cosmochimica Acta 51(10), 2757-2767.

Pacheco, R.I. (2005) Control of Silica Scaling Phenomena in Reverse Osmosis Systems. Ph.D. Dissertation, The University of Texas at Austin.

Paige, C.R., Snodgrass, W.J., Nicholson, R.V., Scharer, J.M. and He, Q.H. (1996) The effect of phosphate on the transformation of ferrihydrite into crystalline products in alkaline media. Water, Air, and Soil Polution 97, 397-412.

Parkhurst, D.L. and Appelo, C.A.J. (2008) PHREEQC Interactive, A hydrogeochemical transport model. USGS.

Paul, D.R. (1972) The role of membrane pressure in reverse osmosis. Journal of Applied Polymer Science 16, 771-782.

Paul, D.R. (2004) Reformulation of the solution-diffusion theory of reverse osmosis. Journal of Membrane Science 241, 371-386.

Perry, R.H. and Green, D.W., (Ed.) (1997) Perry's Chemical Engineers' Handbook. McGraw Hill, New York.

Petry, M., Sanz, M.A., Langlais, C., Bonnelye, V., Durand, J.-P., Guevara, D., Nardes, W.M. and Saemi, C.H. (2007) The El Coloso (Chile) reverse osmosis plant. Desalination 203, 141-152.

Pitzer, K.S. (1973) Thermodynamics of electrolytes. I. Theoretical basis and general equations. The Journal of Physical Chemistry 77(2), 268-277.

Pitzer, K.S. (1975) Thermodynamics of electrolytes. V. Effects of higher-order electrostatic terms. Journal of Solution Chemistry 4(3), 249-265.

Pitzer, K.S. (1991) Activity Coefficients in Electrolyte Solutions. CRC Press, Inc., Boca Raton, FL.

Pitzer, K.S. and Mayorga, G. (1973) Thermodynamics of Electrolytes. II. Activity and osmotic coefficients for strong electrolytes with one or both ions univalent. The Journal of Physical Chemistry 77(19), 2300-2308.

Plottu-Pecheux, A., Houssais, B., Democrate, C., Gatel, D., Parron, C. and Cavard, J. (2002) Comparison of three antiscalants, as applied to the treatment of water from the River Oise. Desalination 145, 273-280.

Pobiner, H. (1961) Determination of hydroperoxides in hydrocarbon by conversion to hydrogen peroxide and measurement by titanium complexing. Analytical Chemistry 33(10), 1423-1426.

Popov, K., Niskanen, E., Ronkkomaki, H. and Lajunen, L.H.J. (1999) P-31 NMR study of organophosphonate protonation equilibrium at high pH. New Journal of Chemistry 23(12), 1209-1213.

Popov, K., Ronkkomaki, H. and Lajunen, L.H.J. (2001) Critical evaluation of stability constants of phosphonic acids (IUPAC technical report). Pure and Applied Chemistry 73(10), 1641-1677.

Pytkowicz, R.M. (1979) Activity Coefficients in Electrolyte Solutions. CRC Press, Inc., Boca Raton, FL.

Rahardianto, A., Gao, J., Gabelich, C.J., Williams, M.D. and Cohen, Y. (2007) High recovery membrane desalting of low-salinity brackish water: Integration of accelerated precipitation softening with membrane RO. Journal of Membrane Science 289, 123-137.

Rahardianto, A., McCool, B.C. and Cohen, Y. (2008) Reverse osmosis desalting of inland brackish water of high gypsum scaling propensity: Kinetics and mitigation of membrane mineral scaling. Environmental Science & Technology 42(12), 4292-4297.

Rahardianto, A., Shih, W.-Y., Lee, R.-W. and Cohen, Y. (2006) Diagnostic characterization of gypsum scale formation and control in RO membrane desalination of brackish water. Journal of Membrane Science 279, 655-668.

Ravizky, A. and Nadav, N. (2007) Salt production by the evaporation of SWRO bring in Eilat: a success story. Desalination 205, 374-379.

Reddy, M.M. and Hoch, A.R. (2001) Calcite crystal growth rate inhibition by polycarboxylic acids. Journal Of Colloid And Interface Science 235(2), 365-370.

Reddy, M.M. and Wang, K.K. (1980) Crystallization of calcium carbonate in the presence of metal-Ions.1. Inhibition by magnesium-ion at Ph 8.8 and 25 ^{o}C. Journal of Crystal Growth 50(2), 470-480.

Reverberi, F. and Gorenflo, A. (2007) Three year operational experience of a spiral-wound SWRO system with a high fouling potential feed water. Desalination 203, 100-106.

Sandia (2003) Desalination and water purification roadmap - A report of the executive committee. U.S. Department of the Interior, Bureau of Reclamation and Sandia National Laboratories, DWPR Program Report #95 http://wrri.nmsu.edu/tbndrc/roadmapreport.pdf. May 25, 2008.

Sanz, M.A., Bonnélye, V. and Cremer, G. (2007) Fujairah reverse osmosis plant: 2 years of operation. Desalination 203, 91-99.

Sauvet-Goichon, B. (2007) Ashkelon desalination plant - A successful challenge. Desalination 203, 75-81.

Sawada, K. (1997) The mechanisms of crystallization and transformation of calcium carbonates. Pure and Applied Chemistry 69(5), 921-928.

Sawada, K., Araki, T. and Suzuki, T. (1987) Complex formation of amino polyphosphonates. 1. Potentiometric and nuclear magnetic resonance studies of nitrilotris(methylenephosphonato) complexes of the alkaline-earth-metal ions. Inorg. Chem. 26, 1199-1204.

Sawada, K., Miyagawa, T., Sakaguchi, T. and Doi, K. (1993) Structure and thermodynamic properties of aminopolyphosphate complexes of the alkaline-earth metal ions. J. Chem. Soc. Dalton Trans., 3777-3784.

Schick, R., Strasser, I. and Stabel, H.-H. (1997) Fluorometric determination of low concentrations of H_2O_2 in water: Comparison with two other methods and application to environmental samples and drinking-water treatment. Water Research 31(6), 1371-1378.

Sedlak, D.L. and Andren, A.W. (1991) Oxidation of chlorobenzene with Fenton's reagent. Environmental Science & Technology 25(4), 777-782.

Sehested, K., Holcman, J., Bjergbakke, E. and Hart, E.J. (1984) Formation of ozone in the reaction of O_3^- and the decay of the ozonide ion radical at pH 10-13. The Journal of Physical Chemistry 88, 269-273.

Seigal, L. and Zelonis, J. (1995) Water desalination. Rensselaer Polytechnic Institute http://www.rpi.edu/dept/chem-eng/Biotech-Environ/Environmental/desal/intro.html. February 13, 2008.

Semiat, R., Sutzkover, I. and Hasson, D. (2003) Characterization of the effectiveness of silica anti-scalants. Desalination 159, 11-19.

Service, R.F. (2006) Desalination freshens up. Science 313, 1088-1090.

Shadyro, O.I., Sosnovskaya, A.A. and Vrublevskaya, O.N. (2003) C-N bond cleavage reactions on the radiolysis of amino-containing organic compounds and their derivatives in aqueous solutions. International Journal of Radiation Biology 79(4), 269-279.

Shih, W.-Y., Albrecht, K., Glater, J. and Cohen, Y. (2004) A dual-probe approach for evaluation of gypsum crystallization in response to antiscalant treatment. Desalination 169, 213-221.

Shih, W.-Y., Gao, J., Rahardianto, A., Glater, J., Cohen, Y. and Gabelich, C.J. (2006) Ranking of antiscalant performance for gypsum scale suppression in the presence of residual aluminum. Desalination 196, 280-292.

Snoeyink, V.L. and Jenkins, D. (1980) Water Chemistry. John Wiley & Sons, Inc., New York.

Sotelo, J.L., Beltrán, F.J., González, M. and Domínguez, J. (1989) Effect of high salt concentrations on ozone decomposition in water. Journal of Environmental Science and Health A24(7), 823-842.

Speitel Jr., G.E., Symons, J.M., Diehl, A.C., Sorensen, H.W. and Cipparone, L.A. (1993) Effect of ozone dosage and subsequent biodegradation on removal of DBP precursors. Journal American Water Works Association 5, 86-95.

Staehelin, J. and Hoigné, J. (1982) Decomposition of ozone in water: Rate of initiation by hydroxide ions and hydrogen peroxide. Environmental Science & Technology 16, 676-681.

Staehelin, J. and Hoigné, J. (1985) Decomposition of ozone in water in the presence of organic solutes acting as promoters and inhibitors of radical chain reactions. Environmental Science & Technology 19, 1206-1213.

Stemmler, K., Glod, G. and von Gunten, U. (2001) Oxidation of metal-diethylenetriamine-pentaacetate (DTPA)-complexes during drinking water ozonation. Water Research 35(8), 1877-1886.

Stumm, W. and Morgan, J.J. (1996) Aquatic Chemistry: Chemical Equilibria and Rates in Natural Waters. Wiley-Interscience, New York.

Sudmalis, M. and Sheikholeslami, R. (2000) Coprecipitation of $CaCO_3$ and $CaSO_4$. Canadian Journal of Chemical Engineering 78(1), 21-31.

Suty, H., DeTraversay, C. and Cost, M. (2004) Applications of advanced oxidation processes: present and future. Water Science and Technology 49(4), 227-233.

Tang, Y.M., Yang, W.Z., Yin, X.S., Liu, Y., Yin, P.W. and Wang, J.T. (2008) Investigation of $CaCO_3$ scale inhibition by PAA, ATMP and PAPEMP. Desalination 228(1-3), 55-60.

Tomiyasu, H., Fukutomi, H. and Gordon, G. (1985) Kinetics and mechanism for ozone decomposition in basic solution. Inorganic Chemistry 24, 2962-2966.

von Gunten, U. (2003) Ozonation of drinking water: Part I. Oxidation kinetics and product formation. Water Research 37, 1442-1467.

Vrouwenvelder, J.S., Manolarakis, S.A., Veenendaal, H.R. and van der Kooij, D. (2000) Biofouling potential of chemicals used for scale control in RO and NF membranes. Desalination 132, 1-10.

Wada, N., Yamashita, K. and Umegaki, T. (1995) Effects of divalent cations upon nucleation, growth and transformation of calcium carbonate polymorphs under conditions of double diffusion. Journal of Crystal Growth 148(3), 297.

Walha, K., Amar, R.B., Firdaous, L., Quéméneur, F. and Jaouen, P. (2007) Brackish groundwater treatment by nanofiltration, reverse osmosis and electrodialysis in Tunisia: performance and cost comparison. Desalination 207, 95-106.

Wang, F.L. and Tarabara, V.V. (2008) Pore blocking mechanisms during early stages of membrane fouling by colloids. Journal of Colloid and Interface Science 328(2), 464-469.

Wanielista, M.M.E. (1997) Advanced oxidation and biodegradation of drinking water. Civil Engineering, The University of Texas at Austin, Austin, TX.

Watts, R.J., Udell, M.D. and Monsen, R.M. (1993) Use of iron minerals in optimizing the peroxide treatment of contaminated soils. Water Environment Research 65(7), 839-844.

Westin, K.J. and Rasmuson, A.C. (2005) Nucleation of calcium carbonate in presence of citric acid, DTPA, EDTA and pyromellitic acid. Journal of Colloid and Interface Science 282(2), 370-379.

Wiesner, A., Katz, L. and Chen, C.-C. (2006) The impact of ionic strength and background electrolyte on pH measurements in metal ion adsorption experiments. Journal of Colloid and Interface Science 301(1), 329-332.

Wijmans, J.G. and Baker, R.W. (1995) The solution-diffusion model: A review. Journal of Membrane Science 107, 1-21.

Wilf, M. (1997) Application of RO desalting technology for potable water production in USA. Hydranautics http://www.membranes.com/docs/papers/15_tokyo.doc.pdf. May 17, 2008.

Wilf, M. and Klinko, K. (2001) Optimization of seawater RO systems design. Desalination 138, 299-306.

Williams, M.D. and Cohen, Y. (2004) Two-stage reverse-osmosis treatment using interstage chemical precipitation to achieve high water recovery. Abstracts of Papers, 227th ACS National Meeting: Anaheim, CA, March 28 - April 1.

Williams, M.D., Evangelista, R. and Cohen, Y. (2002) Non-thermal process for recovering reverse osmosis concentrate: process chemistry and kinetics. Proceedings - Water Technology Conference, American Water Works Association, 1246-1263.

Wolfe, P. (2005) Fujairah marks major milestone for desalination in Middle East. Water & Wastewater International http://ww.pennnet.com/display_article/227597/20/ARTCL/none/none/1/Fujairah-marks-major-milestone-for-desalination-in-Middle-East/. May 25, 2008.

Wolff, G. (2006) The economics of desalination. Pacific Institute http://texas.sierraclub.org/water/conference/SAWConfPPTs/GaryWolff.pdf. February 13, 2008.

Wolthers, M., Charlet, L. and Van Cappellen, P. (2008) The surface chemistry of divalent metal carbonate minerals; A critical assessment of surface charge and potential data using the Charge Distribution Multi-Site Ion Complexation Model. American Journal of Science 308(8), 905-941.

Yang, Q., Ma, Z., Hasson, D. and Semiat, R. (2004) Destruction of anti-scalants in RO concentrates by electrochemical oxidation. Journal of Chemical Industry and Engineering (China) 55(2), 339-340.

Yang, Q.F., Liu, Y.Q., Gu, A.H., Ding, J. and Shen, Z.Q. (2001) Investigation of calcium carbonate scaling inhibition and scale morphology by AFM. Journal of Colloid and Interface Science 240(2), 608-621.

Vita

Lauren Fay Greenlee was born to Samuel D. and Jan S. Greenlee on April 8, 1979 in Camp LeJeune, North Carolina. She was raised in Limerick, PA with her younger sister Emily. After graduating as valedictorian from Spring-Ford High School, Lauren attended the University of Michigan, studied chemical engineering, and earned a Bachelor's of Science in Engineering from the College of Engineering in 2001. Lauren spent three years working; she completed an internship with Hoffmann-La Roche in Basel, Switzerland, taught English in Moulins, France, and worked in marketing in Spain, before returning to the U.S. to work as a chemical engineer for OmniGene Bioproducts, Inc. in Boston, MA. While working in Boston, she was inspired to pursue graduate studies and started at The University of Texas at Austin in the fall of 2004. She completed her Master's in Environmental and Water Resources Engineering in the summer of 2006 and continued in Chemical Engineering for her Ph.D. During her graduate studies, she was awarded a Thrust 2000 Fellowship from The University of Texas, a Graduate Research Fellowship from the National Science Foundation, an International Research and Education in Engineering Fellowship from the National Science Foundation, and a P.E.O. Scholar Award from P.E.O. International in support of her Ph.D.

Permanent address: 184 Zorro Court, Schwenksville, PA, 19473

This dissertation was typed by the author.